

Integrated simulation for improved mineral recovery processes

Caroline Izart

Thesis submitted for the Degree of Doctor of Philosophy

Department of Geology

School of Natural Sciences

Trinity College Dublin

2021



Trinity College Dublin

Coláiste na Tríonóide, Baile Átha Cliath

The University of Dublin

Declaration

I declare that this thesis has not been submitted as an exercise for a degree at this or any other university and it is entirely my own work. Wherever there is joint published or unpublished work included, it is duly acknowledged in the text. I agree to deposit this thesis in the University's open access institutional repository or allow the library to do so on my behalf, subject to Irish Copyright Legislation and Trinity College Library conditions of use and acknowledgement.

C. Izart – September 2020



Abstract

The consumption of mineral and metals is increasing as the population grows and the demand for mineral resources will remain high and evolve as society moves towards a carbon-neutral future. The increasing demand for metals, combined with the pressure from citizens and industries for more responsible production methods, creates the necessity to establish more sustainable mining and mineral processing practices. This project investigated the usefulness of modelling and simulation tools to enable sustainability improvement in industry in general and in the mining industry specifically. Simulation offers opportunities for better resource management, impact assessment, planning and personal training within an accessible software tool. Mineral processing simulation must consider the variability of properties (mineralogy, texture, grade, hardness etc.) within the plant feed in order to predict the processing recovery and grade of the final concentrate along the entire mine lifetime. The integration of geological, mineral processing and metallurgical concepts is thus a central part of the simulator. The present process models were developed in the Sim module of Outotec HSC Chemistry® 10 software. Two of these models, which have passed through all modelling steps are presented in detail in this thesis. The first, focusing on a geometallurgical approach, aimed at providing a more accurate description of the grinding behaviour of the ores in a mill by considering the grinding parameter variations depending on the particle composition. This model, once programmed and integrated in the HSC Sim environment, was tested against pilot test results. The second model presented in this thesis is a dynamic mill model. It was conceived for digital twin simulators. This model was also validated against data gathered in a mineral processing plant sampling campaign. The study then describes how models are applied in simulators through two industry cases co-developed during this thesis project. The first case describes an operator training simulator designed to improve the operational skills of spodumene flotation plant staff. The second case study focuses on the development of a digital twin simulator for a gold processing plant. In this case study, the geometallurgical approach was critical to achieve comprehensive planning and optimization of the mine and processing plant operations.

Summary

In 2050, the world population is estimated to reach over nine billion individuals. The consumption of minerals and metals, related to agriculture, construction, new technologies and transport is expected to follow the population growth. Studies show that the exploitation of new primary mineral resources will still be required, as reserves and recycling options will not be sufficient to provide for humanity's needs. With this in mind, and to exploit these non-renewable resources in the best way, the extraction and processing of mineral resources must use the most sustainable method available, in the context of the particular resource geology and characteristics. The processes must be optimized to preserve the majority of water and energy resources while increasing recovery of the commodity. Mining industries also need to consider their impact on society and on the environment by disclosing their exploitation method and environmental footprint in a transparent way and allowing traceability of their products.

To achieve this aim, the minerals industry still has to establish several key operational components. Firstly, reliable performance indicators and benchmarking tools, such as life cycle assessments, must be developed specifically for mining. To attain this level of information integration, a renewed approach from extraction to metal production must be implemented. Holistic mine planning or a geometallurgical approach needs to consider the geological background and mineral processing technologies at the same time. Presently, these two sectors still have a tendency to work in silos. New methods to integrate real-time optimization, better operator training and prediction of the plant's key performance indexes are features considered in the industry 4.0 concept, which has the potential to improve current practices in the mining industry.

The potential capabilities of simulation to improve mineral processing performance is presented in this study, firstly by showing how the performance of other industries improved by implementing simulation tools. With increasing computer power, which is more easily available, for instance with the emergence of cloud computing, simulations are becoming more widely used in a larger scope and in more detailed ways. However, some simulation features are still lacking and need to be introduced

for this method to become widely accepted and utilised. Up to now, simulators have only concerned certain parts of the plants, and few have considered the entire process, limiting the use to the study of isolated phenomena without a global integrated view or tailored approach. Moreover, they have seldom considered the geometallurgical aspect of processing, dealing with heterogeneous particles and natural minerals as materials in large scale simulations, i.e. over several different process circuits. Lastly, some of this simulation work was limited in terms of accessibility. Sometimes programmed in a generic environment, many simulations were not easily modifiable by end users, and required a deep knowledge of the modelling background.

In this study, the author introduces some of the requirements and best practices for an integrated simulation of mineral processing plants, compatible with the concept of digital twins. “Integrated” in this context means capturing each of the metal production steps, from mine to metal production, with user choice of modelling depth from high fidelity resolution to less detailed scope, depending on current process knowledge. The thesis then presents some of the models implemented in the Outotec HSC Sim platform during this PhD work, aiming at the creation of more holistic, multi-purpose simulators. Firstly, an upgraded mill model is presented that concerns different grindability characteristics in its feed stream. This model allows different ore mixes having different behaviour in a mill to be taken into account. It helps, for instance, in the planning of ore blending. Then, a dynamic mill model showing transient phases and time dependence behaviour built for control system testing or operator training is introduced. Field work data gathered during the PhD work was used to validate both presented models.

Finally, the conception of two simulators is described and some preliminary results are given. One is focused on operator training and was specifically developed to be a generic flotation training case. Even though the principal purpose of this simulator is training, it also has the capability to be implemented for other usages. The other simulator was conceived for integrated dynamic simulation from mine to metal production, based on a real mining installation, using models developed during this PhD and pre-existing models from HSC Sim library. This simulator is the first step of

an integrated geometallurgical digital twin to be used for the planning and process optimization of a large-scale gold mine.

Acknowledgements

This work was supported by the project European Industrial Doctorate (EID) in future efficient minerals analysis, processing and training MetalIntelligence, funded by the European Union Horizon 2020 Marie Skłodowska-Curie Innovative Training Networks (grant number 722677).

I would like to thank my supervisors from academia and from Metso Outotec. Thanks to Prof. Balz Kamber for his help on this manuscript and his guidance these past years. Thanks to Dr. Antti Roine for his trust and for making me feel at home in the HSC team. And finally, thanks to Dr. Séan McClenaghan for his support in the past year.

Thanks to First Quantum Minerals Ltd. for letting me organize tests in Pyhäsalmi plant and use the results in this thesis. Thanks to GTK Mintec and Pirjo Seppälä for letting me use their samples from the Prochaine course project pilot. And thanks to Newcrest Mining company for letting me present their mine to mill simulator in this thesis.

A huge thank to Dr. Antti Remes, I do not count the number of times he helped and advised me these past years.

I thank MetalIntelligence project team, and especially Dr. Una Farrell for her help and support. Thanks to all my fellows in this project: Alex, Marco, Temi, Cheche and Pedro. We had great discussions about our own work and that really helped me contextualise mine.

And many thanks to the HSC team who helped me so much these past three years, Matias, Matti and Matti, Deepak and Petri. Thanks to Jussi who helped me and Pedro with our first training simulator.

Finally, I would like to thank my partner Loïc, for all the support and his help on this manuscript. I also thank my family in France for the encouragement.

Co-author statement

Section 3.1 and Section 4.1 was presented at a conference (Izart, C. (2020) Mill Simulation using Multi-particle Grindability Parameters, Sweden: Implications for Mineral Processing, Conference in Minerals Engineering 2020. Luleå, Sweden). The author collected the bibliographical references, reviewed multi-particle mill conceptual models and coded the model in the HSC Sim environment. The author analysed samples (XRF, microscopy), studied the results and developed the simulations associated with the pilot test. The pilot test was run by GTK Mintec, and samples were collected with the help of Pirjo Seppälä (GTK).

Sections 3.2 and 4.2 has not yet been presented at any conference. The author conducted the literature review for dynamic SAG/AG mill conceptual models and coded the model in the HSC Sim environment. The author organized the sampling campaign around the primary mill with the help of First Quantum personnel, prepared the samples for analysis and studied the results. The author prepared the simulations and analysed the results, which were reviewed by Antti Remes (Outotec (Finland) Oy).

Section 3.3 and section 3.3 are in preparation for submission as a conference paper. The author improved HSC Sim dynamic flotation cell and conditioner model codes, conducted a literature review for conceptual models, created the simulation flowsheet, parametrized the units and created the feed streams. Pedro Bergamo (Luleå University of Technology) participated in the creation of the exercises and gave the training to the operators. Jussi Leinonen (Outotec (Finland) Oy) made the coupling between HSC and the process control platform.

Section 3.4 and section 3.4 will not be presented as a separate publication as it is, but some of the simulation results will be used in conference proceedings and publications. The author conducted the literature review for conceptual models, implemented and improved the code for old and new units (crushers, stockpiles, mills, conveyors), parametrized, ran and debugged simulations, with the help of Antti Remes.

Contents

Declaration	i
Abstract	ii
Summary	iv
Acknowledgements.....	vii
Co-author statement.....	viii
Contents	ix
List of Tables.....	xiii
List of Figures.....	xv
List of Abbreviations.....	xxi
Chapter 1 Introduction.....	22
1.1 Current status of mining and mineral processing.....	1
1.1.1 Resources and mining projects	1
1.1.2 Mining and mineral processing.....	4
1.1.3 The integration issue of mining and mineral processing operations.....	15
1.2 Future trends.....	18
1.2.1 Evolution of the mineral and metal demand.....	18
1.2.2 Future trends in mineral processing.....	18
1.2.3 Implication for modelling and simulation.....	21
1.3 Research questions, aim and scope of this study	22
Chapter 2 Literature review	24
2.1 Simulator Capabilities in Mineral Processing Plants	26
2.1.1 Terminology.....	26
2.1.2 Modelling process.....	26
2.1.3 Simulation building process	29
2.1.4 State of the art and future trends	32
2.2 Specificities of mineral processing simulations.....	35

2.2.1	Terminology employed.....	35
2.2.2	Stream description	36
2.2.3	Models for mineral processing	41
2.2.4	Choosing a simulation environment.....	43
2.3	Simulator applications in mineral processing plants.....	46
Chapter 3	Materials and methods	53
3.1	Multi-particle mill model study	55
3.1.1	Material.....	55
3.1.2	Modelling methods.....	55
3.2	Dynamic SAG/AG mill model study.....	64
3.2.1	Material.....	64
3.2.2	Modelling methods.....	68
3.3	Training simulator conception	83
3.3.1	Background and process description.....	83
3.3.2	Simulator requirements	86
3.3.3	Simulator construction	87
3.4	Gold Processing Plant Digital Twin.....	100
3.4.1	Background and process description.....	100
3.4.2	Simulator requirements	103
3.4.3	Simulator construction	104
Chapter 4	Results	116
4.1	Multi-Particle Mill Validation Results	117
4.2	Dynamic Mill Model Validation Results.....	119
4.3	Flotation Training Simulator Results	128
4.4	Gold processing plant simulation results	130
4.4.1	Process replication validation.....	130
4.4.2	Optimisation case-study.....	130

Chapter 5	Conclusions, discussion and recommendations for future work.....	134
5.1	Research questions	134
5.2	Discussion	135
5.3	Recommendation for future work.....	138
References	139
Appendices	152
6.1	Appendix 1: Version history of HSC models (from 2015, updated for April 2021 release version 10.0.5) from HSC Chemistry User's Guide – Chapter 46 (Antti Remes & Izart, 2021) – In bold are version updates made by the author.....	152
6.2	Appendix 2: Manual pages from the author describing the implementation of , from HSC Chemistry User's Guide – Chapter 46 (Antti Remes & Izart, 2021).....	157
6.3	Appendix 3: Murske size analysis and mineral reconstruction	181
6.4	Appendix 4: TMT size analysis and mineral reconstruction.....	182
6.5	Appendix 5: 2SA size analysis and mineral reconstruction	183
6.6	Appendix 6: KMT size analysis and mineral reconstruction.....	184
6.7	Appendix 7: Mineral reconstruction in streams and enrichments.....	185
6.8	Appendix 8: Pyhäsalmi grinding circuit flowsheet.....	186
6.9	Appendix 9: Data table from Pyhäsalmi SAG automation process control during	test 187
6.10	Appendix 10: LM2J power consumption (kW) and feed rate (tph) evolution graph. Blue arrows show when feed was momentarily interrupted	189
6.11	Appendix 11: Sample timing, D80, D50 and fine (-38µm) particles amount (%)	table 190
6.12	Appendix 12: LM2J product size evolution graph. Blue arrow shows when feed was briefly interrupted	191
6.13	Appendix 13: Screenshot of the user interface of the economic calculator tool used in the VeX-Li training simulator.....	192

6.14 Appendix 14: Parameter simulation results from grinding / flotation circuits and expected results from plant survey. (Note: mass pulls and recoveries are not disclosed, and simulation results are given as a function of the expected results)

..... 193

List of Tables

Table 1: Illustration of locked, semi-liberated and liberated sulphides. Particle sizes are around 1mm. Images taken with reflected light microscopy on a polished section from Kylylahti grinding test samples. Sulphides are bright yellow grains and dark grey grain are gangue (mainly quartz).....	8
Table 2: Most common mineral separation methods for ores. Suitability depends on the specificity of the ore being processed. This list is not exhaustive and does not mention all separation methods and subprocesses, it rather aims to give an overview of the most commonly found processes in mineral processing plants. Information and characteristics are extracted from SME Mineral Processing and Extractive Metallurgy Handbook, ed. 2019 (Young, 2019).	12
Table 3: Description summary of hydro, pyro and hybrid methods for primary ore treatments. Recycling is not taken into account. Information and characteristics are extracted from SME Mineral Processing and Extractive Metallurgy Handbook, ed. 2019 (Young, 2019), unless stated otherwise.....	14
Table 4: Example of stream architecture and information contained.	40
Table 5: Example of particle architecture and information contained.....	41
Table 6: Example of mineral architecture and information contained.....	41
Table 7: Proportion of grains bearing non-liberated sulphides (size threshold above 50µm ²)	57
Table 8: Pyhäsalmi ROM sample AG/SAG breakage parameters.....	65
Table 9: Crushed ore (LM2J feed) sieve analysis results.....	66
Table 10: Flotation models in HSC 10.....	89
Table 11: Input and output variables used in the conveyor model.....	111
Table 12: Input and output variables used in the stockpile model.	112
Table 13: Integrated crusher models and summary of their relationships.	113
Table 14: Fitted parameters used for the simulation of primary crushing and grinding circuits units (NA: Not Applicable).	115
Table 15: Experimental, mass balanced and simulated results with original ball mill model (Sim1) and multi-particle model (Sim2). Stream names are shown on the flowsheet in Figure 21 (RM = Rod mill, OS = Oversized, US = Undersized, UF =	

Underflow, OF = Overflow, BM = Ball mill). P80 “bulk” design the 80% particle passing size for the entire solid flow.	117
Table 16: Sim 2 results with base case feed flow rate (0.67t/h) and increased flow rate (+5% and +10%), representing the cyclone overflow (OF) P80 for the sulphide population and for the “bulk” -i.e. the sulphides and NSG populations – and the mill circuit power consumption.	119
Table 17: Virtual Training satisfaction evaluation (or reaction evaluation), scaled from 1 (satisfied) to 5 (not satisfied), from the training participants. (SD: Standard Deviation) Figure from Bergamo et al. (2021)	129
Table 18: Relative error between expected P80, specific energy, mass pull and recovery for each alteration type.	130

List of Figures

Figure 1: Diversity and variability in a deposit type class and strong heterogeneities in a deposit intrinsic characteristic raise a need for specific and adjustable mineral treatment methods. Left, tonnage / grade of the major VMS type deposits (Mosier et al., 2009). Right, three pictures from the same VMS deposit in different ore zones – Hood deposit, Nunavut, Canada (from Mills, Piercey and Toole, 2016).....	3
Figure 2: a/ Cross section of a geological model, constructed from information from several drill holes, coupled to surface geochemistry of geophysical information - used to prepare the mine planning b/ block model of a deposit – each block has an associated grade information, interpolated from data points (assays from drill holes, grab samples). For the sake of simplicity, the size of the blocks is constant in this representation, which is not always true.	5
Figure 3: Classical stress forces of rock mechanics used in comminution.....	6
Figure 4: Evolution of the studied material along the comminution circuit, from large, heterogeneous rock boulders in the crusher feed, to particles (composed of several minerals) to mineral before the separation. PSD and initial grade control are the main monitored variables.....	10
Figure 5: Evolution of the studied material slurry along the separation circuit, with a magnetic separation and a flotation. For the flotation process, the aqueous phase characteristics become an important variable to monitor.....	13
Figure 6: Evolution of the studied material (gold ore concentrate pulp) along a carbon in leach process, wherein activated carbon particles (C) and cyanide (NaCN) are added to the pulp. The cyanide leaching and precious metals adsorption onto the activated carbon occur simultaneously in the tanks. Gold is then stripped from loaded carbon and is finally isolated in electrowinning cells.....	15
Figure 7: Schematic view of a mining operation, with the evolution of the available routine information data, its quality and focus. This view also shows the transformation of the studied material scale from a geological to an elemental/atomic object.	17
Figure 8: Historical and predicted copper demand (in Tg) from 1980 to 2050, displaying the four scenarios defined by the United Nation Environment Program	

(UNEP) (MF – Market first ; PF – Policy first ; SF – Security first ; EF – Equitability first) (from Elshkaki et al., 2016).....	18
Figure 9: Historical Cu ore grades for selected countries and projected global ore grades 2010 onwards. Figure from Northey et al. (2014).	20
Figure 10: Conceptual modelling, model coding and experimentation, the three steps of the modelling process, adapted from Robinson, 1997.	27
Figure 11: Relationships between simulator purpose and general scope, also known as “what” aspects (adapted from Kellner et al., 1999).	30
Figure 12: Evolution of the simulation purposes over time (adapted from Miettinen, 2008).....	31
Figure 13: Purposes of simulators in the 2000’s (adapted from Ylén et al. 2005).....	32
Figure 14: Digital Factory concepts, benefits and investments. The dashed line represents the benefits realised by a plant over start-up time with a conventional approach. The plain line represents the benefits over start-up time with a digital factory approach. (Comm. = Commissioning) (Adapted from Kühn, 2006).	33
Figure 15: Simplified example of the organization of circuit, streams and units.	36
Figure 16: Pictures of mineral streams at different stages of the process. a) Pyhäsalmi crusher charge, composed of heterogeneous particles in terms of size and composition, with no water added (picture J. Joutsenvaara, 2019 for Minetrain project). b) – Cleaner launder streams from Pyhäsalmi plant, almost 30wt% solid, with relatively more homogeneous particle sizes and compositions (picture C. Izart, 2019).....	37
Figure 17: Solid material in streams – different level of description. From HSC Chemistry® User’s Guide, Chapter 45 (Antti Remes & Lamberg, 2021).	39
Figure 18: Effect of simulator deviation compared to real plant operation. The relevance of the simulation is tied to the amount of information available. The original, or initial simulator, conceived for preparing the start-up does not have a lot of information about the real process. With no maintenance, the simulator is not even updated when the plant starts operation and is thus already outdated compared to the amount of data gathered during the start-up. With little or only reactive maintenance, the simulation is adapted intermittently when issues are spotted. With proactive maintenance, the simulator is regularly updated and stays relevant. Finally, using opportunity assessment on the simulator enables to improve its relevance....	48

Figure 19: Mine lifecycle and use of mineral processing simulators.....	50
Figure 20: Particle-based geometallurgical model after Lamberg (2011).....	51
Figure 21: Grinding circuit model with collection points from the pilot test – red circles show where the flow rate, particle size distribution and solid percentage of the pulp were measured – green arrows show where polished sections and chemical analysis by size fractions were performed.	56
Figure 22: a and b: polished sections of hydrocyclone underflow (ball mill feed), c and d: polished section of ball mill product. The bright yellow grains are sulphides and dark grey grains are the gangue (mainly quartz, with some carbonates).....	57
Figure 23: Perfect mixing mill model illustration: for a given size class, all entering particles and all particles generated from the coarser fraction in the mill are either discharged or broken down into smaller sizes.	59
Figure 24: Rod mill plug flow model separated in breakage stages.	62
Figure 25: Particle size evolution when the crushed ore feed flow rate was changed from 120tph to 90tph.....	67
Figure 26: Particle size evolution when the crushed ore feed was changed from 90tph to 118tph.....	68
Figure 27: Steps for the dynamic calculation of the mill model content and product PSD.....	70
Figure 28: High energy appearance functions for various size fractions for a given mill content state.	71
Figure 29: Discharge function for the SAG/AG mill.....	73
Figure 30: Flowsheet used for the dynamic simulation of LM2J.....	79
Figure 31: LM2J parameters for the simulation.....	80
Figure 32: Screenshot of HSC Sim Dynamic Dialog tool set parameters page.	81
Figure 33: Screenshot of HSC Sim Dynamic Dialog tool get parameters page.....	81
Figure 34: Spodumene flotation simulator flowhseet used for operator training, as seen in HSC Sim.	85
Figure 35: Purpose, scope, result variables, process abstraction and input parameters of the spodumene flotation simulator.	86
Figure 36: Effect of reagents on the infinite recovery of every particle in the rougher flotation bank a) collector (NaOl – Sodium oleate) dosage b) pH regulator (NaOH –	

Sodium hydroxide) c) frother dosage. Mineral abbreviations: Spd, Qtz, Ab, Ms, Mc, Mgt - Spodumene, Quartz, Albite, Muscovite, Microcline, Magnetite.	91
Figure 37: Recovery of minerals from the collection zone through the froth zone. ...	93
Figure 38: Screenshot of the XRF on-line analyser simulation data page. On the parameters page, any number of analysis lines, the elements being analysed, and the time required for the filling, measuring and washing steps can be defined. In the Assay Accuracies tables, the analysis parameters (detection limit and standard deviation for each element) can be filled in. Each line can be bypassed or requested for analysis.	95
Figure 39: Schematic structure of process simulation for the OTS case-study of spodumene flotation plant.	97
Figure 40: Screenshot of the user interface of a pump sump controller. Controlled values are the level setpoint, the switching on/off of the motor and valve opening. The evolution of pulp level and pump frequency are shown as separate graphs.	99
Figure 41: Lihir gold deposit 3D model showing the different alteration zones: argillic, advanced argillic, leached soaked group, boiled zone and anhydrite sealed group. The Lihir mineralised envelope is approximately 3km along strike, 1.5km down dip and 0.5km depth (Newcrest Mining Limited, 2014).....	101
Figure 42. Simplified flowsheet for the processing of Lihir ore (Newcrest Mining Limited, 2014). The ROM is first separated into three piles for crushing: soft, medium and hard ore, directed to Abon, gyratory and jaw crushers respectively. The crushed ore is then stored into three piles, depending on grade. The high-grade ore is directly fed to the POX then to the CIL. Flotation grade ore is directed to flotation, and the concentrate is oxidized and leached. The pregnant solution is then treated via electrowinning to recover gold.	102
Figure 43: Mineralogical stream composition (Cal = calcite, Py = pyrite, Qtz = quartz, Au = gold) of the different streams.	105
Figure 44: HSC definition of the different types of ores, mixed into three primary stockpiles according to their crushing properties.	107
Figure 45: Dynamic ball mill with overflow discharge algorithm.	108
Figure 46: Grinding, flotation lines and dewatering of the Lihir process (front-end) implemented in HSC Sim.....	109
Figure 47: Schematic representation of the conveyor model with main parameters.	110

Figure 48: Schematic representation of the stockpile model with main parameters a) conical stockpile “live” and “dead” volumes for single loading and reclaiming points b) stockpile layering effect on the discharge composition.	112
Figure 49: HSC screenshot of crushing circuits for each of the three primary stockpiles. The hard ore pile is crushed with jaw crushers, medium hard ore with a gyrator crusher and soft ore passes through an ABON sizer. The crushed material is then separated into three stockpiles to feed the three main processing lines HGO1, HGO2 and FGO, according to their grade and mineralogy.	114
Figure 50: Particle size distributions of the ball mill output (Bal = balanced, Sim 1 = simulated with perfect mixing mill model, Sim 2 = simulated with multi-particle perfect mixing mill model). Bulk refers to PSD for the complete particle flow and is shown in black. For the balanced and Sim 2 results, sulphide particle population PSD is represented in orange and NSG particle population PSD is in yellow. The simulated results are coherent with experimental observations, both for the bulk and the gangue and sulphide distributions.	118
Figure 51: Simulated and experimental power consumption evolution across the step change.	121
Figure 52: Simulated and experimental P80 and P50 evolution across the step change.	122
Figure 53: Particle size evolution when the crushed ore feed was changed from 125tph to 90tph.....	123
Figure 54: Particle size evolution when the crushed ore feed was changed from 90tph to 120tph.....	124
Figure 55: Simulated and experimental power consumption evolution during the step test with average feed rate input.....	126
Figure 56: Simulated and experimental P80 and P50 evolution during the step test with average feed rate input.....	127
Figure 57: Concentrate and feed grade as a ratio of the initial (t=0) value with and without cell operation parameter adaptation for the concentrate. At 10 minutes, the feed grade is increased by 3.5%. With no adaptation of the flotation cell operation parameters, the concentrate grade follows the increase progressively. If the air flow and pulp level to the cells is increased at t = 10 minutes, then the grade decreases and	

stabilises later to a grade closer to the initial concentrate grade. X-axis (time) is given in hours:minutes:seconds..... 132

Figure 58: Instant Au recovery as a ratio of the initial ($t=0$) recovery value with and without cell air flow adaptation. The spike between 10 and 20 minutes, corresponding to the change of operation parameters value, is due to the instantaneous calculation of the recovery, based concentrate stream amount of Au per feed Au amount at a given time t , and is thus non representative. In the long term trend, we can see that the modification of pulp level and air flow to the cell increases the recovery by almost 2%. 132

List of Abbreviations

AG/SAG mill	Autogenous / Semi-Autogenous mill
CAPEX	Capital expenditure
CSS	Closed Size Setting
DCS	Distributed Control System
F80	Sieve size for which 80% of the feed sample mass passes
ICP-OES/MS	Induced Coupled Plasma – Optical Emission Spectrometry / Mass Spectrometry
KPI	Key Performance Index
LCA	Life Cycle Assessment
MLA	Mineral Liberation Analysis
OPEX	Operational expenditure
OTS	Operator Training Simulator
PGE	Platinum Group Elements
PSD	Particle Size Distribution
P50	Sieve size for which 50% of the product sample mass passes
P80	Sieve size for which 80% of the product sample mass passes
ROM	Run of Mine
SG	Specific Gravity (unitless)
UI	User interface
XRF	X-Ray Fluorescence

Chapter 1 Introduction

This chapter gives a general introduction to mining and mineral processing techniques, as well as background information related to the development timeline of a mining project. Several basic concepts of geology, metallogeny, mining, mineral processing and metallurgy used in the next chapters are outlined in the following sections. Next, some of the issues and topics raised within the mining industry are presented. Following this factual review, the future trends for the mining industry, from 2020 to the mid-century are discussed in terms of the anticipated external and internal drivers. Problems such as social acceptance, environmental concern and grade decline will be discussed, and I will show how digitalization and especially modelling and simulation can respond to these new challenges.

1.1 Current status of mining and mineral processing

Mineral and metal resources are a pillar of our modern economy: building, transport, chemistry, ceramic and many other technologies are all dependent on the availability of various mineral resources. Indeed, the United States Geological Survey (USGS) estimated in 2019 that a US citizen consumed about 5kg of both copper and lead per year, in addition to 124 kg of iron ore (USGS, 2020). Among the commodities needed for societal development, most of the current reserves are commensurate with our current consumption rate. This is true for coal, bauxite, vanadium, platinum-group elements (PGE) or rare earth elements (REE). Other resources, such as zinc, lead, copper or nickel are more problematic, with current reserves estimated to last for from 10 to 50 years (S E Kesler & Simon, 2015). Information on reserves alone is not sufficient to suggest the risk of shortage by itself. Such a risk also depends on the capacity and the time needed to find new reserves and bring them into production. If new reserves are easily found, minable and processable, then the supply will remain safe. However, these international measures do not address national interest concerns, which are subject to geopolitical events.

1.1.1 Resources and mining projects

By definition, a mineral deposit is a natural accumulation of a valuable mineral commodity. It results from geological or other natural phenomena and consists of a localized concentration of a specific mineral or element, above its relative abundance in the Earth's crust, also known as the Clarke. For instance, gold's Clarke is 0.3ppb. In the case of this element, an enrichment factor of 3,000 to 30,000 is necessary to obtain a gold deposit of 1 to 10 g/t.

The combination of geological phenomena resulting in the birth of a specific deposit may help to classify it as belonging to a group: a genetic type or metallogenic group. For instance, deposits issued from volcanic events may be classified as epithermal, volcanic massive sulphides (VMS), sedimentary exhalative (SEDEX) etc., depending on the volcanic setup. Metallogenic provinces are geographical areas where a distinctive style of deposits of a similar geological context are found. These provinces may result in production clusters of specific commodities, such as the great belt of porphyry copper deposits in Chile and Peru, where about 40% of the global copper

production was concentrated in 2018 (Reichl & Schatz, 2020). Classification by genetic type gives a preliminary idea of the deposit's characteristics. However, even when the general process is the same, the intensity of the mineralisation and the pre-existing rock conditions might differ. This results in different sizes and grades of deposit and influences the mineral paragenesis, rock textures and deposit morphologies. Deposits belonging to the same metallogenic group will exhibit variable tonnage and grades. Moreover, geological phenomena are sometimes coupled to surface and climatic processes, such as weathering, which further modify the characteristics of the deposit in a unique way. In addition, a deposit is a complex and heterogeneous object. The mineralogy and texture of the rock can change drastically from one place to another, making its exploitation a complex exercise (Figure 1).

A deposit is usually composed of ore and waste rock and this distinction is made using the cut-off grade. The cut-off grade is the grade above which it is economically viable to extract the commodity from the rock and it has a great influence upon the life of a mine. It depends on the deposit geology, mining method, processing technology and the price of the commodity. Thus, it is subject to change. The implications of the cut-off grade upon the mine's life are crucial and some studies focus on this topic (Asad & Dimitrakopoulos, 2013; Cairns & Shinkuma, 2004). Metals or mineral of interest are extracted from the ore with mineral processing methods as a concentrate, while the tails are stored away. Penalty elements, such as As or Hg, can be found in the concentrate and reduce its economic value. On the contrary, other elements known as by-products, for instance Ag or Ge in zinc deposits, may increase the selling price of the concentrate. Due to the high diversity of deposit types and internal heterogeneities in the deposits, mineral processing technologies must be specific and adjustable, as illustrated in Figure 1. These methods will be presented in section 1.1.2.

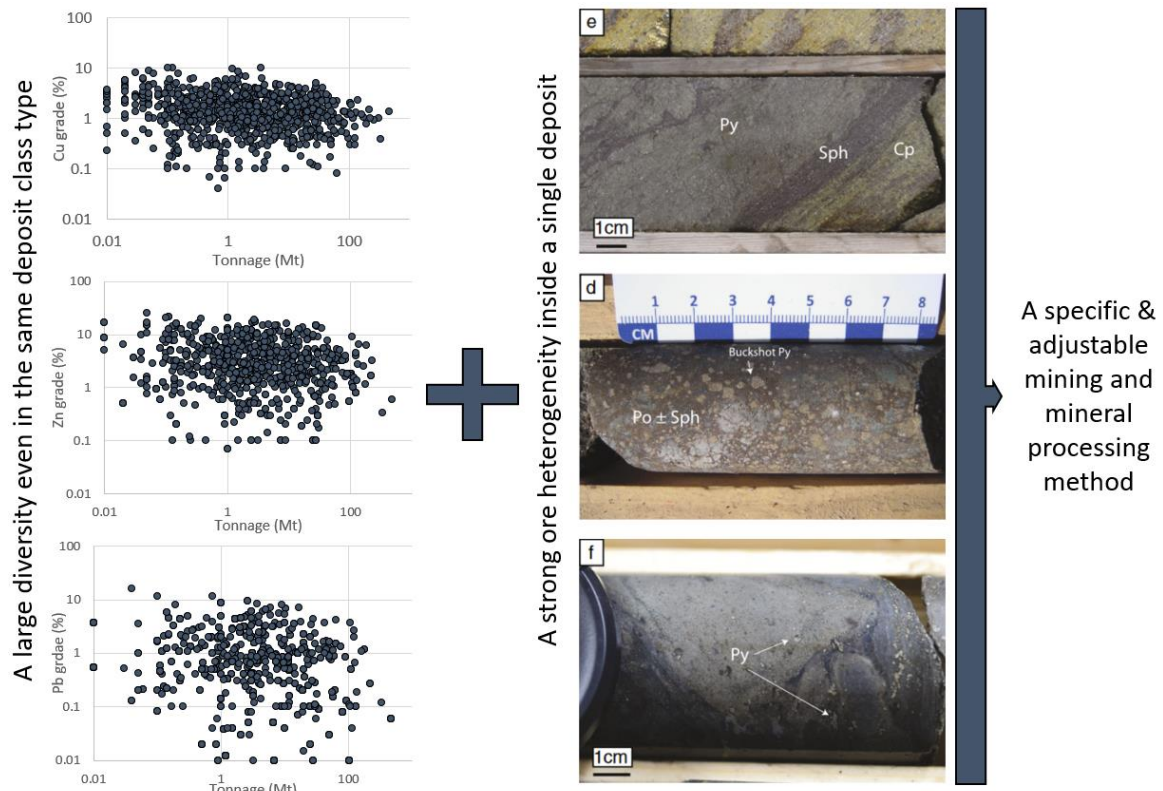


Figure 1: Diversity and variability in a deposit type class and strong heterogeneities in a deposit intrinsic characteristic raise a need for specific and adjustable mineral treatment methods. Left, tonnage / grade of the major VMS type deposits (Mosier et al., 2009). Right, three pictures from the same VMS deposit in different ore zones – Hood deposit, Nunavut, Canada (from Mills, Piercey and Toole, 2016).

A new – or “greenfield” – project usually starts with the exploration phase, when the deposit is found. Following that discovery, the amount of resources is estimated, usually via drilling. When confidence in the estimations is sufficiently high, a pre-economic assessment (PEA) can be made. In this step, the definition of the resource is still quite vague and the cut-off grade, which permits definition of the amount of ore resources, is assumed from comparison with similar known projects. The PEA enables the project to attract investors and funds more drilling to enhance the resource estimation, as well as carrying out processing test work. This information leads to a pre-feasibility study (PFS), a document in which a more accurate estimation of resources and reserves is given, as well as the initial proposals and plans on how the ore could be extracted and processed. The amount of reserves describes the quantity of ore which can be recovered economically. The definitive feasibility study (DFS) contains an exhaustive resource and reserve evaluation, usually accompanied by a

block model, a description of the land usage and a final plan on how the ore will be extracted and processed based on pilot tests in conditions as close as possible to the final plant operating specifications.

All these steps progress synchronously with several permit phases. The permit process is more or less complex and time-consuming depending on the relevant jurisdiction. The applicant must inform the community/state/regional organizations of its project type, method of extraction, number of tons to be extracted per year, generated waste and emissions as well as the construction plan and land usage. Depending on the complexity, maturity and size of the project and location, the permit time varies. For instance, Pettersson *et al.* (2015) compare the regulatory framework in various Northern European countries and state that (p. 243) “...the most important issue regarding the time frame for granting of applications is therefore probably the issue of predictability in terms of what should be considered to be part of the activity and thus what shall be included in the assessment”.

Once the permit and feasibility steps have been completed, the construction of the mine can begin. If no suitable existing mineral processing plant capacity (commonly referred to as “mill”) is available in the mine’s vicinity, then a new installation is built as part of the project.

1.1.2 Mining and mineral processing

1.1.2.1 Extraction and mine planning

Depending on the deposit geometry, accessibility and grade, mining takes place either in an open pit or underground. It is quite common for a mine to start as an open-pit operation and then evolve into an underground operation when surface exploitation diminishes. Several different underground operation strategies exist, and they are usually more costly than open-pit mining, requiring a higher cut-off grade. The details of the various exploitation methodologies are beyond the scope of this study and will instead be summarized.

The mining method employed has an impact on what is known as the mining plan. This plan details the order of exploitation for each ore block, the exploitation design (pit, decline etc.) and its preparation for processing (Figure 2). Once the ore is

extracted – then called “run-of-mine” – it may be crushed directly in the exploitation area before being transported to the mineral processing plant, via shafts, conveyors or hauling trucks. It is common practice, when a deposit is heterogeneous or when several ore bodies are being processed in the same plant, to blend the ores, so that the feed characteristics stay as constant as possible.

In this work, the focus will be on the beneficiation methods used for metallic ores such as base and precious metals (Cu, Zn, Pb & Ag, Au and PGE), alloying metals (Ni, Cr, Mo, W and Nb), iron ores and technology metals (Li, Co and Ta). However, some of the tools developed in this thesis may also be employed for mineral processing of other deposit types, such as industrial minerals (kaolinite, talc etc.), aggregate production or mineral fuels like coal.

During exploitation, the object of study for the miner or geologist is a block, commonly integrated in a block model of the deposit (Figure 2 b). The dimension of the block differs widely, from tens to several hundreds of cubic meters, depending on the exploitation type and geometrical constraints, and more importantly, on the support effect. This last notion relates the size of a block bearing grade information to the actual amount of assayed material (drill hole or grab samples from the front when accessible). The information associated with each block is based on the estimated grade value of the elements of interest, not on the real block grade, which is unknown. The defined size of a block has a large influence on mine planning and consequently on processing (Jara et al., 2006).

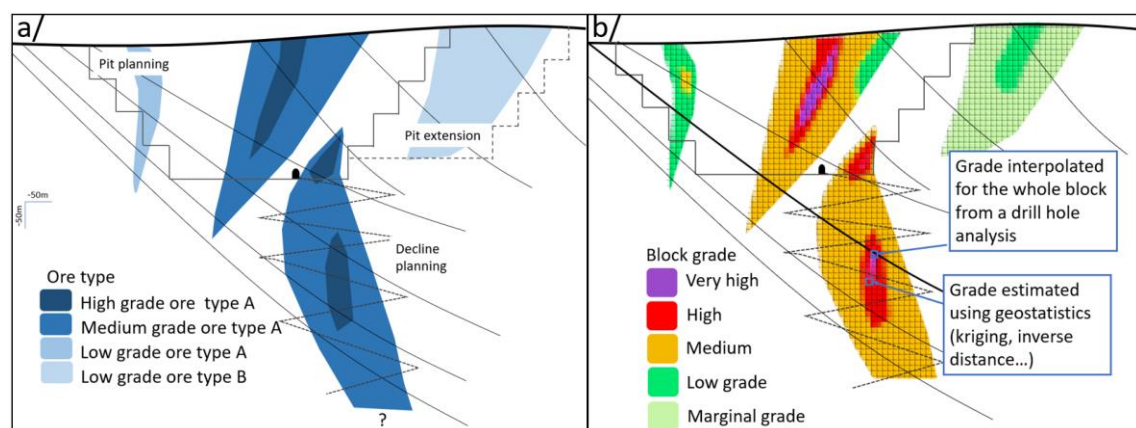


Figure 2: a/ Cross section of a geological model, constructed from information from several drill holes, coupled to surface geochemistry of geophysical information - used to prepare the mine planning b/ block model of a deposit – each block has an associated

grade information, interpolated from data points (assays from drill holes, grab samples). For the sake of simplicity, the size of the blocks is constant in this representation, which is not always true.

1.1.2.2 Liberation

Beneficiation, or ore processing, aims at separating the mineral(s) carrying metal(s) of interest from the gangue. In order to achieve this, the valuable mineral(s) have to initially be separated from the gangue.

Liberation is accomplished by comminution, which involves processes such as crushing, grinding and the separation of particles by size. The main mechanisms used to reduce the size of a material are attrition, impact, compression and shearing (Figure 3). These processes may happen in a dry environment, thus creating dust emissions, or a wet one, thus increasing the weight of the processed material, also known as pulp (solid + liquid).

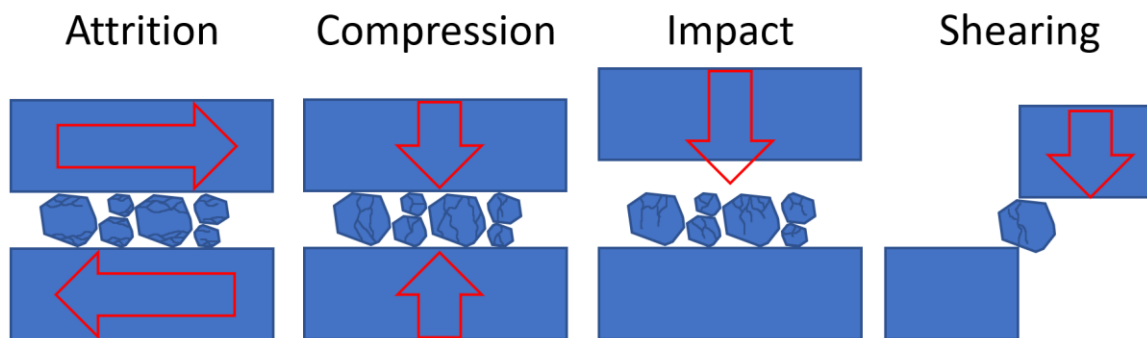


Figure 3: Classical stress forces of rock mechanics used in comminution.

Crushing is the first process to occur after extraction to bring the feed material from a size of up to a meter to one of a few millimetres. The most common crushing units are jaw and gyratory crushers, which are used first with larger rock particles – or boulders – and then followed by cone crushers for further grinding. A pre-crushing phase may occur directly on the mine site. Crushers can be combined with screens (referred to as “closed-circuit” crushing because the oversized particles produced by crushing are recirculated in the same crushing unit until they are fine enough to pass through the screen).

Crushing is usually followed by grinding, which is generally the step when the liberation of the particles occurs. Tumbling mills have several forms, depending on their usage (Napier-Munn et al., 1999; Wills & Napier-Munn, 2005):

- AG/SAG mills are mills used for coarse grinding, at a feed size of up to 400mm and a product as fine as 70 μ m. In so-called autogenous mills, the tumbling effect permits the efficient breakage of the rock by itself. Large rocks – usually referred to as “pebbles” – are sorted out during crushing and fed to the mill at the same time as the crushed ore and are thus used as grinding media. In semi-autogenous mills, these pebbles are complemented by steel ball media. Not using media in a mill can be a great advantage in terms of operational expenditure (OPEX), as steel media need to be replaced due to wear.
- Ball mills are generally smaller than SAG/AG mills and are used to reduce material of up to 15mm to sizes as fine as 20 μ m. In a ball mill, a media charge, up to 35% of the mill volume composed of steel balls of various sizes, is used to effectively grind the feed material.
- Rod mills are less common than SAG/AG mills or ball mill and can be used with feed sizes of up to 90mm and product sizes of up to 600 μ m. Like the ball mill, the rod mill is partially filled with steel media, but in the shape of rods. Using rods is preferable for material with a tendency to be over-ground or with a high hardness contrast between the particles. Indeed, rods have a protective effect towards smaller particles which are less susceptible to being broken down. Rod mills are used when the mineral of interest is brittle in a hard gangue, for example ferberite (FeWO_4) in quartz gangue.

Some other mill types, such as vertical mills, are different from tumbling mills and grind through a stirring action. They can be found in regrinding circuits to obtain very fine products, down to 2 μ m. Regrinding usually occurs between separation steps and is intended to liberate finer mineral(s) or to refresh the mineral surfaces for separation based on mineral surface properties. This step limits the grinding of gangue material and overgrinding of already liberated minerals and thus improves the energy efficiency of the comminution process (de Bakker, 2014).

For some ores, liberation may not require intensive comminution efforts. For instance, some lateritic nickel ores are simply separated using trommels (rotary screens); the valuable part of the ore being highly weathered and friable compared to the hard, low-grade material.

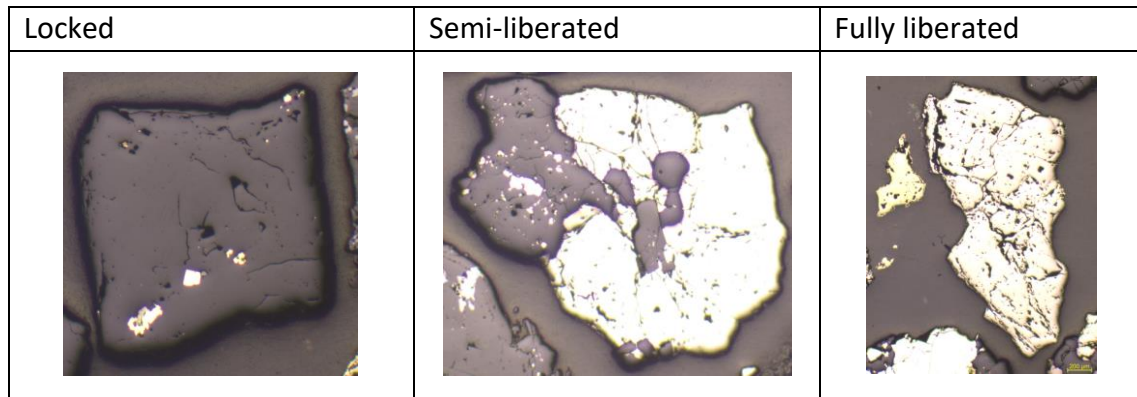
The material is frequently separated or classified by size during comminution, with instruments such as hydrocyclones, screens or screw classifiers, depending on the desired separation and on the solid percentage of the pulp.

The particle size distribution (PSD) describes the size repartition into several size classes of granular or particularly solid material. This distribution is widely used as the principal parameter to describe the comminution step and is often summarized by two parameters, the P80 and P50, which are the sieve sizes at which 80% and 50%, respectively, of the material mass can pass. Additionally, the proportion of fine particles, i.e. the amount of material passing the smallest sieve, can be used with P80 and P50 to characterize the size distribution. To obtain the PSD, the most common method is to sieve a sample of the material in the lab but nowadays, PSD parameters may be obtained directly in the plant circuit via automatic on-line laser measurement tools. It is worth noting that laser diffraction size measurements are best suited for homogeneously sized material, for instance in regrinding circuits (Kongas & Saloheimo, 2009).

Although PSD, P80 and P50 are the most widely used parameters to assess a comminution circuit, they do not fully represent the liberation degree of the mineral. A particle may be composed of several minerals, as shown by the locked and semi-liberated examples in Table 1. If a mineral is associated with other minerals in a particle then the separation process is less effective (Jameson, 2012; R. P. King, 1994; Miller et al., 2009). Different liberation degrees are shown in Table 1. Nowadays, automated mineralogy tools, such as the Quantitative Evaluation of Minerals by Scanning electron microscopy (QEMScan®) or Mineral Liberation Analysers (MLA), which use polished section and scanning electron microscopy, are used to describe the liberation degree of a material. However, these methods remain expensive and time-consuming. Thus, they are not widely used as a daily routine to assess a mineral processing plant's performance. When a mineralogical study of the material is available to give the average liberation size of the valuable mineral(s), then PSD helps to estimate the liberation degree of said mineral(s).

Table 1: Illustration of locked, semi-liberated and liberated sulphides. Particle sizes are around 1mm. Images taken with reflected light microscopy on a polished section from

Kylylahti grinding test samples. Sulphides are bright yellow grains and dark grey grain are gangue (mainly quartz).



It is important to appreciate that comminution may consume up to 50% of the total plant power consumption (Department of Environment, 2007). Crushing generally does not consume water, but some is usually added in the grinding circuits to avoid dust production and increase the milling efficiency. If energy is a key part of the cost of mills, the replacement of parts, grinding media and liners (elements covering the inside of the mill), can account for up to 40% of the mill OPEX, and up to 60% for ball mills (Massola et al., 2016).

To plan and assess liberation, the main information that metallurgists are interested in is the PSD, and, for the later grinding stages, the extent of mineral liberation. The size and denomination of the material varies considerably: at the beginning of crushing, the notion of “boulder” (up to a meter diameter) can be used, in comparison to particles (50 – 1mm) later on, ending up with individual mineral fragments at the end of the process. Figure 4 summarizes the main information on the studied material that is gathered through the comminution process.

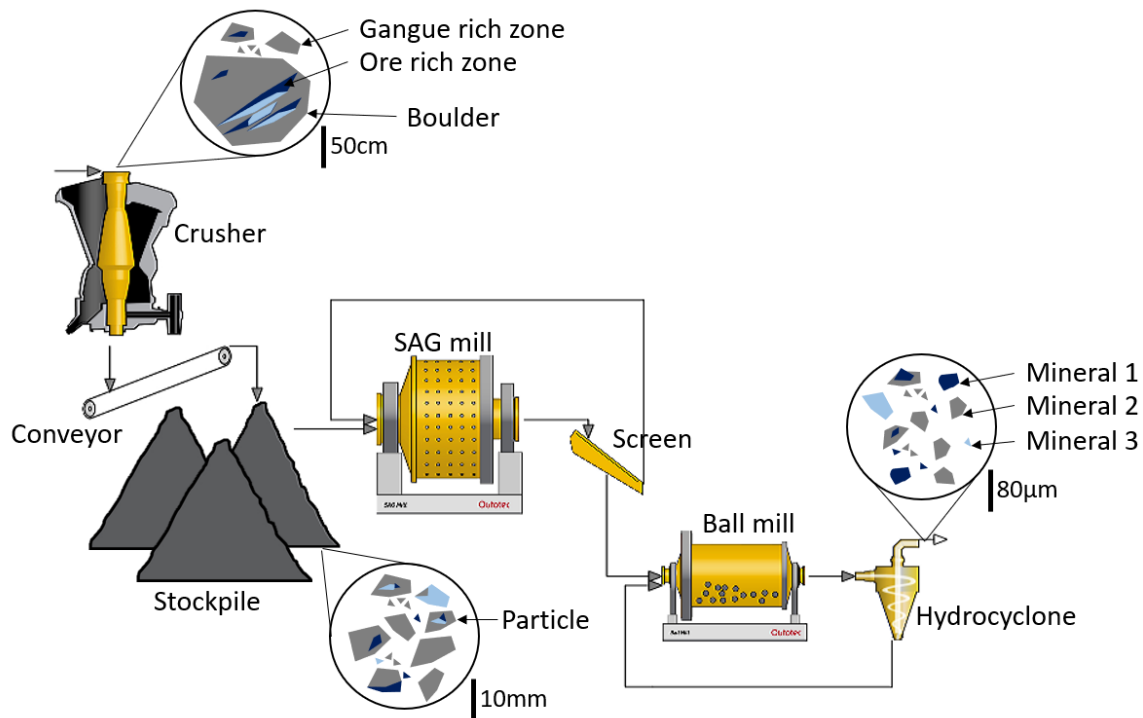


Figure 4: Evolution of the studied material along the comminution circuit, from large, heterogeneous rock boulders in the crusher feed, to particles (composed of several minerals) to mineral before the separation. PSD and initial grade control are the main monitored variables.

1.1.2.3 Separation

In this section, the focus is on the separation methods used for metallic ores. The efficiency of every separation process is largely a function of the liberation of valuable mineral(s).

The oldest separation method is probably manual sorting based on optical properties of the ore, such as mineral colour or reflectivity. Nowadays, the availability of new and more sophisticated sensors allows the automatic replication of this procedure, based on various properties of the ore: X-ray transmission, X-ray luminescence, near infrared radiation reflection, colour, and many more (Robben & Wotruba, 2019).

Separation by density is another well-known separation method using jigs, spirals and shaking tables. These rely on the differential movement of the particle in water according to form factor and density. Separation via dense media lets particles sink or float depending on their density and is commonly employed in coal processing.

The most frequent separation method, flotation, is based on the surface properties of minerals. In this case, the liberation factor is extremely important, as the mineral surface needs to be exposed. Depending on the mineral, its surface can be naturally hydrophobic or hydrophilic. In other cases, these properties are acquired synthetically using reagents. The main reagents used for flotation are collectors, which are adsorbed on the mineral's surface rendering them hydrophobic or hydrophilic; regulators, which either inhibit or activate the reactivity of some minerals with the collectors via pH modification for instance; and frothers, which maintain bubble stability in the froth area. Flotation can be used to float valuable minerals (direct flotation) or gangue material (inverse flotation).

Finally, magnetic separation is used to concentrate ferro-magnetic minerals such as magnetite (Fe_3O_4) when used at low intensity, or paramagnetic minerals such as hematite (Fe_2O_3) when a high intensity separation is used. A summary of these methods is given in Table 2.

During separation, the most important information to be gathered is the chemical composition of the streams, concentrates and tails. For processes like flotation, it is also crucial to monitor the chemistry of the slurry liquid phase, the pH, dissolved species and reagent concentration. Samples are gathered daily to monitor recovery and grade and to assess plant efficiency. On-line elemental analysers, commonly using XRF and more recently Laser Induced Breakdown Spectroscopy (LIBS) (Khajehzadeh et al., 2017), are implemented to monitor slurries in the plant. Figure 5 shows the evolution of the studied material, which becomes more homogeneous through the separation process.

Table 2: Most common mineral separation methods for ores. Suitability depends on the specificity of the ore being processed. This list is not exhaustive and does not mention all separation methods and subprocesses, it rather aims to give an overview of the most commonly found processes in mineral processing plants. Information and characteristics are extracted from SME Mineral Processing and Extractive Metallurgy Handbook, ed. 2019 (Young, 2019).

	Description	Characteristics, comparative advantages and disadvantages
Ore sorting	Sensor-based method which separates particles (particle sorting) or batches of material (on a conveyor or trucks) based on their properties assessed by sensors. Most common sensors are optical (e.g. using visible light), based on conductivity (to separate massive base metal sulphides from non-sulphidic gangue for instance), or using medium wave IR, X-rays, or gamma-rays.	<ul style="list-style-type: none"> -Water and reagent-free -Applied in pre-concentration stages -Require strong heterogeneities between particles and/or on block level -Generally low tonnage for particle-sorting
Magnetic Separation	Separate particles based on their magnetic susceptibility. Depending on the susceptibility contrast between particles, which can be ferromagnetic, paramagnetic or diamagnetic, the separator can be high intensity or low intensity.	<ul style="list-style-type: none"> -Can be operated in dry or wet conditions -Reagent free -Can be applied for tramp metal removal before crushing/grinding
Gravity Separation	Separate particles based on their specific gravity. Different methods can be used, depending on the material PSD. Jigs, shaking tables, spiral, sluices and enhanced gravity concentrators such as Knelson and Falcons are example of gravity separation machines. Dense medium separation is also considered as a gravity separation method, the dense media being usually created using magnetite suspension in water.	<ul style="list-style-type: none"> -Usually low-CAPEX -Reagent-free
Flotation	Group of processes and setups with a variety of configuration, which separates minerals based on their surface properties. Flotation may be pneumatic, as in column flotation, or mechanical, as in cell flotation. Surface properties can be modified by the application of reagents such as pH modifiers, collectors, depressants.	<ul style="list-style-type: none"> -Require large amounts of water -Versatility: it can be applied to various types of ores using different configurations
Electrostatic separation	Separates particles based on their conductivity and chargeability. This method mostly applies on sand ores, to produce concentrates of zircon, rutile or monazite for instance.	<ul style="list-style-type: none"> -Separation efficiency affected by moisture and surface contamination

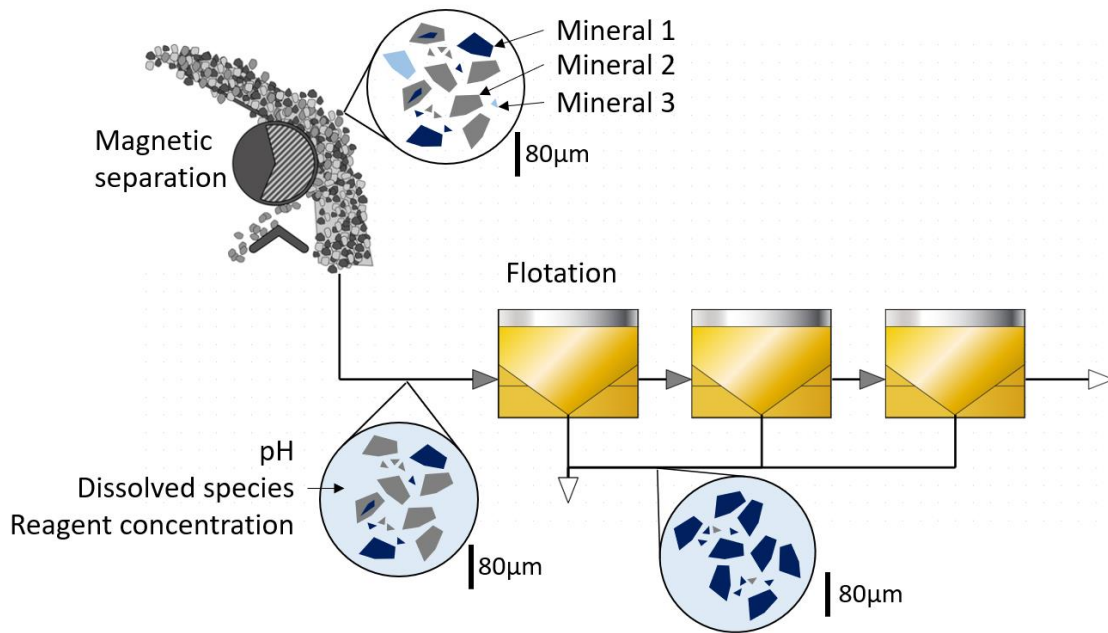


Figure 5: Evolution of the studied material slurry along the separation circuit, with a magnetic separation and a flotation. For the flotation process, the aqueous phase characteristics become an important variable to monitor.

1.1.2.4 Pyro and Hydro treatments of the ore

Pyrometallurgy is a common process to produce metal from concentrate using reduction, via smelting or blast furnaces. Pyro treatment is a low-cost way to produce metals suitable for large scale production. Pyro processes are also applied for the pre-treatment of ore, such as roasting or calcination (Ray & Ghosh, 1991). For instance, roasting is used to treat refractory ores, when a valuable element, often gold, is disseminated in another mineral lattice, often sulphides. In such a case, roasting oxidizes the sulphides to become oxides, sulphates and sulphur dioxide, thereby freeing the gold for further hydro-processing. However, harmful elements such as As, SO₂, Sb and Hg may be extracted in the gas phase and need to be recovered to prevent enduring changes to the ecosystem of the area (Van Den Berghe et al., 2018). As another pre-treatment example, the pyro process is also used for the treatment of spodumene (LiAl(SiO₃)₂). High temperature conditions change the spodumene phase, which renders it reactive for later leaching (Gasafi & Pardemann, 2020). A summary of pyro, hydro and combined treatment methods is presented in Table 3.

For refractory gold ores, carbon-in-leach (CIL) technology (Figure 6) is commonly used in association with high pressure oxidation (POX) of the sulphides.

Table 3: Description summary of hydro, pyro and hybrid methods for primary ore treatments. Recycling is not taken into account. Information and characteristics are extracted from SME Mineral Processing and Extractive Metallurgy Handbook, ed. 2019 (Young, 2019), unless stated otherwise.

	Description	Comparative advantages	Comparative limits	Examples
Hydrometallurgy	Branch of metallurgy containing processes aiming at: -dissolving metallic elements from an ore or a concentrate, in an aqueous solution by chemical reagents and/or bacterial agents, -removing impurities and recover metal by precipitation, solvent, extraction, electro-winning	(*compared to pyrometallurgy) -Produces few gaseous emissions, -Generates limited dust amounts, -Consumes less energy to process low-grade materials	-May cause secondary pollution (Xiang et al., 2019) -Many parameters to survey and disturbances requiring very robust control systems (Xie et al., 2018; Zhang et al., 2018)	Vat-leaching, tanks leaching, pressure leaching & oxidation, heap leaching, in-situ leaching, bio-leaching, CIL/CIP Redox precipitation, gaseous reduction, solvent extraction, electrowinning and electrorefining, ion exchange
Pyrometallurgy	Branch of metallurgy containing processes using high-temperature and pressure conditions to modify or decompose concentrate minerals.	-Wide application range & products	-High energy consumption -Safety risks (thermal exposures, gases production)	Drying, roasting, calcination, smelting, conversion & refining
Hybrid pyro/hydrometallurgy	-Combine one or several processes from hydro and pyrometallurgy (Yun et al., 2020)	-Enable the processing of specific types of ores, which could not be treated with only one option -Combined advantages of pyro and hydro processes	-Applies to specific application cases -Combined limits of pyro and hydro processes	-Laterite treatment (Oxley & Barcza, 2013) -Rare-earth phosphate minerals treatment with roasting and leaching (Abhilash et al., 2016)

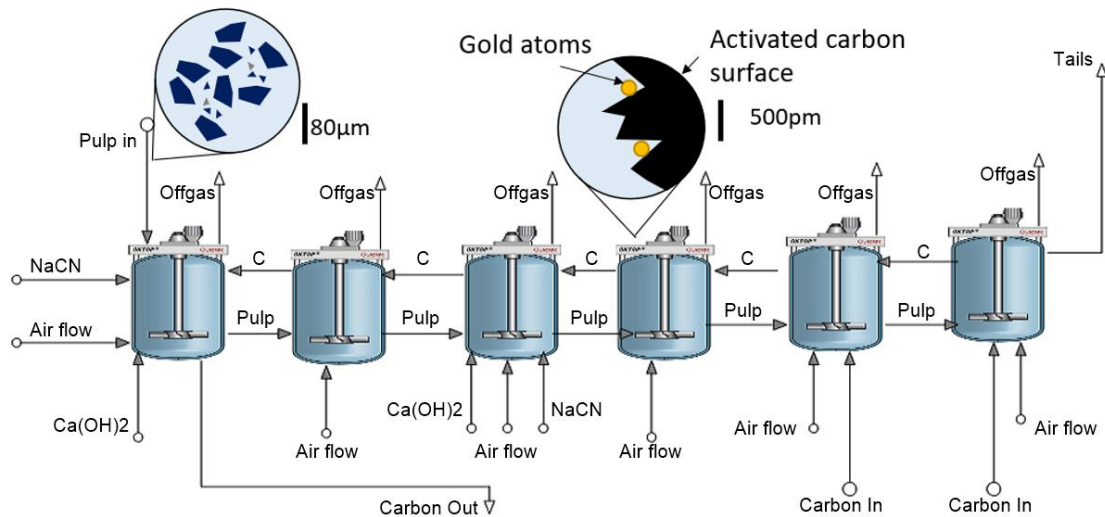


Figure 6: Evolution of the studied material (gold ore concentrate pulp) along a carbon in leach process, wherein activated carbon particles (C) and cyanide (NaCN) are added to the pulp. The cyanide leaching and precious metals adsorption onto the activated carbon occur simultaneously in the tanks. Gold is then stripped from loaded carbon and is finally isolated in electrowinning cells.

1.1.3 The integration issue of mining and mineral processing operations

The previous sections have explained the complexity of mineral processing operations, which needs to be considered together with mining and metallurgical processes to understand the big picture of the full operational chain.

The issue related to the integration of these different processes is mainly related to the variability of the material being processed, as well as the main characteristics studied. During mine planning, the main variable examined is the grade, and interpolated and quite uncertain information that is derived from the chemical analysis of rocks. The comminution stage mainly observes the particle size distribution, when the principal monitored variable of separation is the mineral/elemental grade. Finally, pyro and hydro processes convert the mineral particles to pure metals and chemicals using several processes, including metallurgical refining, oxidation and reduction steps.

The object studied varies in terms of scale, homogeneity, confidence level and in the sampling and analysis methods applicable to it, from the mine stope to the final product (Figure 7). The terminology used and knowledge/training requirements (geology, mineralogy, chemistry, geostatistics, geotechnics, etc.) used to operate a

mine are largely different from those used to operate a pyro/hydro process (chemistry, physics, etc.). These complexities drive the need for an integrated solution to communicate easily from one point to the other along this intricate production chain.

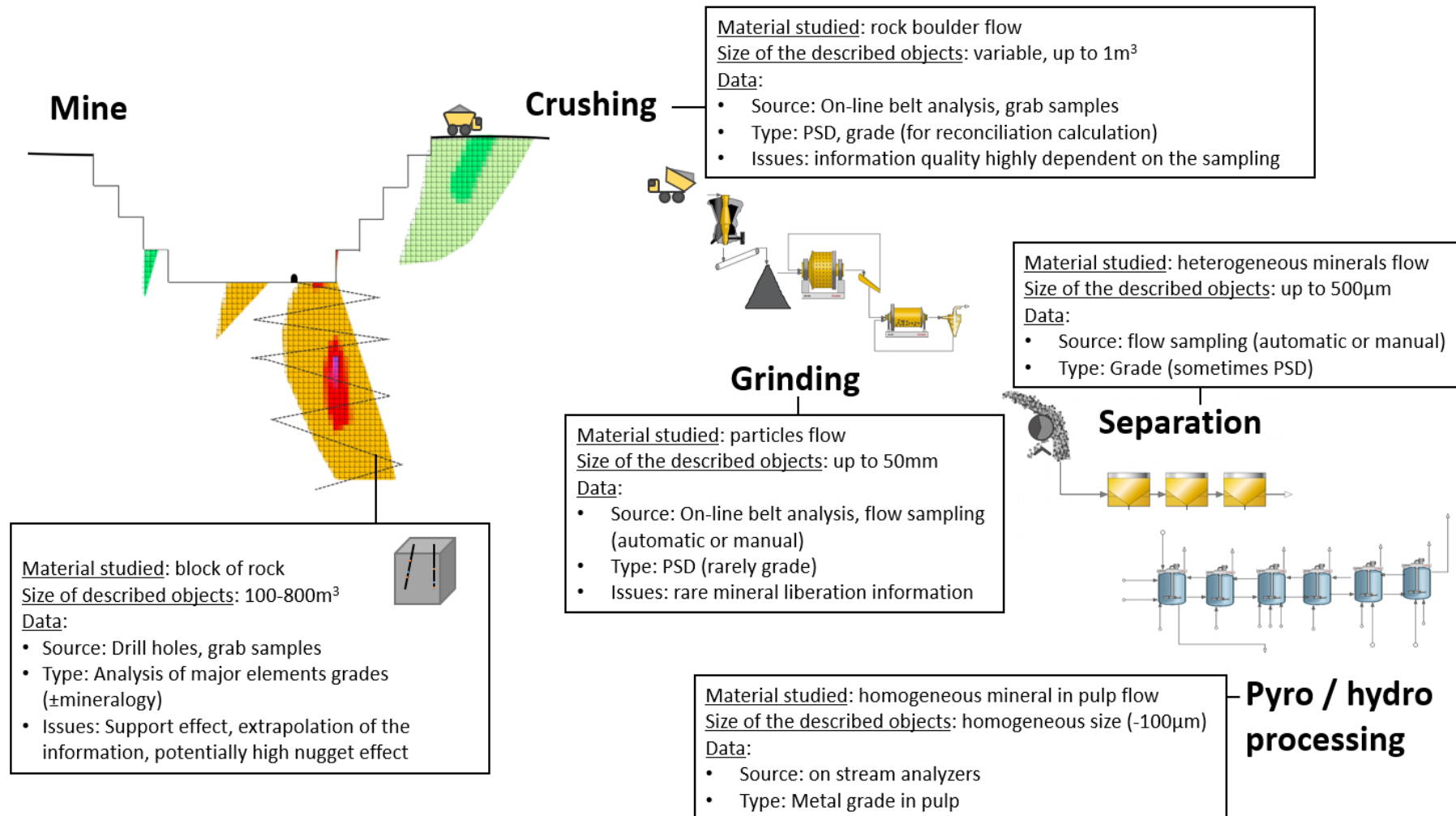


Figure 7: Schematic view of a mining operation, with the evolution of the available routine information data, its quality and focus. This view also shows the transformation of the studied material scale from a geological to an elemental/atomic object.

1.2 Future trends

1.2.1 Evolution of the mineral and metal demand

Minerals and metals are required by society for uses such as transportation, housing and communication, and for an almost infinite array of products and services. Demographic growth will lead to increased use for major metals in the coming years when recycling is predicted to remain a modest fraction of the future supply (Elshkaki *et al.*, 2016; Elshkaki, T. E. Graedel *et al.*, 2018). In some scenarios, the demand for copper is projected to increase by 300% above current levels by 2050 (Elshkaki, T E Graedel *et al.*, 2018) (Figure 8) and some forecasts already predict a market deficit of 600 metric kilotons of copper metal by 2021 (Valenta *et al.*, 2019).

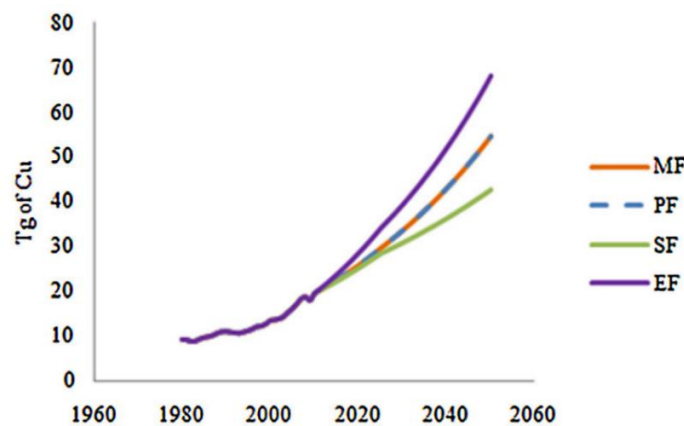


Figure 8: Historical and predicted copper demand (in Tg) from 1980 to 2050, displaying the four scenarios defined by the United Nation Environment Program (UNEP) (MF – Market first ; PF – Policy first ; SF – Security first ; EF – Equitability first) (from Elshkaki *et al.*, 2016)

Some minerals and metals are urgently needed in order to achieve a low carbon emission future. They include lithium, cobalt, graphite, indium or vanadium to cite just a few. They are nowadays considered as “critical raw materials” or “technologically critical elements” (Sovacool *et al.*, 2020). These commodities are necessary for batteries, solar cells, wind turbine or electric vehicle motors, and are at a higher risk of price volatility (Innovation Union, 2010).

1.2.2 Future trends in mineral processing

Mining companies and process solution providers must consider the current issues related to mining and future consumption trends. Techniques in mineral processing

have evolved and are more and more efficient, turning impossible-to-mine deposits into economically viable projects. Improvements are still possible and forthcoming and allow the treatment of ores in a more sustainable way, especially in terms of the following points:

- *Reduced energy consumption and CO₂ emissions.* As mentioned previously, mineral processing is an energy-intensive process. Benchmarking initiatives have been commissioned by different governments in order to assess mine energy consumption standards and estimate potential savings (Ballantyne & Powell, 2014; Mining Association of Canada, 2005). In the 2007 benchmark, the US Department of Energy estimated that metallic ore mining industries could save up to 37% of their energy consumption – with proportional repercussions on their CO₂ emissions – by implementing best practices in comminution and ore handling (Department of Environment, 2007). To help with these initiatives, indicators have to be developed to assess the efficiency of mines (Pitis, 2016).
- *Sustainable water use.* In some regions where water is a scarce resource, frictions between social and private sectorial users exist (Adler et al., 2007; Bauer, 2004). The legal framework is diverse, complex and not fully comprehensive, depending on the region (López Steinmetz & Fong, 2019; Schoderer et al., 2020; Thomashausen et al., 2018). Benchmarking water consumption is a complex task, as water withdrawal, uses and discharges vary a lot between mining operations and over time (Gilsbach et al., 2019; S. A. Northey et al., 2018, 2019). Moreover, it has been reported that the impacts of future climate change and regional climate evolution may be adverse for mines in some regions, with increased evaporation and less available water or more erratic precipitation patterns (S. A. Northey et al., 2017).
- *Improved waste management.* Many issues have arisen from poor mineral processing waste management in the past (Leblanc et al., 2000; Rico et al., 2008; Soldán et al., 2001). New technologies and innovations, such as thickened tailings, dry stacking or paste backfilling are now available for future, safer mine waste management planning (Fourie, 2009; Franks et al., 2011). The reuse of inert waste material in a circular economy is another

possible way, already implemented by some mining companies (Kinnunen & Kaksonen, 2019; van Beers et al., 2007).

- *More complex and low-grade deposits.* For some time, the grade of exploited ore deposits has been falling, due to several factors. A predictive model of the evolution of copper grade in the 21st century is presented Figure 9. Mined ores are also generally becoming finer-grained (Mudd, 2007; Norgate & Jahanshahi, 2006). As treatments become more efficient, parts of existing mines which would have not been exploited in the past, due to low grade or fine-grained ore, become economically viable (Calvo et al., 2016; West, 2011). This enables a mine to continue production in the same site, while opening a new exploitation would demand new investments in feasibility studies, permit applications and would be economically riskier. Some studies also show that the advances in mineral processing technologies could be implemented to reprocess historic mine tailings (Lutandula & Maloba, 2013), which are by nature relatively low-grade material compared to the primary resource.

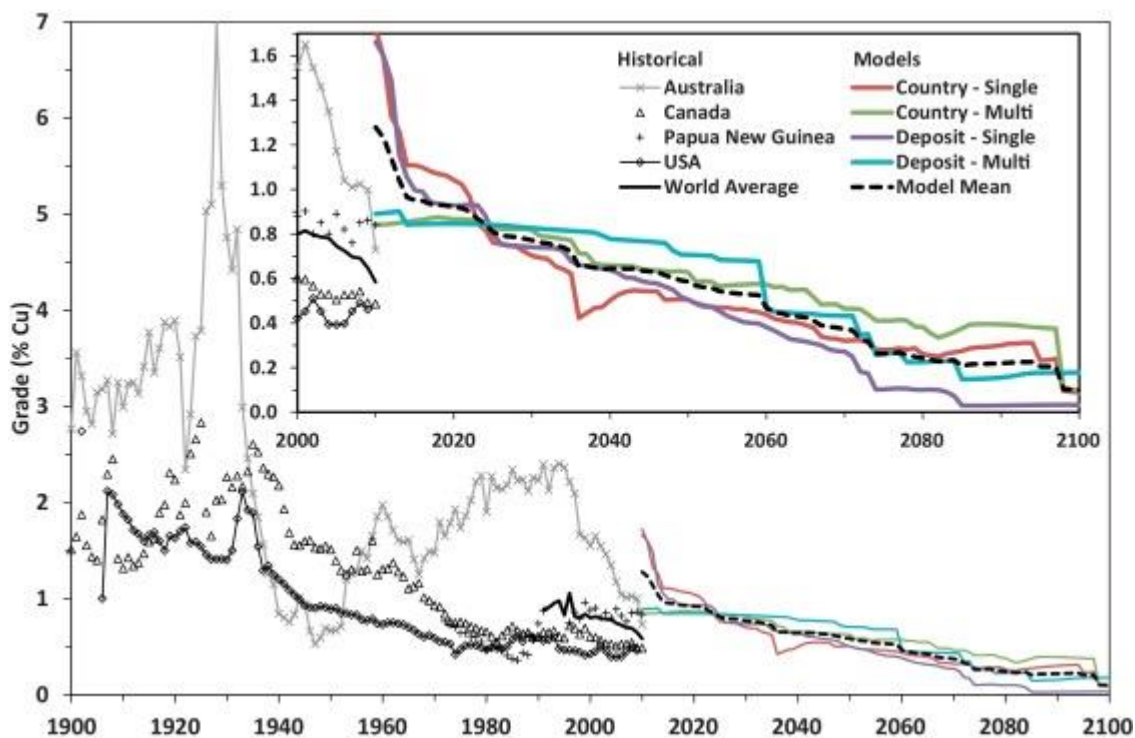


Figure 9: Historical Cu ore grades for selected countries and projected global ore grades 2010 onwards. Figure from Northey et al. (2014).

- *Higher sustainability and social requirements standard.* The social license to operate (SLO) is a growing factor to be considered before opening a mine (Prno, 2013). Local resistance impacts a company's reputation and affects its profitability (Prno & Scott Slocombe, 2012). For better social sustainability in a region, mine sites must hire and train personnel adequately, safely and responsibly. Another global trend is the increasing willingness and ability for consumers and producers to trace and label metal and mineral provenance. When buying a manufactured product, good traceability would give details of the supply chain, such as the legality of the working conditions or environmental impact of the product. Internally, better transparency and communication tools can reduce individual spreadsheet use which lead to inconsistent decisions and management, and thus a less sustainable process, such as with a metallurgical and metal accounting information management system (Ghorbani et al., 2020).

1.2.3 Implication for modelling and simulation

These future trends require an evolution in the organization and integration of mining and mineral processes:

- Benchmarking, monitoring and optimizing energy and water consumption to build more sustainable processes for the environment and society, with reliable indicators, as well as proposing better traceability for the minerals and metals used in our daily lives.
- Knowledge of the chemistry of water used through the plant and as an output to mitigate aquifer pollution risks and achieve more sustainable consumption.
- Prediction not only of the concentrate tonnage and grade, but also the composition and size distribution of waste tails, in order to prepare their management, storage options or re-usability.
- Adapting the process through changing grades and mineralogy, as a mine continues to expand to handle more complex and low-grade ore zones.
- Proposing mineral processing courses and training for operators adapted to the specific issues of a site, to prevent accidents and move towards safer operations.

1.3 Research questions, aim and scope of this study

The aim of this study was to explore to what extent the completion of the requirements described in previous section can be facilitated through the implementation of modelling and simulation techniques. Several research questions, and their limitations, can be formulated related to this work:

- 1/ How modelling and simulation applied to mining and mineral processing can improve the processes in theory, based on comparable industries and customer case-studies?

This research question is addressed by the literature review presented in Chapter 2, and additionally, by the direct study of two customers' requests for mineral processing plant simulation.

- 2/ What are the requirements in terms of modelling, in order to answer to the industry needs?

This research question is addressed by the literature review, where the modelling detail depth and functionalities (e.g. static, dynamic, geometallurgical approach) of mineral processing models is examined and put into perspective.

- 3/ How well dynamic and static geometallurgical mill models can reproduce the performance of a circuit simulation?

This research question will be answered by the presentation of two model validation cases, one for the dynamic mill model and the second for the geometallurgical (multi-component) mill model and in the final chapter. This concerns the ability of the simulation, once fitted to the process, to predict important KPI such as power consumption and PSD in a reliable way.

- 4/ How virtual training can be a tool for the formation of operators mineral processing industry?

To answer this question, the implementation and result of a training course held for a customer case will be examined. Because of the required amount of time to assess the actual implications and improvements induced by such a training would be much longer than the time span of a PhD, and rather on a plant life scale,

i.e. decades, the actual comparison with current training method won't be analysed in this work scope. Assumptions and extrapolations based on other researcher's work will be presented.

- 5/ How modelling and simulation, aiming to be integrated into digital twin, may help with optimisation problem in a gold processing plant?

Finally, this question will be examined using another customer case which required the integration of a gold plant simulation model into a digital twin platform to improve the reliability of their process. To answer this question, the example of an optimisation case will be used. The digital twin integration, which embed the real-plant / simulation connection medium, via online sensors connectivity, is out of the research scope, which only focuses on the simulation perspective. As such, the real-plant response will be given through realist example-case, in order to respond to the research question. In the same way as for the examination of the virtual training, only assumptions and extrapolations based on other researcher's works will be presented for the general case. As a comparison with a similar plant, but without a simulation-based digital twin system, would be needed on the long term, i.e. decades, the measurement of actual improvements induced by the simulation system is out of this work's scope.

Chapter 2 Literature review

Process simulation is a common tool that has been used in the chemical industry since the 1970s (Motard et al., 1975) and is implemented as a predictive tool during project planning, pre-engineering and the design phase. Simulation reduces the time and expenses engaged in initial experimentation, which is supported by an increasing number of research publications related to the simulation of industrial processes (e.g. automotive, chemical, nuclear and electronics) (Jahangirian et al., 2010; Mourtzis et al., 2014). In various industries, the use of simulation has the potential to increase both the revenues and sustainability of the process, as presented by Kuntzsch (2014) or Widok *et al.* (2012).

Despite the increasing importance of simulation, integrated in the fourth industrial revolution (Gunal, 2019), there are few occurrences of detailed process simulators on plant scale in the mineral processing industry. Some of the first description of process models in the mineral processing industry mainly focused on flotation circuits (Dobby & Finch, 1986; R. King, 1978; Moys, 1984; D. N. Sutherland, 1977; Woodburn, 1970) and grinding circuits (Austin et al., 1984; Herbst & Fuerstenau, 1980; S. Morrell & Morrison, 1996; Napier-Munn & Lynch, 1992; Whiten, 1974).

The main challenge of modelling and simulation in the mineral processing industry has been the diversity and complexity of the processed material. Indeed, the ore input can be described as a sum of particles of different sizes, each particle being composed of different minerals in variable proportions. The processed material is thus best described by several distributions of various properties, rather than single values for elemental weight percentages and masses. Although mineral processing plant performance is mainly dependent on the composition, mineralogy, texture and grain size of its ore input, these parameters can vary a lot and are complicated to predict, due to technical and cost-efficiency limitations of deposit modelling and feed sampling (Dominy et al., 2002). However, current techniques, such as mineral liberation analysis methods, are reducing the uncertainty factors linked to ore

characterisation and are being used to adapt concentrator flowsheets during the design stage (Lotter et al., 2013; Talikka et al., 2018).

This chapter gives an overview of the past and present uses of simulators in industry, especially in the chemical industry where the technology has been used for several decades. The specificities relating to the simulation of mineral processing, such as the description of the processed material, are then explained. A review of existing simulators in the mineral processing industry highlights the areas where enhancements are still necessary.

2.1 Simulator Capabilities in Mineral Processing Plants

2.1.1 Terminology

Models are used in the scientific and engineering world, as well as in social sciences. One definition of a model is: *“a simplified representation of a system at some particular point in time and/or space intended to promote the understanding of the real system”* (Jana, 2018 p. 4). Here a “system” refers to one or a collection of various unit operations. In the engineering domain, a model usually describes a system with a set of equations linking variables. These variables are commonly known as input, output or state variables. Sometimes, constants appear in the equations, such as the gravity constant.

A simulation (or process simulation) consists of predicting the behaviour of a system by solving the model equations for a given state. The simulation environment feeds the models all the information needed to perform the calculations. To start a simulation, all of the input variables and constant parameters should be known. In this study, two simulation types are used:

- a “static” simulation, meaning that the predicted behaviour of the system is in a steady state – state variables do not change with time.
- a “dynamic” simulation, meaning that the behaviour of the system is predicted as a function of time.

2.1.2 Modelling process

The first step of the modelling process is to construct a conceptual model. This model, and therefore the algorithm, can be of various degrees of complexity and representation depth. This will depend on the accuracy of the result compared to the real-world problem that the modeller wants to implement. As such, a very simple model with fast calculation may, in some cases, be preferred to a complex, detailed model that is slow to compute. As shown in Figure 10, the modelling process starts with the observation of a real-world system and gathering of datasets. From these observations, a conceptual model is proposed and validated against this real-world system. The conceptual model can be one or several mathematical relationships between some inputs and outputs. Then, a computer model, which is an algorithmic

representation of the conceptual model, is implemented. Experimentation aims to evaluate whether the computer model can reproduce whole or parts of the real-world system behaviour. In addition, each step requires validation with the original observation of the system.

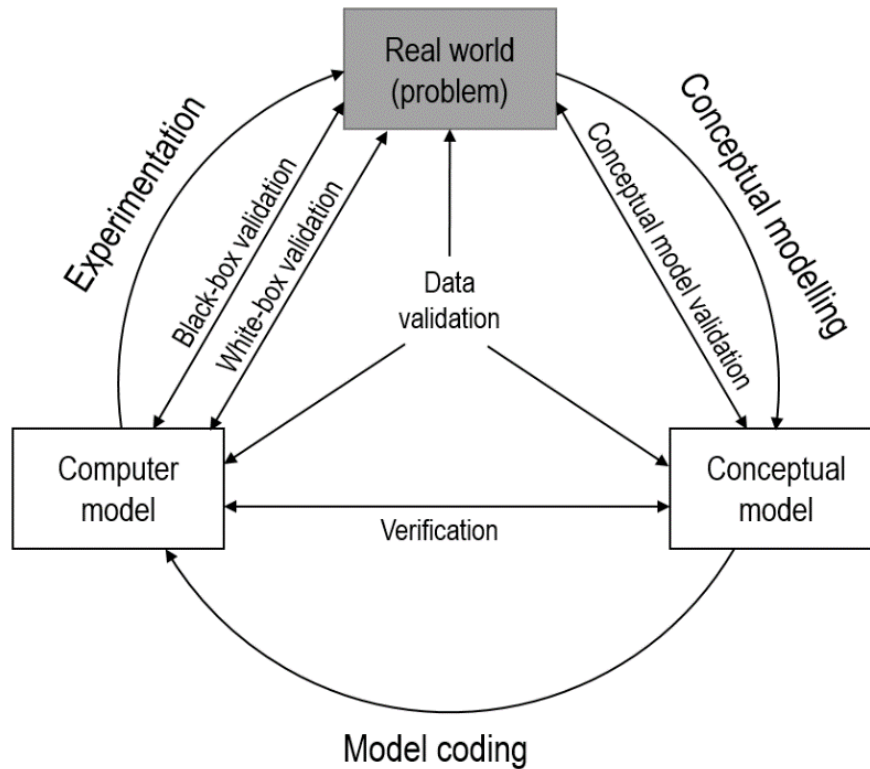


Figure 10: Conceptual modelling, model coding and experimentation, the three steps of the modelling process, adapted from Robinson, 1997.

2.1.2.1 Model classes

Three main categories of models exist:

- Theoretical or “white box” model: these models are based on the physical and chemical phenomena inherent to the process, predicted with thermodynamic laws and chemical equilibrium between phases. They are also called first principle models.
- Empirical models or “black box”: these models are entirely based on data collected from the system. A good example of an empirical model is a linear regression model between data points. They may also be known in some cases as surrogate models.

- Semi-empirical models or “grey box”: these are based on physical and chemical realities but do not yield a complete model. Some data are used to “fit” some parts of the equations in order to reproduce the system in an appropriate way.

Empirical and semi-empirical model accuracy and precision are predominantly a function of the quality of the data used. Semi-empirical models may be preferred in cases when the simulation is intended to explore operating contexts far from the experimental situation, where empirical models have no data to rely on. White and grey box models may be converted into surrogate, black box models, for example, by using artificial neural networks. An advantage of surrogate modelling is a higher calculation speed, which is a requirement of predictive process control and training simulators.

2.1.2.2 Validation process

Verification – testing whether the model is working correctly – and validation – testing whether the model is sufficiently accurate in other cases, are crucial parts of the modelling process. Validation proves whether the simulation and the underlying models are operable and predictive, i.e. whether the simulated process is close enough to reality. The American Nuclear Society established a standard ANSI/ANS-3.5-1998 for the sufficient degree of accuracy and completeness of a plant-referenced simulator. This standard takes different criteria into account, for instance the plant parameters in the stationary or quasi-stationary state should differ by less than 5 % (Miettinen, 2008).

There are several methods for validating a model against a real-world process. Black-box validation is a comparison of the overall output of the model to the real-world output. In white-box validation, parts of the computer model are verified separately. Real-world data used for validation comes with accuracy and precision issues related to sampling and measurement methods. Thus, modellers should keep in mind that absolute validity is unachievable, and rather than proving that the model is correct, validation should aim at showing where and to what extent the model is incorrect. Moreover, one can check validity only for existing systems, i.e. validity cannot be guaranteed if the simulation parameters differ from the real-world (Robinson, 1997).

2.1.3 Simulation building process

The first and most important question to ask before starting to build a simulator is “Why?”, i.e. what is its purpose? According to Kellner, Madachy and Raffo (1999), a hierarchy exists between the simulation purpose, the scope, the desired result variables, the process abstraction and the input parameters (Figure 11).

The purposes may be as diverse as process optimization, testing of an automation system, operator training or design of the plant’s safety procedures, to name just a few. The purpose is always closely related to the implementation timing of the simulation and the plant lifetime. The implementation of a simulator during the planning phase gives a faster plant start-up, when risks and uncertainties are usually at their highest (new personnel, new equipment). A study carried out by ARC Advisory Group for Honeywell in 2009, cited by Ahmad, Low and Shukor, (2010), showed how the incorporation of simulation technologies during a plant start-up lead to early operation readiness. Additionally, a study by Hosseinpour and Hajihosseini (2009) gives the example of an initial start-up time reduced by eight days thanks to the implementation of an operator training simulator (OTS) for an ethylene plant.

Evidently, it is a complex task to estimate the profit resulting from a simulator implementation, as it usually requires long-term studies. Nowadays, the objective of a simulator is also linked to project-specific needs along the plant lifecycle, from the planning to the site remediation (Molson et al., 2005; Shanmugasundaram et al., 2016). Degrees of simulator maturity and purpose differ based on the implementation stage. Due to the small amount of data and knowledge gathered, the sophistication of a simulation model in the start-up phase is much different from what is achievable during the production stage, where expertise and process data collection are more established, reliable and mature.

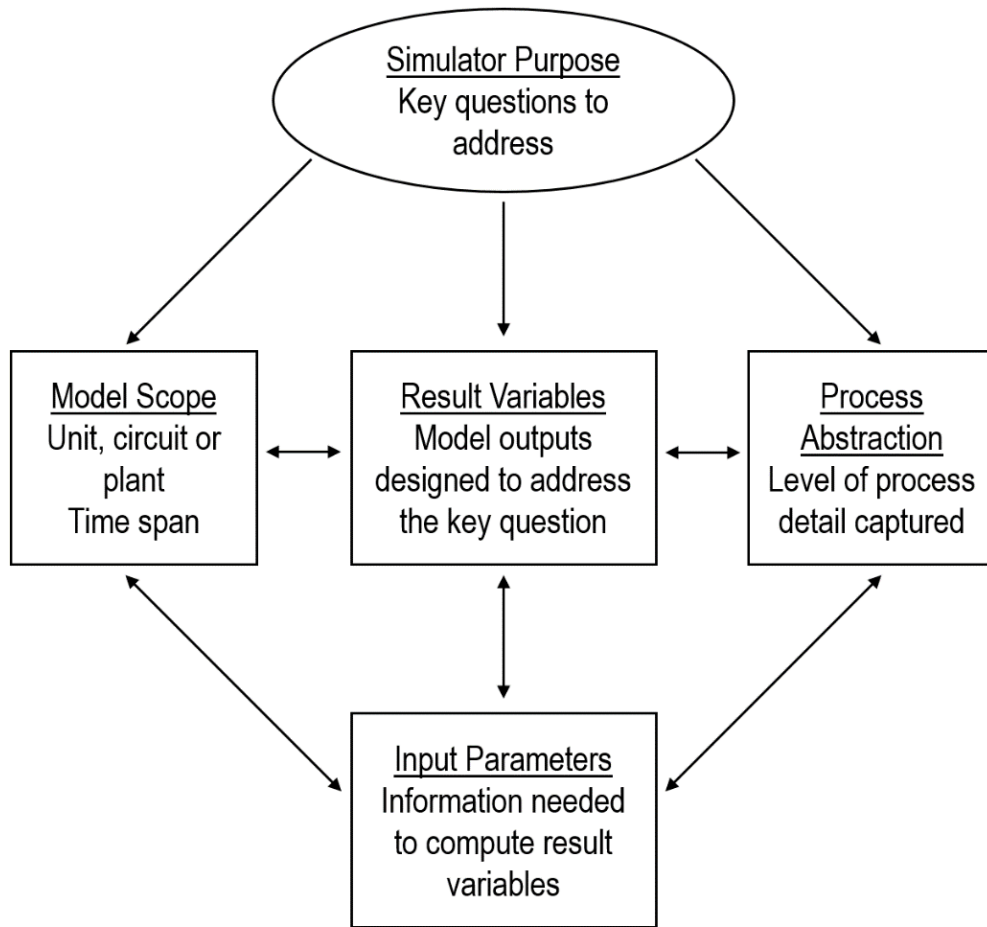


Figure 11: Relationships between simulator purpose and general scope, also known as “what” aspects (adapted from Kellner et al., 1999).

2.1.3.1 The evolution of simulators

The first instance of a simulation process may be recorded as Buffon’s needle problem in the 18th century. By the mid 1940’s, with the first computers, simulation was used in the hydrogen bomb conception for neutron diffusion predictions (Goldsman et al., 2009). However, engineering simulators only became widespread in the late 1970’s and 1980’s. At this time, simulation became a standard tool for specific design questions. There is a strong antinomy between large scope and low detail simulators, used for a training, and small scope and high detail simulators, used for very specific analytical questions as illustrated in Figure 12.

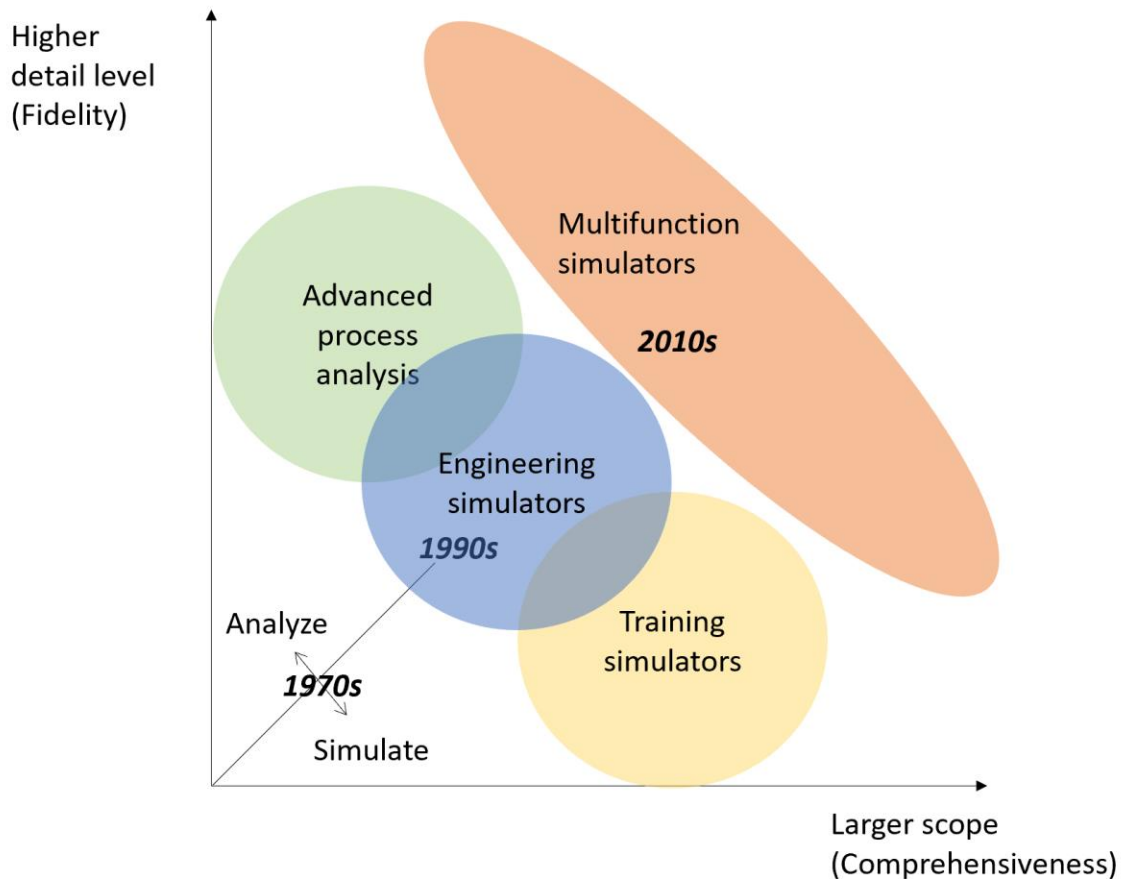


Figure 12: Evolution of the simulation purposes over time (adapted from Miettinen, 2008).

Between the 1990s and 2010s, the gap between high fidelity simulators and their large scope counterparts was reduced as multifunction simulators started to emerge, due to the increased computer power available (Jones, 1992). For instance, Balasko *et al.* (2007) showed that simulation is a powerful tool for detailed analysis and numerical optimization of complex chemical reactor systems. This a priori predictive modelling enables new recipes or catalyst tests with reduced costs or system failures merging process phenomena simulation with an engineering optimization study. In addition, Ylén *et al.* (2005) presented several case studies with the application of a dynamic process simulation (APROS software) for a large array of industries from nuclear reactors to processes in the pulp and paper industry. These authors proposed that several purposes should be considered before or even after the implementation. The purposes can generally be classified as advanced process analysis (or research and development) that requires a high level of detail for computer aided research,

operation and maintenance that requires a larger scope for operator training or process troubleshooting and finally engineering purposes, requiring medium sized scope and detail level for optimization, controller testing and feasibility study, as shown in Figure 13. There are simulators that fall in between these categories, having several purposes, such as the one presented by Balasko *et al.* (2007). It was predicted that by the 2010s, multi-purpose simulators would become the dominant type (Ylén *et al.*, 2005).

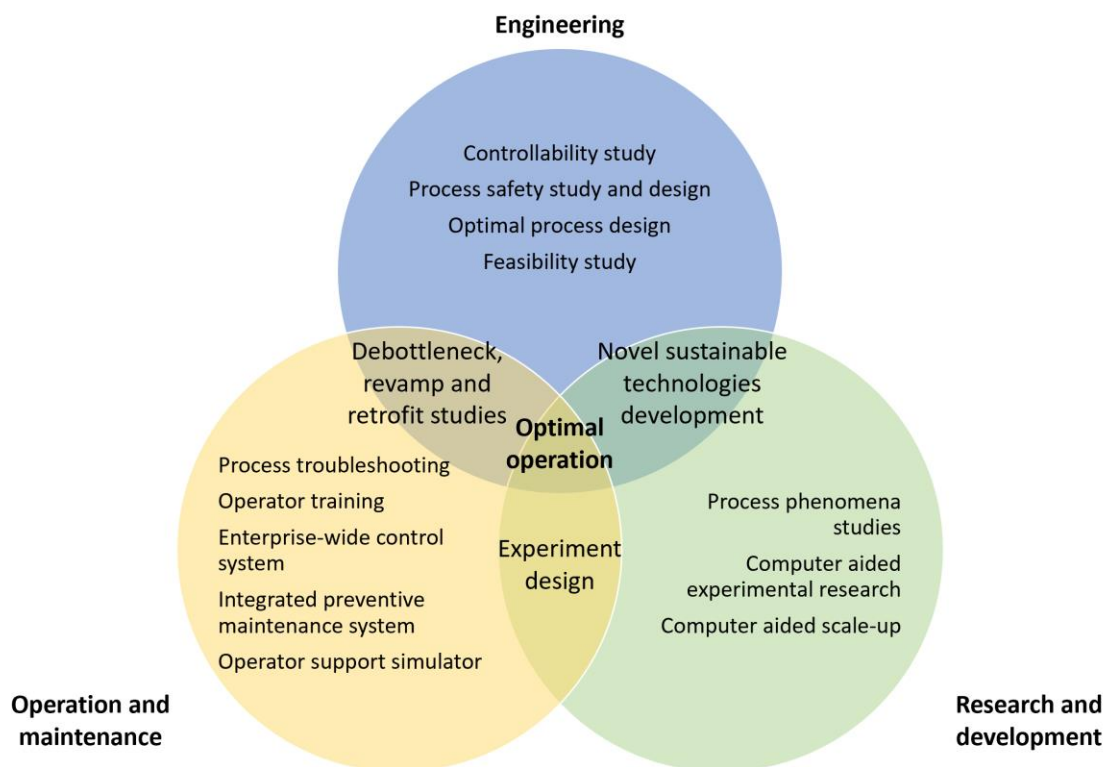


Figure 13: Purposes of simulators in the 2000's (adapted from Ylén *et al.* 2005).

2.1.4 State of the art and future trends

Nowadays, simulators are becoming more flexible, thanks to increased accessible computational power. Multifunctional simulators in combination with computer-aided design (CAD) form the backbone of the *Digital Factory concept* – or *Digital Twin* (Wenbin *et al.*, 2002). Digital factory is defined by the Association of German Engineers (VDI) as: “the generic term for a comprehensive network of digital models, methods and tools – including simulation and 3D visualization – integrated by a continuous data management system. Its aim is the holistic planning, evaluation and ongoing improvement of all the main structures, processes and resources of the real

factory in conjunction with the product.” (Verein Deutscher Ingenieure (VDI), 2008, guideline n° 4499). This approach enables the creation of a virtual layout that completely mimics an industrial facility: integrating process simulator, control system and plant design. Such an approach is beneficial for identifying and lowering potential error handling time during both planning and commissioning phases, as illustrated in Figure 14.

Full plant dynamic process simulation included in the digital factory approach enables the exploration and identification of potential issues before the production start-up and direct modification upon the 3D conception plant layout. During the production phase, the connectivity between real-time sensors (as in the smart factory concept, a highly digitized and connected production facility) and the digital factory (see e.g. Shariatzadeh *et al.*, 2016) is a crucial part in continuously maintaining and updating the process simulation. The digital twin approach needs to consider all phases of a plant or process lifecycle.

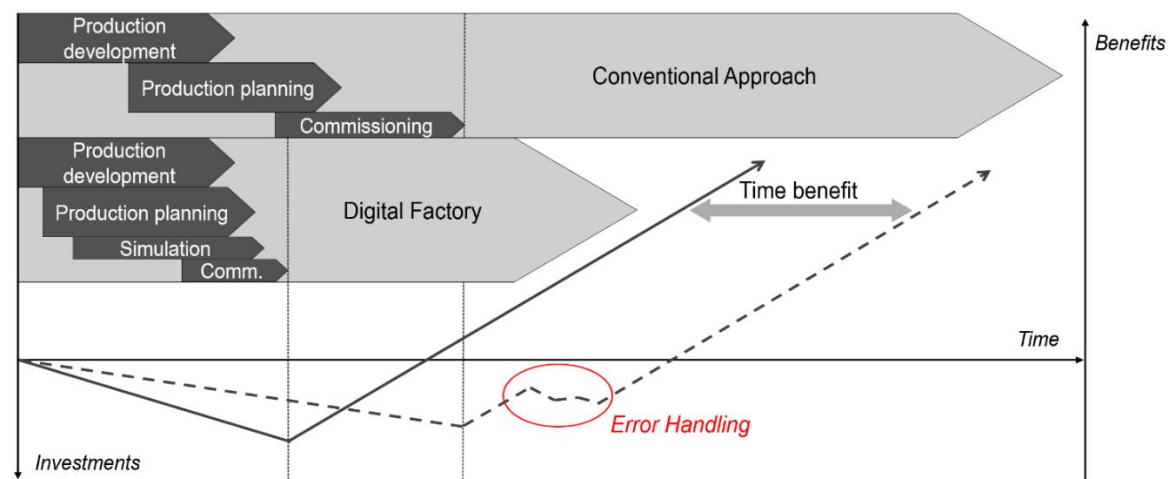


Figure 14: Digital Factory concepts, benefits and investments. The dashed line represents the benefits realised by a plant over start-up time with a conventional approach. The plain line represents the benefits over start-up time with a digital factory approach. (Comm. = Commissioning) (Adapted from Kühn, 2006).

As identified by Rodič (2017), the shift to the digital factory approach requires some changes in the conception of simulators:

- Holistic approach: the simulated system should contain several resolution levels and must be holistic. In short, the simulation must be multipurpose.

- Automatic adaptation: the modification and adaptation of each model's variable and parameter in the simulation must be automatic, based on the smart factory concept.
- Connectivity: the simulation must be connected to the global information system of the plant / enterprise (sensors, databases, operators logs, etc.).

The digital twin concept is sound and several studies have shown its importance (Geissbauer et al., 2016). However, it remains to be widely implemented, especially in the mining world. In planning, design and improvement projects, modelling and simulation are often not included in the plant development budget (Ylén et al., 2005).

2.2 Specificities of mineral processing simulations

This section describes several important issues relevant to the simulation of mineral processing: the description of the processed material - in general and in the HSC 10 algorithm - and the modelling of the equipment. Finally, some of the parameters to consider for choosing between different simulation environments will be presented.

Several professional software programs exist for mineral processing simulation: HSC Sim for HSC Chemistry¹, JKSimMet², Metsim³, UsimPac for Caspéo⁴, to list the most widely known. They contain a specific material description procedure, ready-made models, a user interface and extra tools, such as mass-balancing or model-fitting. In the academic world, simulations are often programmed using the Matlab/Simulink⁵ tools, as these permit the researchers to construct and test his/her own models. This option gives the user more freedom but also limits the simulation scope to the models implemented by the modeller. It also has a reduced distribution in the industry world, as the programmed solution do not pass the software certification standard procedures.

2.2.1 Terminology employed

For this study, specific terminology is defined as follows:

- A unit is a model representing a piece of equipment. For example, a flotation cell, a grinding mill or a size separator;
- A circuit is comprised of several units having a common purpose (liberation, separation, purification...). For example, a flotation circuit would be composed of several flotation cells and conditioners, a grinding circuit of one or several mills and size classifiers;
- A stream is a mix of solid, liquid and gas – the description of a stream is given in the following section. Depending on the context, a stream can be called ROM

¹ <https://www.outotec.com/products-and-services/technologies/digital-solutions/hsc-chemistry/>

² <https://jktech.com.au/jksimmet>

³ <https://metsim.com/>

⁴ <https://www.caspeo.net/>

⁵ <https://www.mathworks.com/products/simulink.html>

(Run of Mine), feed, crushed ore, pulp (when mixed with water) or cake (when the concentrate is dried). In the separation process, stream may be a concentrate or tail.

Units are linked by streams to form circuits, as illustrated in Figure 15.

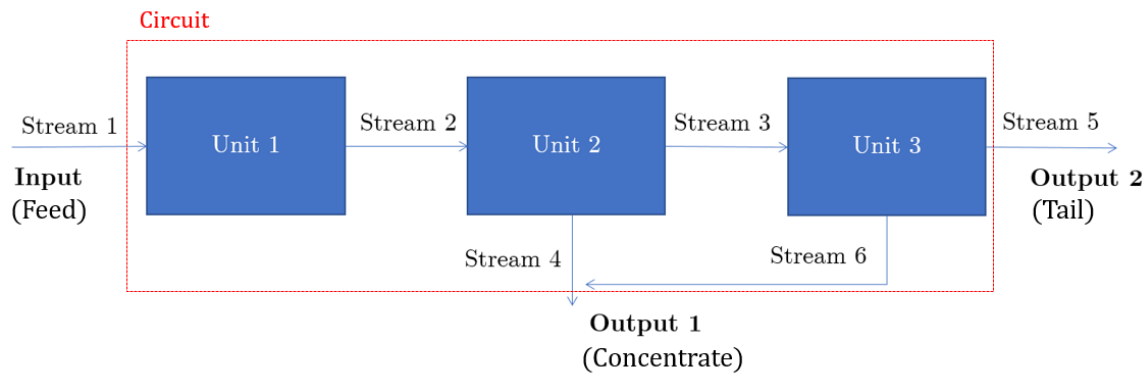


Figure 15: Simplified example of the organization of circuit, streams and units.

2.2.2 Stream description

Along the process, the streams can take on a wide variety of different forms. During the crushing phase, the material is mostly dry, composed of rock fragments, as shown in Figure 16 a. During the flotation phase, rock fragments will be much smaller (less than 200µm), hardly distinguishable with the naked eye and they are mixed with a large amount of water, as shown in Figure 16 b. In this type of stream, impurities play a larger role and have a measurable impact on the process (Michaux et al., 2018).

Therefore, the description of the stream in the simulation has to take into account the diversity of forms and the wide range of physical and chemical properties it may take, in addition to flow rate information.



Figure 16: Pictures of mineral streams at different stages of the process. a) Pyhäsalmi crusher charge, composed of heterogeneous particles in terms of size and composition, with no water added (picture J. Joutsenvaara, 2019 for Minetrain project⁶). b) – Cleaner launder streams from Pyhäsalmi plant, almost 30wt% solid, with relatively more homogeneous particle sizes and compositions (picture C. Izart, 2019).

2.2.2.1 Generic description

A stream is composed of three phases: liquid, solid and gas. The most generic information of the stream is its flow rate, its apparent density and its tonnage.

The liquid phase is commonly water and its amount is given either in absolute terms, in flow rate or tonnage, or relative to the solid content, in weight percent. Additionally, the liquid phase is defined by a specific pH and may contain various elements such as ions and reactants, which are reported as concentrations. The gas phase is commonly used for flotation processes, and later in pyro and hydro processing. The information for flotation is generally limited to giving volume per unit of time, mostly in l/min.

⁶ http://minetrain.eu/pilot_course.html

The solid phase is described with multiple levels of detail. The most basic information which can be generated is the mass of solids transported by the stream per unit of time, generally expressed in metric tons per hour in an operation plant, in kilograms or grams per hour for a pilot or a test, or in metric tons per year for a global, long-term study of an installation. This information may also be given in the volume of solids per hour, when the apparent density of the material is known and when no water is added. The apparent density of the processed material is a difficult parameter to access to. It is the ratio of the mass and the total volume of the solids, including the internal porosity and inter-particle void volume. In addition to the material properties, this is also dependent on the particle size distribution.

A more advanced level of detail of the solid part is reached by knowing the chemical composition. This is achieved through the chemical analysis of a sample (bulk sample in Figure 17), with XRF analysis or induced coupled plasma – mass spectrometry or optical emission spectrometry (ICP MS or OES) being the most common. Another information level is reached with determination of the particle size distribution, for example from sieve data. The combination of chemical information by particle size fraction is called assay by size.

When only the chemistry is known, the mineral composition of the stream can be recalculated. This requires knowledge of the minerals present in the solid phase, and their precise composition. Then, each element can be associated to a mineral amount by solving a matrix problem. However, some mineral compositions need access to more data: for instance, copper-bearing sulphides (chalcopyrite, covellite, bornite, etc.) contain the same elements (Cu, S and Fe) but at different molar ratios, and it is not possible to know their relative proportions when only the chemical composition is known. Because these minerals will not behave exactly the same in the flotation process for instance, it is important to know how much of each is present in the stream. To solve this problem, additional analysis is needed, for instance differential copper dissolution (water, acid, cyanide and nitric acid copper dissolution) to work out the proportion of each copper sulphides originally present.

The most advanced level of detail concerning the solid part is the access to the particle composition. In fact, a particle may be composed of only one mineral (and is thus

called liberated) or of several minerals (which are thus called non-liberated). The fastest way to have access to the distinction between liberated and non-liberated minerals is to use automated mineralogy tools. The heterogeneity of the material processed has a large impact on its behaviour in different processing units, and the better the description of the material, the more accurate the modelling of the process will be. However, increasing the amount of data gathered on a stream means increasing the analysis effort and cost. The size of a representative sample may also change and render the analysis inoperable. Figure 17 summarizes all possible terminology and features used to describe the modelling detail level of a stream's solid phase.

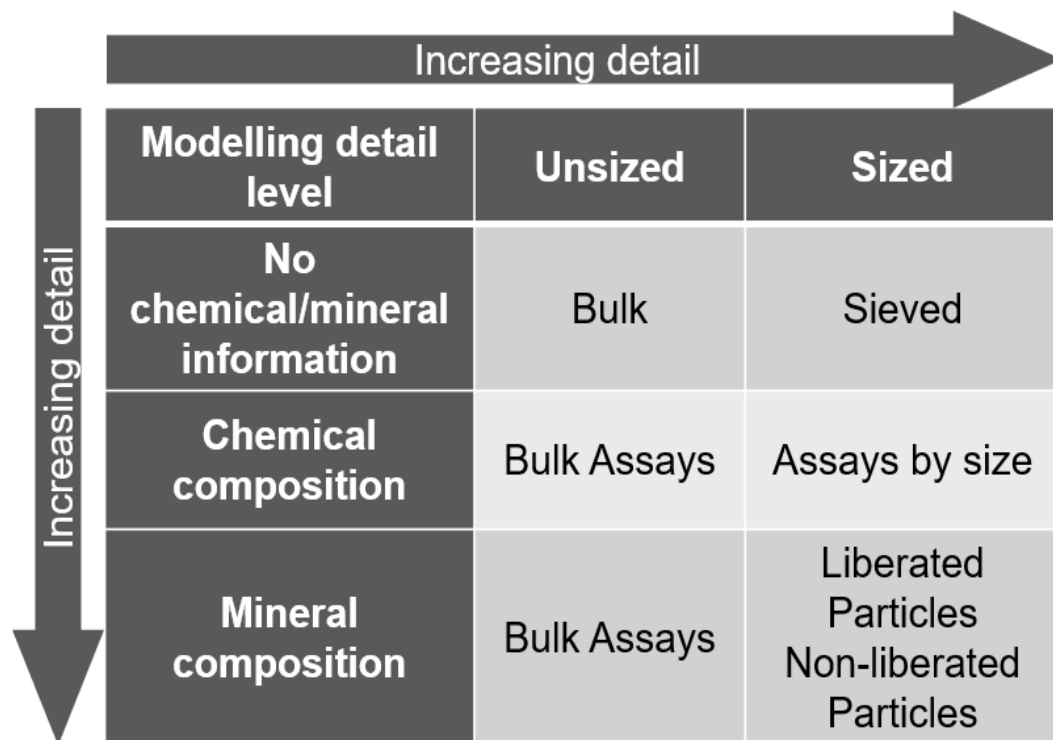


Figure 17: Solid material in streams – different level of description. From *HSC Chemistry® User's Guide, Chapter 45* (Antti Remes & Lamberg, 2021).

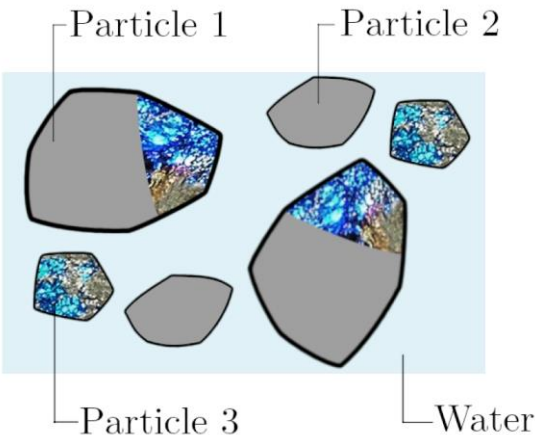
2.2.2.2 Description used in HSC Sim

The material flowing through the plant is either a slurry, i.e. a mixture of water and rock, (in the flotation circuit for instance) or solid rock (usually for the first crushing steps). In HSC 10 environment, the objects *streams* are described as the sum of *water* and *particles*. Particles are themselves objects composed of one or several *minerals* which have their own properties.

In mineral processing, streams cannot be defined by their chemistry alone, i.e. mass of oxide or elemental masses. Physical processing (flotation, magnetic separation, etc.) typically uses properties of minerals, not proportions of elements.

Each stream carries information about the quantity of matter (cubic meters per hour or tonnage per hour) going from one unit to another. It also contains information on the water content and the density of the slurry. The solid part of the stream is composed of particles, and the software records which and how many of each particle is present in each stream. See for example Table 4.

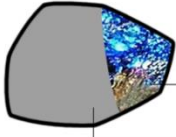


Table 4: Example of stream architecture and information contained.

<p>Stream 1</p>  <p>Particle 1</p> <p>Particle 2</p> <p>Particle 3</p> <p>Water</p>	<p>Stream Information</p> <ul style="list-style-type: none"> -Coming from: Unit 1 (Conditioner) -Going to: Unit 2 (Flotation cell) -Flow rate: 100m³/h -Water content*: 50% -Solid composition* <p>90% Particle 1 12% Particle 2 8% Particle 3</p> <p>*For simplicity composition is here shown as volumetric (area) to correspond with the illustration – but may also be expressed as mass percentage.</p>
--	--

The class object *particle* carries information on density, size fraction, the amount and nature of the mineral(s) contained and other parameters such as flotation kinetics. Indeed, particles may contain several minerals and thus carry crucial information on the liberation degree for each mineral. If not completely liberated, separation from non-valuable minerals (gangue) is difficult and yields poor recovery and concentrate grade. It is the purpose of the comminution steps to free the majority of valuable minerals from the gangue.


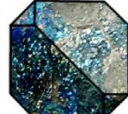
Parameters used for separation (i.e. density or flotation kinetic rate) are a function of the proportion of mineral(s) and thus are recalculated for the whole particle if it consists of several minerals. See for example the particle information presented in Table 5.

Table 5: Example of particle architecture and information contained.

Particle 1 	-Size fraction: +250 μ m -Minerals*: Mineral 1 – 70% Mineral 2 – 30% -Density: medium -Flotation Kinetic: slow
Particle 2 	-Size fraction: 0-250 μ m -Minerals: Mineral 1 – 100% -Density: low -Flotation Kinetic: slow
Particle 3 	-Size fraction: 0-250 μ m -Minerals: Mineral 2 – 100% -Density: high -Flotation Kinetic: fast

Finally, the mineral class object contains mineral information, such as density or magnetic susceptibility. It gives the formulae of the mineral as well, which is required to calculate the oxide or elemental weights of the whole stream.

Table 6: Example of mineral architecture and information contained.

Mineral 1 	-Mineral name: quartz -Density: 2.65 g/cm ³ -Formula: SiO ₂
Mineral 2 	-Mineral name: chalcopyrite -Density: 4.20 g/cm ³ -Formula: CuFeS ₂

2.2.3 Models for mineral processing

The development of the first matrix analyses to model a comminution process (Broadbent & Callcott, 1956), and the original mathematical equations developed for flotation (K. L. Sutherland & Wark, 1955) date back to the 1950s. They were mainly based on an empirical approach and, as such, data used for the development of models was the critical aspect. Nowadays, more information is collected daily in the plant

thanks to on-line analysers. Data processing capability are increasing with less costly computing power and cloud data storage. As a result, models are continuously being improved by taking these new resources into account in the modelling process.

A major review of existing mineral processing unit models was provided by King (2012). It describes quantitative models based on first principle laws (e.g. mass conservation), phenomenological models (e.g. bubble – particle collision model for flotation modelling) completed by the implementation of empirical factors. Early semi-empirical models for comminution devices (Whiten, 1974), flotation (Savassi, 2005) and dewatering (Scales & Usher, 2015) already have a significant advantage over purely empirical models: they offer an extrapolated range of applications in a more reliable way, i.e. they are less prone to failure when simulated conditions move further from the experimental situation. Indeed, these models require some retrofitting, i.e. the adaptation of one or several parameters to experimental data.

One of the main predictability issues was raised by Powell and Morrison (2007). It relates to mineral liberation for comminution circuits, which is both crucial and complex to predict even with retrofitting methods. Recent publications propose modelling solution for mineral liberation, such as in Hamid *et al.* (2019) and Pérez-García, Bouchard and Poulin (2018) works. These models require several parameters to be fitted to the process (4 per mineral of interest in Pérez-García, Bouchard and Poulin (2018) model, 2 per mineral and per size class for Hamid *et al.* (2019) model for β -distributions). As a consequence, and as expressed in these publications, the need for good quality, representative samples are exacerbated. In addition, these models have been validated in their case study against single operation condition sample, limiting the validation of the model for extended operation range prediction.

Models are strongly influenced by ore characteristics, such as mineralogy and texture for comminution, but also by mineral chemistry for the flotation process, as illustrated with the example of sphalerite flotation, which is strongly dependent on the iron content of the sphalerite (Boulton et al., 2005).

Depending on the purpose of the simulator, the modelling depth of the model can vary. Simple, low-detail models are typically sufficient for controller design and testing, where the essential parameters received from the model are the process

variables. Best suited for this purpose are purely empirical mathematical models, fast to calculate and easy to maintain (Hodouin, 2011). On the other hand, very detailed simulations exist, for instance in computational fluid dynamics (Schwarz et al., 2015). These are suitable for process analysis and optimization. However, this type of model demands a lot of input parameters as well as more computational power and thus is currently cost-efficient only in particular equipment design cases.

A modelling process has three steps, as presented in Figure 10. The most critical step is data validation. Modelling requires reliable data in sufficient quantity, especially for mineral processing models, which are most often empirical or semi-empirical (R. P. King, 2012). The quality of the data is of importance, especially knowledge of the heterogeneity and complexity of the material processed. It is crucial to ensure that data collected for the validation of a model responds to sampling law theory (P. M. Gy, 1976) and is representative of the material. Measurement techniques are evolving and enable the formulation of more reliable and advanced models, especially with real-time analyser techniques. New types of information, collected on a more regular basis, help to improve models. For instance, micro-tomography studies, as illustrated by Xu *et al.* (2013) or Guntoro *et al.* (2019), and quantitative mineralogical analysis enable more comprehensive breakage testing techniques and thus more reliable predictive models.

In general, most of the models are steady state, as they are usually more straightforward to program and require less computational power than dynamic models. Dynamic models enable the simulation of transient states which can be a significant aspect to include in dimensioning (for example in a pump sump dimensioning), controller testing or an operator training simulator for greater realism (P. Karelovic et al., 2016; Liu & Spencer, 2004; D. N. Sutherland, 1977). This type of model tends to be more common with increasing access to computational power as originally proposed by Lynch and Morrison (1999).

2.2.4 Choosing a simulation environment

As introduced at the beginning of section 2.2, several environment options are available for mineral processing modelling. The choice of one or another is a function of a sum of parameters, the main difference being between a specialized environment,

such as HSC or the JKSim suite, and generalist, such as Matlab Simulink. A simulator could also be programmed from scratch; however, this case is not discussed at length here.

The most obvious variables to consider are the time available to construct the simulation and the end users. A simulation in a specialized environment is easier and faster to implement when a database of the model pre-exists, and the processed material is already implemented as mineral-based particles with their chemical and physical properties. This type of environment is more accessible for its end-user, as it has been conceived for a precise aim, with defined user inputs, for instance to modify the amount of pulp in a feed stream. User-interface wise, mineral processing simulation environments will generally look the same. In a generic environment, the user-interface would have to be parametrized by the programmer, requiring more time. The adaptability of the simulation (ability to change any model parameters easily) is usually reduced on these simulators, and they are made for a specific study, with a high detail level and generally reduced scope.

Additional features and connection to external databases may be added to the simulator, depending on its purpose. Usually, a tool to balance the collected data is needed. Mass balancing ensures that the information collected on the streams is coherent within itself and that the mass balance is respected (no matter is lost or “created” during the process). This is a critical part of the data treatment before considering simulation, as the sampling of particulate material in mineral processing may be tricky. In several specialized software programs, mass balance is already integrated (e.g. JKSim, HSC Sim). Database of existing minerals is another additional feature to consider, for a more efficient modelling of a case. When the simulation is to be used for a life cycle assessment (LCA) a link to databases (e.g. GABI⁷, openLCA⁸) has to be implemented. For a capital / operational expenditure assessment, a database for metal prices, consumables and equipment prices would be necessary. In

⁷ <http://www.gabi-software.com>

⁸ <http://www.openlca.org/>

the case of a control system design, testing, optimization or operator training simulator, an automation system model must be implemented. Two options exist: control system replication within the simulation software or distributed control system software (DCS) linkage to the process simulation. DCS provides the simulator user interface (UI) in the latter case.

The UI is an important feature to consider, as it represents the interaction between the user and the simulation. It can be integrated in the simulator software or it can use the DCS software's UI in case of external control software. For engineering simulators, i.e., dimensioning, optimization or controller testing, the interface allows the user to change the process model and controller parameters freely and ideally in an intuitive way. It also allows to direct change of the circuit connectivity and input stream properties in the graphical representation of the flowsheet. The simulated results are then easily accessible directly or as an export for further data analysis.

OTS requires the implementation of two separated and different interfaces with different functionalities; one for the trainers and one for the trainees. The trainer UI enables a review of training results, helps to set exercises and change the simulation parameters for each session. The trainee UI is an immersive experience of the operator workstation. For instance, it may require a graphical reproduction or mock-up of the plant control system, e.g. DCS, a 3D representation of the plant in virtual reality, including visualisation of trends (grade, flow rate, etc.) and alarm capabilities. The UI gives also access to the exercise steps and to the didactic content in order to facilitate the training.

2.3 Simulator applications in mineral processing plants

Scientific publications list several applications for simulators in the mining industry. Dimensioning of comminution units is the most widely studied task and many authors have addressed it already (S. Morrell & Morrison, 1996). A few training simulators have been implemented for separate circuits, such as flotation, grinding and classification (Roine et al., 2011; Toro et al., 2012). Remes et al. (2010) and Karelovic et al. (2015) presented examples of simulators aiming at evaluating and testing control strategies in flotation and comminution circuits. Finally, some simulators describe entire plants for optimization purposes (Seppälä et al., 2014; Talikka et al., 2018) or geometallurgical studies (Lishchuk, 2016) in steady-state mode. Despite the tremendous effect of dewatering on water management, previous examples show that dewatering circuits and water-related models are usually not included in current mineral processing simulators, although some models do exist (R. P. King, 2012; Antti Remes & Vesa, 2014). These models have to handle water chemistry and are considered separately from other mineral processing models (Sinche Gonzalez et al., 2016). Therefore, water management optimization may benefit from a simulation that integrates these models in the future.

Currently, a holistic mineral processing plant simulation describing every unit and stream used in the process, in a flexible and multi-purpose manner, has not yet been reported in the scientific literature. However, a simplified theoretical approach has been developed by Lishchuk *et al.*, (2018) but it was not based on a real plant. As seen with the introduction of the industry 4.0 concept and digital twins, this type of simulator would find various applications throughout the processing plant lifecycle. Figure 19 aims to summarize the applications of a simulator in a mine lifecycle, the stages of which were described in 1.1.

During the greenfield project evaluation phase and prefeasibility data is relatively scarce, resources estimation is still uncertain, and few processing tests are yet made on the ore. Some process simulations using these “basic” pieces of information about the deposit can be made using preliminary results from feasibility study tests. These simulations are used to find the best extraction and processing technologies available for the potential future mine. For better primary economic appraisal and a faster

permit application process, it is important to access reliable data and predictions of the future mine operations. Another important aspect in the evaluation phase, and crucial throughout the mine's lifetime, is the preparation of the mining plan. This encompasses the determination of the correct cut-off grade, exploitation sequencing and ore blending. There is no simple analytic solution to determine the correct plan in practice. According to Bradley's (1980) study, mining engineers apply simulations to available data to determine an optimal mining plan. For instance, the approach for evaluating metal price uncertainty is to simulate the effects of different price scenarios on returns with given parameters of exploitation and processing methods, recovery and grade.

During the planning and construction of the plant, once the technology has been selected for the project, the plant simulator can be implemented. At this stage, a simulator can represent the entire process, and is progressively tuned to the specificities of the mine with increasing knowledge of the deposit and process. In association with CAD and 3D layout representation (e.g. Aveva⁹ or AutoDesk¹⁰), process simulation can be used for the first dimensioning of the machinery. Safety procedures, control testing and operator training can also be implemented using simulation.

A simulator conceived initially for training and start-up procedure, needs to be maintained and has to evolve with time (Figure 18). Firstly, the information about the process increases and improves when the plant becomes operational, and thus more sophisticated models can be used. Additionally, the real plant response will slowly deviate from the original simulation. This may be due to modifications to the process itself (for instance with units added or bypassed), or natural wearing of some units. For training simulators, new experiences can be included in the simulation, such as information captured from incidents and new operation scenarios. An important aspect of the integrated simulator is that its adaptability allows it used throughout the

⁹ <https://www.aveva.com/>

¹⁰ <https://www.autodesk.com/>

mining lifecycle and incorporate different levels of modelling, with more or less detail, without modifying the global simulator architecture. Simulation can then be used for process analysis, troubleshooting, for new/remedial operator training or even process optimization.

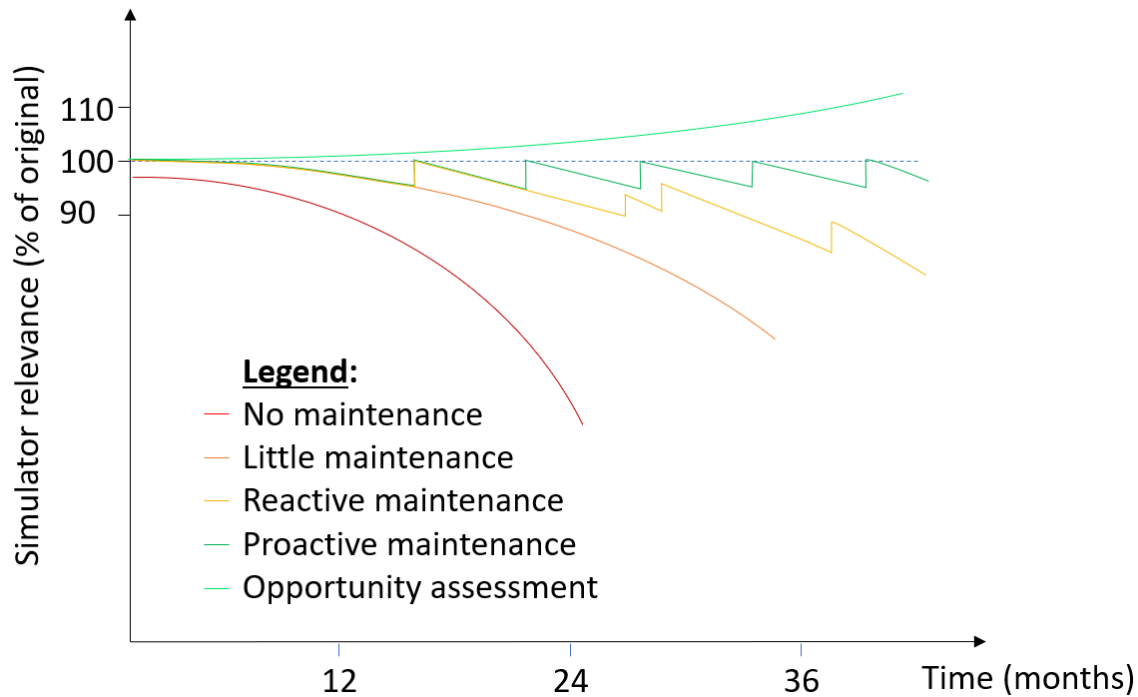


Figure 18: Effect of simulator deviation compared to real plant operation. The relevance of the simulation is tied to the amount of information available. The original, or initial simulator, conceived for preparing the start-up does not have a lot of information about the real process. With no maintenance, the simulator is not even updated when the plant starts operation and is thus already outdated compared to the amount of data gathered during the start-up. With little or only reactive maintenance, the simulation is adapted intermittently when issues are spotted. With proactive maintenance, the simulator is regularly updated and stays relevant. Finally, using opportunity assessment on the simulator enables to improve its relevance.

When the operation is running, process optimization may be a complex task, as it requires the current process line to be reduced, stopped, rerouted to test a new parameter settings or material routes, resulting in a loss of productivity for an amount of time. However, this time can be reduced if different options have already been pre-tested using simulation. The optimization and planning work undertaken during the entire mine lifecycle has an impact on the closure and remediation stages, for instance thanks to better control of the tailing composition and better management of resources. For example, simulation can be used to show the relationship between PSD

and water consumption in a plant (Donoso et al., 2013), opening up new opportunities for better water management. Finally, mine remediation would benefit from an optimised management of process outputs. Waste volume and properties (mineralogy, PSD, pH, etc.) can be simulated and predicted in advance, enabling a better preparation of storage capacity and condition. Better remediation planning could be achieved by using such a simulation already at the exploitation phase of the mine.

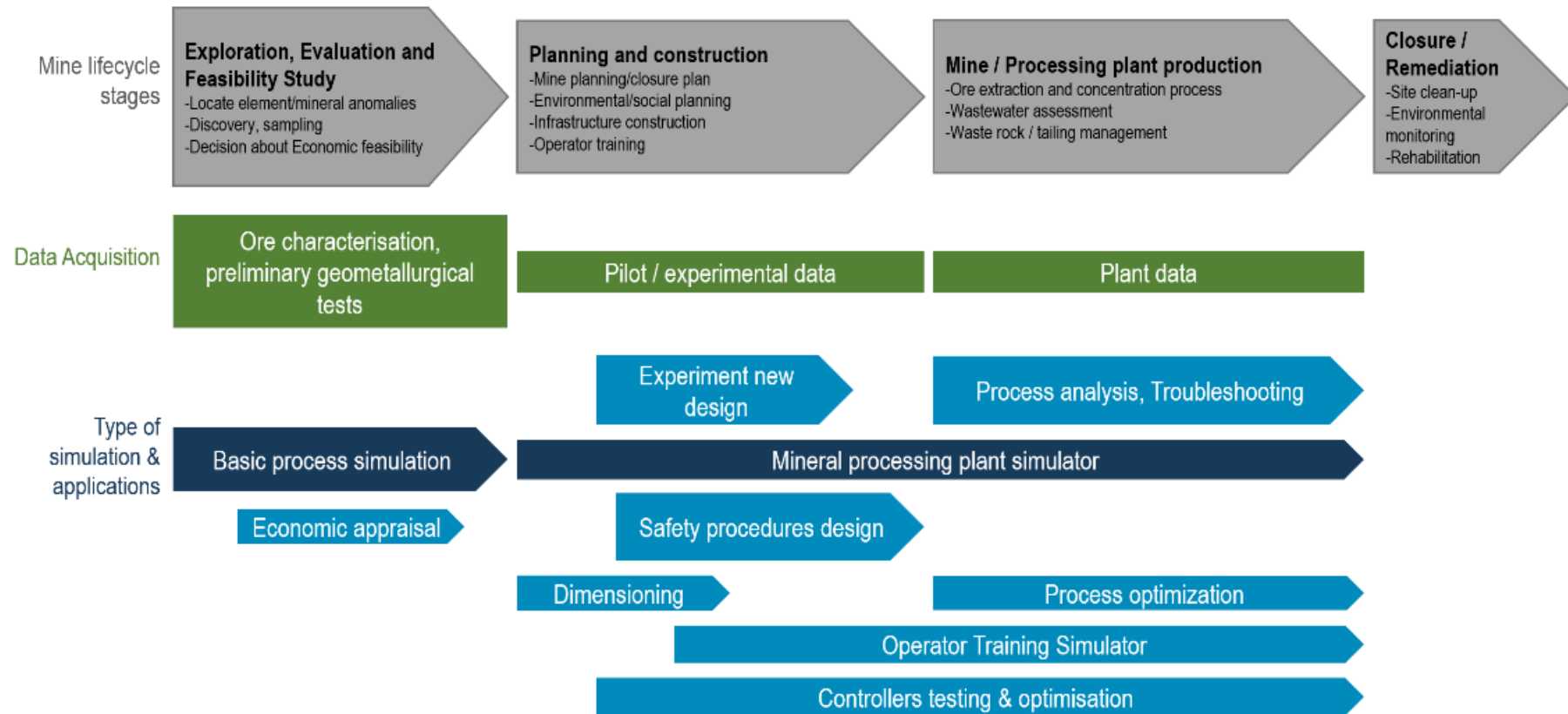


Figure 19: Mine lifecycle and use of mineral processing simulators.

As a conclusion, a holistic simulation of mineral processes must consider the geological information and its variations in order to auto-adapt to the deposit heterogeneity as the deposit is being mined. The geometallurgical approach proposed by Lamberg (2010) aims at describing the ore body with a predictive spatial recovery model using a detailed mineralogical study (grain size, texture, chemical composition, etc.). In order to fully embrace such an approach, the simulation should consider particle behaviours, with liberated and non-liberated minerals, and not only the bulk chemical composition of the feed input. This process starts with the definition of a geological block model, containing not only ore grade, but also metallurgical properties, such as mineralogical textures or grindability parameters. From this block definition, a breakage model can be extrapolated for both blasting and comminution. Then, the predicted outputs of the separation process (tonnage, grade, recovery, tailings volumes & properties, water properties, etc.) are obtained through simulation for every block of the block model, as illustrated in Figure 20, enabling the construction of a fully comprehensive economic block model. The primary goals of this approach are better resource management throughout the mine's lifetime and reduction of operational risks due to ore feed variability. The geometallurgical characterization of a deposit can be completed during the development of the mining project (exploration, evaluation and prefeasibility stage) in order to improve the accuracy of resource estimation.

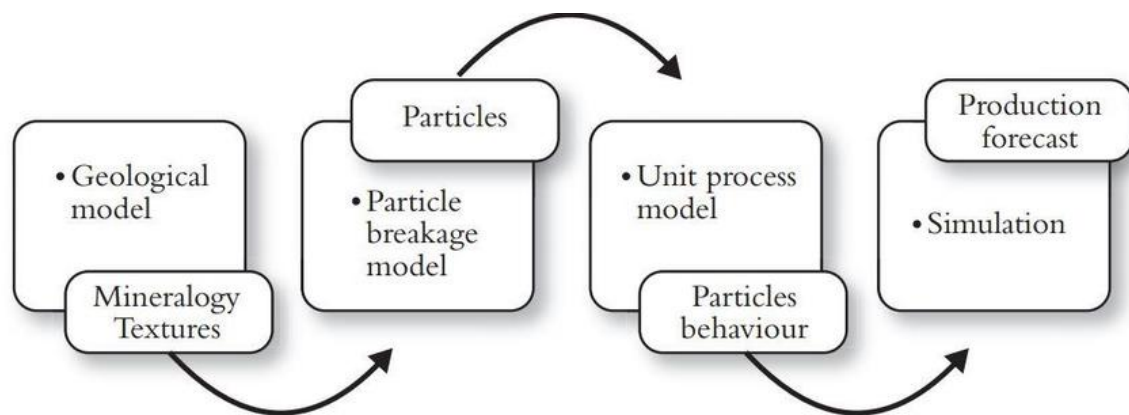


Figure 20: Particle-based geometallurgical model after Lamberg (2011).

In the following chapter, I will show the improvements and additions made to the HSC Sim platform during this project, in order to build the first instance of a fully integrated, geometallurgical, from mine to metal process simulation.

Chapter 3 Materials and methods

This chapter describes the materials and methods used for the development of new and improved models implemented in the HSC Sim environment, as well as the conception of case-study simulator. These models respond to specific necessities, they have to communicate with each other and can be integrated in a multifunctional simulator. During this thesis work, several models were developed, and two examples illustrate the entire modelling process, from conceptual model to validation with field and laboratory work. Several new models have been implemented as part of this project. The main additions to HSC Sim unit library made by the author are displayed in Appendix 1 and 2. All these additions are based on conceptual models originating from distinct projects, research groups or universities, and as such, a major improvement is to be able to use all these individual models together within one environment.

In these following examples, the author programmed the models and integrated them into the HSC Sim environment. The author made the data analysis and section observations on the Kylylahti pilot samples. GTK Mintec provided the pilot process and related samples. Data acquisition for validation of the dynamic mill model (i.e., organization of the sampling campaign, sampling and sample analysis) was completed by the author in collaboration with First Quantum Mineral Ltd. Pyhäsalmi mine personnel.

In the training simulator case, the author was responsible for the simulator construction, model choice, dimensioning, parametrization and research work for the description of a generic spodumene flotation circuit, in coordination with the Outotec business lines. In the digital twin simulator case, the author contributed to the parametrization of the units, flowsheet internal calculation for ore blending and developed specific unit models, such as the stockpile or conveyor models. During the construction of these simulators, the author also improved several model

calculations, such as flotation cells and conditioners. These models will be described in the following sections.

3.1 Multi-particle mill model study

The mill charge composition strongly affects the comminution behaviour, and yet the effect of varying ratios between hard and soft material is not considered in most mill models and is difficult to extrapolate from individual component properties (M. Bueno & Powell, 2011). Blending occurs frequently in mining, either with the aim of reaching a certain plant feed grade and reducing fluctuations or diluting certain undesired elements (Chanda & Dagdelen, 1995). Behaviour of blends during grinding is no trivial question, especially for AG and SAG mills, where an ideal ratio of competent ore can be added to serve as the grinding media (M. Bueno & Powell, 2012) and thus reduce the OPEX costs of the operation.

The following conceptual model is based on the Whiten perfect mixing mill model (Whiten, 1974), upgraded with Bueno's multicomponent approach (M. P. Bueno et al., 2013). In this study, a ball mill model is studied, but the same approach would also be valid for most tumbling mills, such as SAG/AG mill or rod mills. Other models used for the simulation, such as size separator units, are described below.

3.1.1 Material

The material and pilot plant run used as a basis for this modelling work was carried out as part of Prochaine EIT RawMaterial project. This test work was conducted at GTK Mintec (Finland) for training purposes. The ore came from an Outokumpu type-VMS type deposit and the considered material contained between 15 and 20% mostly disseminated sulphides (Malmberg, 2018). The main sulphides observed in the feed samples were pyrite, pyrrhotite, chalcopyrite, Co-pentlandite and sphalerite. Gangue was mainly composed of quartz with traces of calcite and tremolite.

For the pilot test, the run of mine was crushed with a jaw crusher and two cone crushers in a closed loop, with a 6mm final screen (Figure 21). The grinding circuit consisted of a rod mill and a ball mill in a closed loop with hydrocyclone separation. The cyclone overflow, with an overall P80 of 86 μm , was directed to the first flotation stage where copper and nickel-bearing minerals were recovered to the concentrate stream and sent to a copper flotation stage. The first flotation tails were directed to a sulphide concentration flotation stage. The simulation presented below is restricted to the mill circuit with a focus on the ball mill. At several collection points shown, in

Figure 21, the flow rates and solid percentages were measured, and samples were taken. An aliquot of these samples was sieved to determine the particle size distribution. For the feed, rod mill output, ball mill output and cyclone overflow and underflow samples, sieved fractions were ground and then analysed by X-ray fluorescence (Hitachi XMET-8000) – see Appendices 3 to 6 - and another aliquot of the original sample was used to produce polished sections. The mineralogy was then reconstructed based on the major elements with principal minerals and the NSG (non-sulphidic gangue).

Comminution circuit flowsheet

Total Solids Flow (t/h)

Collection points measurements:

- -Flow rate
- -Percentage solid
- -PSD
- ➔ -Chemical analysis by size fraction
- ➔ -Polished section

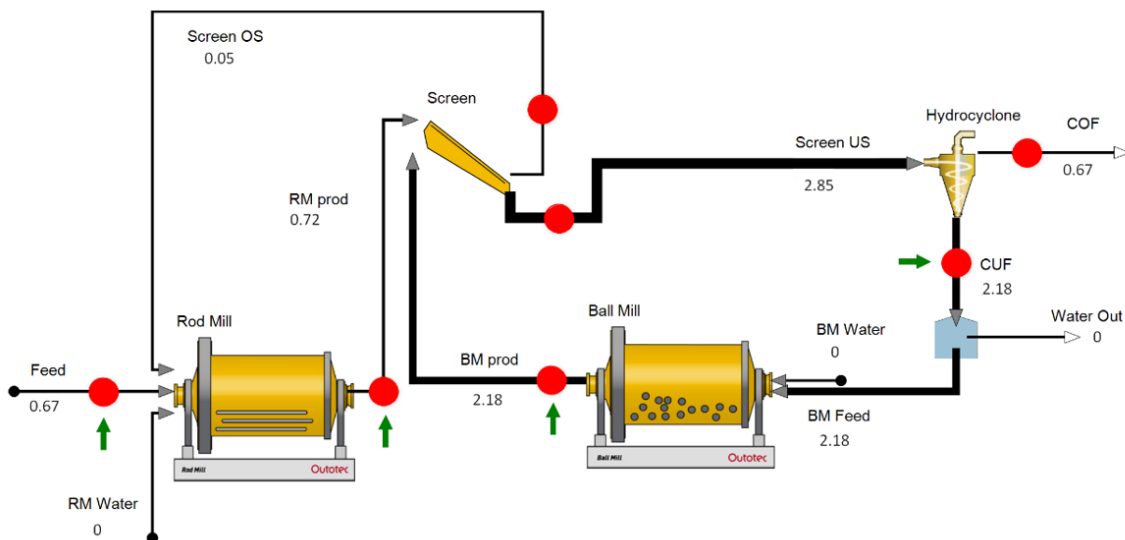


Figure 21: Grinding circuit model with collection points from the pilot test – red circles show where the flow rate, particle size distribution and solid percentage of the pulp were measured – green arrows show where polished sections and chemical analysis by size fractions were performed.

Based on image counting with ImageJ (Collins, 2007) on the hydrocyclone underflow polished section (examples are shown in Figure 22 a and b), 94% of the sulphides having an area larger than $50\mu\text{m}^2$ were found to be free. Only particles larger than $50\mu\text{m}^2$ were considered for this model as the minimum limit for recovery with the

flotation process. In Figure 22 c and d, which are pictures taken of ball mill product polished section, sulphide particles are also clearly separated from gangue particles with very rare binary particles, i.e. two separate particle populations - gangue and sulphides - are clearly distinguishable (Table 7).

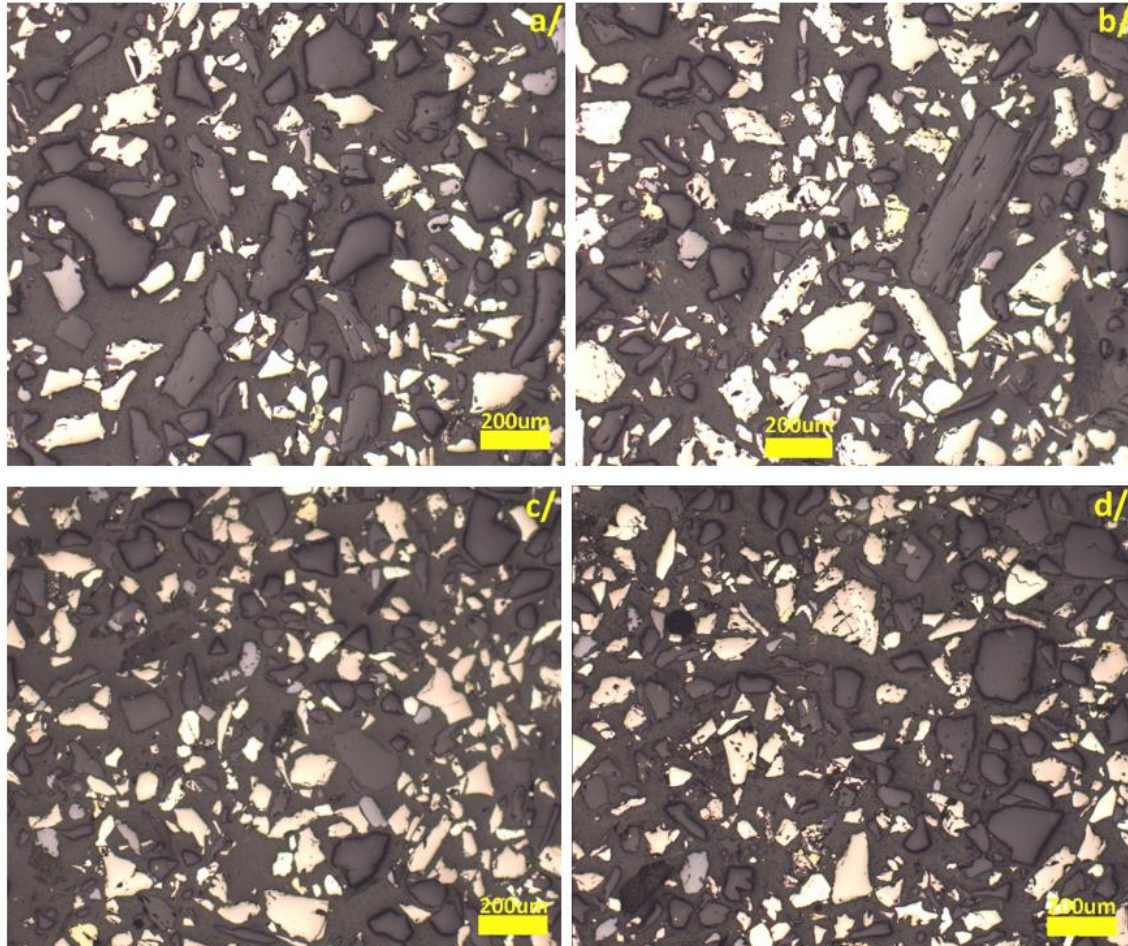


Figure 22: a and b: polished sections of hydrocyclone underflow (ball mill feed), c and d: polished section of ball mill product. The bright yellow grains are sulphides and dark grey grains are the gangue (mainly quartz, with some carbonates).

Table 7: Proportion of grains bearing non-liberated sulphides (size threshold above $50\mu\text{m}^2$)

Total number of sulphides	1,723
Total cumulative area of sulphide (μm^2)	4,663,326
Total number of grains bearing non-liberated sulphides	153
Total cumulative area of non-liberated sulphide (μm^2)	274,865
Proportion of non-liberated sulphide	5.9 %

The heterogeneity of the ball mill input allows to distinguish two main particle populations, one consisting of sulphides and the other being gangue, which can be based on the large difference in specific gravity – 3.9 g/cm³ for the lightest sulphide (sphalerite) versus 2.6 g/cm³ for the gangue. While, in the classic mill model, these two populations would have the same particle size distribution in a simulation, the multi-particle model will consider both populations separately. Noteworthy is that if more bimodal particles were identified, it would have been possible for the model to handle a third population. For example, a population of gangue associated with a certain percentage of sulphide or a dense non-sulphidic mineral, such as an oxide. More populations based on different liberation degree for each mineral would be the ideal case.

From the chemical composition analysis of the different streams for a given fraction, it became apparent that elements are not distributed equally between size fractions. Mineral composition by size fraction is reconstructed based on the chemical analysis, and the various minerals seem to show a different behaviour during comminution (Appendix 7). For instance, gangue material seems to produce proportionally more particles under 90µm than sulphides. This may be due to the presence of brittle minerals, such as diopside, in the gangue or due to the better development of cleavage planes in many gangue minerals.

3.1.2 Modelling methods

3.1.2.1 Ball mill model

The HSC Sim Ball Mill model is based on population balances of each size fraction in the mill, affected by the rate of breakage and material transportation. The model is called the perfect mixing ball mill model, since it is assumed that the mill contents are perfectly mixed, see Figure 23.

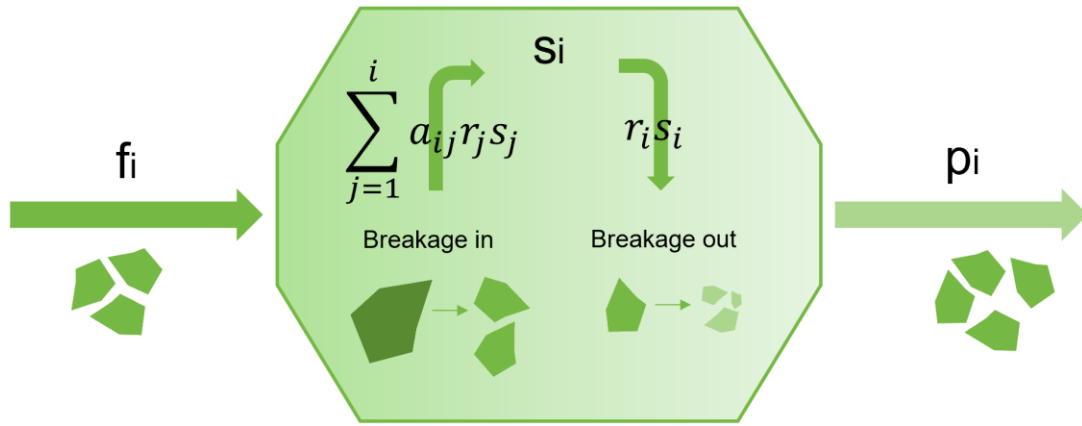


Figure 23: Perfect mixing mill model illustration: for a given size class, all entering particles and all particles generated from the coarser fraction in the mill are either discharged or broken down into smaller sizes.

The following notations are used for the perfect mixing ball mill model:

- f_i = feed in of size fraction i
- p_i = product out of size fraction i
- s_i = material of size fraction i inside the mill
- r_i = rate of breakage of size fraction i
- a_{ij} = appearance matrix, describing which part of the broken particles from fraction i reports to fraction j
- d_i = discharge rate of fraction i out of the mill related to the mill content

The overall balance of a stationary operating mill with the above terms is:

$$f_i + \sum_{j=1}^i a_{i,j} r_j s_j = p_i + r_i s_i \quad (1)$$

The mill contents for each size fraction can be solved from: $p = d \times s$, thus $s = p/d$, and by substituting this in formula (1). Thus, we obtain the mill balance equation that is used in the HSC Sim Ball Mill model for computing the output particle size fractions:

$$\left(f_i + \sum_{j=1}^i \frac{a_{ij} r_j p_j}{d_j} \right) = p_i + \frac{r_i p_i}{d_i} \quad (2)$$

from which the product of size i is obtained with:

$$p_i = \frac{1}{1 + \frac{r_i}{d_i}} \left(f_i + \sum_{j=1}^i \frac{a_{ij} r_j p_j}{d_j} \right) \quad (3)$$

The appearance matrix a_{ij} is assumed on the basis of similar ores (Broadbent & Callcott, 1956) thus, the only terms that need to be fitted to calibrate the ball mill model are r , the breakage rate and d , the discharge rate, with laboratory or pilot tests.

The power calculation is based on the Morrell C-model (Stephen Morrell, 1993), which gives the total power of the mill as the sum of the no-load power and the net theoretical impact power, a function of the charge density, mill dimension and speed settings. The details of the power calculation are described in section 3.2.2.4. This model is scaled up by using the simulated (upscaled) / nominal (laboratory, pilot) ratio of various parameters, such as mill size, mill speed or work index on the breakage rate.

The first simulation of our case study uses the ball mill model described above and has served as a base case for comparison. For the second simulation, a multicomponent ball mill model was selected. The general principle is the same as the one described for the Whiten model, except that instead of giving one breakage and discharge rate function, individual function for each particle population are used. This choice, based on analysis of polished section, separates the particles into two or more, more homogeneous, populations. In this example, this means the heavy sulphides - and particles of interest for the flotation - are one population, and the light gangue the other. Equation 1 is thus adapted for each population, referred to with the index k :

$$f_{i,k} + \sum_{j=1}^i a_{i,j,k} r_{j,k} s_{j,k} = d_{i,k} s_{i,k} + r_{i,k} s_{i,k} \quad (4)$$

In the same way as for the original model, r and d are the main parameters to be fitted. Instead of fitting them to the bulk particle sized distribution, they can be fitted so that

the simulated PSDs match the experimental PSDs for each defined particle population. The fitting of the parameters was achieved with an iterative method, which aims at the minimization of the square-root difference between the experimental process data and the simulated results. These compared values may be PSD, flow rates, or an operational target such as pressure drop in hydrocyclones.

3.1.2.2 Cyclone model

The proportion of particles of a given size d_i directed to the underflow and noted p_i , is calculated using the Plitt/Reid separation efficiency curve (Flintoff et al., 1987):

$$p_i = R_f + (1 - R_f) \left(1 - 0.5 \left(\frac{d_i}{d_{50c}} \right)^m \right) \quad (5)$$

with R_f being the water recovery to the underflow and m the sharpness of separation factor.

The corrected cut size is obtained using cyclone dimensions D_c , D_i , D_o , D_u and h , respectively cyclone, inlet, overflow (vortex finder) and underflow (apex) diameters and cyclone height:

$$d_{50c} = F_1 \frac{39.7 D_c^{0.46} D_i^{0.6} D_o^{1.21} \eta^{0.5} \exp(0.063\phi)}{D_u^{0.71} h^{0.38} Q^{0.45} \left[\frac{(\rho_s - 1)}{1.6} \right]^k} \quad (6)$$

with F_1 being a fitting parameter, Q the flow rate in m^3/h , ρ_s being solid density, ϕ the solid fraction of the feed, k the hydrodynamic exponent and η being fluid viscosity parameter (cP).

In this simulation, the size separation was calculated by particle. The equations used are the same as above, but the solid density ρ_s is then for the specific particle rather than the average of the solid. A more detailed description of the model is available in Appendix 2.

3.1.2.3 Rod mill model

The model used for HSC is adapted from Lynch (1977) and reproduces the plug flow operation of this type of mill. In this model, the tumbling mill is discretized in v stages, which are defined as the length of the mill necessary to eliminate the largest size interval from the pulp, defined as $\sqrt{2}$ times the top size (Figure 24). The number of necessary stages is calculated based on the mill constant.

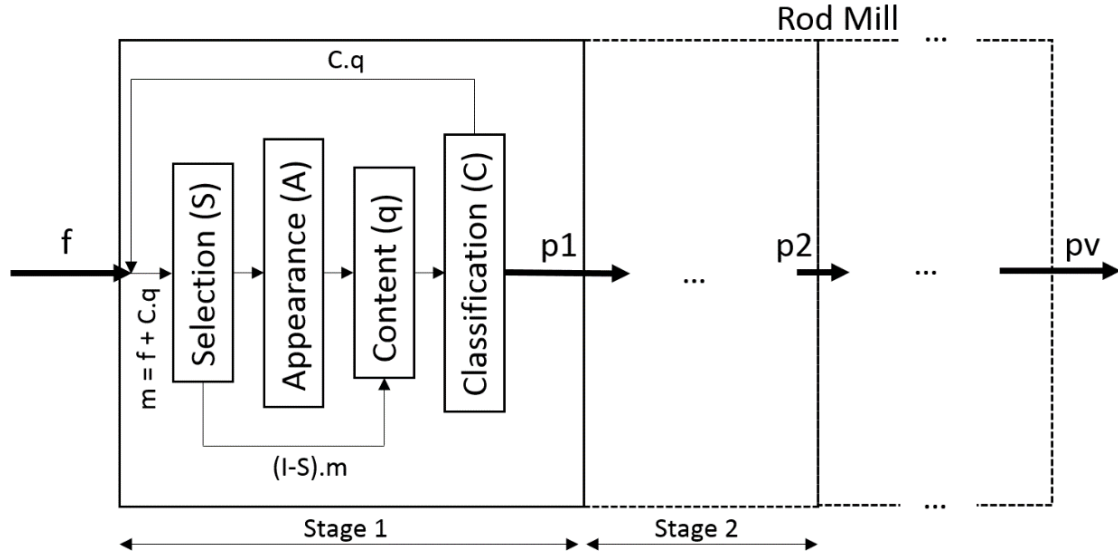


Figure 24: Rod mill plug flow model separated in breakage stages.

The main equations are given below, for stage n and size i , with p representing the product, q the mill content, c the classification parameter, a the appearance matrix, s the selection parameter and m the sum of the current stage feed and post-classified particles:

$$p_{i,n} = (1 - c_{i,n})q_{i,n} \quad (7)$$

$$q_{i,n} = (1 - s_i)m_{i,n} \sum_{j=0}^i (a_{ij}s_j) \quad (8)$$

$$m_{i,n} = c_{i,n}q_{i,n} + p_{i,n-1} \quad (9)$$

The selection function is usually fitted to the laboratory or pilot results, and the model is scaled up by adjusting the mill constant with the simulated to fitted ratio of the mill size, load fraction, speed and feed size.

3.2 Dynamic SAG/AG mill model study

The vast majority of mill models describe steady state and does not consider transient phases, such as fill-up or changes in the feed rates. For training simulators and safety procedure design it is important to include transient phases in the mills. Indeed, reaction time between a parameter change and its impact on the process is a critical variable to take into account for process optimization. For instance, an interesting OTS exercise consists of changing a parameter in the comminution circuit, such as increasing the mill rotation speed, and getting the mill operators to observe how long they have to wait to see an actual change in the flotation recovery. For the system control validation and testing, the time dependence of the process is an important parameter to simulate as well. The validation of the model presented below rely on a sampling campaign realized with the help of First Quantum Mineral Pyhäsalmi personnel on the primary SAG mill of their processing plant.

The conceptual model chosen for this update is initially proposed by Valery and Morrell (1995). This model is selected because it is easily adaptable to HSC Sim SAG/AG mill model and reuse several parameters already present for static calculation. Moreover, it was successfully implemented, in parts or entirely, in several studies (Li et al., 2018; Salazar et al., 2009) and recent studies continues to use and update it (Yu et al., 2018).

3.2.1 Material

The dynamic model was validated against a step test conducted in the Pyhäsalmi plant (Finland). This plant is operated by First Quantum Minerals and processes a copper-zinc ore. The Pyhäsalmi deposit is a VMS type, and the ore is mainly composed of chalcopyrite and sphalerite associated with pyrite and pyrrhotite.

The first part of the Pyhäsalmi plant grinding circuit consists of a SAG grinding mill (LM2J) fed by crushed ore (P80 ~ 15mm) and pebbles (P80 ~ 175mm). The pebbles consist of ore coming from the oversized fraction of the crushing circuit. The LM2J mill is followed by a closed circuit of hydrocyclones clusters and SAG mills in parallel, where the cyclones overflow P80 is around 140µm. The overflow is directed to a last

closed circuit with a ball mill and a cyclone cluster (the feed is separated between several hydrocyclones gathered in a cluster), the overflow of which goes to flotation at an average P80 of 100 μ m. Appendix 8 shows the grinding circuit flowsheet.

Comminution test work of run of mine sample was carried out by Ammtec for Outotec in 2009. The breakage parameters obtained with JK drop weight tests (Stark et al., 2008), summarized in Table 8, were used for the HSC simulation.

Table 8: Pyhäsalmi ROM sample AG/SAG breakage parameters.

Sample Identity	AG/SAG parameters			
	A	b	A x b	Ta
ROM sample	69.4	2.51	174.2	0.72

3.2.1.1 Sampling method

Samples were taken to characterise the behaviour of the first SAG mill (LM2J). The step test involved changing LM2J crushed ore feed rate from 120tph to 90tph and back to 120tph. The 90tph step started at 11:20 and stopped at 13:00 for a total duration of 1h40. Total power consumption monitored by the plant was collected from 10:24 to 14:36 (in time steps of 6 minutes) and data are listed in Appendix 9. It is noticeable that the water input to the mill was not controlled and stayed the same throughout the experiment (40.5 \pm 0.5tph). As a result, the percentage solid and the pulp density of the feed, mill content, and mill product changed as well.

The crushed ore stream was sampled from the feed belt with a belt cutter and 10kg of sample was collected before the step test.

The SAG output stream was sampled with a stream cutter and each sample was 1.2L \pm 0.2L of pulp. The first sample (sample 0) was collected at 11:10, just before the step. Then, samples were collected every 10 minutes while the crushed ore feed rate was at 90tph (sample 1 at 11:25 to sample 10 at 12:54). After the crushed ore feed rate returned back to 120tph, the SAG output was still sampled every 10 minutes for 1h (sample 11 at 13:11 to sample 16 at 14:00). During the experiment, pulp changed from 2.5g/cm³ at 77% solid (at 120tph of crushed ore) to 2.3 g/cm³ at 65% solid (at 90tph of crushed ore).

All SAG output samples were dried at the plant and brought back to Outotec Research Centre for sieving analysis along with the crushed ore sample.

Crushed ore sieving analysis results are presented Table 9 and the SAG product samples sieve analysis results are presented Appendix 11.

Table 9: Crushed ore (LM2J feed) sieve analysis results.

Size (µm)	Retained (g)	Retained (%)	Cumulative passing (%)
25000	860	9	91
10000	1468	15	76
8000	404	4	72
5000	529	5	67
4000	226	2	64
2500	547	6	59
1250	1108	11	47
850	798	8	39
710	144	1	38
200	2109	22	16
150	492	5	11
106	357	4	8
38	542	6	2
-38	207	2	

The step used for this experiment, a variation of 25% of the crushed ore feed rate, was sufficient to observe the impact of the change on the mill energy consumption as well as on the discharge particle size distribution. According to the plant manager, the steady state following the step change was expected to happen about 1.5h after the change in the feed rate. According to the results, a steady state was almost completely reached after 1h40 at 90tph, before returning back the feed rate to the usual tonnage.

3.2.1.2 Results of the sampling campaign

There were short interruptions (less than 2 minutes) of the mill feed before and during the step test. One before 10:33am and one at 12:15, which are noted in Appendix 10. These kinds of event are typical in the lifecycle of the plant and thus such occurrence offers the opportunity to assess the simulation ability to predict and analyse downstream consequences of such instabilities. For instance, it appears that

the size distribution became slightly coarser (see Appendix 12) as a possible reaction to the interruption.

Particle size analysis and mill power consumption show consistent results with the step test. As expected, the power consumption diminished when the feed flow rate was decreased, as did the product size distribution (Figure 25). Conversely, when the feed tonnage increased back to the normal working value (120tph), the particle size distribution became coarser again (Figure 26) and power consumption increases back as well. Individual PSD data are reported in Appendices 11 and 12.

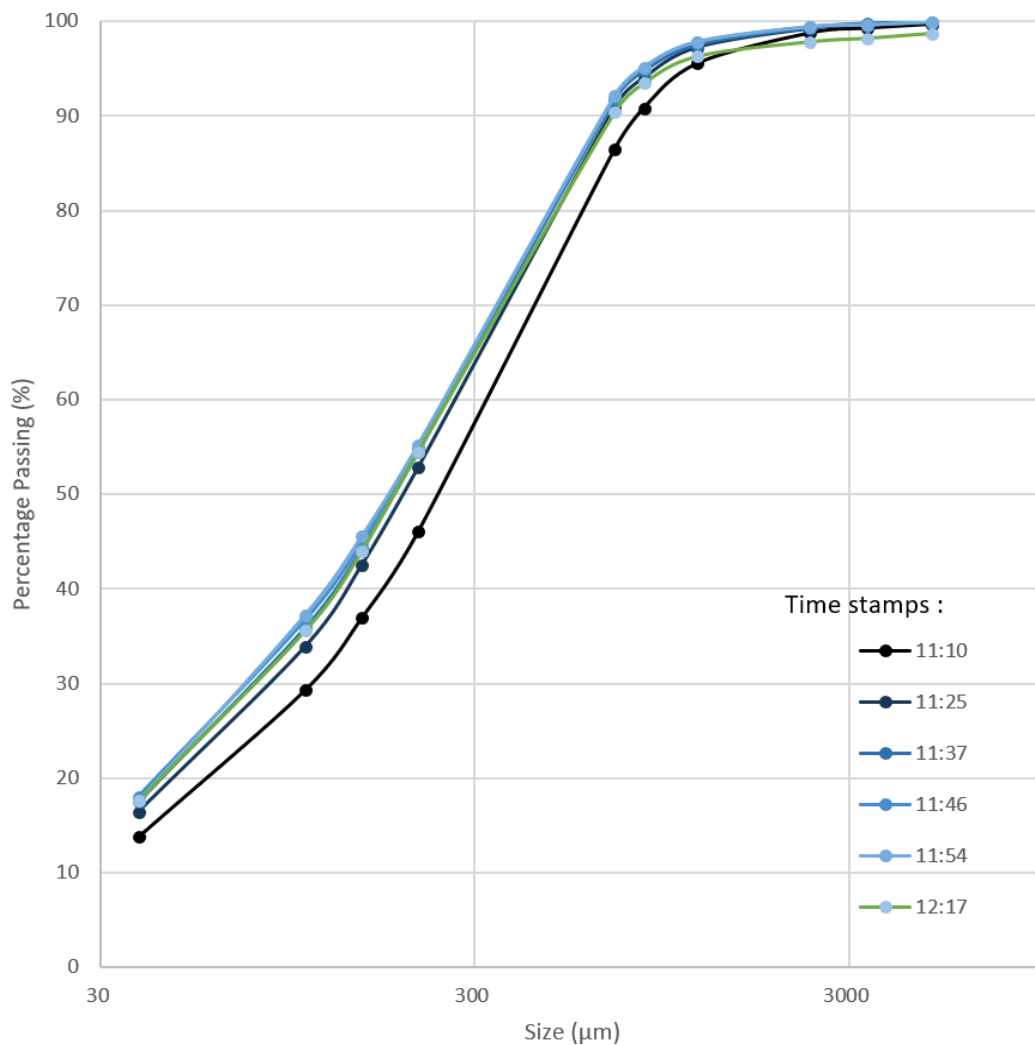


Figure 25: Particle size evolution when the crushed ore feed flow rate was changed from 120tph to 90tph.

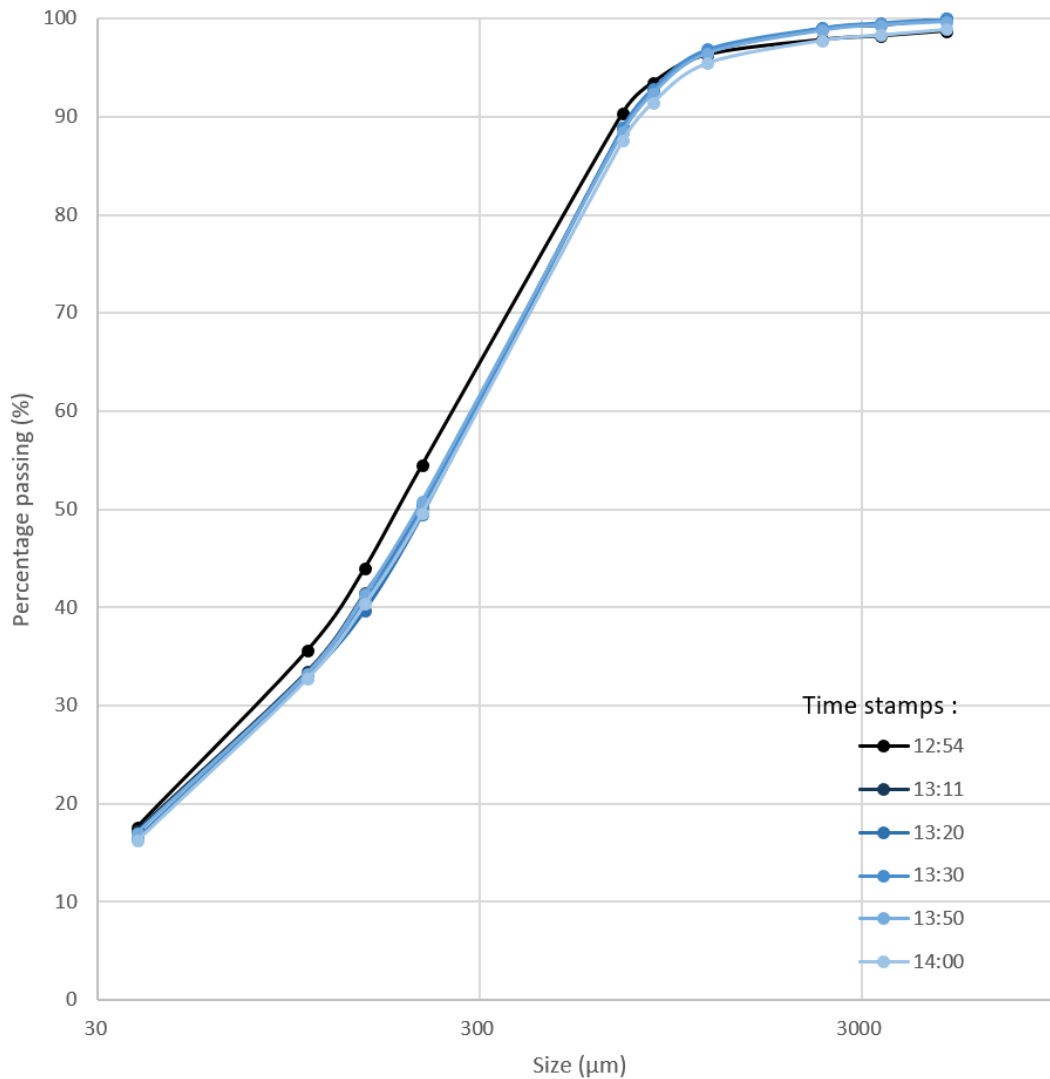


Figure 26: Particle size evolution when the crushed ore feed was changed from 90tph to 118tph.

The following steps of this sampling experiment were to build a simulation around the LM2J mill and to try to reproduce the variation in the feed rate.

3.2.2 Modelling methods

3.2.2.1 Perfect mixing mill model

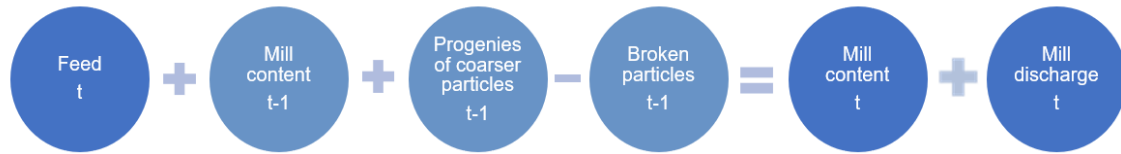
HSC Sim SAG/AG models in static mode are considered as a perfectly mixing ball mill model, in which the grinding process can be described as the function of both transportation through the mill and breakage inside the mill. It is possible to use this model as well in dynamic mode while preserving mass preservation hypothesis.

The following notation will be used:

- f_i : feed in of size fraction i in tons
- p_i : product out of size fraction i in tons
- s_i : mill content of size fraction i in tons
- r_i : rate of breakage for size fraction i (in 1/h)
- a_{ij} : appearance matrix, describing how much of the size i particle broke into class j
- d_i : discharge rate for the size fraction i (in 1/h)
- Δt the time step in hours

3.2.2.2 Population balance model in the dynamic model

The particle size distribution of the system can be evaluated based on the balance of the masses for a given size i and at a given step of time t . This equation stays valid during the mill filling phase when the mill output is simply equal to 0:



Which gives with the above-mentioned notation:

$$s_{t,i} = s_{t-1,i} + \sum_{j=1}^i a_{ij} r_j \Delta t s_{t-1,j} - r_i \Delta t s_{t-1,i} + f_{t,i} - p_{t,i} \quad (10)$$

With $p_{t,i} = d_i \Delta t s_{t,i}$

In this model, three parameters are needed: the rate of breakage, discharge rate and appearance matrix. The mill content is then computed at each time step and in case the mill is discharging, the product is calculated and removed from the content (see Figure 27).

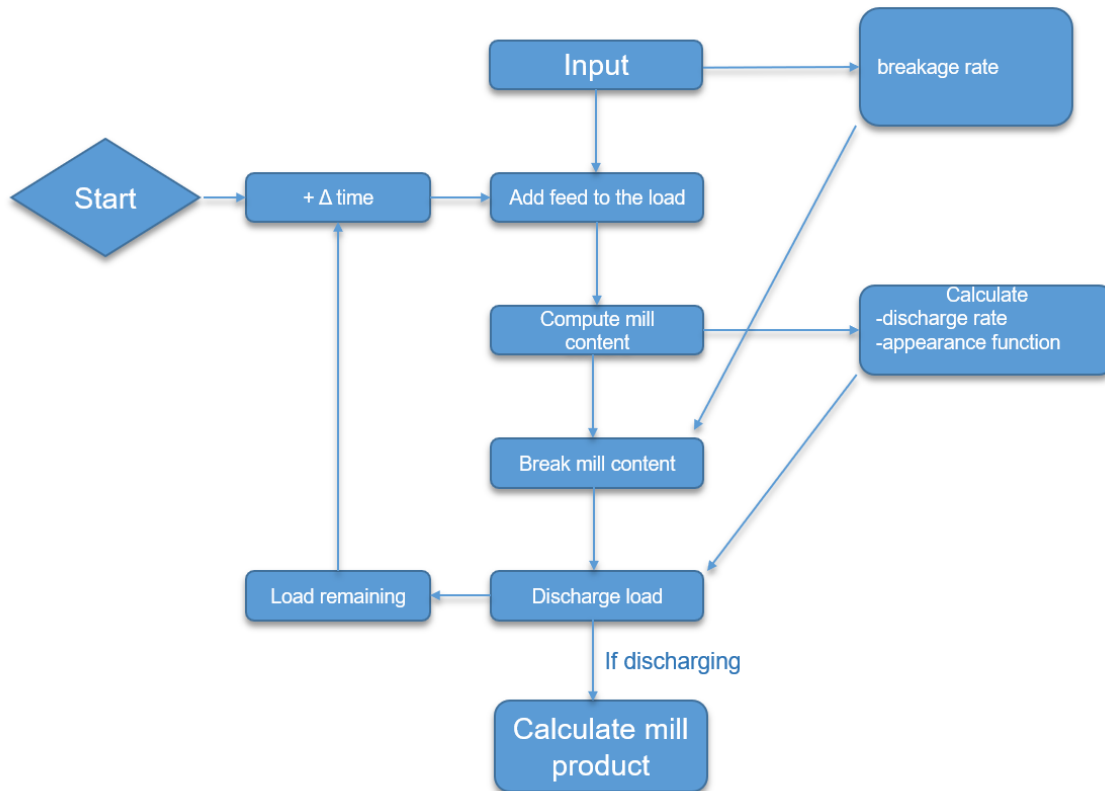


Figure 27: Steps for the dynamic calculation of the mill model content and product PSD.

The calculation of the appearance functions for the AG/SAG is the same as in static mode and describes the distribution of the progeny size of a particle being broken down. It uses A , b and T_a parameters which are measured using drop weight and abrasion tests (Bearman et al., 1997). The appearance function can be divided into two subfunctions:

- The high energy appearance function, described by the A and b parameters, which represents how particles break from high energy mechanism such as impact or compression forces. This is dominant for medium to fine sized particles.
- The low energy appearance function, described by the T_a parameter, which represents how a particle breaks from attrition forces, dominant for coarse particles.

The high energy appearance function is based on the specific energy parameter (E_{cs}), calculated for each size fraction and as function of the mill content (Figure 28). As such, the high energy appearance function changes for each size fraction at each time

step, as a function of the mill charge and particle size distribution. The low energy function; however is non-size specific and non-dependent on the mill content thus it is not updated through time. The compilation of appearance functions for each size class eventually gives the appearance matrix.

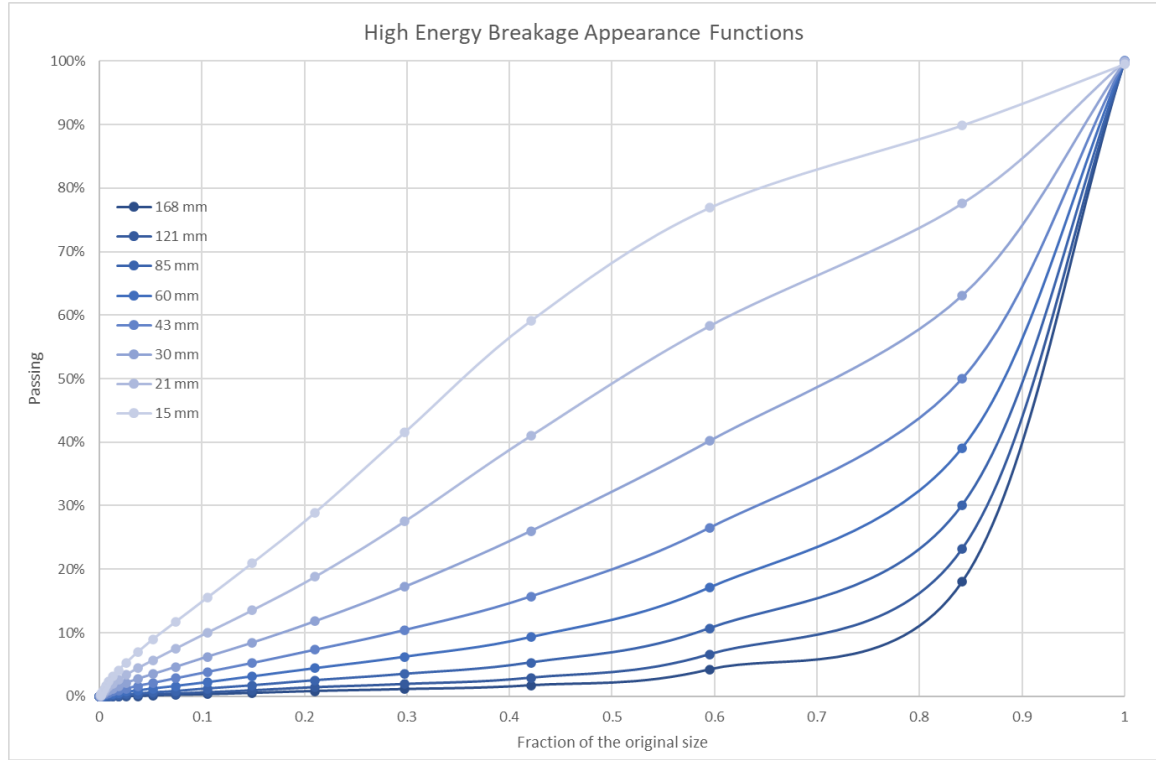


Figure 28: High energy appearance functions for various size fractions for a given mill content state.

3.2.2.3 Discharge and breakage rates calculation method

As in the static calculation, the breakage rates are fitted to the experimental results. It is best to have several steady states results for optimal fitting. With other parameters such as X_m (see below), the breakage rates are part of the critical parameters to be fitted to the process for SAG/AG mill simulation.

In dynamic mode, the equations developed by Morrell and Stephenson (1996) are used to compute the maximum discharge rate, which is determined by the relation between holdup and flow rate out of the mill. The flow rate out uses two equations to describe the slurry flow via the grinding media (Q_m in m^3/h):

$$Q_m = k_m J p_m^2 \gamma^{2.5} D^{0.5} A \phi^{-1.38} \quad (11)$$

and via the slurry pool (Q_t in m^3/h):

$$Q_t = k_t J p_t \gamma^2 D^{0.5} A \quad (12)$$

where k_m and k_t are two constants, $J p_m$ and $J p_t$ the fractional slurry holdup in the media and in the slurry pool, respectively, γ the mean relative radial position of the grate apertures, D the diameter (m), A the open area percentage and ϕ the critical speed fraction.

Then, the maximum discharge rate, D_{max} (h^{-1}), is computed being equal to the ratio of the outflow rate by of the mill content volume:

$$D_{max} = \frac{Q_m + Q_t}{\text{Mill Content volume}} \quad (13)$$

The complete discharge rate function is subsequently calculated based on X_m (size of particle behaving like water), X_g (grate size), X_p (size of pebble aperture) and the pebble port aperture percentage, as show in Figure 29. X_m , X_g , X_p and the pebble port aperture are variables that may be fitted to the process.

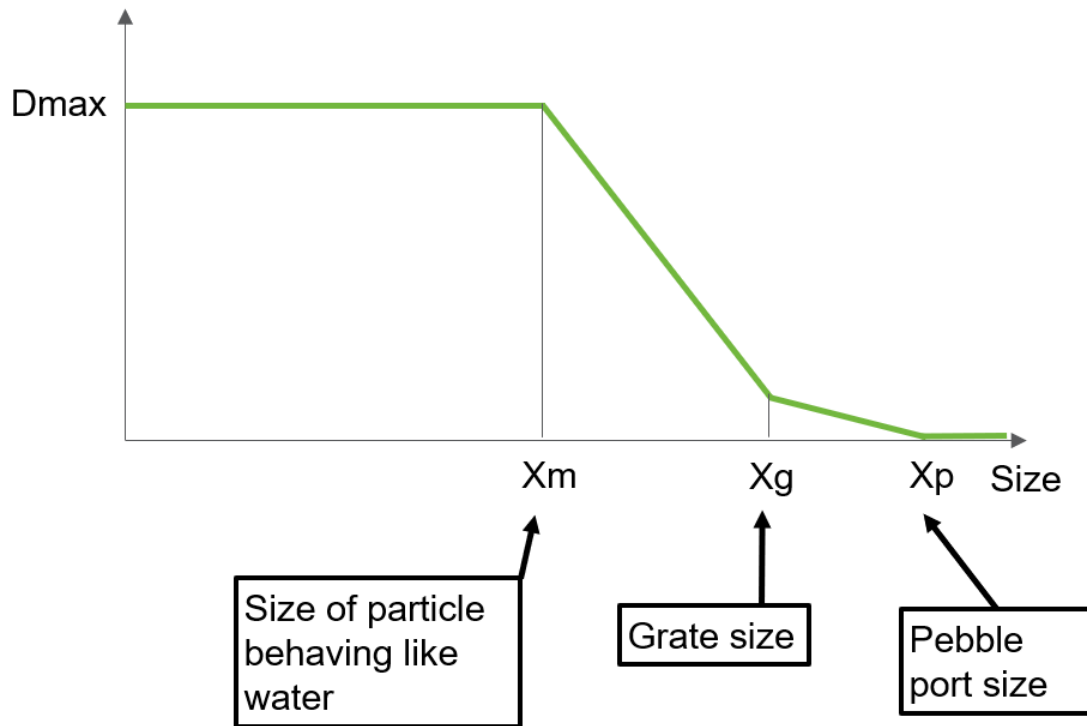


Figure 29: Discharge function for the SAG/AG mill.

3.2.2.4 Power model

The HSC Sim SAG mill model uses the Morrell C-model (S. Morrell, 1996) which estimates the *Total Power* draw of the mill as a sum of:

- *No Load Power*, referring to mill power draw without any load inside;
- *Net Power*, which is a calculated net theoretical impact power multiplied by a calibration factor. The calculation takes into account whether the mill is a grate or overflow type.

The calculation procedure includes the following steps:

Calculate the trunnion diameter ($D_{Trunnion}$) from the mill diameter (D):

$$D_{Trunnion} = 0.251 \times D \quad (14)$$

Calculate the centre line length (L_c) from the mill length (L), the feed and end cone angles (α_{Feed} , $\alpha_{Discharge}$ in degrees), and the trunnion diameter:

$$L_c = L + 0.5(D - D_{Trunnion}) \left(\tan(\pi\alpha_{Feed}) + \tan(\pi\alpha_{Discharge}) \right) \quad (15)$$

Net theoretical impact power is calculated by using:

- Total charge density
- Mill speed
- Mill diameter (inside liners)
- Centre line length
- Trunnion diameter
- Mill load fraction
- Fraction of critical speed

No load power is calculated by using:

- Mill length
- Centre line length
- Mill diameter (inside liners)
- Fraction of critical speed

Firstly, HSC calculates the charge density, with m_{ball} , m_{water} , and m_{solid} being, respectively, the mass of the balls, water, and solids component of the slurry and V_{charge} being the total volume of charge in the mill:

$$d_{charge} = (m_{ball} + m_{water} + m_{solid})/V_{charge} \quad (16)$$

The mill RPM is obtained from the mill fraction of critical speed ϕ :

$$RPM = \phi \times \frac{30}{\pi} \times \sqrt{\frac{9.81}{D/2}} \quad (17)$$

The toe angle position (t) in radians, defined as:

$$t = A(1 - e^{-B(\phi_c - \phi)}) + \frac{\pi}{2} \quad (18)$$

is estimated, where A and B parameters are functions of the mill fractional filling, and ϕ_c is the mill critical speed.

The mill shoulder angle position (s) in radians is estimated using:

$$s = \frac{\pi}{2} - (t - \frac{\pi}{2})(E + FJ_t) \quad (19)$$

where E and F parameters are functions of the mill fraction of critical speed and J_t is mill fractional filling.

Then the mill charge inner surface radius (r_i) is calculated using the relation between mill radius (r), s and t from equations 18 and 19, and the mill fractional filling (J_t):

$$r_i = r \sqrt{1 - \frac{2\pi\beta J_t}{2\pi + s - t}} \quad (20)$$

by using:

- The active fraction of the charge (β)

$$\beta = \frac{t_c}{t_c + t_f} \quad (21)$$

with t_c being the mean time to travel between the toe and the shoulder:

$$tc = \frac{2\pi + s - t}{\pi(RPM/60)} \quad (22)$$

- The mean time to travel from the shoulder to the toe in free fall (tf):

$$tf = \sqrt{\frac{(\sin(s) - \sin(t))}{9.81}} \times r \left(1 + \sqrt{1 - \frac{2\pi J_t}{2\pi + s - t}} \right) \quad (23)$$

In addition, an extra variable z is used to relate the charge inner radius (r_i) to the theoretical normalised radius (r_0) at which the tangential velocity is supposed to be null. The relation between r_i and r_0 is found to be a function of the fractional filling, and is interpolated from laboratory tests realised in glass mill (Stephen Morrell, 1993):

$$z = (1 - Jt)^{0.4532} \quad (24)$$

The kinetic energy allowance (KE) is calculated as follows, using equations 17, 20 and 24:

$$KE = L d_c \left(\frac{\pi r RPM/60}{(r - z r_i)} \right)^3 ((r - z r_i)^4 - ((z - 1) r_i)^4) \quad (25)$$

A correction parameter due to the presence of a slurry pool ($Corr_{Overflow}$), which will decrease the power draw of an overflow mill compared to a grate-discharge mill, is obtained using:

The angle of the slurry pool (to), which is equal to t in the case of a grate mill discharge. Estimated angle to be 3.395 rad in the case of an overflow mill discharge.

$$Corr_{Overflow} = \frac{(9.81 \pi L d_{pulp} r RPM/60)}{3 r - z r_i} (2r^3 - 3 z r_i r^2 + (3z - 2)r_i^3) (Sin(t) - Sin(to)) \quad (26)$$

Then, we need to calculate the correction factors ($Corr_{Cone}$) due to the conical end section, taking into consideration the charge moving in these sections of the mill, by calculating the power used (P_{Cone}) and kinetic energy allowance in these sections (KE_{Cone}) with r_t being the radius of the trunnion:

$$P_{Cone} = \frac{9.81 \pi (Lc - L) RPM/60}{3(r - r_t)} (r^4 - 4 r r_i^3 + 3r_i^4) \times [d_{charge}(Sin(s) - Sin(t)) + d_{pulp}(Sin(t) - Sin(to))] \quad (27)$$

$$KE_{Cone} = \frac{2 (Lc-L) d_c (\pi RPM/60)^3}{5 (r-r_t)} (r^5 - 5 r r_i^4 + 4 r_i^5) \quad (28)$$

$$Corr_{Cone} = P_{Cone} + KE_{Cone} \quad (29)$$

The first part of the total power, the theoretical impact power ($NTIP$, kW), is finally calculated as:

$$NTIP = \frac{(9.81 \pi L d_{charge} r RPM/60)}{3 r - z r_i} (2r^3 - 3 z r_i r^2 + (3z - 2)r_i^3) (Sin(s) - Sin(t)) + KE + Corr_{Overflow} + Corr_{Cone} \quad (30)$$

The second part of the total power, the “no-load” power (NLP , kW), i.e., the power used by the mill when emptied, is estimated by using the fraction of critical speed (fCs) and the mill dimensions:

$$NLP = K D^{2.05} (fCs(0.33 Lc + 0.67 L))^{0.82} \quad (31)$$

where K is a constant accounting for the optional use of gear and pinion drives.

Finally, the mill total power (TP , kW) is calculated, using the results of equations 30 and 31, as:

$$TP = NLP + k \times NTIP \quad (32)$$

where k is a factor to convert the power draw of the mill charge into observed gross motor power.

In the SAG/AG mill model in dynamic mode, these calculations are carried out for every time step. Indeed, at every step, the mill content – amount of pulp, pulp density, size distribution of the solid fraction – varies and so does the power consumption.

3.2.2.5 Simulation process

The process was simulated with the HSC Sim grinding AG/SAG mill model, presented above, compatible with dynamic simulations. Three streams were modelled to feed the mill: the fine (crushed) ore stream, pebble stream and water stream (Figure 30).

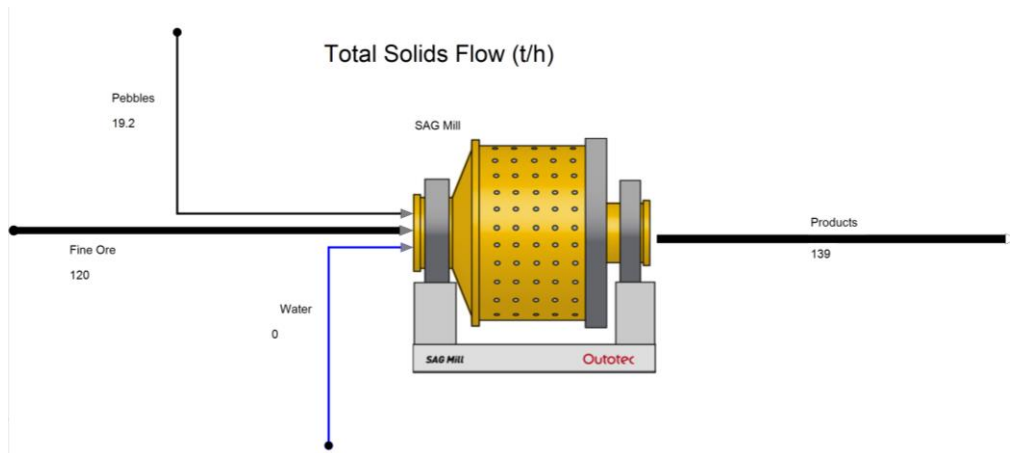


Figure 30: Flowsheet used for the dynamic simulation of LM2J.

The mill parameters and dimensions (diameter, length, feed and discharge angles, speed and media charge) obtained from the Pyhäsalmi plant personnel are presented within the HSC interface in Figure 31. The breakage function (A , b and T_a) parameters were derived from the Ammtec study (Table 8). The X_g and port fraction used were derived from a previous simulation study on LM2J, conducted for audit work. X_m was fitted to the process as detailed in section 3.2.2.6.

Parameter	Value	Unit	Description
Settings			
Tolerance	0.0001		For mineral balance iteration
Max Iteration	25		For mineral balance iteration
Activate Warning Messages	<input type="checkbox"/>		Activate load / max throughput warning messages
Dimensions and Physical Properties			
Mill Type	SAG		SAG or AG mill
Variable Rates	<input type="checkbox"/>		Breakage rates calculated using Variable Rates model based on mill operating point
Diameter	3.1	m	Without liners
Length	4.2	m	Mill length
Feed Cone Angle	11	degrees	Feed end geometry
Discharge Cone Angle	0	degrees	Discharge end geometry
Liners	100	mm	Thickness
Backing Rubber	6	mm	Thickness
Ball Load Fraction	5.8	%	Ball charge (Typical: 0-12)
Ball Diameter	100	mm	Grinding media top size
Ball Density	7.84	kg/dm3	Grinding media
Charge Porosity	40	%	Ball/Rock charge porosity
Calibration Constant for Mill Power	1.34	*	(default = 1.26)
Fraction of Critical Speed	75	%	Typical: 55%-80%
Ore Properties			
Ore Work Index	14	kWh/t	
Ore Abrasion Index	0.3		
Grate Parameters			
Xg	3	mm	Grate aperture size (Typical: 15-30mm)
Xm	0.28	mm	Fine size behaving as water in outflow
Pebble port fraction	0	%	
Weighted Radius Fraction	0.75		Gamma - mean relative radial position of the grate apertures
Open Area	9.6	%	Area of the apertures (without pebble ports)
Rn	0.91	*	(Dynamic) Radius of the outermost row of grate holes, relative to mill radius
Discharge Coefficient	10 000		For mill outflow calculation
Breakage Function and Mass Transfer			
Breakage Parameter A	69.4	%	High energy breakage relation parameter
Breakage Parameter b	2.51	*	High energy breakage relation parameter
Ta	0.72	*	Abrasion parameter
m1	0.44	*	Mass transfer parameter
m2	0.5	*	Mass transfer parameter

Figure 31: LM2J parameters for the simulation.

During the simulation, feed flow rates were changed with the Dynamic Dialog tool *SET* page (Figure 32). On this page, it is possible to define which values are to change, when, and to what new value. In this example, two values were changed: the crushed ore (fine) tonnage (tph) and the pebble feed rate (tph). These two values and their variations were obtained from Pyhäsalmi control system logs, as shown in Appendix 9.

In order to smoothen and remove data noise in the variations of the feed rate, real tonnage values from Pyhäsalmi control log (see Appendix 9) were actually fed to two PID (proportional integral derivative) controllers via the Dynamic Dialog. The first controls the crushed ore feed rates, while the second adapts the pebble feed rate. Even though the pebble feed rate was not the subject of this step tests, some variations were detected and were thus reproduced in this simulation.

rate was above 120tph, at an average value of 125ph of crushed ore. During the step test, the feed rate was around 90tph and after the step, feed rate returned to a value lower than 120tph, at about 118tph. These three actual feeding states are thus chosen to fit the model to these different steady state phases.

The model fitting for these three steady states consisting of reproducing particle size distribution and power consumption with the adaptation of the breakage rates by minimize the residual between observation and simulation. The first state, at 125tph used a target mill power consumption of 457 ± 3 kW, a P80 of 600 μ m and a P50 of 248 μ m. The second state at 90tph used a target mill power consumption 426 ± 3 kW, a P80 of 518 μ m and a P50 of 182 μ m. Finally, the last step at 118tph was fitted to a power consumption of 440 ± 3 kW, a P80 of 585 μ m and P50 of 205 μ m.

3.3 Training simulator conception

This case-study simulator was constructed to train operators to run a flotation circuit at a greenfield plant. The process simulation was developed using Outotec HSC Sim software and was based on a generic spodumene flotation plant flowsheet.

3.3.1 Background and process description

This case study intended for operator training was conceived for generic use and is based on open-source research publication and knowhow, with references given below.

The model feed composition mimics a typical spodumene-bearing pegmatitic ore. The process simulation involved the modelling of a desliming step with hydrocyclones, magnetic separation to remove ferromagnetic mineral, a mica flotation step and rougher spodumene flotation, followed by two cleaning steps with tails recirculation. The flowsheet model also included several dewatering units for the spodumene concentrate, flotation tails, ferromagnetic product water removal and a drying step for adjusting the moisture of the final spodumene product.

3.3.1.1 Flotation training process

Certain theoretical knowledge, such as flotation cell parts and flotation parameters, is key training aspects for process operators. Trainees have to understand the roles of froth phase, frother addition, conditioners, collectors, depressants and pH conditions. A basic understanding of flotation stages– cleaner, scavenger and rougher - and their roles, as well as the organization of cells in banks, is an important goal of the training.

The training also aims at assisting the operators with calculation steps, by provision of tips, particularly for calculation performed regularly when dealing with a flotation cell. This encompasses conversion from one unit (kg to tons, l/min to m³/h, etc.) to another and calculation of concentration (from reagent dosage for instance), process recovery or the flotation bank mass pull. All these calculations are usually implemented in the control system of the plant. However, an operator may detect abnormal behaviour just by recalculating some parameters, in case of a captor fault for instance. The operators also need to be trained to understand system controllers, detect problems and find their potential causes.

Some practical competencies cannot be learned by theoretical training alone. This includes reaction to alarms, a skill which can only be gained when confronted with the situation. For instance, training to operate pump-sumps, a component of a flotation circuit, is often overlooked but knowledge of the most common issues and alarm situations is quite important to avoid pulp floor spills. Elements of procedure training, for which a real situation training is impossible, can be reproduced in a simulation environment. This includes start-up or emergency shutdown. Finally, the training also aims to give operators optimization skills in order to achieve maximal recovery and thus more sustainable operation, e.g. optimization of the reagent consumption or machine down time and limitation of pulp losses.

3.3.1.2 Construction of the flowsheet

The particular simulator feed composition used here represents a typical spodumene-bearing pegmatitic ore, composed of quartz, feldspars, mica (muscovite), spodumene and iron-bearing oxides (Stephen E. Kesler et al., 2012). Usually, spodumene flotation involves reverse flotation of the gangue (Filippov et al., 2019), where amines are employed as collectors. For the direct flotation of spodumene, the usual collector is oleic acid in an alkaline pH setting. Even though the training mainly focuses on flotation, other important steps of the process are incorporated into the simulation, such as desliming, magnetic separation and dewatering. The final flowsheet consisted of:

- A desliming step with hydrocyclones. The desliming process stage is used to remove fine particles which have a negative impact on flotation recovery;
- Magnetic separation to remove ferromagnetic mineral, such as magnetite, from the deslimed stream;
- A reverse flotation step, which can be bypassed for training purposes;
- A rougher spodumene flotation step followed by two cleaning steps with recirculation;
- Several dewatering phases for spodumene concentrate, flotation tails, ferromagnetic product as well as a drying step for the final spodumene product.

The entire circuit is illustrated in the Figure 34.

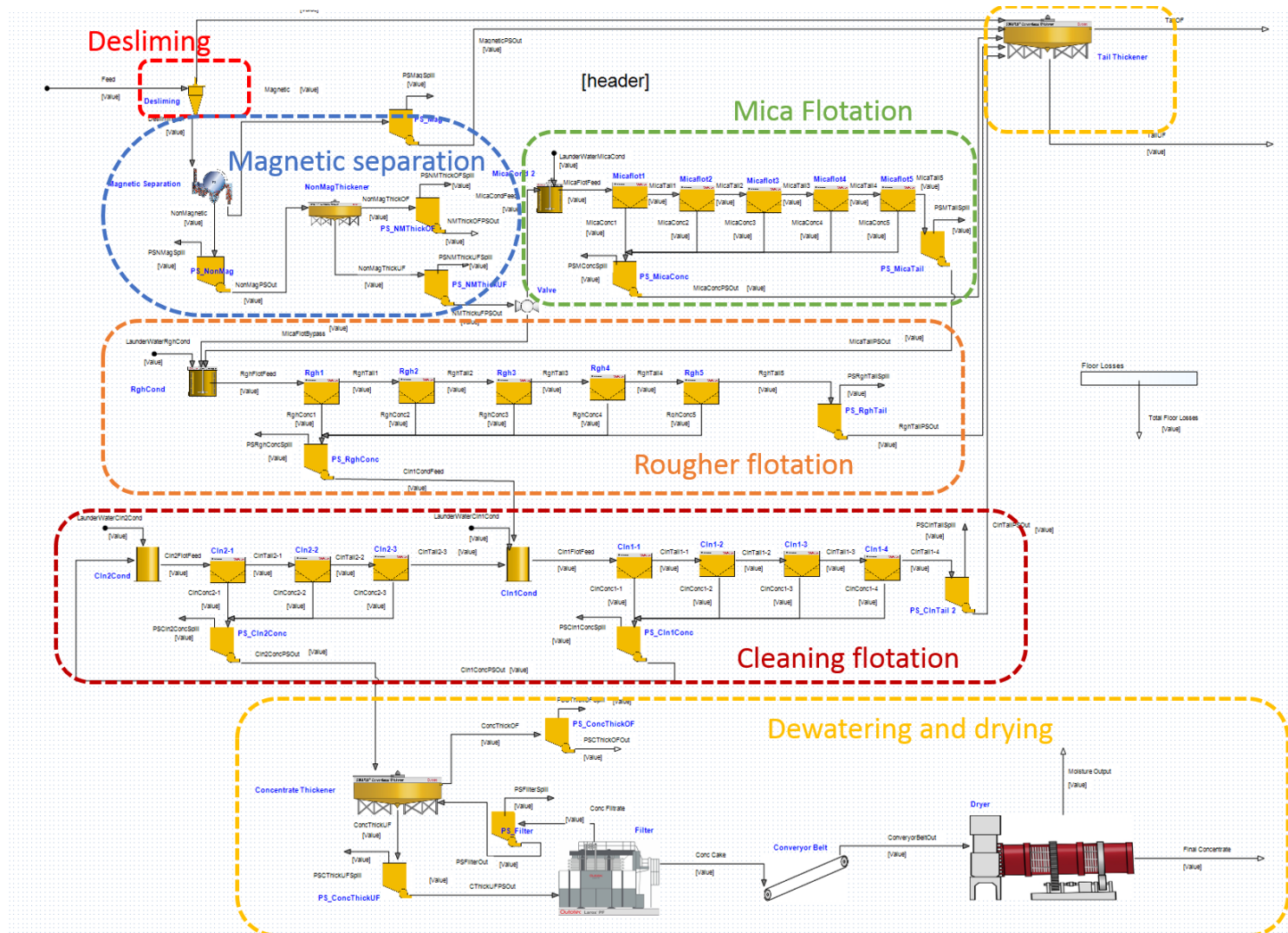


Figure 34: Spodumene flotation simulator flowseet used for operator training, as seen in HSC Sim.

3.3.2 Simulator requirements

The purpose of this simulator and the central question to address was how to train operators to maintain a spodumene flotation circuit in optimal conditions during transient and steady-state phases. A real-time simulator enables the trainees to get used to start-up and shutdown procedures, and to the temporary effects of control parameter changes. It is also more comprehensive than a steady-state simulator, for instance with integration of the filling time of pump sumps, a detail which can be overlooked in classical simulation.

The purpose and general scope of the simulator were defined prior to its conception and are presented in Figure 35. These specifications guided the choice of models, UI conception and controller implementation.

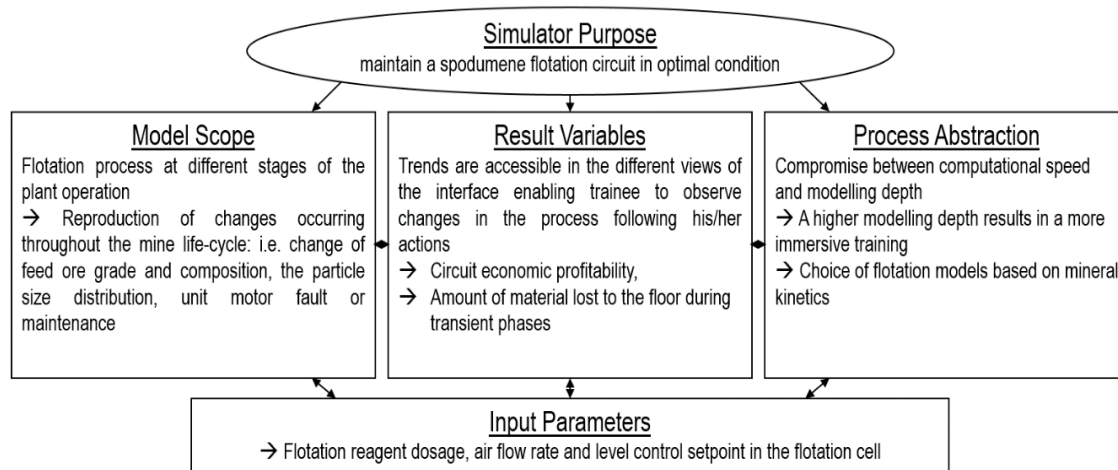


Figure 35: Purpose, scope, result variables, process abstraction and input parameters of the spodumene flotation simulator.

The training consists of several exercises, each depicting a situation an operator could encounter during plant operation (e.e.: modification of the feed grade and PSD or issue with the machinery). The first exercises aim to familiarise the trainee with the simulation environment and system control itself and get to know the accessible parameters and UI operation. Subsequent exercises require increasing knowledge of the process and put the operator in less usual contexts, such as emergency procedures or a programmed shutdown.

This simulator is also used to evaluate trainees at the end of their course. The practical exercises and evaluations are integrated in the simulation. In these practical exercises, the operator will be required to change reagent dosages, air flow rate and cell level to achieve the best circuit profitability. In addition, the simulator is designed to be combined with an external theory notebook and evaluation tests.

3.3.3 Simulator construction

This section summarizes the construction process of the simulator, firstly by defining the input stream content and then by choosing and implementing the relevant unit models.

3.3.3.1 Feed and particles used

A feed blender unit (perfect mixer) is implemented in HSC to control the head grade of the circuit described above in the automation system. This unit does not reflect a real plant process and is simply a means to create an easily adjustable feed. Four input streams are directed to the feed blender:

- Spodumene, 100% solid, composed of 100% spodumene (Spd)
- Magnetite, 100% solid, composed of 100% magnetite (Mgt)
- Gangue, 100% solid, composed of:
 - 25% quartz (Qtz)
 - 25% muscovite (Ms)
 - 25% albite (Ab)
 - 25% microcline (Mc)
- Water 100% liquid

The output stream of this unit is the “Blend Feed”, which is the sum of the four input streams.

As the solid and liquid flow rates of each input stream can be a manipulated variable in the automation system PID controllers, it is thus possible to control the grade of spodumene and magnetite (in %) and the solid percentage of the Blend Feed stream.

The blend feed is then directed to a unit designed to modify the particle size distribution of the stream. It uses the “Fixed PSD” unit model, which changes the

amount of particles in each size class so that the output PSD corresponds to the user given Rosin-Rammler distribution. In this circuit, five size classes are in use:

- 1.4-2 mm
- 0.7-1.4 mm
- 0.35-0.7 mm
- 0.02-0.35 mm
- <0.02mm

The Fixed PSD unit enables the operator to change the D63.5 (μm) and the Rosin-Rammler slope of the output distribution, which is the Feed stream, directed to the first process unit of the circuit (Desliming). The default parameters are:

- D63.5: 150 μm
- Slope: 1.5

3.3.3.2 Newly implemented and improved models

The HSC Sim process simulation software provides dynamic empirical and semi-empirical models of flotation cells, conditioners and pump sumps coupled with steady-state models for dewatering and classification units. The flotation cell and conditioner models need to be combined, as explained below.

3.3.3.2.1 Conditioner and flotation cell models

The flotation cell models separate particles into concentrate and tails streams according to the recovery equation and kinetic parameters set in the conditioner unit, described further below. Kinetic parameters were defined for each particle, and were modified by the dosage of frother, collectors and pH modifier, based on studies Grau, Laskowski and Heiskanen (2005) and Tian *et al.* (2017).

The kinetic parameters are inputted into the conditioner model. The conditioner model assigns flotation characteristics to each particle depending on the chosen behaviour such as infinite recovery, fast floating proportion, slow floating proportion, etc. In HSC Sim, four flotation models are available: rectangular distribution, one-component distribution, two-component distribution and three-component distribution. For this simulation, a rectangular distribution was chosen for the three

flotation processes (mica flotation, rougher flotation and cleaning flotation). Flotation parameters are defined for each of these flotation stages.

The rectangular distribution is a discretized version of the Klimpel (1980) model. The advantage of this model is that with only two parameters, a distribution of flotation behaviours is generated resulting in various flotabilities of particles. Particles are divided into a discrete number of floatability types, ending up with the maximum kinetic rate k_{max} . The second parameter, infinite recovery R_{∞} , describes the proportion of floating particles had the process lasted an infinite amount of time. These parameters and their relation to particle recovery (R) are given in Table 10, for batch laboratory recovery and continuous recovery simulation. When experimental flotation data is available, the procedure would be first to model fit kinetic parameters with the laboratory equation with the aim of reproducing observed batch recoveries. Then, the simulation of the continuous process would use these fitted kinetic parameters with the continuous equation. In this theoretical case, no real experimental flotation data exist, and kinetic parameters were established based on discussion with Outotec experts, with long-time experience in flotation separation.

Aside from attributing the flotation kinetics, in dynamic mode the conditioner model also has a pump parameter, which can be set to *On* or *Off* by the operator, or to *Fault* by the trainer. In cases where the pump is *Off* or in a *Fault* state, and the volume in the conditioner grows to equal to or larger than the conditioner capacity, then slurry overflows and is directed to the *Floor losses* unit, which gathers all the losses from the operation.

Table 10: Flotation models in HSC 10.

Model	Laboratory equation (batch)	Continuous equation (plant)	Constraints
Rectangular Distribution	$R = \frac{R_{\infty}}{n} \sum_{i=1}^n (1 - \exp(-k_i \tau))$ $k_1 = \frac{k_{max}}{n}, \quad k_{i>1} = k_{i-1} + k_1$	$R = \frac{R_{\infty}}{n} \sum_{i=1}^n \left(\frac{k_i \tau}{1 + k_i \tau} \right)$ $k_1 = \frac{k_{max}}{n},$ $k_{i>1} = k_{i-1} + k_1$	$R_{\infty} \leq 1$

To model the impact of reagent concentration, the infinite recovery of each particles is adjusted, as illustrated by the curves presented in Figure 36 for rougher cells.

The collector, here sodium oleate (NaOl) has an optimal set point of 600g per ton of pulp addition. This optimum was established based on internal discussion with Outotec experts. If insufficient collector is added, then spodumene infinite recovery will be reduced. However, if too much collector is added, then the infinite recovery of gangue (quartz) will be increased.

Sodium hydroxide (NaOH) is added to maintain pH at an alkaline level in the pulp. If insufficient NaOH is added, then recovery deteriorates. The optimum NaOH addition rate (10g/t) was calculated for a stable pulp pH, which has been estimated based on the feed mineralogy in equilibrium with pure water. This optimum pH was again established with flotation experts.

Finally, frother addition has a simplified impact on recovery by reducing the infinite recovery parameters of all particles when insufficient amount is added.

All the above-mentioned behaviours are represented in Figure 36. They were based on internal communication with Outotec flotation experts and represent a simplified average behaviour that is suitable for training purposes.

In addition, for all flotation processes, coarse ($>1,414\mu\text{m}$) and ultra-fine ($<20\mu\text{m}$) particles infinite recoveries are lowered by different factors (x0.6 for ultra-fine, x0.7 for coarse) estimated based on Grau, Laskowski and Heiskanen (2005) work and discussions with Outotec experts.

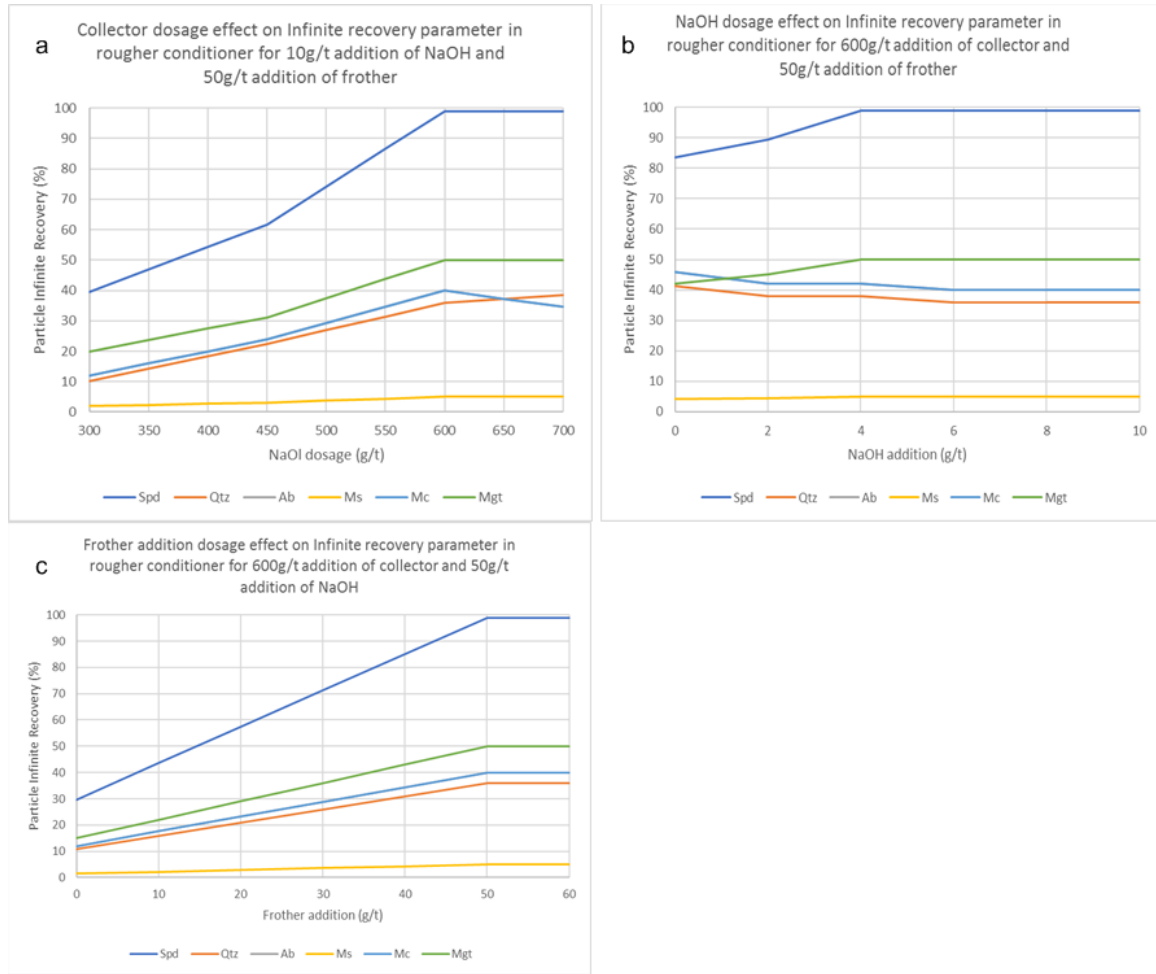


Figure 36: Effect of reagents on the infinite recovery of every particle in the rougher flotation bank a) collector (NaOl – Sodium oleate) dosage b) pH regulator (NaOH – Sodium hydroxide) c) frother dosage. Mineral abbreviations: Spd, Qtz, Ab, Ms, Mc, Mgt - Spodumene, Quartz, Albite, Muscovite, Microcline, Magnetite.

Dynamically flotation recovery calculation was based on the compartment model proposed by Savassi (2005). Roine et al. (2011) summarized the description of equations for true flotation, entrainment and froth recovery used in the model. The verification and validation of these models against a real case were presented in an earlier study (Karttinen et al., 2013).

These models were improved and debugged during this project, notably with respect to recovery from the froth zone calculation (Equation 36) and its algorithmic integration. Indeed, in the previously programmed solution, the steady-state recovery and mass pull used to be incorrectly dependant on the chosen simulation time step (an increasing time step was giving reduced overflow flow rate).

In this model, the kinetic rate constants k_c (1/min) for each particle is calculated based on the mineral floatability k obtained from the conditioner model and on the ratio between simulated and nominal bubble surface area flux S_b (in s^{-1}):

$$k_c = k \cdot \frac{S_{b_{sim}}}{S_{b_{nom}}} \quad (33)$$

where S_b nominal is usually fitted to the process, and S_b simulated is recalculated for each time step to account for changes in the air flow rate (Gorain et al., 1999) with:

$$S_b = \frac{6J_g}{d_b} \quad (34)$$

with d_b (mm) being the Sauter bubble diameter in the pulp phase and J_g being the superficial gas velocity (cm/s) calculated as:

$$J_g = \frac{Q_{Air}}{A_{cell}} \quad (35)$$

with A_{Cell} being the cell area and Q_{Air} the air volumetric flow rate. This parameter is modifiable by the trainee via *Air flow valve opening*, which can be changed from 0 to 100%. In this particular training, an S_b nominal of $63.6 s^{-1}$ is used.

The flotation model in HSC Sim consists of a collection (pulp) zone and a froth zone. The overall recovery of a cell can be derived from the balance illustrated in Figure 37.

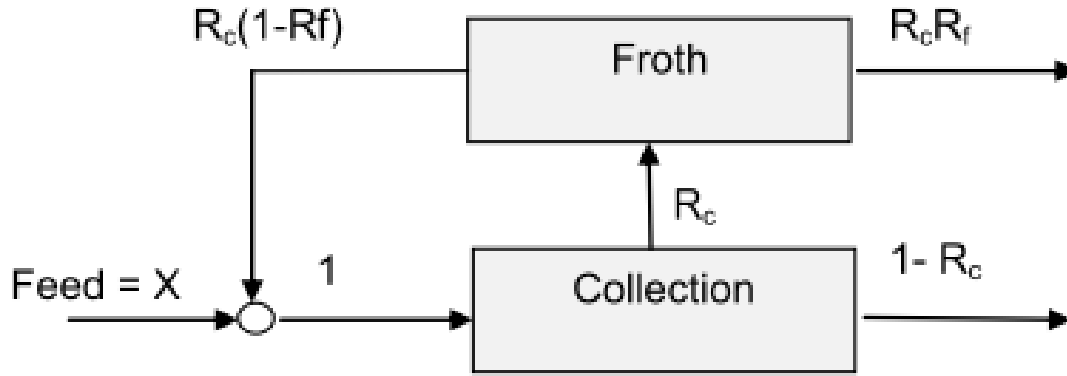


Figure 37: Recovery of minerals from the collection zone through the froth zone.

In dynamic calculation, it is assumed that the particle removal rate from the pulp zone to the froth is proportional to the mass available in the pulp zone:

$$\frac{dM}{dt} = k_c M \quad (36)$$

where M is the mass of particles in the pulp zone. For each time step, the amount of particles directed to the froth zone can be expressed as R_c the pulp recovery.

In this simulation, the global froth recovery R_f is modelled function of the gas residence time in the froth λ_{air} and thus is dependant to the froth thickness and superficial gas velocity. Indeed, the recovery of particles from the froth is largely correlated to the time spent by these particles in the froth (Gorain et al., 1998). As such, R_f is expressed as:

$$R_f = 1 - (1 - e^{-\alpha \lambda_{air}}) \quad (37)$$

where α is a constant adjusted to the process.

The combination of R_c and R_f is used to calculate the amount of particles directed to the concentrate, for each time step, as illustrated in Figure 37.

The status of each flotation cell rotor motor can be changed manually and can be set to *On* or *Off*. Depending on the scenarios of the exercise, the trainer can also set or program the rotor motors to turn to *Fault* mode. After entering *Fault* mode, the motor cannot be turned back *On* immediately. In the case where the motor is *Off* or in *Fault* mode while the cell should be in operation, no concentration process happens in the model and the feed, concentrate and tails move toward an identical composition. *Tail valve opening* is normally controlled by a PID but can also be manually changed, from 0 to 100%. This variable enables control of the cell pulp level, related to the froth depth in the cell and thus changes the froth recovery.

3.3.3.2.2 PSD and chemistry on-line analyser model

On-line analysers models are specifically developed for training purposes. Both PSD and chemistry analysers are implemented in training for certain practicalities related to on-line analysers, such as:

- The sequencing of the analysis – each stream (also called line) is analysed in a certain order, and the analysis is not immediate. In general, the sequence follows three steps: the filling of the analytical device chamber, the measurement proper and finally the washing (or flushing) of the analysis chamber. All these steps combined can take up to two minutes per line. Thus, if a single analyser has to measure six different lines, there will be 12 minutes between two data points from the same line.
- Due to the overall time constraint, sometimes some lines must either be bypassed or requested for measurement in priority. The implementation of this type of unit, for PSD or chemistry, is an obvious way to introduce these concepts in training.
- The models include a measurement error simulation and therefore do not return the exact same result all the time. This introduces operators to the concept of margin of error, the standard deviation of a measurement device and the detection limit.
- Finally, the on-line analysers can also be put in maintenance mode. This urges trainees to make decisions based on partial information and therefore set them closer to real operation conditions.

A screenshot of the on-line chemical analyser model is displayed in Figure 38.

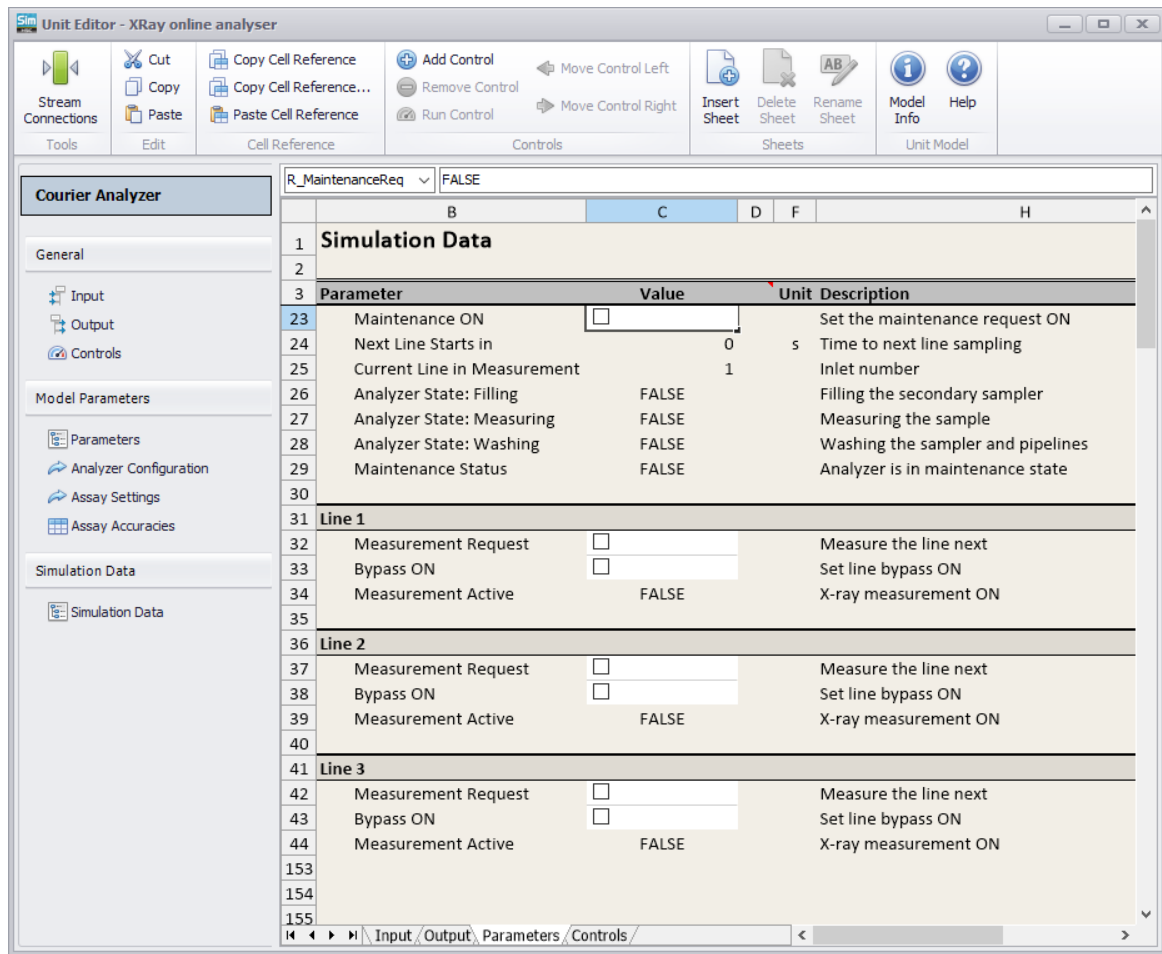


Figure 38: Screenshot of the XRF on-line analyser simulation data page. On the parameters page, any number of analysis lines, the elements being analysed, and the time required for the filling, measuring and washing steps can be defined. In the Assay Accuracies tables, the analysis parameters (detection limit and standard deviation for each element) can be filled in. Each line can be bypassed or requested for analysis.

3.3.3.2.3 Additional models for contextualisation

Additional models were added to the flowsheet in order to place the flotation circuit in context. They are less critical for training centred on flotation circuit operation and thus have a lower level of detail than the flotation cell.

A desliming model based on the Whiten efficiency function was introduced to split the feed stream into underflow and overflow streams based on particle size (Napier-Munn et al., 1999). The pump sump is a simple tank model, introducing delay and overflowing in case of motor fault or pumping under capacity. All the overflowing material is directed to floor losses, and one of the purposes of the training is to limit

the amount of spillage by verifying each pump motor status (*On*, *Off* or *Fault*). Dewatering units (here representing thickener, filter and dryer) are based on an empirical model which separates the water phase from the solid phase into two output streams. A user-given solid percentage for the dewatered stream is needed to compute the amount of water to be removed. Finally, the magnetic separation unit is an empirical model for splitting particles based on their mineralogy. For this training, it is estimated that 98% of the magnetite is removed together with 1% each of the other mineral particles, based on historic information.

An extra calculation unit was added to the process for the economic calculation of the simulation. This unit shows production profit accumulated during the exercise based on the concentrate revenue and operating costs. A screenshot of this unit user-interface is visible in Appendix 13. The following input values from the user are needed:

- the valuable element / mineral / oxide (in this case, Li₂O),
- the price of the valuable element / mineral / oxide, in \$/t,
- the reagent consumption information:
 - number of input points,
 - number of different reagents used,
 - price of reagents, in \$/g of reagent.
 - the tons of solid passing through the reagent addition point and the dosage of each reagents are fetched from the conditioners input data sheet and custom calculation sheet and stored in a consumption table in the economic calculation unit. The size of this table is given by the number of input point input and the number of different reagents used input. Each column represents an addition point and rows are created to store reference to solids t/h passing through and each reagent dosage in g/t for said input point.

In this unit, the revenue (Income, \$) is calculated at each iteration (Δt) based on the valuable element price (Price in \$/t) and its production in the final concentrate (t), Prod, during the time step:

$$Income_{\Delta t} = Price \times Prod$$

38

The same applies for operating costs (Costs, C) which are calculated from the quantity of reagents used. The reagent consumed at each time step is calculated based on the solid tons ($Tons_n$) passed through the input point n, reagent price ($Price_r$) for a reagent r are given in \$/g and the reagent dosage for the input point n and for the reagent r:

$$Costs_{\Delta t} = \sum_n \sum_r Dosage_{n,r} \times Price_r \times Tons_n \quad 39$$

Finally, the difference between Income and Costs is taken as the profit value. Cumulative figures and averages are also available for concentrate and tails (accumulated tonnage, average grade) as well as for floor losses.

Figure 39 shows the schematic structure of the simulator, with principal models and possible actions in the simulation.

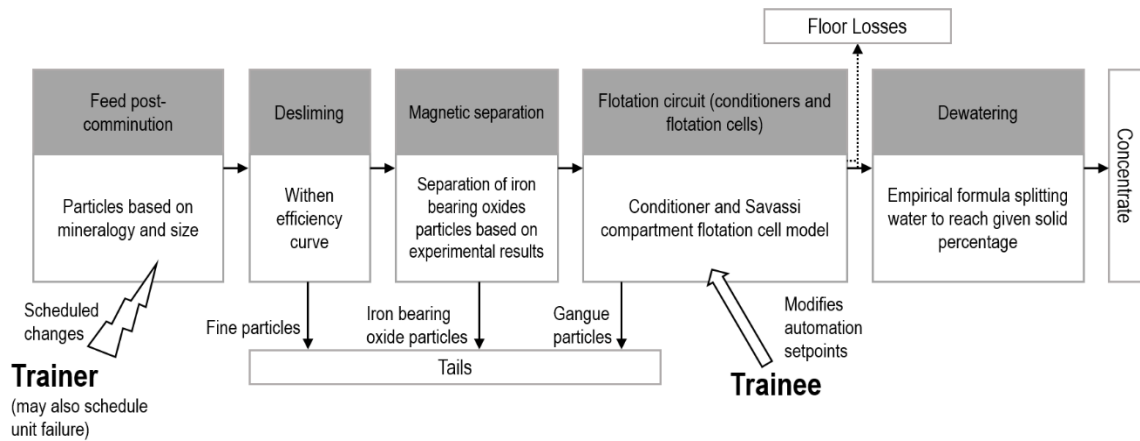


Figure 39: Schematic structure of process simulation for the OTS case-study of spodumene flotation plant.

3.3.3.3 System control and exercises

The automation system and user interface is based on the Outotec ACT Advanced Process Control Platform, presented by Ruhanen *et al.*, (2018). The automation system contained two PID controllers for each of the flotation cells, one for each pump sump and three for each conditioner. In the flotation cell, one controlled the tail valve opening based on the slurry level setpoint, and the other controlled the air valve opening based on the air flow rate set point. In every pump sump, a PID controlled the slurry level in the sump, and finally, for the conditioners, PID were implemented to control reagent dosages. The automation system also acts as the human-machine

interface, enabling the trainee to visualize the entire flowsheet on the main screen and to navigate from it to different views. As such, there were specific views for each flotation line, units and analyzers. In the unit view, the trainee could manipulate the PID set points, such as reagent dosage. An example of this interface is shown in Figure 40.

The simulator described above was used in operator training alongside a complementary theoretical background course in flotation. The simulation illustrated several concepts: the influence of the particle size distribution upon the flotation process, and the impact of the feed mineralogy and the flow rate. The user interface developed for this simulation was tailored to mimic the customer control software used in the plant. Therefore, operators trained with this tool are capable of monitoring and regulating the process without having to learn separately how to use another control system. This represents an important gain in terms of time and is likely to improve training impact and trainee involvement.

Process flowsheet simulation together with ACT-based automation control system are called by the Outotec Virtual Experience training software. This software has two parts: for the trainees it enables to enter a selected training session and will display exercise instructions on top of the ACT-based user interface. For the trainer, the software enables to create new exercises with a set of instructions and optionally to schedule changes of some parameters during the exercise. For instance, the main goal of one of the exercises was to maintain the concentrate grade throughout the process subject to feed changes, programmed into the training software.

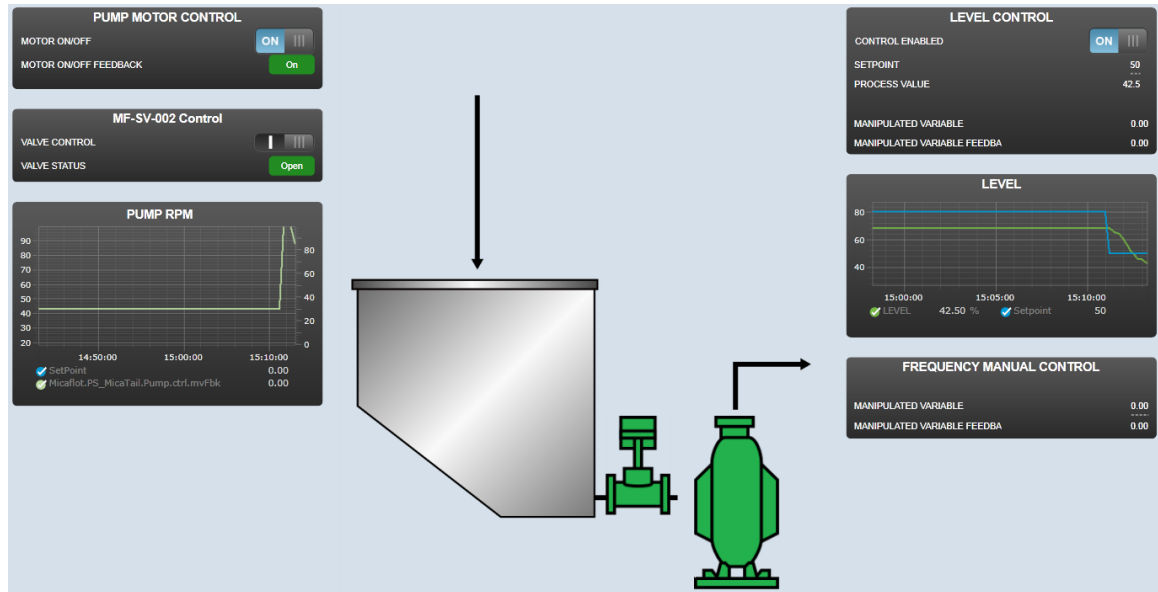


Figure 40: Screenshot of the user interface of a pump sump controller. Controlled values are the level setpoint, the switching on/off of the motor and valve opening. The evolution of pulp level and pump frequency are shown as separate graphs.

Another important feature of the training was the management of start-up and shut-down situations. Several exercises were especially based on the management of circuit start-up: the operator had to follow and manage each unit during the filling period, opening and closing valves and turning on the pumps and rotor motors in the correct sequence. In the same way, this simulation was used to train operators to react and apply adjustments in the right order when stopping the system due to an unexpected issue. These training options would not be available with traditional steady-state simulation.

3.4 Gold Processing Plant Digital Twin

The second case-study involved the construction of a gold processing plant simulator or *digital twin*, for a client case from Newcrest Mining Limited. This digital twin aimed at being associated with the mine block model as well as the hydro-processing simulation. The intent of client with this simulator is to improve their mine planning and their exploitation methodology, for a complex mineral deposit.

3.4.1 Background and process description

The Lihir gold deposit was explored in the 1980s and 1990s, with a first PFS submitted in 1993. Since 2010, the mine has been owned at 100% by Newcrest Mining Limited. In 2019 the total resources amounted to 680Mt Au@2.3ppm including total reserves of 320Mt Au@2.3ppm¹¹. From 1997 to 2013, the deposit produced 72,813,000 tons of Au@5.09ppm and a total of 10,296,317 oz of gold (320,251kg)¹².

3.4.1.1 Deposit description

The Ladolam gold deposit occupies the centre of the extinct Luise volcano on Lihir Island (Papua New Guinea). The geological consensus (Blackwell et al., 2014; Simmons & Brown, 2006; Sykora et al., 2018) describes it as a superimposed epithermal-style mineralization with porphyry-style alterations. Although the juxtaposition of a porphyry-type with an epithermal-type of mineralization produced a large bulk mineable resource, it also created complexity with regard to mineral processing (Sykora et al., 2018). Two main types of mineralization have been identified:

- A refractory potassium feldspar-sulphide mineralization with sub-micron gold included within the sulphides (refractory). In this type of mineralization, the average sulphide grade is 6%.

¹¹ Values extracted from Dec. 2019 Resources and Reserves report https://www.newcrest.com/investor-centre/results-reports?report_type=7

¹² Technical Report on the Lihir property in Papua New Guinea, March 2014, Newcrest Mining Limited

- A low-sulphidation quartz-chlorite-bladed anhydrite association with occasional free gold.

Metallurgical tests revealed that most of the gold is refractory. As a result, direct cyanidation is used, only 30% of the gold is recovered and coarse, free gold is rare. Auriferous pyrite and marcasite are the main minerals bearing gold. They are associated with other sulphides and sulphosalts in variable amounts (chalcopyrite, sphalerite, arsenopyrite and tennantite-tetrahedrite).

The mine block model constructed in 2012 separates nine structural domains, determined by fault boundaries, and five alteration domains (Newcrest Mining Limited, 2014). Each domain exhibits very specific mineralogy, Au grade and mineral textures.

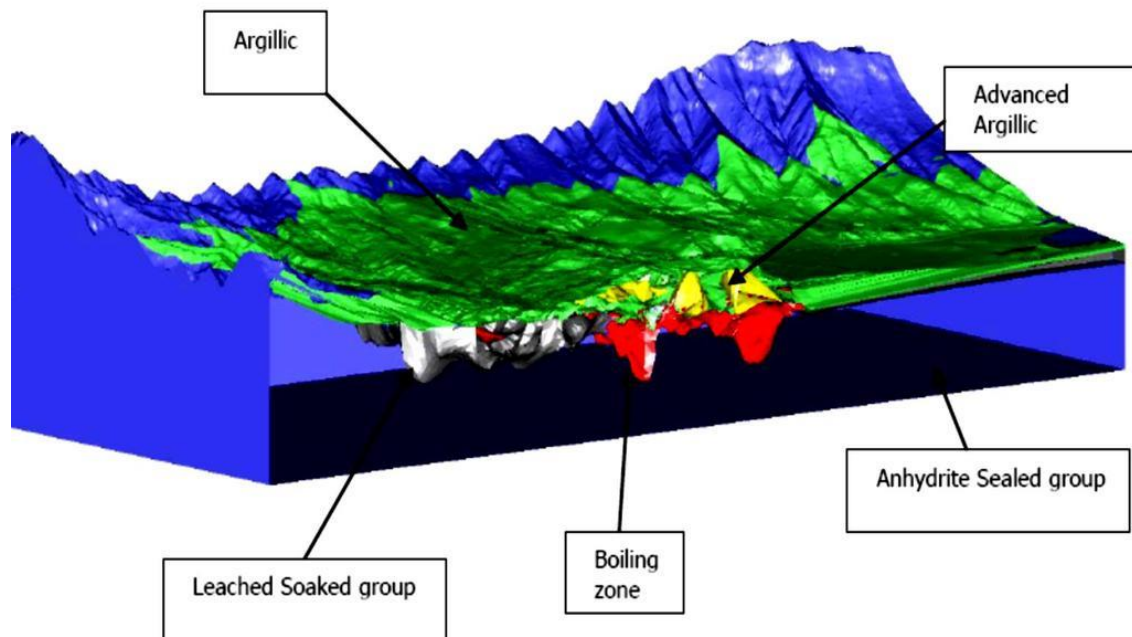


Figure 41: Lihir gold deposit 3D model showing the different alteration zones: argillic, advanced argillic, leached soaked group, boiled zone and anhydrite sealed group. The Lihir mineralised envelope is approximately 3km along strike, 1.5km down dip and 0.5km depth (Newcrest Mining Limited, 2014).

3.4.1.2 Exploitation and processing

The following information was extracted from a Newcrest technical report from 2014 (Newcrest Mining Limited, 2014). The processing operation in Lihir started in 1997 with a high-grade ore (HGO). For these high-grade ores, the process consisted only of

grinding and pressure oxidation (POX) followed by carbon-in-leach (CIL) (see 1.1.2). In 2007, a flotation circuit was added to concentrate the sulphides and process the low-grade ore, also known as flotation-grade ore (FGO). Pregnant solution from the leach of high-grade ore and flotation concentrate from FGO is finally directed to an electrowinning step to produce bullion. A simplified flowsheet of the plant is shown in Figure 42.

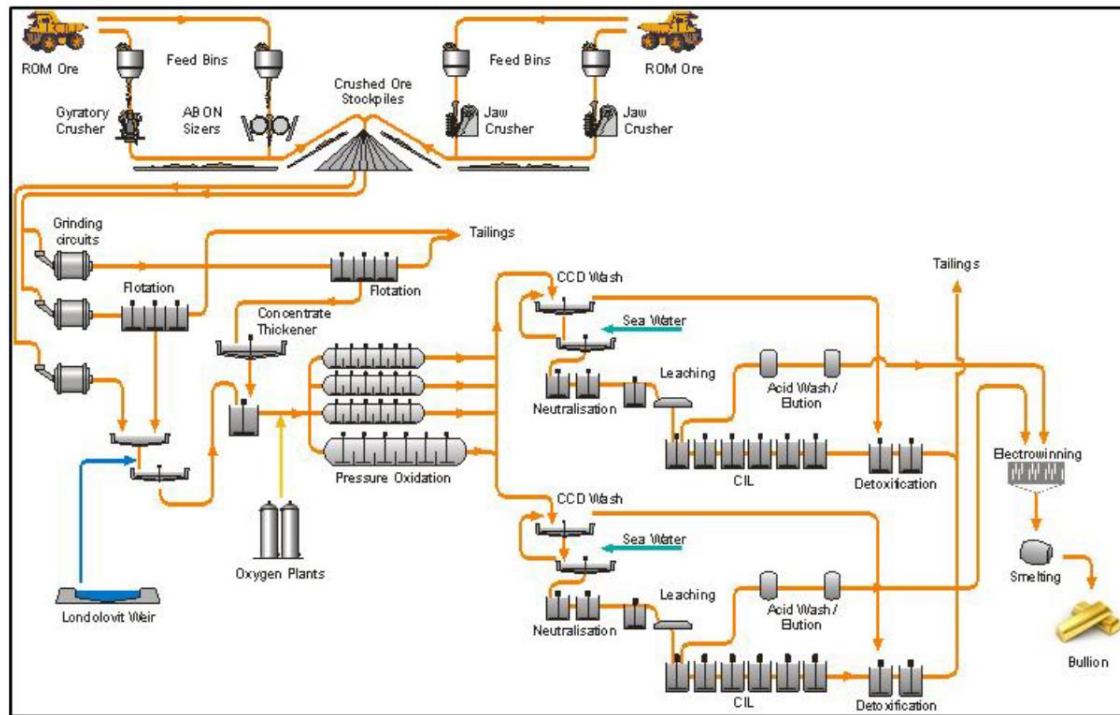


Figure 42. Simplified flowsheet for the processing of Lihir ore (Newcrest Mining Limited, 2014). The ROM is first separated into three piles for crushing: soft, medium and hard ore, directed to Abon, gyratory and jaw crushers respectively. The crushed ore is then stored into three piles, depending on grade. The high-grade ore is directly fed to the POX then to the CIL. Flotation grade ore is directed to flotation, and the concentrate is oxidized and leached. The pregnant solution is then treated via electrowinning to recover gold.

The ROM ore, coming from different parts of the deposit, is crushed via two primary crushing circuits. For the first circuit, the ore is processed in a gyratory crusher or in an Abon crusher depending on its competence. The other primary crushing circuit is used for more competent and lower-grade ores and consists of two parallel jaw crushers. Mechanical and lithological tests and data gathered since the operation started have identified five main alteration zones of increasing hardness (see Figure 41 for distribution of main alteration types):

- Argillic Clay
- Advanced Argillic
- Leached Soak Domain
- Boiling Zone
- Anhydrite Sealed

Once the ROM is crushed, the products are stockpiled and stored before being transported to the grinding circuits.

There are three grinding circuits: one (HGO2) is used for high grade ore, which is routed to POX. The second and third circuits (FGO and HGO) grind the flotation grade ore. All three grinding circuits have a primary SAG mill, followed by a secondary ball mill in a closed circuit with classifying hydrocyclones.

Ground FGO is first directed to a bulk rougher flotation in a single roughing stage consisting of a bank of five 150m³ flotation tanks. The ground ore from the HGO line goes through five 300m³ flotation tank cells. The flotation concentrates are then thickened to reduce their water content and blended with high grade slurry to achieve the required target autoclave feed sulphide grade. Raw water is used in addition for the front-end process (comminution, flotation and dewatering) whereas the back-end process (hydro-processing) may use sea water. As of 2013 y-o-y production totalled 6.94Mt of ore with an overall gold recovery of 85%.

3.4.2 Simulator requirements

A crucial aspect of this particular processing of the treatment plant is how to consider the heterogeneities of the ore in the deposit. Five types of ore need to be processed in the plant and they all have different treatment routes depending on their physical, chemical and mineralogical properties. POX and CIL processing require a constant feed grade for best operation, which is difficult to achieve, especially with changing ore types in the front-end process.

This type of management requires a lot of transversal communication across the different parts of the operation, including between geologists, miners and metallurgists in an integrated geometallurgical approach. A simulator developed by

Outotec for this case study proposed a common management tool for all these aspects, easily accessible through a dedicated platform.

As part of this integrative geometallurgical approach, one requirement for this simulator is to be connected to the exploitation block model. The block model will give information (grade and composition) for each mined block and its stockpile destination. These data are then transformed into stream data for the process simulation.

The complex stockpile management – for the crusher feed and for the grinding lines – is integrated in the simulator as well. Developed for this purpose, a dynamic stockpile model serves to monitor and predict the average pile properties and discharge, depending on the reclaiming method. As part of the simulation, the model helps to predict possible blending scenarios with a view to optimal choice.

The mineral processing simulation, comminution, separation and dewatering, have to be connected to the hydrometallurgical parts, POX and CIL. In HSC Sim the integration of both parts is possible, as the mineral processing models are compatible with hydro-processing models in the same environment. Thus, the resulting simulator integrates all parts of the process from the mine to metal production.

The simulator built for this study aims to meet all the requirements mentioned above. In addition, it displays KPIs for the entire plant, including the energy consumption from comminution, gold recovery, plant water balance and water chemical composition for the back-end process.

3.4.3 Simulator construction

The following sections describe the models that were implemented in the front-end simulation and the methodology used for the streams' descriptions.

3.4.3.1 Description of the streams

As explained in section 3.3.3.1, various streams are directed to the blending units. Specifically, the three blending units represent the three feed stockpiles. Each blending unit is fed with nine incoming streams with different compositions, depending on the zone from which the ore was extracted. These nine incoming streams are named according to their alteration domain characteristics:

- ADIB for porphyry anhydrite seal inner biotite zone;
- ADOB for porphyry anhydrite seal outer biotite zone;
- ADDC for porphyry anhydrite seal chlorite zone;
- ADLE for boiled & leached lower epithermal zone;
- ADUE for boiled & leached upper epithermal zone;
- ADSB for boiled & leached epithermal silica breccia zone;
- ADAC for argillic alteration zone;
- ADAA for advanced argillic alteration zone;
- ADUA for upper argillic alteration zone.

These streams exhibit strong compositional and mineralogical differences, as shown in Figure 43. Therefore, each of these streams has its own theoretical grinding and flotation behaviour. Within the HSC simulation, these characteristics are controlled via custom calculation sheets.

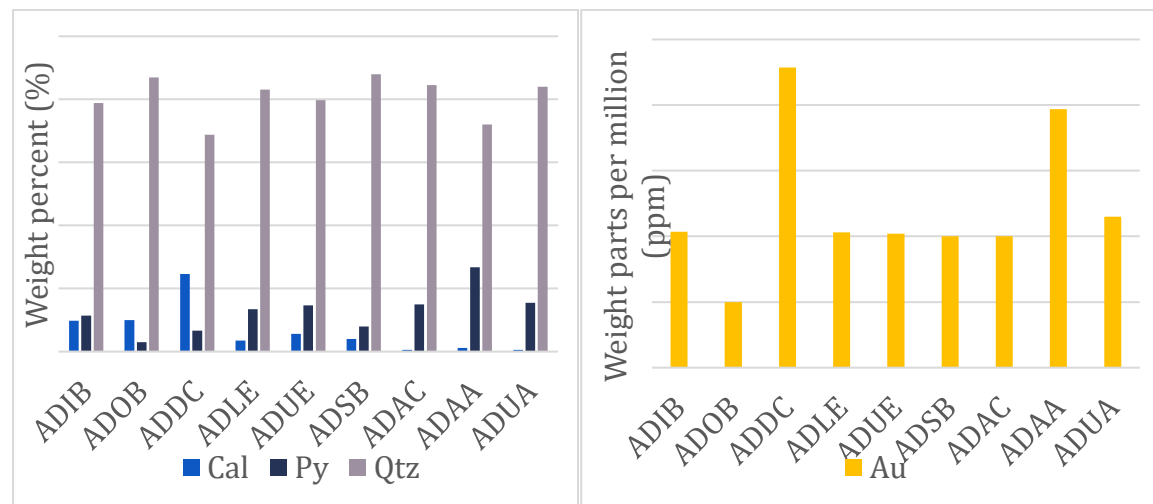


Figure 43: Mineralogical stream composition (Cal = calcite, Py = pyrite, Qtz = quartz, Au = gold) of the different streams.

The mineralogical and chemical composition of each stream is a blend of quartz, calcite, pyrite and gold. The proportion of each stream to each stockpile is controlled via a table, shown in Figure 44. Each stream has 26 different size classes: [0 – 38], [38 – 53 μm], [53 – 75 μm], [75 – 106 μm], [106 – 150 μm], [150 – 212 μm], [212 – 300 μm], [300 – 500 μm], [500 – 1000 μm], [1000 – 1800 μm], [1800 – 2000 μm], [2000 – 3400 μm], [3400 – 4800 μm], [4800 – 6350 μm], [6350 – 9525 μm], [9525 – 11200 μm], [11200 – 25400 μm], [25400 – 38100 μm], [38100 – 50800 μm], [50800 – 68850 μm],

[68850 – 101600 μm], [101600 – 127000 μm], [127000 – 152400 μm], [152400 – 203200 μm], [203200 – 254000 μm] and [+ 254000 μm].

Each of these ores type has its own breakage parameters (work indexes, breakage and abrasion parameters – derived from weight-drop and abrasion tests) and flotation kinetics for each of its mineral, summarized in an internal study. In terms of comminution response, the argillic alteration ore types (ADAC, ADAA and ADUA) are softer and less competent than the other types, the silica breccia (ADSB) being the most competent. Relatively, and for the same grind size domain, an average ore from porphyry (ADIB, ABOD and ADDC) and from epithermal zones (ADLE, ADUE and ADSB) would have a specific power input (kWh/t) respectively 63% and 66% higher than an average ore from the argillic zone. In terms of flotation response, for a similar mass pull in the flotation circuit, PSD and age of the ore (i.e., the time between the extraction and the processing), the recovery of gold and sulphides decreases as the alteration intensity increases. Relatively to an average ore from the porphyry zone that would have the highest recoveries, the recoveries of sulphides and gold for an average ore from the epithermal zone would respectively be 19% and 9% lower. Compared to recoveries from a porphyry ore, the recoveries of sulphides and gold for an average ore from the argillic alteration zone would respectively be 24% and 13% lower. According to these test results and using the company's R&D knowledge, all these parameters can be interpolated for any stream composed of these ore types.

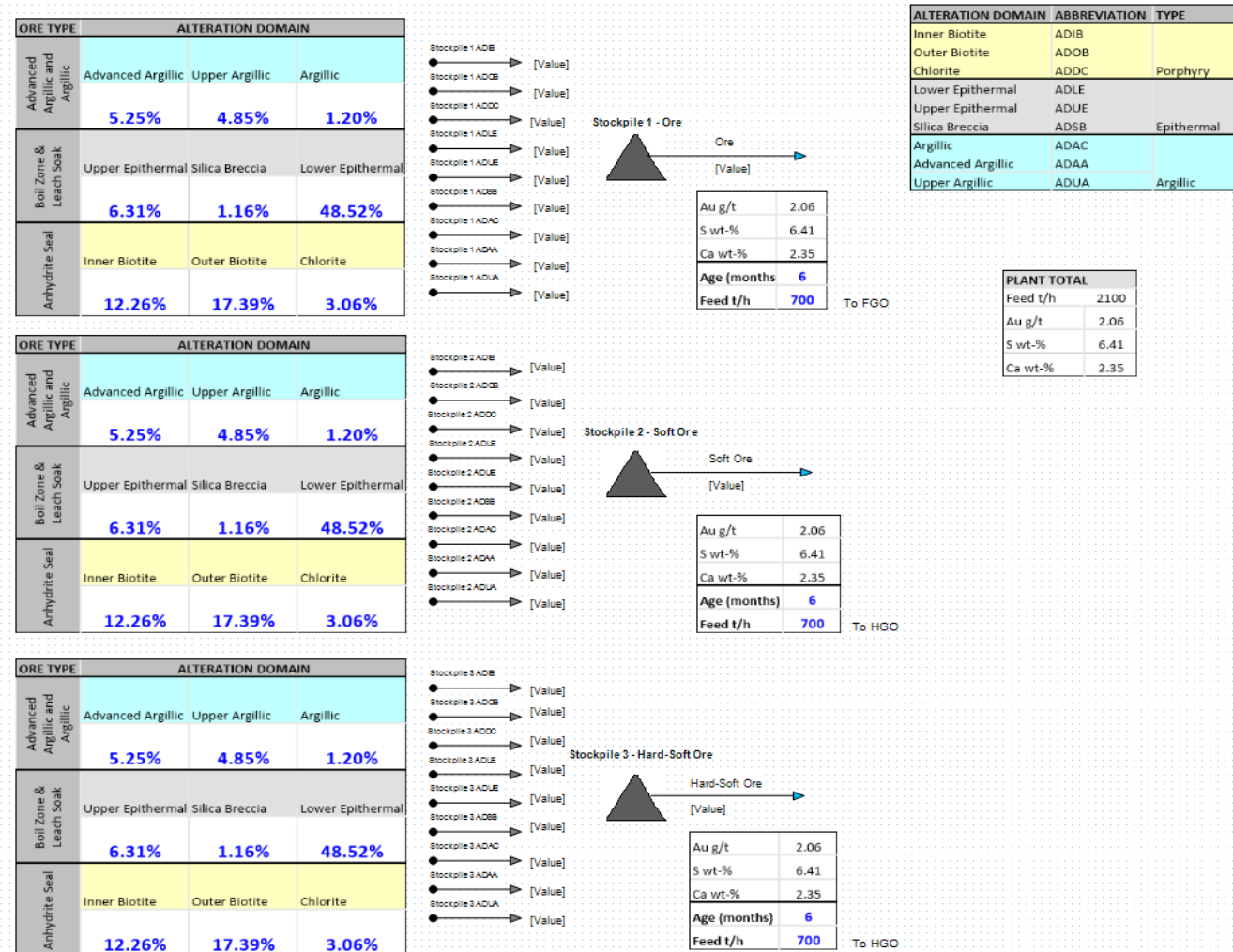


Figure 44: HSC definition of the different types of ores, mixed into three primary stockpiles according to their crushing properties.

3.4.3.2 Models developed and used in the mineral processing simulation

Three of the main models used in this simulation have already been described in earlier chapters and sections of this thesis:

- in section 3.2 for the dynamic SAG mill model,
- in section 3.3.3.2 for the dynamic flotation cell model,
- in section 3.1 for the size separation models.

A new dynamic model for the ball mill was integrated for this simulator. The principle of the model is quite similar to that of the SAG dynamic mill model, presented in section 3.2. The main difference is that the discharge can be calculated as a simple overflow from the mill. The volume of slurry inside the mill is therefore not a function of charge characteristics but simply calculated based on the load fraction, a user-input parameter of the mill. The algorithm is represented on Figure 45.

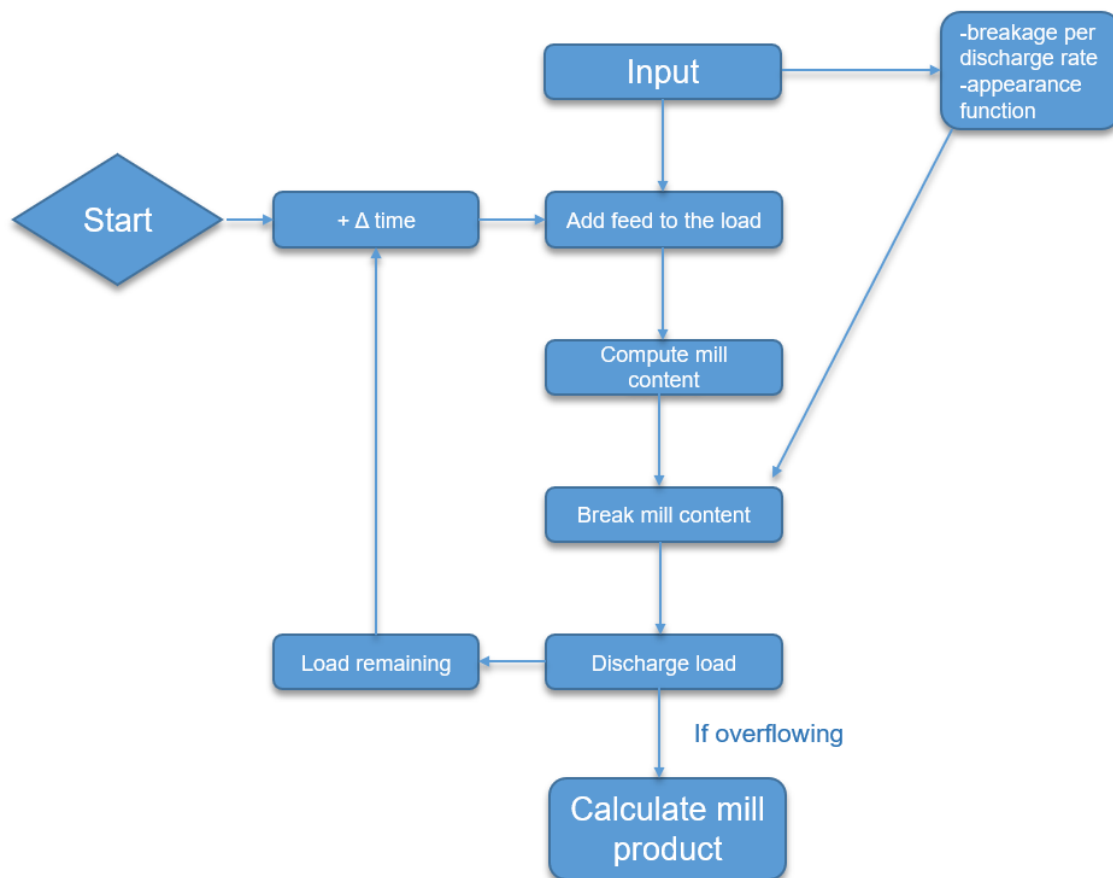


Figure 45: Dynamic ball mill with overflow discharge algorithm.

The Nageswararao et al. (2004) model was implemented for hydrocyclones and the Whiten efficiency curve model for screens. This cyclone model is a newer version of the Plitt model, described in 3.1.2.2. It has been tested and validated at the Julius Kruttschnitt Mineral Research Centre (University of Queensland) and contains a few variations of the calculations and fitting parameters from the Plitt model (Nageswararao et al., 2004).

For dewatering, the models are purely empirical, using the desired underflow solid percentage as user-given input. Finally, the pump sump models, mentioned in 3.3.3.2.3, are also built into the flotation circuit. All the above mentioned models are implemented in the grinding and flotations circuits, shown on Figure 46.

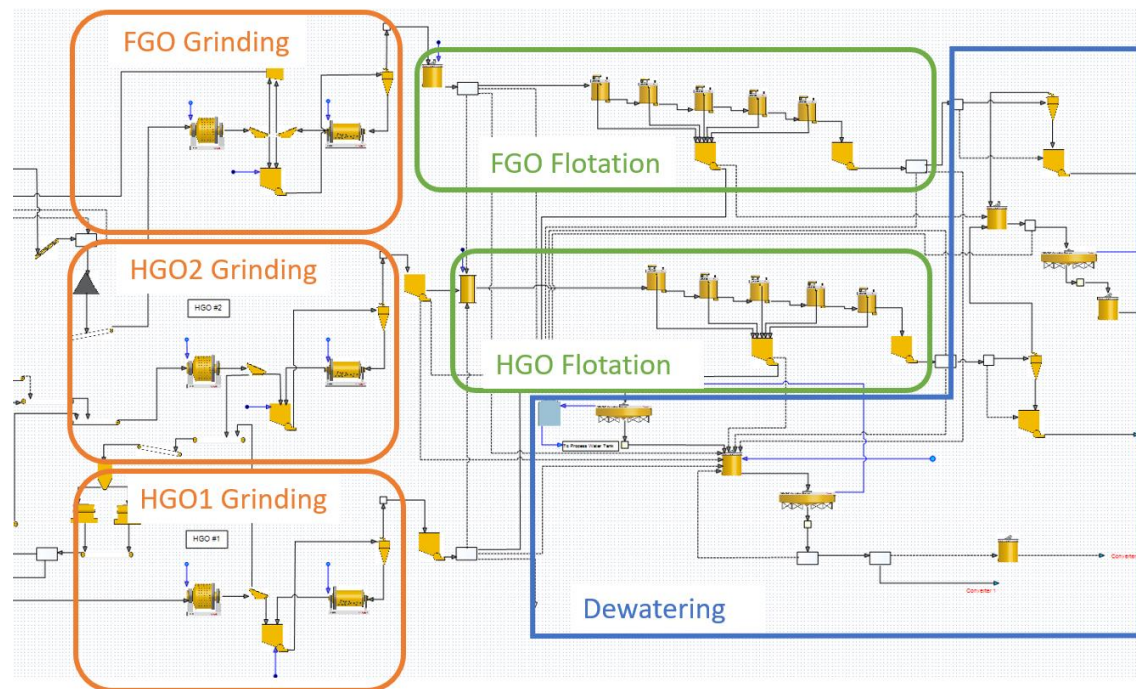


Figure 46: Grinding, flotation lines and dewatering of the Lihir process (front-end) implemented in HSC Sim.

3.4.3.2.1 New and improved models

Two other dynamic models were programmed for this simulator: a stockpile and a conveyor model.

The conveyor model is a straightforward stream delay unit. The input and output variables are described in Table 11. The conveyor dimensions, belt status (ON/OFF and direction) and speed are used to give the discharge at either end of the belt. The belt capacity is calculated based on the material mechanical characteristics and the

idler troughing angle (Figure 47). If the belt capacity is exceeded, then material can be directed to an optional overflow stream. The belt capacity calculation is based on the empirical solution presented by Tsakalakis and Michalakopoulos (2015), expressed as:

$$Q = 390.4 W^{2.1473} [(-0.0002 \lambda + 0.0219) \beta_{dyn} + 0.0408 \lambda^{0.7903}] \quad (38)$$

with Q being the maximum capacity in m^3/h , W the belt width in m, λ the troughing angle in degrees, and β_{dyn} the surcharge angle of the material in degrees.

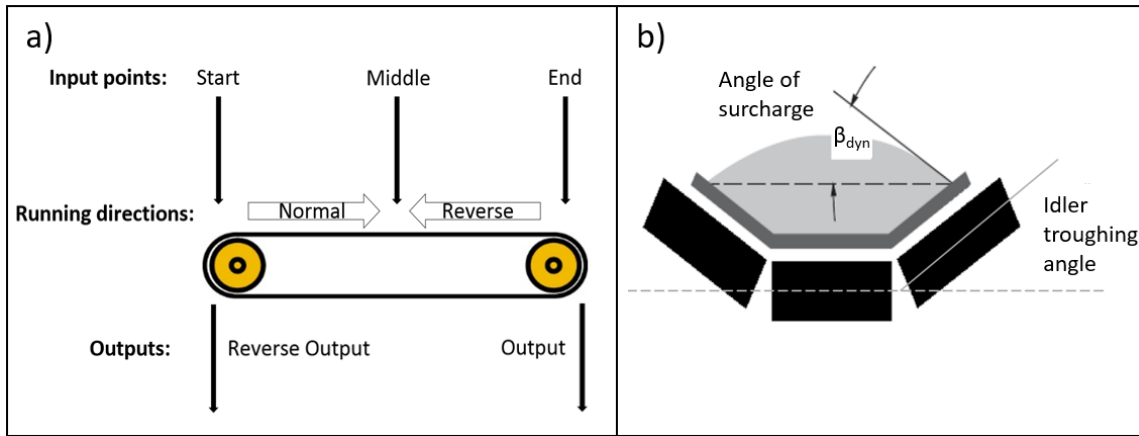


Figure 47: Schematic representation of the conveyor model with main parameters.

Table 11: Input and output variables used in the conveyor model.

Parameter / Variable	Description
Input	
Input stream(s)	Tonnage, %solid, particle amount and composition
Input location	Start, middle or end of the conveyor
Conveyor dimensions	Length, width, idler troughing angle
Material characteristics	Surcharge angle
Operational parameter	Belt speed, On/Off, reverse direction
Output	
Output stream(s) (Output or reverse output)	Tonnage, %solid, particle amount and composition
Overflow	If belt is overcharged, an overflow stream is connected and takes extra material
Belt capacity	In m ³ /h or ft ³ /h

The stockpile model is simple in terms of calculation but has a crucial role in this specific simulator for managing the feed composition. A stockpile can be used to store material for long periods, up to several months, with discontinued feed additions using conveyors, buckets or other surface equipment. The in situ evaluation of an average stockpile composition respecting Gy's sampling theory (P. Gy, 1967) is a difficult task, and the sampling of conveyor feed to reconstruct the pile composition is the preferred method, as mentioned in Petersen et al. (2005). The stockpile is a highly heterogeneous body and depending on the reclamation method (recuperation of the material), the recovered material may have different properties. Reclamation can be done with conveyors under the stockpile or with surface equipment such as bucket wheels, draglines or loaders and dozers, as summarised in Young (2019). For this model, only a single underground draw-point is implemented. A distinction is made between the "live" fraction of the stockpile and the "dead" fraction, which can only be removed using mobile equipment (Figure 48 panel a). Depending on the stockpile storage and reclamation method, the materials directed to the stockpile may be stacked up on one another, with no mixing between them resulting in a layered pile, or a relatively well mixed pile. These behaviours are reproduced by the model by different internal mixing options, illustrated in Figure 48 panel b. The modelled

reclamation process can be switched from ongoing to stopped, and the process speed is adaptable as a percentage of the maximum reclamation speed. Table 12 shows the main input and output parameters used by the stockpile model.

Table 12: Input and output variables used in the stockpile model.

Parameter / Variable	Description
Input	
Input stream(s)	Tonnage, %solid, particle amount and composition
Stockpile characteristics	Type, maximum radius, angle of repose
Buffering effect	High, medium or low buffering effect
Operational parameters	Reclamation ongoing / Reclamation speed
Output	
Output stream(s) (Output or reverse output)	Tonnage, %solid, particle amount and composition
Stockpile capacity	Maximum stockpile capacity in m ³

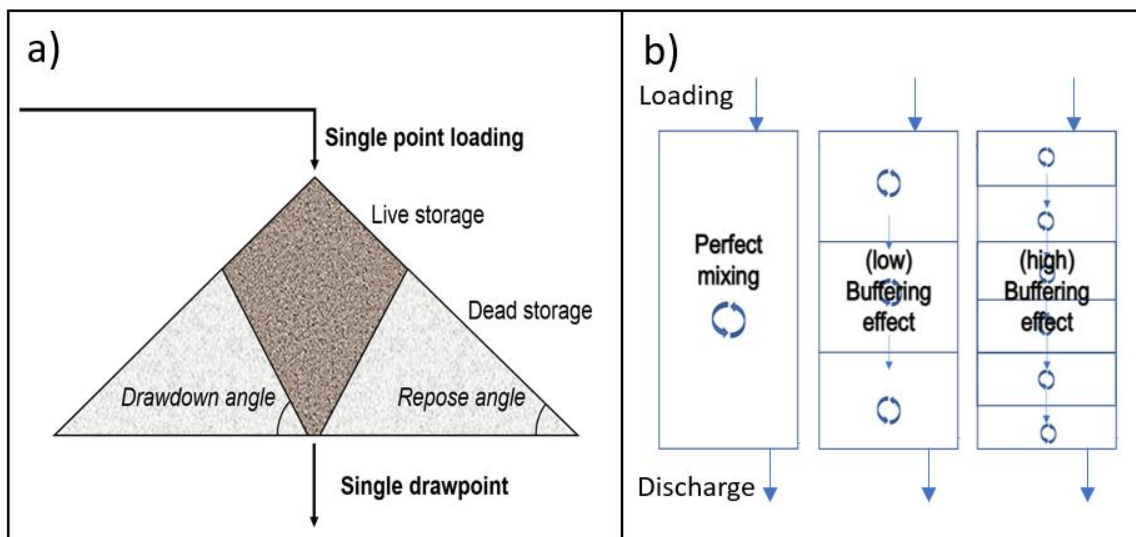


Figure 48: Schematic representation of the stockpile model with main parameters a) conical stockpile “live” and “dead” volumes for single loading and reclaiming points b) stockpile layering effect on the discharge composition.

Several crusher models needed to be implemented in this simulation. Three computer models based on conceptual models developed by Chalmers University were selected for cone, gyratory and jaw crushers (Bengtsson & Evertsson, 2008; Johansson et al., 2017). These models give semi-empirical relationships between the crusher CSS

(Closed Size Settings) and product PSD. The models also use empirical correlations between crusher dimensions, material crushing work index, feed and product PSD as well as power consumption. A summary of the crusher models present in this simulator is given in Table 13.

Table 13: Integrated crusher models and summary of their relationships.

Crusher model	Maximum opening (mm)	CSS range (mm)	Tonnage range (t/h)	Product PSD calculation method	Power calculation method
Jaw	600-1500	60-130	75-1300	CSS & crusher dimension relationship	Bond equation (Bond, 1952)
Gyratory	100-270	25-60	80-900	CSS & crusher dimension relationship	Bond equation
Cone	60-150	10-50	150-450	CSS & crusher dimension & eccentric speed relationship	CSS relationship

These models are shown in Figure 49, integrated on the Lihir crushing flowsheet with pre-grinding circuit stockpiles.

Table 14: Fitted parameters used for the simulation of primary crushing and grinding circuits units (NA: Not Applicable).

Parameters	I Gyratory Crusher	I Jaw Crushers	Flotation grade SAG	High Grade SAG 1	High Grade SAG 2	II Cone crushers
Xm	NA	NA	0.84	2	2	NA
Xg	NA	NA	1.86	0.1	0.5	NA
Xp	NA	NA	71.5	61	71	NA
CSS (mm)	75	100	NA	NA	NA	12

As explained in section 3.4.3.1, ore-specific comminution parameters (A, b, Ta, BWI) and flotation kinetics are then adapted in custom sheets based on the proportion of each ore type feeding the process. Additionally, the age of the ore (i.e., the time between extraction and processing) is integrated as a modifier for the flotation kinetic parameters based on Newcrest internal studies.

Finally, several controllers needed to be set-up in the process. The main purpose of these controllers in this part of the simulation is to regulate the water input into mills and pumps from the flotation circuit, based on the design pulp solid percentages.

Chapter 4 Results

This chapter reports the results of the validation procedure of the mill models described in Chapter 3, as well as implementation results of the simulator case-studies presented also in Chapter 3.

4.1 Multi-Particle Mill Validation Results

The circuit simulation was constructed with previously described models and then fitted with mass balance reconciliated data. In HSC Sim, different controls were set up to find fitted parameter values for the first simulation (referred to as Sim 1). A rod mill selection function was fitted to obtain a PSD similar to the balanced results of the rod mill output. Cyclone efficiency factors were fitted to obtain a similar PSD and water separation to the balanced results of the overflow. Finally, a ball mill breakage rate was fitted to obtain a PSD like the balanced ball mill product. For the second simulation, using the multicomponent ball mill model (referred to as Sim 2), rod mill and cyclone fitting methods were the same as for the Sim 1, but ball mill breakage rates were fitted to match the balanced PSD and recirculation flow rates for both the NSG and sulphide populations. The results, experimental, balanced and simulated, both with the original mill model and with multi-particle model are presented in Table 15.

Table 15: Experimental, mass balanced and simulated results with original ball mill model (Sim1) and multi-particle model (Sim2). Stream names are shown on the flowsheet in Figure 21 (RM = Rod mill, OS = Oversized, US = Undersized, UF = Underflow, OF = Overflow, BM = Ball mill). P80 “bulk” design the 80% particle passing size for the entire solid flow.

Stream name	Feed	RM prod	Screen OS	Screen US	Cyclone UF	Cyclone OF	BM prod
Solid (t/h) Exp	0.65	0.79	0.05	2.03	2.46	0.72	3.13
Solid (t/h) Bal	0.67	0.72	0.05	2.76	2.12	0.65	2.09
Solid (t/h) Sim1	0.67	0.72	0.05	2.85	2.18	0.67	2.18
Solid (t/h) Sim2	0.67	0.72	0.05	2.83	2.16	0.67	2.16
P80 (um, bulk) Exp	3787	229	205	181	204	86	169
P80 (um, bulk) Bal	3786	225	204	182	205	86	165
P80 (um, bulk) Sim1	3786	228	193	184	203	86	166
P80 (um, bulk) Sim2	3786	227	192	185	204	87	171

Bulk particle size distributions (i.e., for the entire solid flow) displayed in Figure 50 are very similar between the classical perfect mixing model and multi-particle model, even though the fitting strategy differed, the first one aiming to match the bulk PSD and flow rate and the other to match each particle type PSDs and flow rates. By

contrast, sulphide and NSG PSD for Sim 2 are close to experimental distributions and the variability between NSG and sulphide distributions is clearly noticeable. The difference of simulated P80 for sulphides (72 μm) and NSG (88 μm) population reflects a different behaviour in terms of grinding, which is amplified in the circuit by the size separation method; the denser particles being more likely directed to the underflow at a similar size.

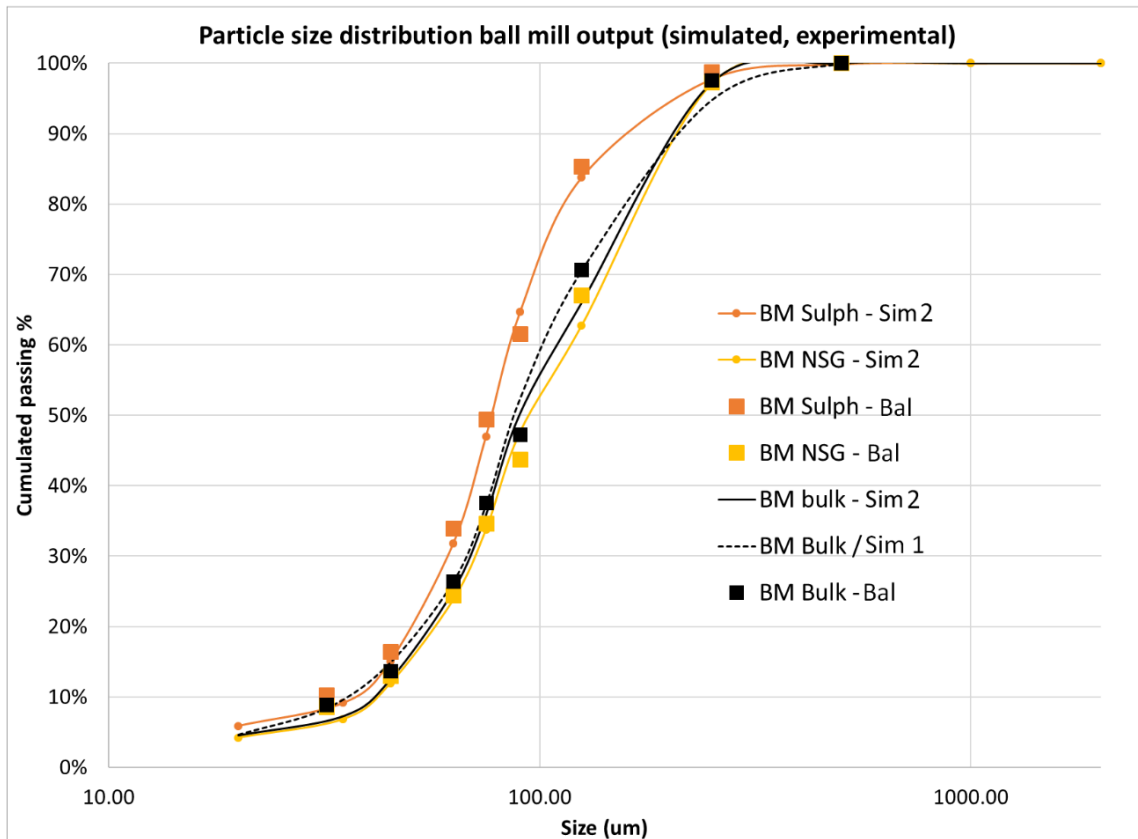


Figure 50: Particle size distributions of the ball mill output (Bal = balanced, Sim 1 = simulated with perfect mixing mill model, Sim 2 = simulated with multi-particle perfect mixing mill model). Bulk refers to PSD for the complete particle flow and is shown in black. For the balanced and Sim 2 results, sulphide particle population PSD is represented in orange and NSG particle population PSD is in yellow. The simulated results are coherent with experimental observations, both for the bulk and the gangue and sulphide distributions.

The multi-particle model exhibits good potential for circuit optimization. For instance, considering in this specific case, that the most important parameter in the cyclone overflow is sulphide size distribution for flotation, and not overall nor gangue distribution. The prediction would limit overgrinding of the sulphides, reduce recirculation flow rate and the average energy consumption of the circuit per ton of

concentrate. Table 16 shows that it is possible to reduce the recirculation load and the mill circuit energy consumption per ton of processed ore by increasing the feed flow rate and considering acceptable an increase of the cyclone overflow P80 of the sulphides. As another option for optimization, different sizing equipment setting could be selected (for instance cyclone number and dimensions).

Table 16: Sim 2 results with base case feed flow rate (0.67t/h) and increased flow rate (+5% and +10%), representing the cyclone overflow (OF) P80 for the sulphide population and for the “bulk” -i.e. the sulphides and NSG populations – and the mill circuit power consumption.

Feed flow rate (t/h)	Cyclone OF Sulphide P80 (um)	Cyclone OF Bulk P80 (um)	Mill circuit power consumption (kW/t)
0.67	71.79	87.53	375.292
0.70	72.54	88.60	359.752
0.75	73.71	90.76	336.738

An important parameter to take into account, which has been observed but not studied in this project, is the difference in ore behaviour, at the earliest crushing stage. Indeed, as seen in the feed analyses, there is a difference in mineral distribution within particle size classes already after the crushing. A more in-depth simulation should also consider using multi-particle modelling for the crushers.

The propositions for optimization described above would only be valid when the liberation size of the sulphide is known and may be verified using polished section analysis or MLA. Multivariate grinding models may also improve the level of detail of blended ore simulation, using different grinding parameters for each ore type. While the multi-particle models require more data than what is usually collected for grinding circuit optimization (chemical analysis by size fraction and section analysis to determine relevant particle populations partition), they offer an alternative representation with a superior definition.

4.2 Dynamic Mill Model Validation Results

Using the Dynamic Dialog tool, a total of 6h40min were simulated, with time steps of 2 minutes. The first recording of the plant control system (10:24:16) for the crushed

ore feed and pebbles started at the simulation time of 2:00 hours, in order to let the system reach a steady state before making the first modification.

The simulated results are presented against plant control log data in Figure 51 and Figure 52. Overall, the simulated power consumption fits the experimental values well. The small deviations are attributed to minor perturbations to the input feed tonnage (as most prominently seen at 12 and 116 minutes).

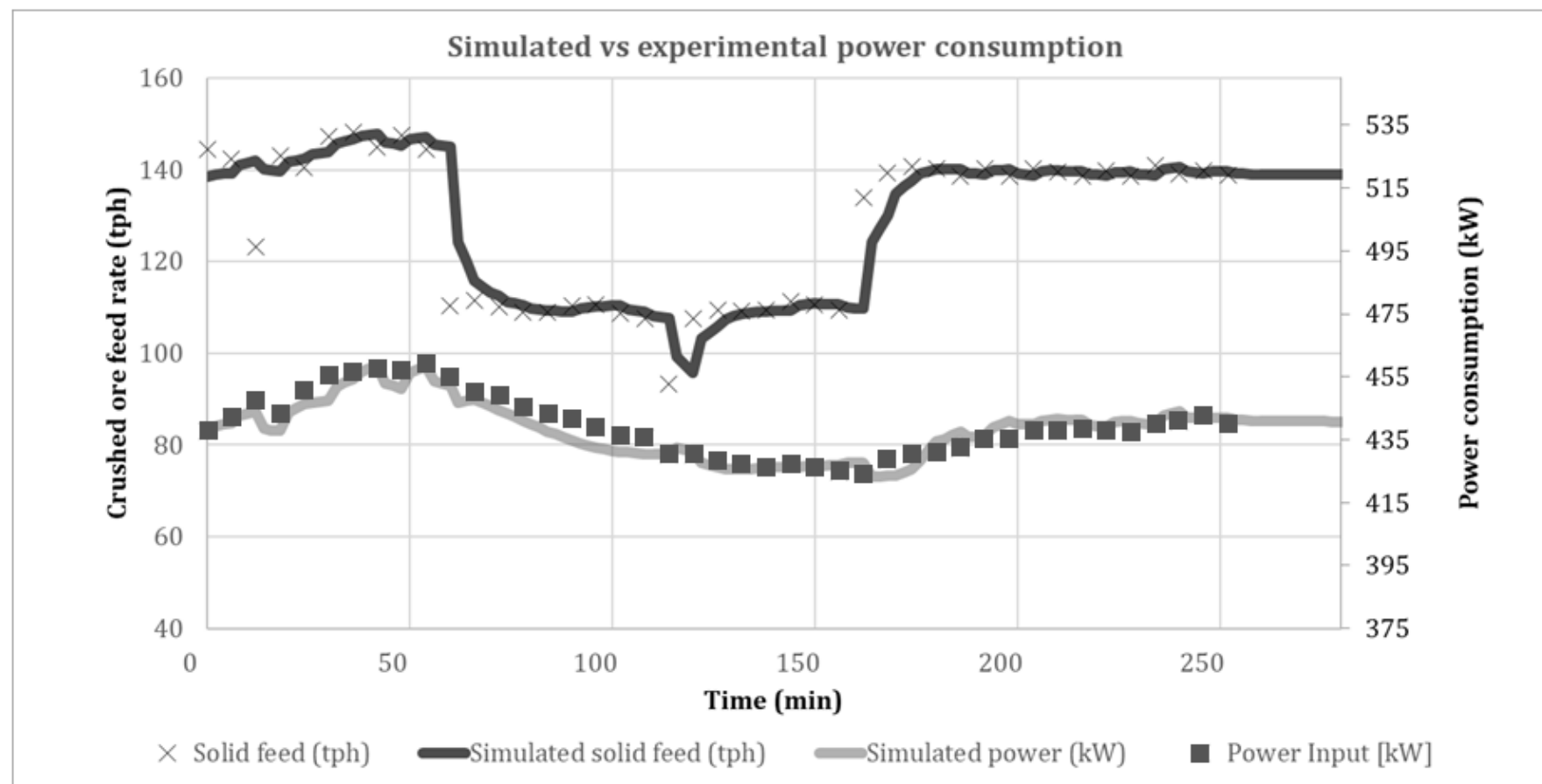


Figure 51: Simulated and experimental power consumption evolution across the step change.

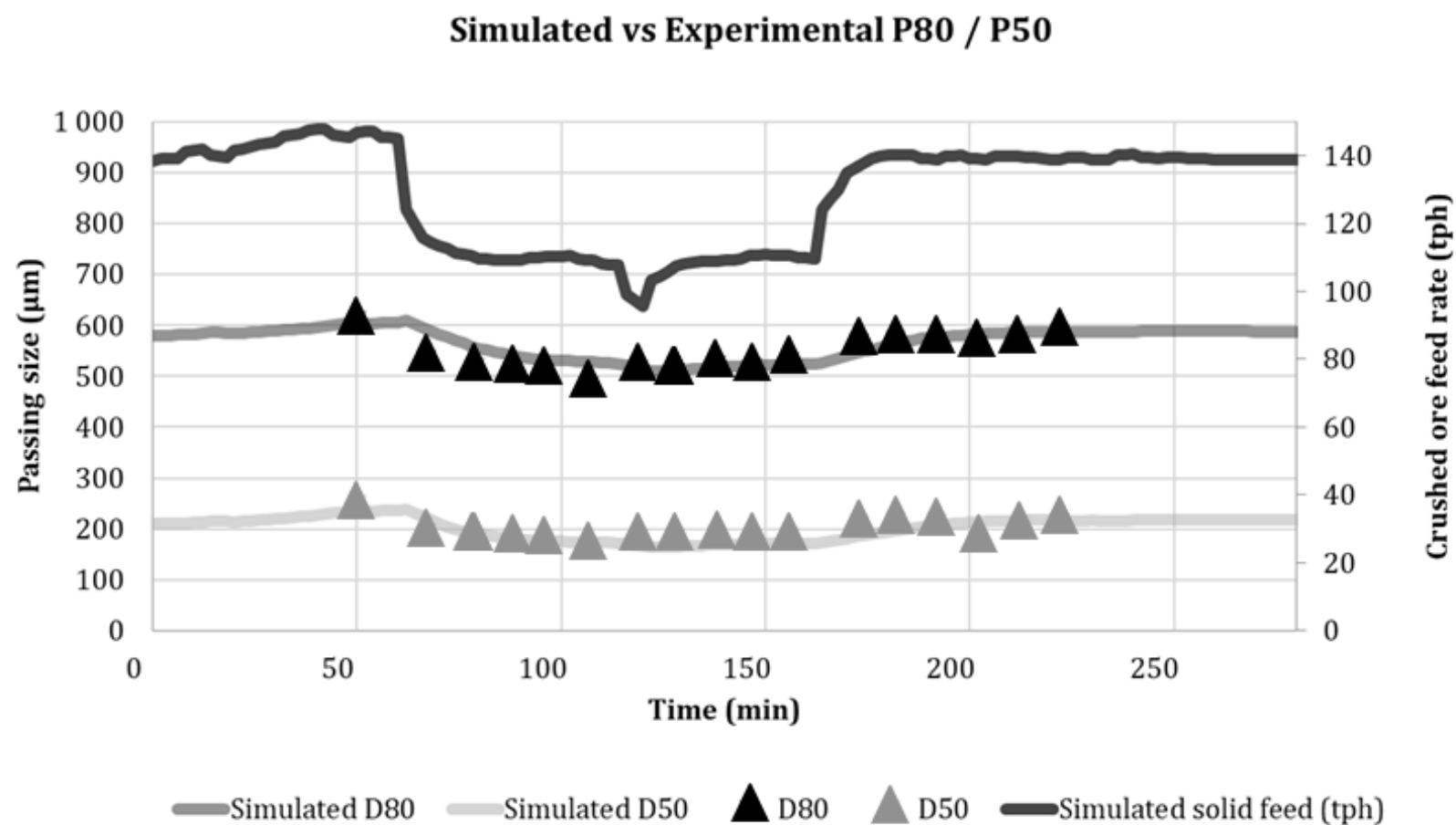


Figure 52: Simulated and experimental P80 and P50 evolution across the step change.

The simulated PSD was also close to the experimental values. Both comparisons between simulation and real data contribute to the validation of this model for dynamic simulation, as can be seen in Figure 53 and Figure 54.

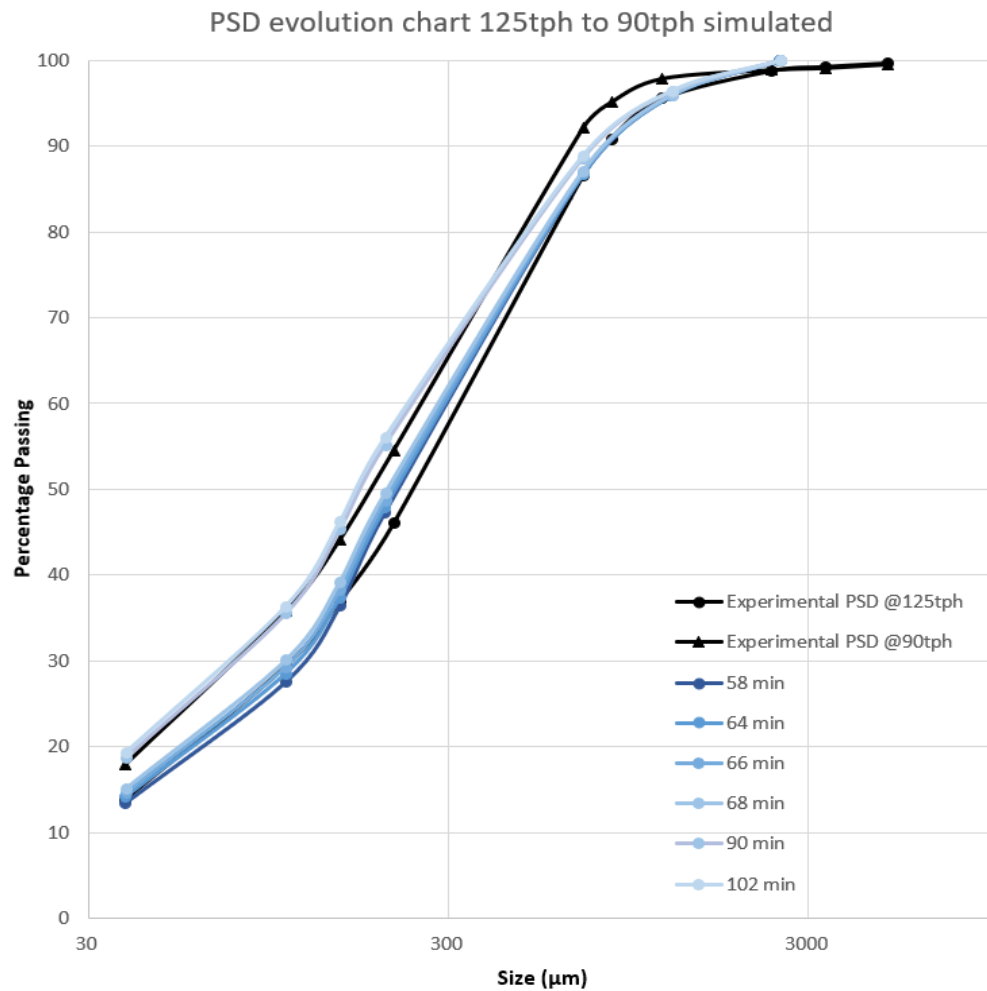


Figure 53: Particle size evolution when the crushed ore feed was changed from 125tph to 90tph.

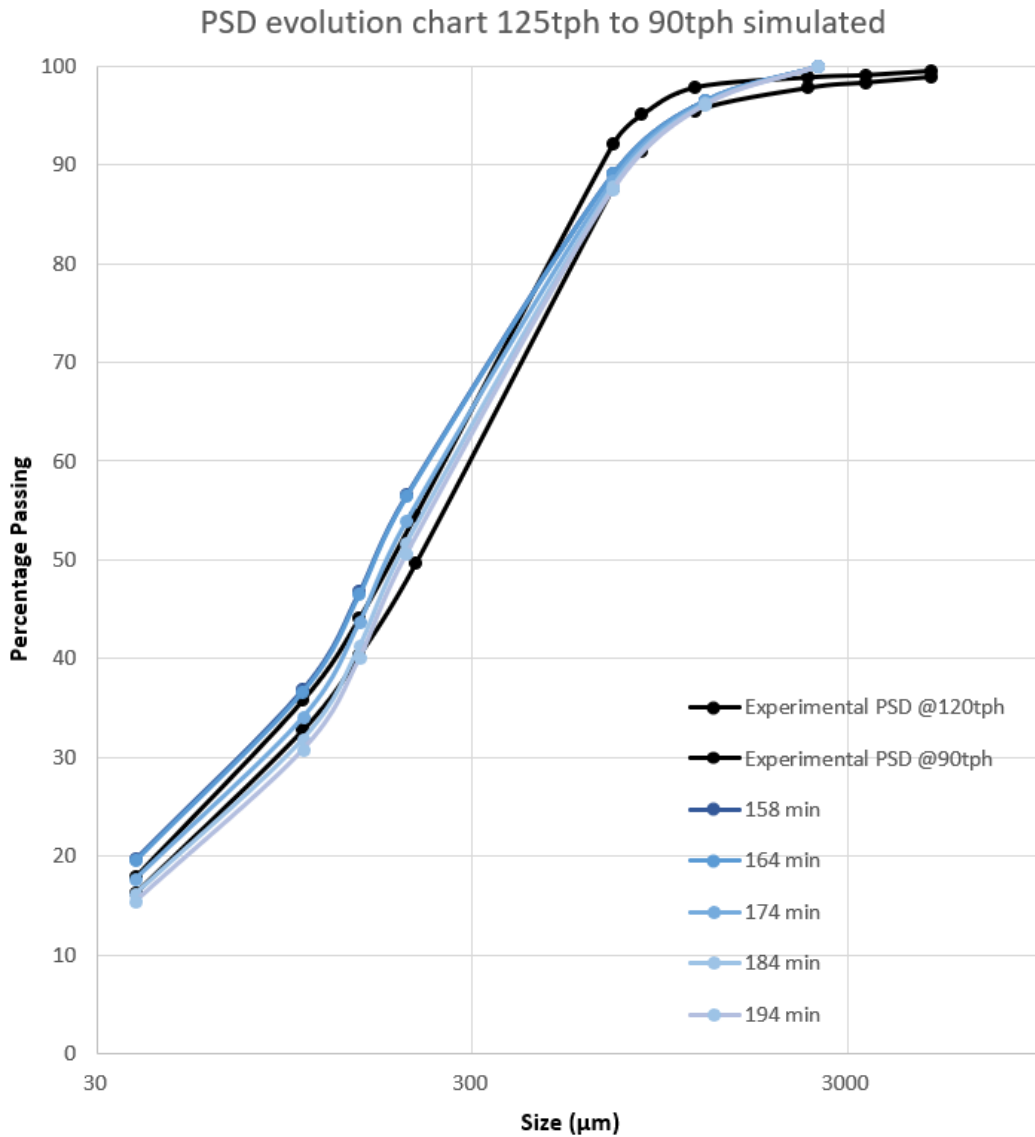


Figure 54: Particle size evolution when the crushed ore feed was changed from 90tph to 120tph.

From the PSD and power consumption simulation, the trend and duration of the transient phase is replicating the experimental data adequately. However, it can be noticed that the model seems more sensitive to short-term changes in the input feed rate than in reality and should have a smoother response. This can be avoided by removing noise from the input data (averaged feed rate values), as illustrated in Figure 55 and Figure 56. Further studies and longer-term experimental data (over a day or a week) would allow the validation of this model to be extended and provide greater confidence for real-world simulation.

Additionally, the impact of the time step used for a simulation task using this model according to the simulated period would also need to be studied further. Indeed, as this model is step based, the choice of a longer time step (ten minutes for instance), would considerably increase the speed of the simulation, but may lead to less accurate results or distorted trends. This would depend on the requirements in terms of computing time and available computing power, especially for more complex flowsheets, containing several mill models and/or other dynamic modules.

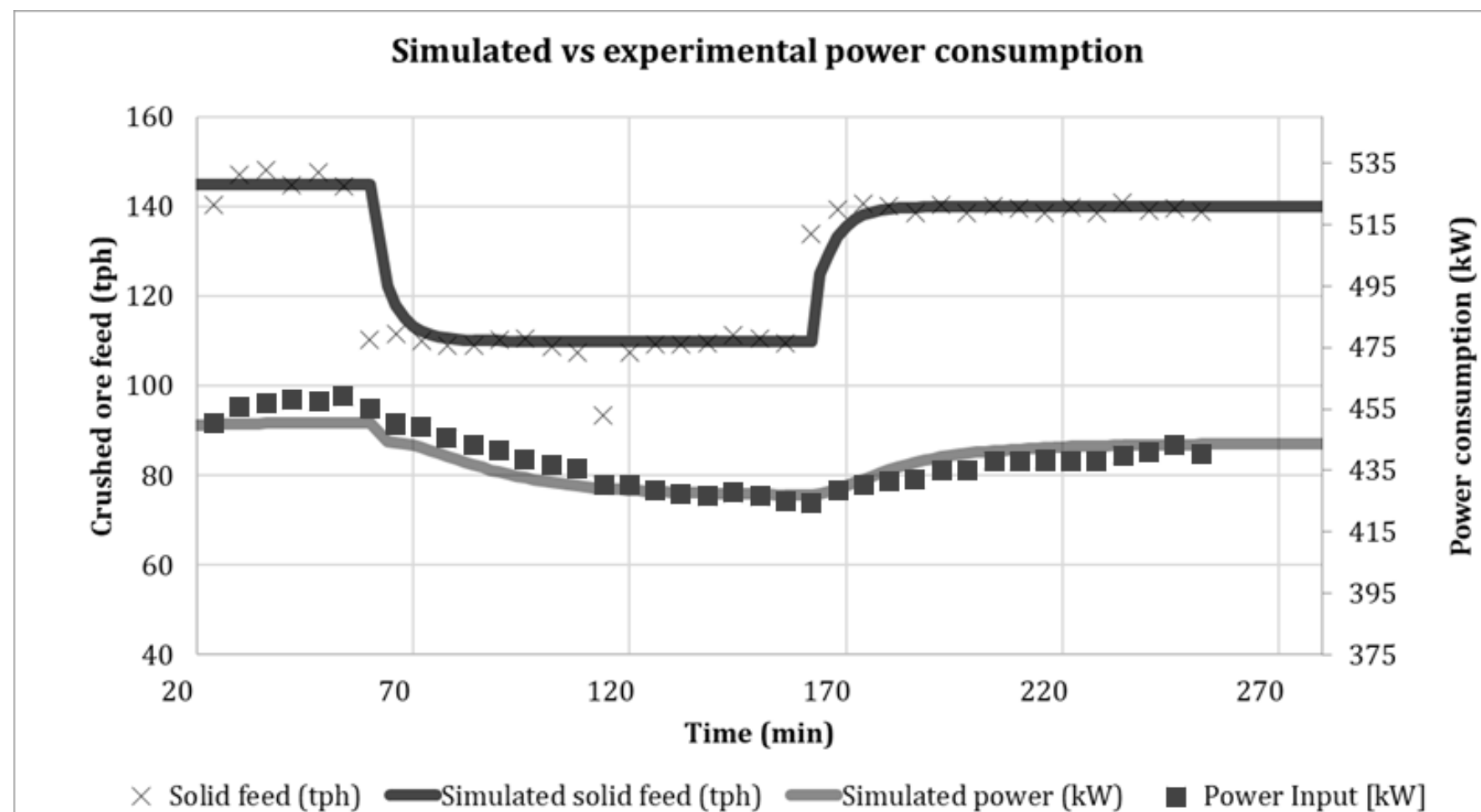


Figure 55: Simulated and experimental power consumption evolution during the step test with average feed rate input.

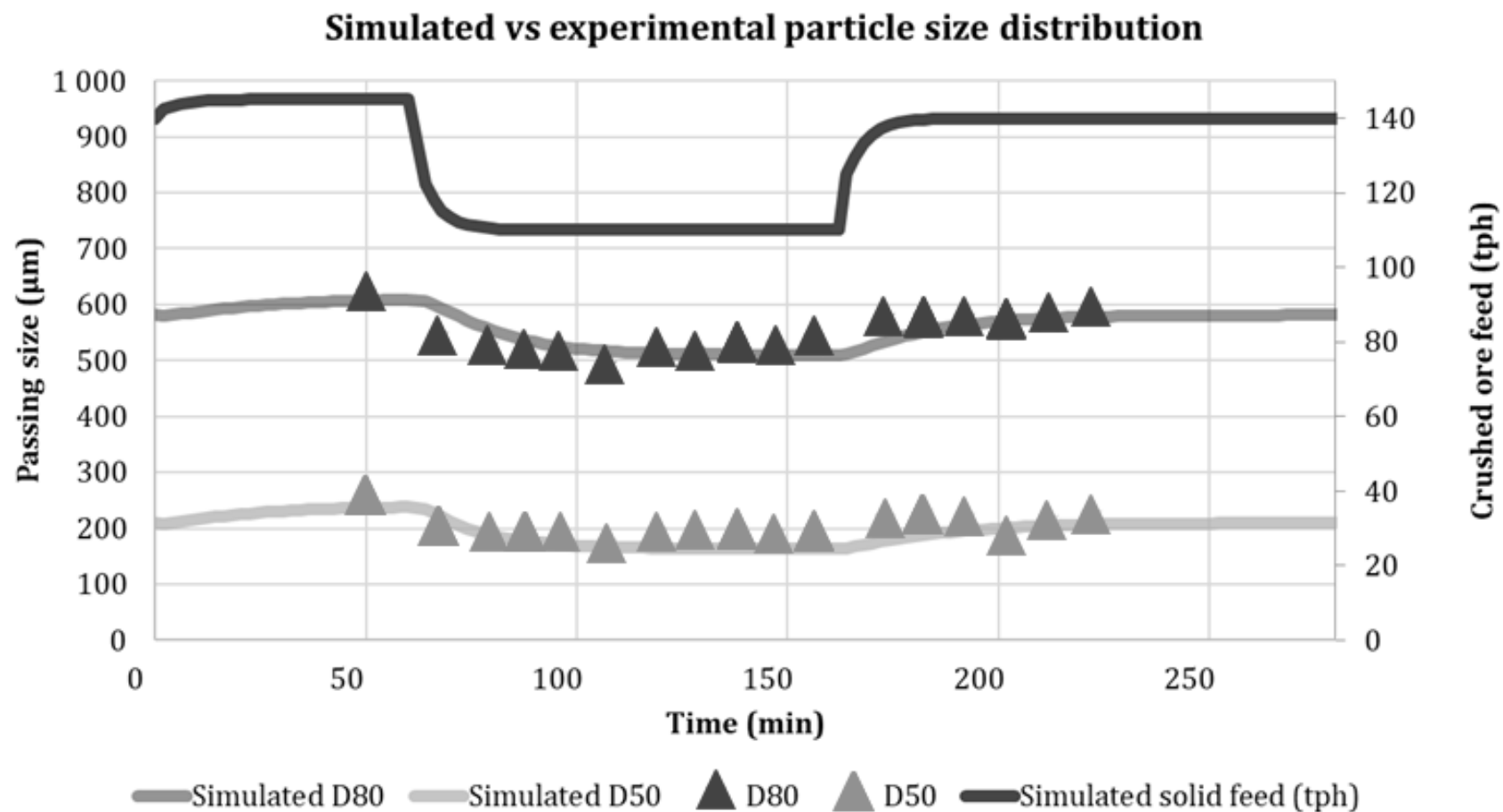


Figure 56: Simulated and experimental P80 and P50 evolution during the step test with average feed rate input.

4.3 Flotation Training Simulator Results

The simulator described in 3.3 was used for on-site flotation operation training courses in 2018 for two operator groups. A complete training handbook, gathering theoretical and practical knowledge used for these exercises was compiled. The training was evaluated on two levels: reaction and learning, from the four proposed by the Kirkpatrick model (Kirkpatrick & Kirkpatrick, 2006). The reaction evaluation comprised a satisfaction feedback from the attendees. The learning evaluation was divided into two parts: a theoretical and a practical examination. The theoretical examination consisted of a pre-questionnaire and a final theory examination, given respectively at the beginning and the at end of the course. The practical examination included five questions that tested the user performance in important Key Performance Indexes, such as decision making. The results of these evaluations are presented in a separated publication (Bergamo et al., 2021).

The Table 17 shows the satisfaction evaluation of the trainees in regard to the training realised using the simulator (also called “Virtual Training”). These results illustrate how the use of simulation met the operator’s requirements for an efficient training.

Table 17: Virtual Training satisfaction evaluation (or reaction evaluation), scaled from 1 (satisfied) to 5 (not satisfied), from the training participants. (SD: Standard Deviation) Figure from Bergamo et al. (2021)

Topic	Average	SD
How would you evaluate the Virtual Learning Experience in general?	4,75	0,45
How well were the learning objectives met?	4,47	0,74
How well the learning theory met your needs?	4,67	0,62
How well the simulation exercises met your needs?	4,60	0,74
How would you evaluate the overall arrangements and the training environment?	4,87	0,35
The pace of the training was good?	4,27	0,59
How would you rate trainers' knowledge of the topic?	4,94	0,25
How understandably did the trainer present the information?	4,79	0,58
How well did the trainer keep you motivated?	4,94	0,25
How well did the trainer support in your learning?	4,94	0,25

From the results showed above, we concluded that using simulation in training satisfied the trainees in terms of efficiency. From several studies, it was shown that using OTS for training operators before a plant start up can improve the operation start-up and its safety (Cheltout et al., 2007; Komulainen et al., 2012), and we can thus expect the same results for this customer case-study when the plant starts its operation. In addition, to measure the real effects of this implementation, a long-term study would be needed with comparative cases. This simulator illustrates the case of a generic simulation designed for training purposes. It is worth noting that the models used, and the level of detail implemented would have been sufficient for supporting a multi-purpose virtual plant design. Adapting the simulator to a real plant layout, characteristics and fitting all the models to a specific process would have required much more time and was beyond the scope of this project.

4.4 Gold processing plant simulation results

4.4.1 Process replication validation

The simulation described above successfully reproduced the expected results from the audit, with correct PSD and recoveries, as well as machine power consumption. Moreover, with varying mineralogy, in accordance with each types of ore fed, these parameters were also accurately modelled as illustrated by the results in Table 18, which shows the relative errors between expected and simulated P80, grinding specific energy, mass pull and Au and S recoveries in the FGO processing line for an average ore from each of the three main alteration zones. These simulation results are obtained in steady state of the dynamic simulation, by adapting the mill speed and load fraction to reach a similar PSD for the flotation feed, and the air feed and cell level to reach the same mass pull during flotation in the three cases. They are compared to Newcrest internal geometallurgical study results mentioned in 3.4.3.1. More complete results are available in the Appendix 14.

Table 18: Relative error between expected P80, specific energy, mass pull and recovery for each alteration type.

Alteration Type	Porphyry (IB, OB & CHL)	Epithermal (LE, UE & SBX)	Argillic (A, AA & UA)
Relative error expected vs. simulated P80 (μm)	0.5 %	1.7 %	1.3 %
Relative error expected vs. simulated grinding circuit specific energy (kwh/t)	-0.8 %	-1.4 %	4.1 %
Relative error expected vs. simulated flotation circuit (FGO) mass pull (%)	4.9 %	-1.7 %	3.3 %
Relative error expected vs. simulated flotation circuit (FGO) Au rec (%)	2.0 %	1.0 %	-3.1 %
Relative error expected vs. simulated flotation circuit (FGO) S rec (%)	-0.6 %	-2.4 %	2.0 %

4.4.2 Optimisation case-study

From the results above, we show that the simulation replicates the real-world process in a satisfactory way. In addition, the digital twin will use the model prediction capabilities for optimization purposes, depending on the cases observed at the plant,

when the simulator is implemented. As a preliminary example of optimisation result, we will take a hypothetical case of a misclassification of a high-grade ore after primary crushing, directed to the low-grade ore stockpile. Using the simulation tool and the on-line sensors in the flotation circuit, a higher actual grade than what is predicted by the simulator is observed, in the flotation feed and concentrate. The error can be identified rapidly and mitigated, for instance by increasing the recovery of the flotation for the laps of time when the error occurs.

In this case, the simulator can be used to determine the changes to make to some operation parameters here, the pulp level and the air input to the flotation cells, in order to preserve a concentrate grade similar to its value post-incident, and a higher recovery. Figure 57 and Figure 58 show the simulation of the FGO line response for 1 hour, when the feed grade is increased. Two cases are represented: in the first one, the issue is not detected, and no parameter is changed immediately in the circuit. In the second case, the issue is detected, the feed grade is abnormally high, and the pulp level is raised (+10 cm) and air flow rate to the FGO flotation cells is increased (+50% of the initial l/m³ air input) in order to boost the recovery. In this example, the recovery can be increased by 2%, while maintaining a similar concentrate grade. It may be noted that the adaptation of the operating parameters could be improved by using specific controller systems in the digital twin implementation, however this is out of the scope of this study.

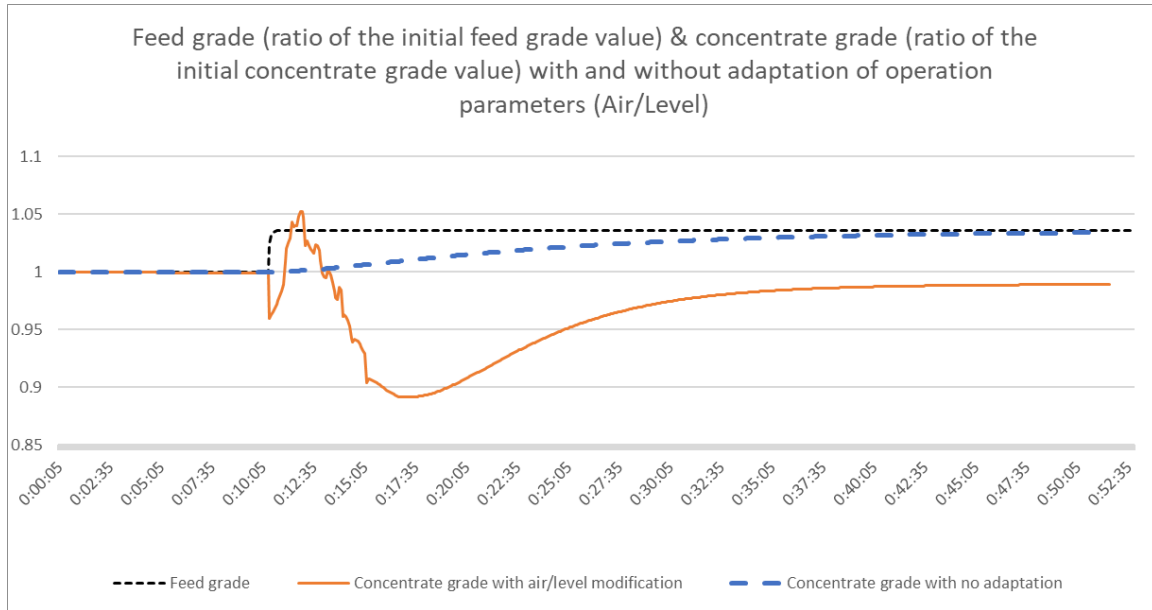


Figure 57: Concentrate and feed grade as a ratio of the initial ($t=0$) value with and without cell operation parameter adaptation for the concentrate. At 10 minutes, the feed grade is increased by 3.5%. With no adaptation of the flotation cell operation parameters, the concentrate grade follows the increase progressively. If the air flow and pulp level to the cells is increased at $t = 10$ minutes, then the grade decreases and stabilises later to a grade closer to the initial concentrate grade. X-axis (time) is given in hours:minutes:seconds.

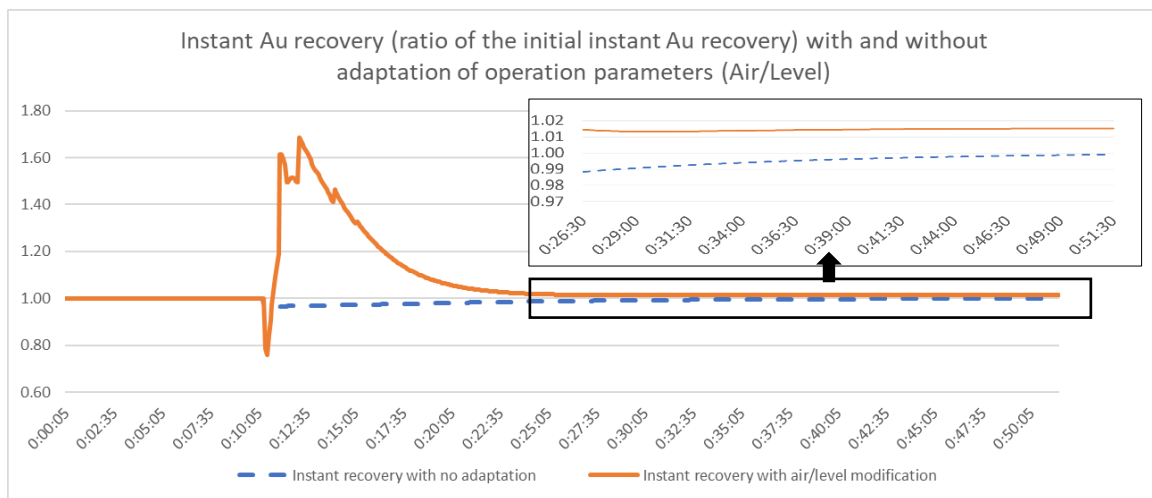


Figure 58: Instant Au recovery as a ratio of the initial ($t=0$) recovery value with and without cell air flow adaptation. The spike between 10 and 20 minutes, corresponding to the change of operation parameters value, is due to the instantaneous calculation of the recovery, based concentrate stream amount of Au per feed Au amount at a given time t , and is thus non representative. In the long term trend, we can see that the modification of pulp level and air flow to the cell increases the recovery by almost 2%.

This example shows the application possibilities of such a simulator. In a real case, in a digital twin application, the warning and adaptation would occur automatically when in this example, the issue is purely simulated. However, these results show a concrete application case for the simulation, in a case of material misclassification.

Chapter 5 Conclusions, discussion and recommendations for future work

5.1 Research questions

- 1/ How modelling and simulation applied to mining and mineral processing can improve the processes in theory, based on comparable industries and customer requests?

In chapter 2, the fact that simulators are widely used in various industries, chemical, pulp and paper, oil and gas, for process optimisation, training simulator, and present as the backbone of the digital twin concept was highlighted. It was showed that the safety of these industries processes was efficiently improved by the implementation of simulators. By analogy, it can be concluded that simulation implementation will have the same long-term impact on mining and mineral processing industry.

- 2/ What are the requirements in terms of modelling, in order to answer to the industry needs?

For implementation of simulation in a plant operation, models need to be implemented for all stages of the processing. In Chapter 2, it was demonstrated that simulation solutions were missing a global overview of the process, needed in the scope of the “Mine to Mill” optimisation. In Chapter 3 we presented the method used to implement several models needed to obtain a simulation from the mine, to the concentrate and thus to be able to conceive an integrated simulation approach, considering the variability of the material being processed. These missing models were added to the software solution presented in the thesis, tested and some were validated.

- 3/ How well dynamic and static geometallurgical mill models can reproduce the performance of a circuit simulation?

In Chapter 4, the method to build a dynamic and a multi-particle (geometallurgical) mill models from Chapter 3, has been tested against real cases from both pilot and plant operations. Both models were able to reproduce the performances of the real case in a very accurate way.

- 4/ How virtual training can be a tool for the formation of operators mineral processing industry?

In Chapter 4, using a simulator which development method was described in Chapter 3, results of operator formation session organised as a virtual training showed a very good satisfaction from the operators' perspective. Based on the feedbacks, the use of simulator based training is demonstrated to offer a viable interactive training opportunity for the mineral processing industry.

- 5/ How modelling and simulation, aiming to be integrated into digital twin, may help with optimisation problem in a gold processing plant?

In Chapter 4 the result of an optimisation case on gold processing plant using a simulator which development method was described in Chapter 3, showed a strong potential to assist the optimisation of a flotation circuit, based on information recovered on the feed stream. The integration of several process units from different circuits (crushing, grinding, flotation in this study) simulated in a common environment and integrating different ore properties is a major novelty contribution for the research and industrial applications.

5.2 Discussion

Mining industry is experiencing deep transformations to align itself with arising sustainability trends. This study explores how modelling and simulation of mineral processing can be instrumental in achieving such transformations.

First, literature review highlighted that mining industry is facing an increasing societal pressure to evolve toward safer, cleaner and more sustainable processes. As a result, key evolutionary trends of mining industry were identified.

In a second time, this study demonstrated that modelling and simulation is to be a major support for the transition towards improved processes in the mineral

processing industry. Indeed, process simulation has been successfully implemented in various industries since 1970s. Nowadays, simulation is used as a backbone for the digital transformation of various industries, in form of digital twins and immersive training simulators.

Examples of successful simulator uses and suggestions for improved implementations in other industries were compiled in order to propose an approach specific to mineral processing. It was showed that a simulator should be conceived for more than one use and for the entire lifecycle of the plant. Such a long-term approach requires regular updates of the simulation. As a consequence, flexibility and ease of maintenance are key desirable features. Based on these observations, the specificities required for the construction of mineral processing simulator are described. Finally, a summary of the existing works is made, and the opportunities offered by the integration of these separate works into a same environment are exposed.

Based on this preliminary context study, it is observed that an integrative simulation environment, encompassing all stages of mineral processing from mine to metal production is lacking and impedes the demand for new simulators in the industry. This shortcoming was alleviated in this study, through the implementation of new and/or improved models in HSC Sim. Indeed, HSC offers a simulation platform that is able to support multi-scale, mine to metal simulations, with state-of-the-art metallurgical and flotation models already implemented in a particle-based environment. The need for a multi-functional and adaptive simulation tool is also considered. This is eased by the adaptive detail scale of the models integrated: dynamic, multi-component, concerning bulk or sized feed, with or without mineralogical information. Both mill models presented in detail in this study participate to this multi-functional approach of a same simulation environment. The multi-particle model option opens new, more detailed possibilities with a geometallurgical approach. The dynamic mill model option is to be used in digital twin and training operators. Finally, simulators developed in HSC Sim during this thesis were successfully implemented and tested in two industrial case-studies. This demonstrates industry interest for such integrated simulation environment.

There is a dire need to improve mining industry understanding of digitalization capabilities for mineral processing. Actual changes may be slow to observe due to the high capital intensity of the mining industry and thus a clear demonstration of the digitalisation potential has to be made through meaningful case-studies such as the ones presented in this thesis.

Thanks to process models either already included or implemented during this study, HSC becomes an ideal environment for integrated mining simulation: from blasting to comminution, flotation, dewatering and even hydro and pyrometallurgy. Associated with the mining plan and geological information, HSC Sim software can be implemented in a digital twin of the plant, reproducing and predicting the mine lifecycle and enabling the optimization of the entire production chain. In addition, HSC particle-based architecture allows for a tailored geometallurgical simulation of a given mineralogical process.

The work carried out during this project demonstrate that simulation capabilities are considered relevant and being investigated by major mining industry actors. However, the practical benefits of simulation use would take a plant lifetime, 10 to 20 years, to be fully recognised and quantified. Nevertheless, the first results, stemming from the simulations detailed in Chapter 4 are promising regarding the potential of simulators to improve mineral processing efficiency.

Further efforts to increase the amount of input data and its quality is expected to enhance the quality of the mathematical models on which simulations rely upon. The mineral processing models are often quite old but are regularly updated, when not completely revisited as new data are acquired. New analysis methods and enhanced computational power enable more accurate and predictive models. For instance, some simulators, such as HSC Sim, already implement tools to import and use mineral liberation analysis (MLA) data as input to their simulation.

In addition, continuous data availability at every stage of the plant lifecycle would help to build, maintain and improve a digital twin simulator. Nowadays, the connection to rapid on-line analysers during operation provides continuous data input and enables better process control. Moreover, early access to rapid geometallurgical tests facilitates the creation of simulators during the plant

commissioning phase. More accessible computational power and more efficient calculation processes enable simulators to be even more multi-purpose. The association with CAD (Computer Aided Design) software layout design turns process simulations more compatible for integration into a comprehensive digital factory solution. The evolution of available data and purposes is expected to prompt a change in simulation use and implementation.

The author believes that an integrated and geometallurgical approach set theoretical ground for mining industry self-improvement in terms of both production efficiency. The work conducted during this thesis aims to bring geometallurgical concepts into a modern and novel, industry adopted, digital simulation solution. Tremendous improvements of the mining process as a whole are expected through the broad adoption of integrated digital solutions.

5.3 Recommendation for future work

The future work within this research may focus on the following:

- Develop the capabilities of dynamic modelling with for other units, such as dewatering.
- Validate the results using more plant or pilot scale results for more models in dynamic mode, in order to ensure their robustness, for instance flotation models.
- Explore further the capacity of surrogate modelling using as a basis semi-empirical simulation result. This may bring increased simulation speed and new opportunities for simulator developments.
- Develop more partnership with industrial users of simulation tools. In order to validate and demonstrate widely the importance of modelling and simulation for the improvement of industrial processes, more cases need to be studied in collaboration with the industry.

References

- Abhilash, S. S., Meshram, P. & Pandey, B. D. (2016). Metallurgical processes for the recovery and recycling of lanthanum from various resources - A review. *Hydrometallurgy*, 160, 47–59. <https://doi.org/10.1016/j.hydromet.2015.12.004>
- Adler, R. A., Claassen, M., Godfrey, L. & Turton, A. R. (2007). Water, mining, and waste: An historical and economic perspective on conflict management in South Africa. *The Economics of Peace and Security Journal*, 2(2). <https://doi.org/10.15355/epsj.2.2.33>
- Ahmad, A. L., Low, E. M. & Shukor, S. R. A. (2010). Safety Improvement and Operational Enhancement via Dynamic Process Simulator: A Review. *Chemical Product and Process Modeling*, 5(1). <https://doi.org/10.2202/1934-2659.1502>
- Asad, M. W. A. & Dimitrakopoulos, R. (2013). A heuristic approach to stochastic cutoff grade optimization for open pit mining complexes with multiple processing streams. *Resources Policy*, 38(4), 591–597. <https://doi.org/10.1016/j.resourpol.2013.09.008>
- Austin, L. G., Luckie, P. T., Klimpel, R. R. & of Mining Engineers of AIME, S. (1984). *Process engineering of size reduction : ball milling*. New York : Society of Mining Engineers of the American Institute of Mining, Metallurgical and Petroleum Engineers.
- Balasko, B., Nemeth, S., Janecska, A., Nagy, T. & Nagy, G. (2007). *Process Modeling and Simulation for Optimization of Operating Processes*. 895–900.
- Ballantyne, G. R. & Powell, M. S. (2014). Benchmarking comminution energy consumption for the processing of copper and gold ores. *Minerals Engineering*. <https://doi.org/10.1016/j.mineng.2014.05.017>
- Bauer, C. J. (2004). Siren song: Chilean water law as a model for international reform. In *Resources for the Future*. <https://doi.org/10.4324/9781936331062>
- Bearman, R. A., Briggs, C. A. & Kojovic, T. (1997). The application of rock mechanics parameters to the prediction of comminution behaviour. *Minerals Engineering*, 10(3), 255–264. [https://doi.org/10.1016/s0892-6875\(97\)00002-2](https://doi.org/10.1016/s0892-6875(97)00002-2)
- Bengtsson, M. & Evertsson, C. M. (2008). Modelling of output and power consumption in vertical shaft impact crushers. *International Journal of Mineral Processing*, 88(1–2), 18–23. <https://doi.org/10.1016/J.MINPRO.2008.04.005>
- Bergamo, P., Izart, C., de Carvalho, M. A., Streng, E., Rosenkranz, J. & Ghorbani, Y. (2021). The use of different evaluation methods for simulation-based training - a flotation study. *Evaluation and Program Planning, Submitted*.
- Blackwell, J. L., Cooke, D. R., McPhie, J. & Simpson, K. A. (2014). Lithofacies associations and evolution of the volcanic host succession to the minifie ore zone: Ladolam gold deposit, Lihir Island, Papua New Guinea. *Economic Geology*, 109(4), 1137–1160. <https://doi.org/10.2113/econgeo.109.4.1137>

References

- Bond, F. C. (1952). The third theory of comminution. *Transactions of AIME Mining Engineering*. <https://doi.org/10.1016/j.mineng.2006.01.007>
- Boulton, A., Fornasiero, D. & Ralston, J. (2005). Effect of iron content in sphalerite on flotation. *Minerals Engineering*. <https://doi.org/10.1016/j.mineng.2005.03.008>
- Bradley, P. G. (1980). Modelling mining. Open pit copper production in British Columbia. *Resources Policy*, 6(1), 44–59. [https://doi.org/10.1016/0301-4207\(80\)90006-9](https://doi.org/10.1016/0301-4207(80)90006-9)
- Broadbent, S. R. & Callcott, T. G. (1956). A Matrix Analysis of Processes Involving Particle Assemblies. *Philosophical Transactions of the Royal Society of London. Series A, Mathematical and Physical Sciences*, 249(960), 99–123.
- Bueno, M. P., Kojovic, T., Powell, M. S. & Shi, F. (2013). Multi-component AG/SAG mill model. *Minerals Engineering*, 43–44, 12–21. <https://doi.org/10.1016/j.mineng.2012.06.011>
- Bueno, M. & Powell, M. (2012). How to Use Hard Ore Components as Grinding Media. *Auslmm 11th Mill Operators Conference*.
- Bueno, M. & Powell, M. S. (2011). The dominance of the competent. *5th International Autogenous and Semi-Autogenous Grinding Technology*.
- Cairns, R. D. & Shinkuma, T. (2004). The choice of the cutoff grade in mining. *Resources Policy*, 29(3–4), 75–81. <https://doi.org/10.1016/j.resourpol.2004.06.002>
- Calvo, G., Mudd, G., Valero, A. & Valero, A. (2016). Decreasing Ore Grades in Global Metallic Mining: A Theoretical Issue or a Global Reality? *Resources*, 5(4), 36. <https://doi.org/10.3390/resources5040036>
- Chanda, E. K. C. & Dagdelen, K. (1995). Optimal blending of mine production using goal programming and interactive graphics systems. *International Journal of Surface Mining, Reclamation and Environment*, 9(4), 203–208. <https://doi.org/10.1080/09208119508964748>
- Cheltout, Z., Coupier, R. & Valleur, M. (2007). Capture the long-term benefits of operator training simulators. *Hydrocarbon Processing*, 86(4), 111–116.
- Collins, T. (2007). ImageJ for microscopy. *BioTechniques*, 43(S1), S25–S30. <https://doi.org/10.2144/000112517>
- de Bakker, J. (2014). Energy use of fine grinding in mineral processing. *Metallurgical and Materials Transactions E*, 1(1), 8–19.
- Department of Environment. (2007). Mining Industry Energy Bandwidth Study. In *US Department of Energy*. https://www1.eere.energy.gov/manufacturing/resources/mining/pdfs/mining_bandwidth.pdf
- Dobby, G. S. & Finch, J. A. (1986). Flotation Column Scale-up and Modelling. *CIM Bulletin*, 79, 89–96.
- Dominy, S. C., Noppé, M. A. & Annels, A. E. (2002). Errors and uncertainty in mineral resource and ore reserve estimation: The importance of getting it right. *Exploration and Mining Geology*, 11(1–4), 77–98. <https://doi.org/10.2113/11.1-4.77>

References

- Donoso, M., Robles, P. A., Gálvez, E. D. & Cisternas, L. A. (2013). Particle size effect on the efficient use of water and energy in mineral concentration processes. *Industrial and Engineering Chemistry Research*, 52(49), 17686–17690. <https://doi.org/10.1021/ie402099n>
- Elshkaki, A., Graedel, T. E., Ciacci, L. & Reck, B. (2016). Copper demand, supply, and associated energy use to 2050. *Global Environmental Change*, 39, 305–315. <https://doi.org/10.1016/j.gloenvcha.2016.06.006>
- Elshkaki, A., Graedel, T. E., Ciacci, L. & Reck, B. K. (2018). Resource Demand Scenarios for the Major Metals. *Environmental Science and Technology*, 52(5), 2491–2497. <https://doi.org/10.1021/acs.est.7b05154>
- Filippov, L., Farrokhpay, S., Lyo, L. & Filippova, I. (2019). Spodumene flotation mechanism. *Minerals*, 9(6). <https://doi.org/10.3390/min9060372>
- Flintoff, B. C., Plitt, L. R. & Turak, A. A. (1987). Cyclone Modelling: A Review of Present Technology. *CIM Bulletin*.
- Fourie, A. (2009). Preventing catastrophic failures and mitigating environmental impacts of tailings storage facilities. *Procedia Earth and Planetary Science*, 1(1), 1067–1071. <https://doi.org/10.1016/j.proeps.2009.09.164>
- Franks, D. M., Boger, D. V., Côte, C. M. & Mulligan, D. R. (2011). Sustainable development principles for the disposal of mining and mineral processing wastes. *Resources Policy*, 36(2), 114–122. <https://doi.org/10.1016/j.resourpol.2010.12.001>
- Gasafi, E. & Pardemann, R. (2020). Processing of spodumene concentrates in fluidized-bed systems. *Minerals Engineering*, 148. <https://doi.org/10.1016/j.mineng.2020.106205>
- Geissbauer, R., Vedso, J. & Schrauf, S. (2016). *Industry 4.0: Building the digital enterprise*. PWC, 2016 Global Industry 4.0 Survey. <https://www.pwc.com/gx/en/industries/industries-4.0/landing-page/industry-4.0-building-your-digital-enterprise-april-2016.pdf>
- Ghorbani, Y., Nwaila, G. T. & Chirisa, M. (2020). Systematic Framework toward a Highly Reliable Approach in Metal Accounting. *Mineral Processing and Extractive Metallurgy Review*, 1–15. <https://doi.org/10.1080/08827508.2020.1784164>
- Giltsbach, L., Schütte, P. & Franken, G. (2019). Applying water risk assessment methods in mining: Current challenges and opportunities. *Water Resources and Industry*, 22, 100118. <https://doi.org/10.1016/j.wri.2019.100118>
- Goldsman, D., Nance, R. E. & Wilson, J. R. (2009). A brief history of simulation. *Proceedings - Winter Simulation Conference*, 310–313. <https://doi.org/10.1109/WSC.2009.5429341>
- Gorain, B. K., Franzidis, J. P. & Manlapig, E. V. (1999). The empirical prediction of bubble surface area flux in mechanical flotation cells from cell design and operating data. *Minerals Engineering*, 12(3), 309–322. [https://doi.org/10.1016/s0892-6875\(99\)00008-4](https://doi.org/10.1016/s0892-6875(99)00008-4)
- Gorain, B. K., Harris, M. C., Franzidis, J. P. & Manlapig, E. V. (1998). The effect of froth

References

- residence time on the kinetics of flotation. *Minerals Engineering*, 11(7), 627–638. [https://doi.org/10.1016/s0892-6875\(98\)00047-8](https://doi.org/10.1016/s0892-6875(98)00047-8)
- Grau, R. A., Laskowski, J. S. & Heiskanen, K. (2005). Effect of frothers on bubble size. *International Journal of Mineral Processing*, 76(4), 225–233. <https://doi.org/10.1016/j.minpro.2005.01.004>
- Gunal, M. M. (2019). *Simulation and the Fourth Industrial Revolution*. https://doi.org/10.1007/978-3-030-04137-3_1
- Guntoro, P. I., Tiu, G., Ghorbani, Y., Lund, C. & Rosenkranz, J. (2019). Application of machine learning techniques in mineral phase segmentation for X-ray microcomputed tomography (μ CT) data. *Minerals Engineering*, 142, 105882. <https://doi.org/10.1016/j.mineng.2019.105882>
- Gy, P. (1967). *L'échantillonnage des minerais en vrac: t. 1: theorie generale*. Societe de l'industrie minerale.
- Gy, P. M. (1976). The sampling of particulate materials - A general theory. In *International Journal of Mineral Processing*. [https://doi.org/10.1016/0301-7516\(76\)90020-X](https://doi.org/10.1016/0301-7516(76)90020-X)
- Hamid, S. A., Alfonso, P., Oliva, J., Anticoi, H., Guasch, E., Sampaio, C. H., Garcia-Vallès, M. & Escobet, T. (2019). Modeling the liberation of comminuted scheelite using mineralogical properties. *Minerals*, 9(9). <https://doi.org/10.3390/min9090536>
- Herbst, J. A. & Fuerstenau, D. W. (1980). Scale-up procedure for continuous grinding mill design using population balance models. *International Journal of Mineral Processing*, 7(1), 1–31. [https://doi.org/10.1016/0301-7516\(80\)90034-4](https://doi.org/10.1016/0301-7516(80)90034-4)
- Hodouin, D. (2011). Methods for automatic control, observation, and optimization in mineral processing plants. *Journal of Process Control*, 21(2), 211–225. <https://doi.org/10.1016/j.jprocont.2010.10.016>
- Hosseinpour, F. & Hajihosseini, H. (2009). Importance of Simulation in Manufacturing. *World Academy of Science, Engineering and Technology*, 51(3), 292–295.
- Innovation Union. (2010). *Communication From the Commission to the European Parliament, the Council, the European Economic and Social Committee and the Committee of the Regions*. 1–43. <https://eur-lex.europa.eu/legal-content/EN/TXT/?uri=CELEX%3A52017DC0490>
- Jahangirian, M., Eldabi, T., Naseer, A., Stergioulas, L. K. & Young, T. (2010). Simulation in manufacturing and business: A review. *European Journal of Operational Research*, 203(1), 1–13. <https://doi.org/10.1016/j.ejor.2009.06.004>
- Jameson, G. J. (2012). The effect of surface liberation and particle size on flotation rate constants. *Minerals Engineering*, 36–38, 132–137. <https://doi.org/10.1016/j.mineng.2012.03.011>
- Jana, A. K. (2018). *Chemical process modelling and computer simulation*. PHI Learning Private Limited.
- Jara, R. M., Couble, A., Emery, X., Magri, E. J. & Ortiz, J. M. (2006). Block size selection and its impact on open-pit design and mine planning. In *Journal of the Southern African*

Institute of Mining and Metallurgy.

- Johansson, M., Bengtsson, M., Evertsson, M. & Hulthén, E. (2017). A fundamental model of an industrial-scale jaw crusher. *Minerals Engineering*, 105, 69–78. <https://doi.org/10.1016/J.MINENG.2017.01.012>
- Jones, D. R. (1992). Current applications of simulators in the process industries and future trends. *Operator Training Simulators, IEE Colloquium On*, 3/1-3/4.
- Kaartinen, J., Pietilä, J., Remes, A. & Torttila, S. (2013). Using a virtual flotation process to track a real flotation circuit. *IFAC Proceedings Volumes (IFAC-PapersOnline)*. <https://doi.org/10.3182/20130825-4-US-2038.00061>
- Karelovic, P., Putz, E. & Cipriano, A. (2016). Dynamic hybrid modeling and simulation of grinding-flotation circuits for the development of control strategies. *Minerals Engineering*, 93, 65–79. <https://doi.org/10.1016/j.mineng.2016.01.021>
- Karelovic, Pablo, Putz, E. & Cipriano, A. (2015). A framework for hybrid model predictive control in mineral processing. *Control Engineering Practice*, 40, 1–12. <https://doi.org/10.1016/j.conengprac.2015.02.006>
- Kellner, M. I., Madachy, R. J. & Raffo, D. M. (1999). Software process simulation modeling: Why? What? How? *Journal of Systems and Software*, 46(2–3), 91–105. [https://doi.org/10.1016/S0164-1212\(99\)00003-5](https://doi.org/10.1016/S0164-1212(99)00003-5)
- Kesler, S E & Simon, A. C. (2015). *Mineral Resources, Economics and the Environment* (Second Edi). Cambridge University Press.
- Kesler, Stephen E., Gruber, P. W., Medina, P. A., Keoleian, G. A., Everson, M. P. & Wallington, T. J. (2012). Global lithium resources: Relative importance of pegmatite, brine and other deposits. *Ore Geology Reviews*, 48, 55–69. <https://doi.org/10.1016/j.oregeorev.2012.05.006>
- Khajehzadeh, N., Haavisto, O. & Koresaar, L. (2017). On-stream mineral identification of tailing slurries of an iron ore concentrator using data fusion of LIBS, reflectance spectroscopy and XRF measurement techniques. *Minerals Engineering*, 113, 83–94. <https://doi.org/10.1016/j.mineng.2017.08.007>
- King, R. (1978). A pilot-plant investigation of a kinetic model for flotation. *Journal of the South African Institute of Mining and Metallurgy*, July, 325–338.
- King, R. P. (1994). Comminution and liberation of minerals. *Minerals Engineering*, 7(2–3), 129–140. [https://doi.org/10.1016/0892-6875\(94\)90059-0](https://doi.org/10.1016/0892-6875(94)90059-0)
- King, R. P. (2012). Modeling and Simulation of Mineral Processing Systems. In C. L. Schneider & E. A. King (Eds.), *SME* (2nd ed.). Elsevier. <https://doi.org/10.1016/C2009-0-26303-3>
- Kinnunen, P. H. M. & Kaksonen, A. H. (2019). Towards circular economy in mining: Opportunities and bottlenecks for tailings valorization. *Journal of Cleaner Production*, 228, 153–160. <https://doi.org/10.1016/j.jclepro.2019.04.171>
- Kirkpatrick, D. L. & Kirkpatrick, J. D. (2006). *Evaluating training programs : the four levels*. Berrett-Koehler.

References

- Klimpel, R. R. (1980). Selection of chemical reagents for flotation. *Mineral Processing Plant Design*, 2, 907–934.
- Komulainen, T. M., Sannerud, R., Nordsteien, B. & Nordhus, H. (2012). Economic benefits of training simulators. *World Oil*, 233(12), 61–65.
- Kongas, M. & Saloheimo, K. (2009). Online slurry particle size analyzers. In D. Malhotra, P. R. Taylor, E. Spiller & M. LeVier (Eds.), *Recent Advances in Mineral Processing Plant Design*. Society for Mining, Metallurgy, & Exploration.
- Kuntzsch, S. (2014). *Energy Efficiency Investigations with a new Operator Training Simulator for Biorefineries*. Jacobs University.
- Lamberg, P. (2010). Structure of a Property Based Simulator for Minerals and Metallurgical Industry. *51st SIMS Conference on Simulation and Modelling*, 1–5.
- Lamberg, P. (2011). Particles - the bridge between geology and metallurgy. *Conference in Minerals Engineering : Luleå, 8-9 February 2011*.
- Leblanc, M., Morales, J. A., Borrego, J. & Elbaz-Poulichet, F. (2000). 4,500-year-old mining pollution in southwestern Spain: Long-term implications for modern mining pollution. *Economic Geology*, 95(3), 655–661. <https://doi.org/10.2113/gsecongeo.95.3.655>
- Li, H., Evertsson, M., Lindqvist, M. & Hulth, E. (2018). Optimization a SAG Mill-Pebble Crusher Circuit By Controlling Crusher Operational Parameters. *Minerals Engineering*, 127(SI: Comminution '18), 98–104.
- Lishchuk, V. (2016). *Geometallurgical Programs – Critical Evaluation of Applied Methods and Techniques* (Issue June). Dissertation, Luleå Tekniska Universitet.
- Lishchuk, V., Lund, C., Lamberg, P. & Miroshnikova, E. (2018). Simulation of a Mining Value Chain with a Synthetic Ore Body Model: Iron Ore Example. *Minerals*, 8(11), 536. <https://doi.org/10.3390/min8110536>
- Liu, Y. & Spencer, S. (2004). Dynamic simulation of grinding circuits. *Minerals Engineering*, 17(11–12), 1189–1198. <https://doi.org/10.1016/j.mineng.2004.05.018>
- López Steinmetz, R. L. & Fong, S. B. (2019). Water legislation in the context of lithium mining in Argentina. *Resources Policy*, 64, 101510. <https://doi.org/10.1016/j.resourpol.2019.101510>
- Lotter, N. O., Oliveira, J. F., Hannaford, A. L. & Amos, S. R. (2013). Flowsheet development for the Kamoia project - A case study. *Minerals Engineering*, 52, 8–20. <https://doi.org/10.1016/j.mineng.2013.02.014>
- Lutandula, M. S. & Maloba, B. (2013). Recovery of cobalt and copper through reprocessing of tailings from flotation of oxidised ores. *Journal of Environmental Chemical Engineering*, 1(4), 1085–1090. <https://doi.org/10.1016/j.jece.2013.08.025>
- Lynch, A. J. (1977). *Mineral Crushing and Grinding Circuits*. Elsevier.
- Lynch, A. J. & Morrison, R. D. (1999). Simulation in mineral processing history, present status and possibilities. In *Journal of The South African Institute of Mining and Metallurgy*.

References

- Malmberg, M. (2018). *Boliden Summary Report Resources and Reserves Kylylahti*. https://www.boliden.com/globalassets/operations/exploration/mineral-resources-and-mineral-reserves-pdf/2019/resources_and_reserves_kylylahti_2019-12-31.pdf
- Massola, C. P., Chaves, A. P. & Albertin, E. (2016). A discussion on the measurement of grinding media wear. In *Journal of Materials Research and Technology* (Vol. 5, Issue 3, pp. 282–288). Elsevier Editora Ltda. <https://doi.org/10.1016/j.jmrt.2015.12.003>
- Michaux, B., Rudolph, M. & Reuter, M. A. (2018). Challenges in predicting the role of water chemistry in flotation through simulation with an emphasis on the influence of electrolytes. In *Minerals Engineering* (Vol. 125, pp. 252–264). Elsevier Ltd. <https://doi.org/10.1016/j.mineng.2018.06.010>
- Miettinen, J. (2008). Nuclear Power Plant Simulators: Goals and Evolution. *THICKET*, 42, 107–133. www.iaea.org/inis/collection/NCLCollectionStore/_Public/42/101/42101979.pdf
- Miller, J. D., Lin, C. L., Hupka, L. & Al-Wakeel, M. I. (2009). Liberation-limited grade/recovery curves from X-ray micro CT analysis of feed material for the evaluation of separation efficiency. *International Journal of Mineral Processing*, 93(1), 48–53. <https://doi.org/10.1016/j.minpro.2009.05.009>
- Mills, H. K., Piercey, S. J. & Toole, T. (2016). Geology, alteration, and lithogeochemistry of the Hood volcanogenic massive sulfide (VMS) deposits, Nunavut, Canada. *Mineralium Deposita*, 51(4), 533–556. <https://doi.org/10.1007/s00126-015-0612-1>
- Mining Association of Canada. (2005). *Benchmarking the Energy Consumption of Canadian Open-pit Mines*. <http://publications.gc.ca/site/eng/270732/publication.html>
- Molson, J. W., Fala, O., Aubertin, M. & Bussière, B. (2005). Numerical simulations of pyrite oxidation and acid mine drainage in unsaturated waste rock piles. *Journal of Contaminant Hydrology*, 78(4), 343–371. <https://doi.org/10.1016/j.jconhyd.2005.06.005>
- Morrell, S. (1996). Power Draw of Wet Tumbling Mills and its Relationship to Charge Dynamics - Part 1: A Continuum Approach to Mathematical Modelling of Mill Power Draw. *Transactions of the Institute of Mining and Metallurgy*, 105(Section C), 43–53.
- Morrell, S. & Morrison, R. D. (1996). Ag and Sag Mill Circuit Selection and Design By Simulation. *Sag*, January, 769–790.
- Morrell, S & Stephenson, I. (1996). Slurry discharge capacity of autogenous and semi-autogenous mills and the effect of grate design. *International Journal of Mineral Processing*, 46(1–2), 53–72. [https://doi.org/http://dx.doi.org/10.1016/0301-7516\(95\)00060-7](https://doi.org/http://dx.doi.org/10.1016/0301-7516(95)00060-7)
- Morrell, Stephen. (1993). *The Prediction of Power Draw in Wet Tumbling Mills*. <https://doi.org/10.13140/RG.2.1.3189.2248>
- Mosier, D. L. B., Singer, V. I. & Donald, A. (2009). *Volcanogenic massive sulfide deposits of the world: Database and grade and tonnage models*.
- Motard, R. L., Shacham, M. & Rosen, E. M. (1975). Steady state chemical process simulation. *AIChE Journal*, 21(3), 417–436.

References

- Mourtzis, D., Doukas, M. & Bernidaki, D. (2014). Simulation in manufacturing: Review and challenges. *Procedia CIRP*, 25(C), 213–229. <https://doi.org/10.1016/j.procir.2014.10.032>
- Moys, M. H. (1984). Residence time distributions and mass transport in the froth phase of the flotation process. *International Journal of Mineral Processing*, 13(2), 117–142. [https://doi.org/10.1016/0301-7516\(84\)90015-2](https://doi.org/10.1016/0301-7516(84)90015-2)
- Mudd, G. M. (2007). *The Sustainability of Mining in Australia : Key Production Trends and Their Environmental Implications for the Future*. <http://civil.eng.monash.edu.au/publications/>
- Nageswararao, K., Wiseman, D. M. & Napier-Munn, T. J. (2004). Two empirical hydrocyclone models revisited. *Minerals Engineering*, 17(5), 671–687. <https://doi.org/10.1016/j.mineng.2004.01.017>
- Napier-Munn, T. J. & Lynch, A. J. (1992). The modelling and computer simulation of mineral treatment processes — current status and future trends. *Minerals Engineering*, 5(2), 143–167. [https://doi.org/10.1016/0892-6875\(92\)90039-C](https://doi.org/10.1016/0892-6875(92)90039-C)
- Napier-Munn, T. J., Morrell, S., Morrison, R. D. & Kojovic, T. (1999). *Mineral Comminution Circuits - Their Operation and Optimisation*. 413.
- Newcrest Mining Limited. (2014). *Technical Report on the Lihir property in Papua New Guinea*. <https://www.miningdataonline.com/reports/annual/TechnicalLihir2013.pdf>
- Norgate, T. & Jahanshahi, S. (2006). *Energy and greenhouse gas implications of deteriorating quality ore reserves*.
- Northey, S. A., Madrid López, C., Haque, N., Mudd, G. M. & Yellishetty, M. (2018). Production weighted water use impact characterisation factors for the global mining industry. *Journal of Cleaner Production*, 184, 788–797. <https://doi.org/10.1016/j.jclepro.2018.02.307>
- Northey, S. A., Mudd, G. M., Werner, T. T., Haque, N. & Yellishetty, M. (2019). Sustainable water management and improved corporate reporting in mining. *Water Resources and Industry*, 21, 100104. <https://doi.org/10.1016/j.wri.2018.100104>
- Northey, S. A., Mudd, G. M., Werner, T. T., Jowitt, S. M., Haque, N., Yellishetty, M. & Weng, Z. (2017). The exposure of global base metal resources to water criticality, scarcity and climate change. *Global Environmental Change*, 44, 109–124. <https://doi.org/10.1016/j.gloenvcha.2017.04.004>
- Northey, S., Mohr, S., Mudd, G. M., Weng, Z. & Giurco, D. (2014). Modelling future copper ore grade decline based on a detailed assessment of copper resources and mining. *Resources, Conservation and Recycling*, 83, 190–201. <https://doi.org/10.1016/j.resconrec.2013.10.005>
- Oxley, A. & Barcza, N. (2013). Hydro-pyro integration in the processing of nickel laterites. *Minerals Engineering*, 54, 2–13. <https://doi.org/10.1016/j.mineng.2013.02.012>
- Pérez-García, E. M., Bouchard, J. & Poulin, É. (2018). Integration of a liberation model in a simulation framework for comminution circuits. *Minerals Engineering*, 126, 167–176. <https://doi.org/10.1016/J.MINENG.2018.07.009>

References

- Petersen, L., Minkkinen, P. & Esbensen, K. H. (2005). Representative sampling for reliable data analysis: Theory of Sampling. *Chemometrics and Intelligent Laboratory Systems*, 77(1), 261–277. <https://doi.org/https://doi.org/10.1016/j.chemolab.2004.09.013>
- Pettersson, M., Oksanen, A., Mingaleva, T., Petrov, V. & Masloboev, V. (2015). License to Mine: A Comparison of the Scope of the Environmental Assessment in Sweden, Finland and Russia. *Natural Resources*, 06(04), 237–255. <https://doi.org/10.4236/nr.2015.64022>
- Pitis, C. (2016, December 5). New approach on energy conservation measures types applied in mining industry. *2016 IEEE Electrical Power and Energy Conference, EPEC 2016*. <https://doi.org/10.1109/EPEC.2016.7771742>
- Powell, M. S. & Morrison, R. D. (2007). The future of comminution modelling. *International Journal of Mineral Processing*, 84(1–4), 228–239. <https://doi.org/10.1016/j.minpro.2006.08.003>
- Prno, J. (2013). An analysis of factors leading to the establishment of a social licence to operate in the mining industry. *Resources Policy*, 38(4), 577–590. <https://doi.org/10.1016/j.resourpol.2013.09.010>
- Prno, J. & Scott Slocombe, D. (2012). Exploring the origins of “social license to operate” in the mining sector: Perspectives from governance and sustainability theories. *Resources Policy*, 37(3), 346–357. <https://doi.org/10.1016/j.resourpol.2012.04.002>
- Ray, H. S. & Ghosh, A. (1991). *Principles of extractive metallurgy*. Wiley.
- Reichl, C. & Schatz, M. (2020). *World Mining Data 2020* (Volume 35). Federal Ministry for Sustainability and Tourism.
- Remes, A., Aaltonen, J. & Koivo, H. (2010). Grinding circuit modeling and simulation of particle size control at Siilinjärvi concentrator. *International Journal of Mineral Processing*, 96(1–4), 70–78. <https://doi.org/10.1016/J.MINPRO.2010.05.001>
- Remes, Antti & Izart, C. (2021). 46 - Sim Minerals Processing Unit Models. In Metso:Outotec (Ed.), *HSC Chemistry® User's Guide*.
- Remes, Antti & Lamberg, P. (2021). 45 - Sim Mineral Processing. In Metso:Outotec (Ed.), *HSC Chemistry® User's Guide*.
- Remes, Antti & Vesa, L. (2014). Thickener modelling: From laboratory test work to plant scale simulation. *XXVII International Mineral Processing Congress*, 46–57.
- Rico, M., Benito, G. & Díez-Herrero, A. (2008). Floods from tailings dam failures. *Journal of Hazardous Materials*, 154(1–3), 79–87. <https://doi.org/10.1016/j.jhazmat.2007.09.110>
- Robben & Wotruba. (2019). Sensor-Based Ore Sorting Technology in Mining—Past, Present and Future. *Minerals*, 9(9), 523. <https://doi.org/10.3390/min9090523>
- Robinson, S. (1997). Simulation model verification and validation increasing the users's confidence. *Proceedings of The 1997 Winter Simulation Conference*, 7–13. <https://doi.org/10.1109/WSC.1997.640377>
- Rodič, B. (2017). Industry 4.0 and the New Simulation Modelling Paradigm. *Organizacija*,

- 50(3), 193–207. <https://doi.org/10.1515/orga-2017-0017>
- Roine, T., Kaartinen, J. & Lamberg, P. (2011). Training Simulator for Flotation Process Operators. *IFAC Proceedings Volumes*, 44(1), 12138–12143. <https://doi.org/10.3182/20110828-6-IT-1002.02171>
- Ruhanen, E., Kosonen, M., Kauvosaari, S. & Henriksson, B. (2018). Optimisation of paste thickening at the Yara Siilinjärvi plant. In R. J. Jewell, R. J. Jewell, A. B. Fourie & A. B. Fourie (Eds.), *21st International Seminar on Paste and Thickened Tailings* (pp. 75–88). Australian Centre for Geomechanics PP - Perth. https://papers.acg.uwa.edu.au/p/1805_06_Kosonen/
- Salazar, J. L., Magne, L., Acuña, G. & Cubillos, F. (2009). Dynamic modelling and simulation of semi-autogenous mills. *Minerals Engineering*, 22(1), 70–77. <https://doi.org/10.1016/j.mineng.2008.04.009>
- Savassi, O. N. (2005). A compartment model for the mass transfer inside a conventional flotation cell. *International Journal of Mineral Processing*, 77(2), 65–79. <https://doi.org/10.1016/j.minpro.2005.02.003>
- Scales, P. J. & Usher, S. P. (2015). Thickener modelling - from laboratory experiments to full-scale prediction of what comes out the bottom and how fast. *Proceedings of the 18th International Seminar on Paste and Thickened Tailings*.
- Schoderer, M., Dell'Angelo, J. & Huitema, D. (2020). Water policy and mining: Mainstreaming in international guidelines and certification schemes. *Environmental Science and Policy*, 111, 42–54. <https://doi.org/10.1016/j.envsci.2020.04.011>
- Schwarz, M. P., Koh, P. T. L., Verrelli, D. I. & Feng, Y. (2015). Sequential multi-scale modelling of mineral processing operations, with application to flotation cells. *Minerals Engineering*, 90, 2–16. <https://doi.org/10.1016/j.mineng.2015.09.021>
- Seppälä, P., Sorsa, A., Paavola, M., Remes, A., Ruuska, J. & Leiviskä, K. (2014). Pilot plant simulation as a tool for more efficient mineral processing. *IFAC Proceedings Volumes (IFAC-PapersOnline)*, 19, 11506–11511. <https://doi.org/10.3182/20140824-6-ZA-1003.02152>
- Shanmugasundaram, H., Annamalai, S. K., Arunachalam, K. D., Jha, V. N., Sethy, N. K., Sivasubramaniam, K., Krishnan, H. & Pandima Devi, M. (2016). Simulation model for feasibility studies on bioremediation of uranium mill tailings using hyper accumulator *Chrysopogon zizanioides*. *American Journal of Environmental Sciences*, 12(6), 370–378. <https://doi.org/10.3844/ajessp.2016.370.378>
- Shariatzadeh, N., Lundholm, T., Lindberg, L. & Sivard, G. (2016). Integration of Digital Factory with Smart Factory Based on Internet of Things. *Procedia CIRP*, 50, 512–517. <https://doi.org/10.1016/J.PROCIR.2016.05.050>
- Simmons, S. F. & Brown, K. L. (2006). Gold in magmatic hydrothermal solutions and the rapid formation of a giant ore deposit. *Science*, 314(5797), 288–291. <https://doi.org/10.1126/science.1132866>
- Sinche Gonzalez, M., Lamberg, P. & Suup, M. (2016). Geochemical Model and Simulation of Water Balance for Mining Operations: Svappavaara Iron Mine. *Modern*

- Environmental Science and Engineering*, 2, 721–728.
[https://doi.org/10.15341/mese\(2333-2581\)/11.02.2016/002](https://doi.org/10.15341/mese(2333-2581)/11.02.2016/002)
- Soldán, P., Pavonič, M., Bouček, J. & Kokeš, J. (2001). Baia mare accident - Brief ecotoxicological report of Czech experts. *Ecotoxicology and Environmental Safety*, 49(3), 255–261. <https://doi.org/10.1006/eesa.2001.2070>
- Sovacool, B. K., Ali, S. H., Bazilian, M., Radley, B., Nemery, B., Okatz, J. & Mulvaney, D. (2020). Sustainable minerals and metals for a low-carbon future. *Science*, 367(6473), 30–33. <https://doi.org/10.1126/science.aaz6003>
- Stark, S., Perkins, T. & Napier-Munn, T. J. (2008). JK Drop weight parameters: a statistical analysis of their accuracy and precision and the effect on SAG mill comminution circuit simulation. *Australasian Institute of Mining and Metallurgy Publication Series*, 147–156.
- Sutherland, D. N. (1977). An appreciation of galena concentration using a steady-state flotation model. *International Journal of Mineral Processing*, 4(2), 149–162. [https://doi.org/10.1016/0301-7516\(77\)90022-9](https://doi.org/10.1016/0301-7516(77)90022-9)
- Sutherland, K. L. & Wark, I. W. (1955). *Principles of flotation*. Australasian Institute of Mining and Metallurgy.
- Sykora, S., Cooke, D. R., Meffre, S., Stephanov, A. S., Gardner, K., Scott, R., Selley, D. & Harris, A. C. (2018). Evolution of pyrite trace element compositions from porphyry-style and epithermal conditions at the Lihir gold deposit: Implications for ore genesis and mineral processing. *Economic Geology*, 113(1), 193–208. <https://doi.org/10.5382/econgeo.2018.4548>
- Talikka, M., Remes, A., Hicks, M., Liipo, J., Takalo, V.-P., Khizanishvili, S. & Natsvlshvili, M. (2018). Copper Ore Variability – Benefits of Advanced Simulation. *Copper Cobalt Africa, Incorporating the 9th Southern African Base Metals Conference, July*, 75–80.
- Thomashausen, S., Maennling, N. & Mebratu-Tsegaye, T. (2018). A comparative overview of legal frameworks governing water use and waste water discharge in the mining sector. *Resources Policy*, 55, 143–151. <https://doi.org/10.1016/j.resourpol.2017.11.012>
- Tian, J., Xu, L., Deng, W., Jiang, H., Gao, Z. & Hu, Y. (2017). Adsorption mechanism of new mixed anionic / cationic collectors in a spodumene-feldspar flotation system. *Chemical Engineering Science*, 164, 99–107. <https://doi.org/10.1016/j.ces.2017.02.013>
- Toro, R., Ortiz, J. M. & Yutronic, I. (2012). An Operator Training Simulator System for MMM Comminution and Classification Circuits. *IFAC Proceedings*, 1, 1–5.
- Tsakalakakis, K. G. & Michalakopoulos, T. (2015). Mathematical modeling of the conveyor belt capacity. *CHoPS 2015 - 8th International Conference for Conveying and Handling of Particulate Solids*.
- USGS. (2020). Mineral commodity summaries 2020. In *Mineral Commodity Summaries*. <https://doi.org/10.3133/mcs2020>
- Valenta, R. K., Kemp, D., Owen, J. R., Corder, G. D. & Lèbre. (2019). Re-thinking complex

- orebodies: Consequences for the future world supply of copper. *Journal of Cleaner Production*, 220, 816–826. <https://doi.org/10.1016/j.jclepro.2019.02.146>
- Valery, W. & Morrell, S. (1995). The development of a dynamic model for autogenous and semi-autogenous grinding. *Minerals Engineering*, 8(11), 1285–1297. [https://doi.org/10.1016/0892-6875\(95\)00096-9](https://doi.org/10.1016/0892-6875(95)00096-9)
- van Beers, D., Corder, G. D., Bossilkov, A. & van Berkel, R. (2007). Regional synergies in the Australian minerals industry: Case-studies and enabling tools. *Minerals Engineering*, 20(9 SPEC. ISS.), 830–841. <https://doi.org/10.1016/j.mineng.2007.04.001>
- Van Den Berghe, M. D., Jamieson, H. E. & Palmer, M. J. (2018). Arsenic mobility and characterization in lakes impacted by gold ore roasting, Yellowknife, NWT, Canada. *Environmental Pollution*, 234, 630–641. <https://doi.org/10.1016/j.envpol.2017.11.062>
- Verein Deutscher Ingenieure (VDI). (2008). Blatt 1: Digitale Fabrik Grundlagen Digital factory Fundamentals VDI 4499. In *VDI-Gesellschaft Produktion und Logistik* (Issue February).
- Wenbin, Z., Xiumin, F., Juanqi, Y. & Pengsheng, Z. (2002). An Integrated Simulation Method to Support Virtual Factory Engineering. *International Journal of CAD/CAM*, Vol.2(No.1), 39–44.
- West, J. (2011). Decreasing Metal Ore Grades: Are They Really Being Driven by the Depletion of High-Grade Deposits? *Journal of Industrial Ecology*, 15(2), 165–168. <https://doi.org/10.1111/j.1530-9290.2011.00334.x>
- Whiten, W. J. (1974). A matrix theory of comminution machines. *Chemical Engineering Science*, 29(2), 589–599. [https://doi.org/10.1016/0009-2509\(74\)80070-9](https://doi.org/10.1016/0009-2509(74)80070-9)
- Widok, A. H., Schiemann, L., Jahr, P. & Wohlgemuth, V. (2012). Achieving sustainability through a combination of LCA and des integrated in a simulation software for production processes. *Proceedings - Winter Simulation Conference*, 1219–1229. <https://doi.org/10.1109/WSC.2012.6465079>
- Wills, B. A. & Napier-Munn, T. (2005). *Wills' Mineral Processing Technology*. Elsevier Science & Technology Books. <https://doi.org/10.1016/b978-075064450-1/50014-x>
- Woodburn, E. T. (1970). Mathematical modelling of flotation processes. *Minerals Science and Engineering*, 2(2), 3–17.
- Xiang, L., Liu, P. hui, Jiang, X. fu & Chen, P. jia. (2019). Health risk assessment and spatial distribution characteristics of heavy metal pollution in rice samples from a surrounding hydrometallurgy plant area in No. 721 uranium mining, East China. *Journal of Geochemical Exploration*, 207. <https://doi.org/10.1016/j.gexplo.2019.106360>
- Xie, S., Xie, Y., Ying, H., Gui, W. & Yang, C. (2018). A Hybrid Control Strategy for Real-Time Control of the Iron Removal Process of the Zinc Hydrometallurgy Plants. *IEEE Transactions on Industrial Informatics*, 14(12), 5278–5288. <https://doi.org/10.1109/TII.2018.2815659>
- Xu, W., Dhawan, N., Lin, C. L. & Miller, J. D. (2013). Further study of grain boundary

References

- fracture in the breakage of single multiphase particles using X-ray microtomography procedures. *Minerals Engineering*, 46–47, 89–94. <https://doi.org/10.1016/j.mineng.2013.03.016>
- Ylén, J.-P., Paljakka, M., Karhela, T., Savolainen, J. & Juslin, K. (2005). Experiences on utilising plant scale dynamic simulation in process industry. *Simulation in Wider Europe - 19th European Conference on Modelling and Simulation, ECMS 2005*.
- Young, C. A. (2019). *SME Mineral Processing and Extractive Metallurgy Handbook* (Vol. 71, Issue 8). Society for Mining, Metallurgy & Exploration.
- Yu, P., Xie, W., Liu, L. X., Hilden, M. M. & Powell, M. S. (2018). Evolution of a generic, dynamic and multicomponent tumbling mill model structure incorporating a wide-range 4D appearance function. *Powder Technology*, 339, 396–407. <https://doi.org/10.1016/J.POWTEC.2018.08.016>
- Yun, Y., Stopic, S. & Friedrich, B. (2020). Valorization of rare earth elements from a steenstrupine concentrate via a combined hydrometallurgical and pyrometallurgical method. *Minerals*, 10(3). <https://doi.org/10.3390/min10030248>
- Zhang, F., Yang, C., Zhou, X. & Zhu, H. (2018). Fractional order fuzzy PID optimal control in copper removal process of zinc hydrometallurgy. *Hydrometallurgy*, 178, 60–76. <https://doi.org/10.1016/j.hydromet.2018.03.021>

Chapter 6 Appendices

6.1 Appendix 1: Version history of HSC models (from 2015, updated for April 2021 release version 10.0.5) from HSC Chemistry User's Guide – Chapter 46 (Antti Remes & Izart, 2021) – In bold are version updates made by the author.

Type No.	Model	Version	Date	Available since HSC	What's New
100-10	Blasting	1.0	12/2018	9.8	/
		1.1	09/2020	10.0	- Model fit compatibility update
110-10	Perfect Mixer	1.0	06/2015	8.1	/
110-11	Pump Sump	1.0	06/2015	8.1	/
		1.2	03/2015	9.5	- Dynamic calculation improvements
		1.3	10/2018	9.7	- Static calculation: overflow stream is not required
		1.4	06/2019	9.9	- Dynamic calculation optimization
110-12	Water Tank	1.0	06/2019	9.9	/
		1.1-1.2	04/2021	10.0.5	- Corrected calculation of raw water required
110-13	Conveyor Belt	1.0	06/2018	9.6	/
110-14	Ore Bin	1.0	06/2018	9.6	/
		1.1	07/2019	9.9	- Layering calculation addition
110-15	Stockpile	1.0	06/2019	9.9	/
		1.1	07/2019	9.9	- Layering calculation addition
110-16	Overflow Tank	1.0	07/2019	9.9	/
110-20	OreMet Optimizer	1.0	03/2017	9.1	/
		1.1	12/2017	9.4	- Model parameters reorganized, parameter renaming - Option for product price: element or mineral based calculation, using NSR or concentrate price/ton
		1.2	03/2018	9.5	- Table parameter value reading fixed
		1.3	04/2021	10.0.5	- OPEX table refactoring (fixed costs, variable cost tables) - Input stream refactoring - Add comments columns - Product and Penalty elements tables refactoring - Add In-situ Product Element Value table - Add energy price for OPEX costs and field for labor cost calculation

120-10	Efficiency Curve	1.0	06/2015	8.1	/
		1.1	12/2015	9.8	- Support for hydro & pyro material species
		1.2	09/2019	9.9	- Support for bulk particle mixed with sized in feed
		1.3	10/2019	9.9	- Support for NA particle in the feed
		1.4	05/2020	10.0	- Fix bug if feed is empty
		1.5	06/2020	10.0	- Added partition curve
		1.6	08/2020	10.0	- Added separation efficiency
		1.7	09/2020	10.0	- Model fit compatibility update
120-11	Mass Distributor	1.0	06/2015	8.1	/
		1.1	06/2019	9.9	- Table edit lock bugfix.
		1.2	09/2020	10.0	- Model fit compatibility update
120-12	Mineral Splitter	1.0	06/2015	8.1	/
		1.1	12/2016	9.0	- Improved param. table handling routines
		1.2	09/2017	9.3	- Middling water balance error fixed
		1.3	12/2018	9.8	- Support for non-particle solids species
		1.4	09/2020	10.0	- Model fit compatibility update
		1.5	04/2021	10.0.5	- Non-liberated particle separation handling
130-10	Fixed PSD	1.0	06/2015	8.1	/
		1.1	06/2018	9.6	- Parameter min limits changed
		1.2	09/2020	10.0	- Model fit compatibility update
130-20	Size Redistribution	1.0	03/2019	9.9	/
		1.1	07/2019	9.9	- Optimization of particle handling
140-10	Courier Analyzer	1.0	06/2015	8.1	/
		1.1	10/2018	9.7	- Support for Stream References
		1.2	09/2019	9.9	- Empty channel indexing bugfix
140-20	PSI Analyzer	1.0	06/2015	8.1	/
		1.1	10/2018	9.7	- Support for Stream References
		1.0	06/2018	9.6	/
210-10	Jaw Crusher	1.1	03/2019	9.9	- Fine feed calculation improvement. Fix for internal P80 iteration
		1.2	05/2019	10.0	- Fix reference to crusher type
		1.3	01/2020	10.0	- Fix of the retained PSD calculation
		1.4	09/2020	10.0	- Model fit compatibility update
		1.0	06/2018	9.6	/
210-20	Gyratory Crusher	1.1	03/2019	9.9	- Fine feed calculation improvement. Fix for internal P80 iteration
		1.2	01/2020	10.0	- Fix of the retained PSD calculation
		1.3	09/2020	10.0	- Model fit compatibility update
		1.0	05/2017	9.2	/
210-30	Cone Crusher	1.2	06/2018	9.6	- Revised Chalmers correlation model
		1.3	03/2019	9.9	- Fine feed calculation improvement
		1.4	01/2020	10.0	- Fix of the retained PSD calculation
		1.5	09/2020	10.0	- Model fit compatibility update
		1.0	12/2018	9.8	/
220-10	Rod Mill	1.1	11/2019	9.9	- Mtc calculation option added
		1.2	07/2020	10.0	- Volume bug correction
		1.3	03/2021	10.0.5	- Model fit compatibility update
		1.0	09/2017	9.3	/
220-20	Bond Ball Mill	1.1	06/2018	9.6	- Parameter min limits changed

		1.2	10/2018	9.7	- Individual efficiency factors added
		1.3	12/2018	9.8	- Fix of the retained PSD calculation
		1.4	03/2019	9.9	- Option for a user-input total EF
		1.5	07/2020	10.0	- Model fit compatibility update
220-30	Ball Mill	1.0	05/2017	9.2	/
		1.1	12/2017	9.4	- Option to select ore type based appearance matrices - Mill residence time calculation added - r/d^* knot spline interpolation robustness improved
		1.2	03/2018	9.5	- Calculation of ball and liner consumption
		1.3	12/2018	9.8	- New post classification function
		1.4	03/2019	9.9	- Modification of default parameters
		1.5	08/2019	9.9	- Calculation optimization
		1.6	09/2019	9.9	- Fix when bulk particles are mixed in a sized feed
		1.7	11/2019	9.9	- Mtc calculation option added
		1.8	12/2019	10	- Fix slurry SG calc. in the Mtc option
		1.9	05/2020	10.0	- Correction of f4 calculation
		1.10	06/2020	10.0	- Addition of the scaled $\ln R/D^*$ column
		1.11	07/2020	10.0	- Model fit compatibility update
220-40	AG/SAG Mill	1.0	03/2018	9.5	/
		1.1	12/2018	9.8	- Parameter updates, dynamic optimization
		1.2	01/2019	9.9	- Max mill capacity calculation
		1.3	03/2019	9.9	- Liner and ball wear rate calculation - Mill default parameters changed
		1.4	05/2019	9.9	- Added Ore properties and wear rate calculation
		1.5	09/2019	10.0	- Fix recycle stream connectivity
		1.6	10/2019	10.0	- Discard 0tph particles
		1.7	10/2019	10.0	- Calculation optimization
		1.8	11/2019	10.0	- Mtc calculation option added
		1.9	12/2019	10.0	- Fix slurry SG calc in the Mtc option
		1.10	03/2020	10.0	- Variable rate model updated
		1.11	07/2020	10.0	- Model fit compatibility update
		1.12 - 1.13	04/2021	10.0.5	- Calculation speed improvements - Optional dynamic discharge calculation method based on Morrell and Stephenson equations
220-50	HIGmill	1.0	12/2016	9.0	/
		1.1	06/2018	9.6	- Parameter min limits changed
		1.2	03/2020	10.0	- Circuit feed is now optional
		1.3	07/2020	10.0	- Model fit compatibility update
230-10	Screen - Whiten Efficiency Curve	1.0	06/2015	8.1	/
		1.1	12/2018	9.8	- Support for non-particle solids species
		1.2	09/2020	10.0	- Model fit compatibility update
	Screen - Karra	1.0	06/2015	8.1	/

230-11		1.1	12/2018	9.8	- Support for non-particle solids species
		1.2	09/2020	10.0	- Model fit compatibility update
230-12	Screen Batterham et al.	1.0	06/2015	8.1	/
		1.1	12/2018	9.8	- Support for non-particle solids species
		1.2	09/2020	10.0	- Model fit compatibility update
240-10	Hydrocyclone - Plitt	1.0	06/2015	8.1	/
		1.1	12/2018	9.8	- Support for non-particle solids species
	Hydrocyclone	1.0	07/2020	10	- Integration of Plitt & Nageswararao models - Partition curve and efficiency parameters added - Model fit compatibility update
		1.1	12/2020	10.0.5	- Table visualization bugfix
240-11	Hydrocyclone - Nageswararao	1.0	03/2019	9.9	/
	/	/	07/2020	/	- Replaced in Hydrocyclone (240-10) model
310-10	Conditioner	1.0	06/2015	8.1	
		1.1	08/2015	8.1	- New flotation model: Rectangular Distribution
		1.2	12/2016	9.0	- Improved param. table handling routines
		2.0	03/2017	9.1	- Rectangular Distribution as default (Klimpel model obsolete)
		2.1	09/2017	9.3	- Rectangular Distribution tables reordered
		2.2	12/2017	9.4	- Fix for dynamic calculation
		2.3	03/2018	9.5	- Dynamic calculation improvements
		2.5	06/2019	9.9	- Optimized dynamic particle handling
		2.6	10/2019	10.0	- Discard 0tph particles
		2.7 - 2.9	04/2021	10.0.5	- Bugfix for particle duplication issue in dynamic mode - Internal modifications, preparation for v.3.0
310-11	Flotation Cell	1.1	08/2015	8.1.2	- New flotation model: Rectangular Distribution - New residence time option: Feed and Tails Avg - New froth recovery option: Function of Froth Retention
		1.2	10/2015	8.1.5	- Froth vol.% model parameter as default for effective volume calculation - New calculations of: bank froth area and lip load, froth solids% before launder water
		1.3	12/2016	9.0	- Improved param. table handling routines - Calculations of: bank air consumption, bank mass pull, bank lip load, total bank rotor power
		1.4	03/2017	9.1	- Fixed froth recovery parameters available separately for each minerals - Enrichment ratio table
		1.5	09/2017	9.3	- Cells in row can be set to zero - Gives a warning if a conditioner unit prior flotation is missing

		1.6	12/2017	9.4	- Model parameter list reorganized - Stage recovery table - Residence time table - New model parameters: min/max Jg in forth, air calculation based on Jg, selected motor (kW), Lab. Residence Time
		1.8	03/2018	9.5	- Power number for mixer motor and minimum motor size calculation - Dynamic calculation improvements
		1.9	12/2018	9.8	- Support for non-particle solids species
		2.0	03/2019	9.9	- Fix for carry rate and lip load limitation for parallel rows
		2.1	06/2019	9.9	- Dynamic calculation optimization
		2.2	10/2019	10.0	- Discard 0tph particles
		2.3	01/2020	10.0	- Fix water recovery calculation in dynamic mode
		2.4	01/2020	10.0	- Fix water recovery calculation in dynamic mode
		2.5 - 2.9	04/2021	10.0.5	- Dynamic rectangular calculation bugfix - Internal modifications, preparation for v.3.0
310-12	Column Flotation	1.0	12/2017	9.4	/
		1.1	12/2018	9.8	- Support for non-particle solids species
		1.2	10/2019	10.0	- Discard 0tph particles
410-10	Specific Gravity Splitter	1.0	06/2015	8.1	/
		1.1	09/2017	9.3	- Middlings water balance error fixed
		1.2	12/2018	9.8	- Support for non-particle solids species
420-10	WHIMS (Dobby & Finch)	1.0	04/2021	10.0.5	/
510-10	Thickener (General)	1.0	06/2015	8.1	
		1.1	12/2018	9.8	- Support for non-particle solids species
520-10	Filter (General)	1.0	06/2015	8.1	
		1.1	12/2018	9.8	- Support for non-particle solids species
610-10	Sorter	1.0	05/2017	9.2	/
		1.1	09/2017	9.3	- Wash water is now optional
		1.2	03/2018	9.5	- Fix in wash water particle size fractioning
		1.3	12/2018	9.8	- Support for non-particle solids species
		1.4	11/2019	10.0	- Fix separation ratio (division per 0)

6.2 Appendix 2: Manual pages from the author describing the implementation of , from HSC Chemistry User's Guide – Chapter 46 (Antti Remes & Izart, 2021).

Metso:Outotec

HSC - Sim MinPro Unit Models
9/192
Antti Remes, Caroline Izart, et al.
May 27, 2021

46.3.1. **Blasting: MU-100-10**

Modeling scope:	<input type="button" value="QUICK"/>	<input type="button" value="DIMENSIONING"/>	<input type="button" value="ADVANCED"/>
Stream particle sizing:	<input type="button" value="SIZED"/>		
Mode:	Static: <input checked="" type="checkbox"/> Dynamic: -		
Inputs:	In-situ Rock Mass		
Outputs:	Fragmented Rock Pile		

Description and equations

The HSC Sim blasting model is based on the Swebrec function, developed at Swebrec (Swedish Blasting Research Centre at Luleå University of Technology, Sweden) by F. Ouchterlony (2005) /3/. It describes rock fragmentation by blasting with a three-parameter fragment size distribution. It is an empirical model which improves the Kuz-Ram model /1/ and takes the production of fines into account. The main model parameters are:

- The rock mass factor (A), which measures how hard it is to blast an in-situ rock mass by considering the friability, the pre-existing joints and their orientation with respect to the face of the bench
- The geometry selected for the blast holes (spacing between the holes, diameters, depth, height, and position of the charge)
- The properties of the explosive compared to ANFO (ammonium nitrate fuel oil) and its loading (amount per blast hole)

The difference between a Rosin-Rammler distribution and the Swebrec model is illustrated by the experimental data in **Fig. 1**. The fines are underestimated by other models, whereas the Swebrec function offers a better fit in that region.

Metso:Outotec

HSC - Sim MinPro Unit Models
11/192
Antti Remes, Caroline Izart, et al.
May 27, 2021

The blasting simulation is calculated as follows:

First, the rock mass factor A (Lily, 1986) /2/ is calculated by summing the contributions of

- Friability and pre-existing fractures (RMD)
- Specific gravity (RDI)
- Hardness (HF)

$$HF = \frac{E}{3}, E < 50$$

$$HF = \frac{\sigma_c}{5}, E > 50$$

$$RDI = 0.025 \rho_{solids} - 50$$

from which A is obtained

$$A = 0.06(RMD + RDI + HF)$$

Then the uniformity exponent N is calculated based on the geometry of the bench, as illustrated in the figure above:

$$N = \left(2.2 - \frac{0.014B}{D/H}\right) \left(1 - \frac{SD}{B}\right) \sqrt{\frac{1 + \frac{S}{B}}{2} \left(\frac{|Lb - Lc|}{Ltot + 0.1}\right)^{0.1} \left(\frac{Ltot}{H}\right)}$$

The size of the maximum fragment can be estimated by

$$x_{max} = \sqrt{S \cdot B}$$

Then, based on A and the properties of the explosive, the x_{50} is estimated as in the Kuz-Ram model (Cunningham, 1983) /1/

$$x_{50} = \left(A \cdot Q^{\frac{1}{6}}\right) \frac{\left(\frac{115}{S_{ANFO}}\right)^{\frac{19}{30}}}{Q^{0.8}}$$

The undulation coefficient b is calculated using the values x_{50} , x_{max} and N

$$b_{ondul} = 2 * \ln(2) * \ln\left(\frac{x_{max}}{x_{50}}\right) N$$

Alternatively, b can be estimated if a t_{10} value from crushing tests exists

$$b_{ondul} = 1.616 + 0.02735 * t_{10}$$

Metso:Outotec

HSC - Sim MinPro Unit Models
10/192
Antti Remes, Caroline Izart, et al.
May 27, 2021

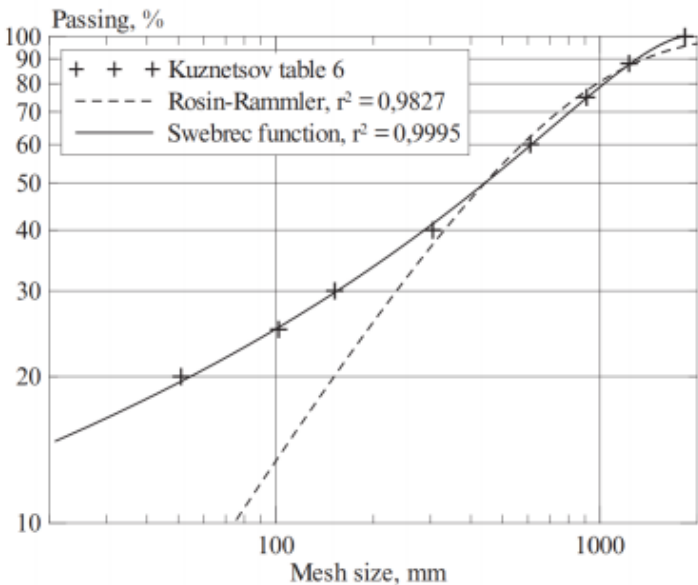


Fig. 1. Difference between the Rosin-Rammler model and Swebrec function for fines (Ouchterlony, 2010) /4/.

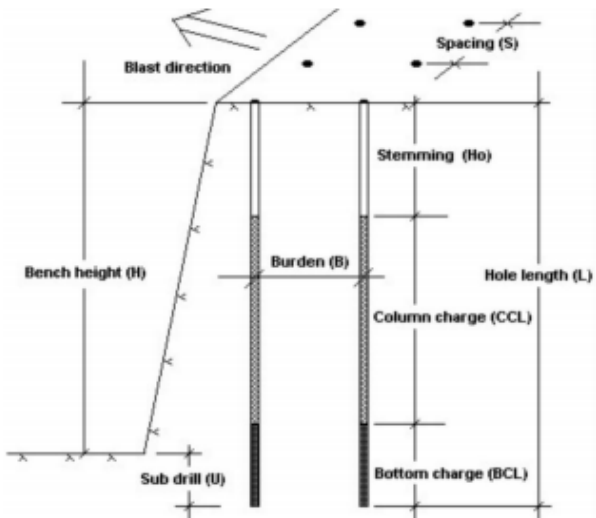


Fig. 2. Difference between the Rosin-Rammler model and Swebrec function for fines (Ouchterlony, 2010) /4/.

Metso Outotec reserves the right to modify these specifications at any time without prior notice. Copyright © 2021, Metso Outotec Finland Oy

Metso:Outotec

HSC - Sim MinPro Unit Models
12/192
Antti Remes, Caroline Izart, et al.
May 27, 2021

If enough experimental data exists, the value of b can be fitted to experimental data and used directly in the model.

Finally, the particle size distribution is evaluated at each point d by

$$P(d) = \frac{1}{1 + \left(\frac{\ln\left(\frac{x_{max}}{d}\right)}{\ln\left(\frac{x_{max}}{x_{50}}\right)} \right)^{b_{undul}}}$$

where

- $P(d)$ = weight passing % to sieve size d
- d = sieve size (μm)
- x_{max} is the size of the maximum fragment
- b is the undulation parameter

Effect of geometry on fines ($x_{50} = 450 \text{ mm}$ and $x_{max} = 2250 \text{ mm}$)

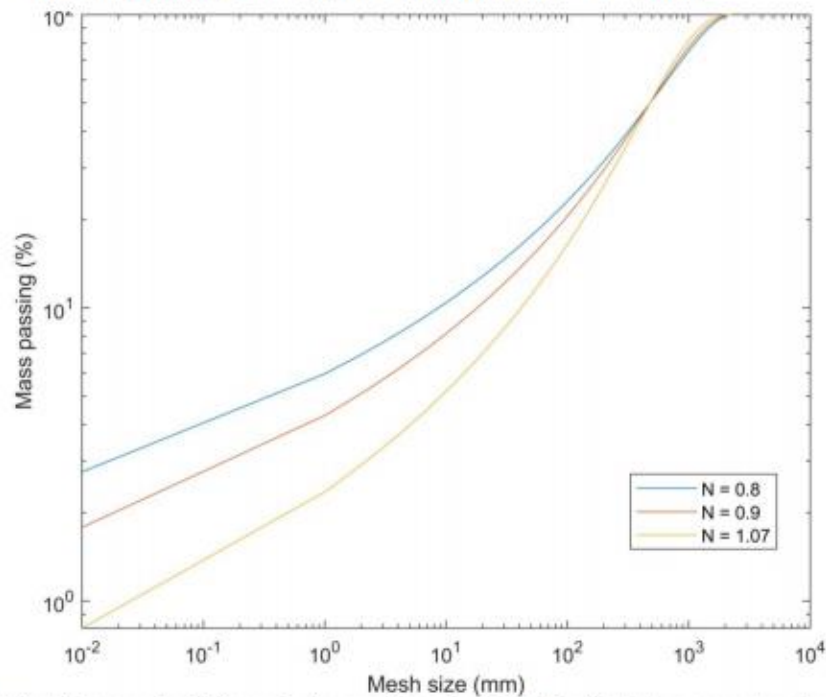


Fig. 3. Effect of parameter N (geometry) on particle size distribution (all other parameters kept constant) according to Ouchterlony (2010) /4/.

Metso Outotec reserves the right to modify these specifications at any time without prior notice. Copyright © 2021, Metso Outotec Finland Oy

Metso:Outotec

HSC - Sim MinPro Unit Models

13/192

Antti Remes, Caroline Izart, et al.

May 27, 2021

Messages from the model:

Message	Reason / What to Do
Mineral balance was not reached within tolerance, max iterations were exceeded	Input – output mineral balancing did not converge. Please increase the <i>Max Iteration</i> parameter or increase the <i>Tolerance</i> for less accuracy. If a large number of iterations (~50) does not help, please check in which minerals and size fractions the balance did not converge, and adjust the tolerance accordingly

Model parameters

Parameter	Val.	Unit	Limits	Description
Settings				
Tolerance	0.0001		>0	For mineral balance iteration
Max Iteration	25		>=1	For mineral balance iteration
Explosive Properties				
Q	9.24	kg	>0	Charge weight per hole (typical: 1...100 kg/hole)
q	0.55	kg.m ⁻³	>0	Specific charge or powder factor. In general <ul style="list-style-type: none"> >0.5 if A>11 0.45 if A = 10 or 11 0.3 if A = 8 – 9 0.15 to 0.25 if A<8
s(ANFO)	62.2	%	[0 – 100]	Explosive's weight strength relative to ANFO
Bench Geometry				
B	1.8	m	>0	Blast-hole burden
S	2.2	m	>0	Spacing
H	5.2	m	>0	Bench height
Dh	0.051	m	>0	Drill-hole diameter. Standard values: 25, 35, 38, 41, 45, 48, 51, 108, 114 up to 445 mm
Lb or BCL	4.2	m	>0	Length of the bottom charge
Lc or CCL	0	m	>0	Length of column charge

Metso Outotec reserves the right to modify these specifications at any time without prior notice. Copyright © 2021, Metso Outotec Finland Oy

Metso:Outotec

HSC - Sim MinPro Unit Models
14/192
Antti Remes, Caroline Izart, et al.
May 27, 2021

Lto	4.2	m	>0	Total charge length (can exceed surface level)
SD	0.25	m	>0	Standard deviation of drilling accuracy
Rock Mass Factor				
RMD	30	[]	>0	Rock mass description <ul style="list-style-type: none"> 10 for powdery/friable rocks JF = JPS + JPA if vertical joints are present 50 for massive rock
JPS	10	[]	>0	Joint plane spacing <ul style="list-style-type: none"> 10 if average joint spacing < 10 cm 20 if joint spacing between 10 cm and oversize x0 50 if higher than oversize
JPA	30		>0	Joint plane angle <ul style="list-style-type: none"> 20 for dip out of face 30 for strike perpendicular to face 40 if dip into face
σ_c	250	MPa	>0	Compressive strength. From 10-20 for soft sedimentary rocks to 500 for basalts.
E	50	GPa	>0	Young's modulus. Usually between 5 and 100.

Simulation Data

Readable:

Parameter	Val.	Unit	Limits	Description
Rock Mass Factor				Calculated
Xmax		m		Maximum block size, Calculated
X50		m		Size of 50% passing, Calculated

Model fitting and calibration

The model is calibrated for the blasting operation by fitting the appropriate value

Metso Outotec reserves the right to modify these specifications at any time without prior notice. Copyright © 2021, Metso Outotec Finland Oy

Metso:Outotec

HSC - Sim MinPro Unit Models
15/192
Antti Remes, Caroline Izart, et al.
May 27, 2021

Usage for optimization:

- The geometry in general has an impact on N as shown in the Fig. 2 above
- The amount of explosive per hole has an impact on the location of x_{50} . The other parameter to change x_{50} is the strength of the explosive compared to ANFO.
- The presence of vertical joints in the rock mass before blasting will decrease the value of A and shift x_{50} as well

Limitations

- The model is designed to approximate the particle size distribution based on existing settings and should not be used to design blasting geometry
- The model is applicable in the range of 0.1–5000 mm. It is not appropriate for fine material since deviations have been observed in the range of 0.02 to 0.001 mm.
- Extensive validation data can be found in Ouchterlony (2005) for different ore types

References

1. Cunningham C. The Kuz-Ram Model for production of fragmentation from blasting. In the Proceedings of the 1st Symposium on Rock Fragmentation by Blasting, Lulea 1983.
2. Lilly P., An Empirical Method of Assessing Rock mass blastability, Large Open Pit Mine Conference, Newman, Australia, October 1986, pp89-92.
3. Ouchterlony, F., The Swabrec© function: Linking fragmentation by blasting and crushing, Transactions of the Institution of Mining and Metallurgy, Section A: Mining Technology 114(1), 2005, pp. 29-44
4. Ouchterlony, F., Fragmentation characterization; the Swabrec function and its use in blast engineering, Rock Fragmentation by Blasting – Sanchidrián (ed), 2010 Taylor & Francis Group, London, ISBN 978-0-415-48296-7

Metso:Outotec

HSC - Sim MinPro Unit Models
22/192
Antti Remes, Caroline Izart, et al.
May 27, 2021

46.3.5. Conveyor Belt: MU-110-13

Modeling scope:	QUICK	ADVANCED
Stream particle sizing:	UNSIZED	SIZED
Mode:	Static: <input checked="" type="checkbox"/>	Dynamic: <input checked="" type="checkbox"/>
Inputs:	Input	
	Output	
Outputs:	Reverse Output	
	Overflow	

Description and equations

The conveyor is used to transfer material from one point to another. If the feed flow exceeds belt capacity, a part of the flow will be transferred to the overflow output instead of the normal output. The belt can be used to transport material in two opposite directions, with an input feed which can be located at different points of the belt. The length can be set or computed based on the elevation and inclination of the belt.

Overflow – Capacity calculation

The belt capacity, Q (in m^3/h), is defined as a function of 4 parameters:

- The idler troughing angle λ
- The surcharge angle β of the transported material
- The belt width W
- The belt speed

Conveyor parameters

The input stream can be inserted at different points of the belt. In dynamic mode, it is possible to change the belt running direction at any time, enabling the shift between the normal output and the reverse output.

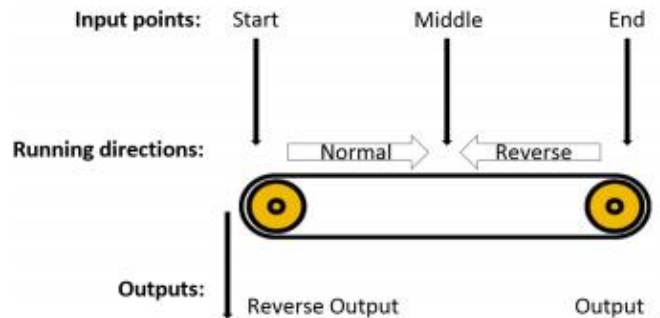


Fig. 5. Schematic diagram of the conveyor belt position of inputs, outputs, and running directions

Metso:Outotec

HSC - Sim MinPro Unit Models
23/192
Antti Remes, Caroline Izart, et al.
May 27, 2021

The idler troughing angle, used in the belt capacity calculation, is the angle formed between the central idler roll and the wing idler roll.

The surcharge angle is dependent on the mechanical characteristics of the transported material and directly linked to the angle of natural friction. For instance, fine rounded particles of uniform size can have an angle of surcharge of 5 degrees, whereas the angle of surcharge of irregular and granular material is about 20 degrees.

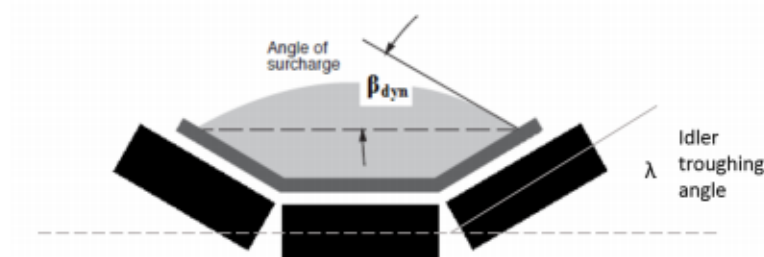


Fig. 6. Schematic representation of a cross-section of the conveyor belt and position of different angles.

Messages from the model

Message	Reason / What to Do
Belt capacity exceeded, overflowing.	Input stream flow is too great for the conveyor belt dimensions. Reduce input stream flow or change belt parameters.
Overflow stream is not connected, excess material is disappearing	Optional 'Overflow' outlet is not connected but the capacity is exceeded. Please connect the Overflow stream.
Reverse output stream is not connected, material is disappearing	Optional 'Reverse Output' outlet is not connected but the belt is running in Reverse direction mode. Please connect the Reverse Output stream.
Conveyor stopped, material is overflowing.	As the conveyor belt has stopped, all the material in input is overflowing. Belt needs to be restarted.

Model parameters

Parameter	Val.	Unit	Limits	Description
Settings				
Units	Metric / Imperial			Units in use in the model
Calculate length	TRUE / FALSE			Calculate conveyor belt length based on elevation and inclination angle parameters
Elevation*	2	m	>0	Elevation of the conveyor belt
Inclination Angle*	10	degrees	[0,45]	Inclination angle of the conveyor belt
Length	10 / 32.8	m / ft		Length of the conveyor belt

Metso Outotec reserves the right to modify these specifications at any time without prior notice. Copyright © 2021, Metso Outotec Finland Oy

Metso:Outotec

HSC - Sim MinPro Unit Models
24/192
Antti Remes, Caroline Izart, et al.
May 27, 2021

Width	0.8 / 31.5	m / in		Width of the conveyor
Maximum Speed	1	m/s / FPM		Maximum speed of the conveyor belt in meters per second or feet per minutes
Feed Point	Middle / Start / End			Define the input point of the feed on the conveyor belt
Surcharge angle	25	degrees	[0,90]	Depends on material natural friction angle (Typical: 20-30 degrees)
Idler angle	35	degrees	[0,90]	Idler troughing angle

*Visible if *Calculate length* parameter is True

Runtime values

Writeable:

Parameter	Val.	Unit	Limits	Description
Percentage of maximum speed	100	%	[0,100]	Conveyor speed percentage
Start/Stop Conveyor	TRUE / FALSE			If selected (True), the conveyor will stop running
Reverse running direction	TRUE / FALSE			If selected, the material will be directed to the reverse output

Readable:

Parameter	Val.	Unit	Limits	Description
Capacity		m ³ /h / ft ³ /h		Volumetric maximum capacity of the conveyor belt

Model fitting and calibration

The model is parameterized according to the equipment dimensions and belt speed. In static calculation mode, the capacity is checked, and the overflow is directed to a separate stream.

Limitations

- The capacity model assumes a conveyor belt moving with no inclination (horizontal) and is calibrated using a trough idler belt with three rolls of equal length.

References

- Tsakalakis, K.G., and Michalakopoulos, Th., Mathematical Modelling of the Conveyor Belt Capacity, The 8th International Conference for Conveying and Handling of Particulate Solids, Tel-Aviv, 2015.

Metso:Outotec

HSC - Sim MinPro Unit Models
25/192
Antti Remes, Caroline Izart, et al.
May 27, 2021

46.3.6. Stockpile: MU-110-15

Modeling scope:	DIMENSIONING	ADVANCED
Stream particle sizing:	SIZED	
Mode:	Static: <input checked="" type="checkbox"/>	Dynamic: <input checked="" type="checkbox"/>
Inputs:	Feed	
Outputs:	Output	

The stockpile model stores material and delivers it by reclaiming [1]. A variable buffering or mixing effect can be simulated.

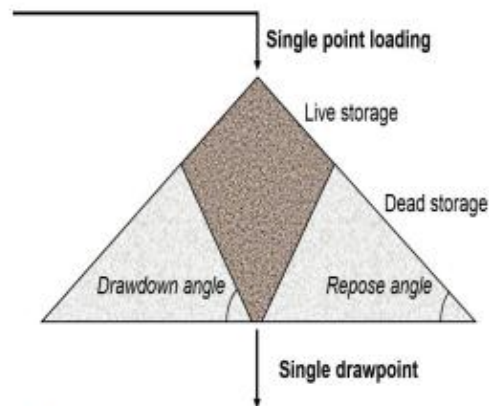


Figure 1: Conical stockpile "live" and "dead" volumes for single loading and reclaiming points.

Relationships:

This model calculates the maximum capacity of the stockpile based on different parameters. Two shape options are available: elongated and conical. For both, the maximum volume capacity can be directly given to the model. Otherwise, the volume is calculated based on the radius (r , meters) / angle of repose (A , degrees) pair or on the maximum height (h , meters) / angle of repose, and with the length (l , meters) of the stockpile if an elongated shape is selected.

For a given conical shape and $r - A$ pair: $V = \pi r^3 \tan(A)$

For a given elongated shape and $r - A$ pair: $V = \pi l r^2 \tan(A)$

For a given conical shape and $h - A$ pair: $V = \pi \frac{h^3}{\tan(A)^2}$

For a given elongated shape and $h - A$ pair: $V = \pi l \frac{h^2}{\tan(A)}$

The maximum weight capacity is then recalculated, considering the material specific gravity and the void fraction (volume of voids / total volume). In dynamic mode, the mean specific gravity of the entire pile is taken into account.

Metso Outotec reserves the right to modify these specifications at any time without prior notice. Copyright © 2021, Metso Outotec Finland Oy

Metso:Outotec

HSC - Sim MinPro Unit Models
26/192
Antti Remes, Caroline Izart, et al.
May 27, 2021

The live volume, calculated with the live volume fraction, is the stockpile volume available for reclaiming by gravity alone, i.e., without external handling.

In dynamic calculation, a buffering or mixing effect can be added to the model. The mixing mode means continuous mixing of the entire pile volume with the input. In the buffering mode, there is a delay between the input loading point and the reclaiming drawpoint. The content of the stockpile is separated into several sub-zones, mixing with each other. The higher the buffering effect, the higher the number of sub-zones.

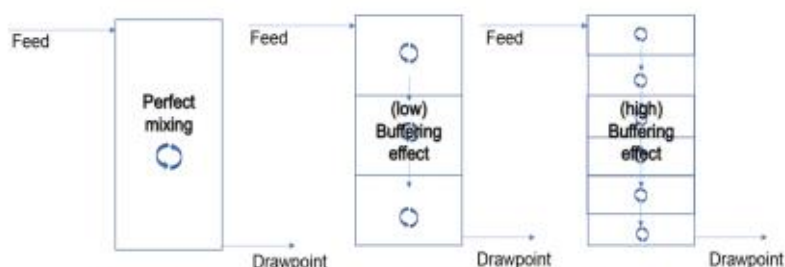


Figure 2: Difference between mixing, low, and high buffering effect models.

Notations:

Messages from the model

Message	Reason / What to Do
Stockpile is overfilled	In dynamic calculation, the stockpile capacity is exceeded. Turn reclaiming ON, increase its capacity, or reduce the input tonnage.
Stockpile is empty	In dynamic calculation, the stockpile is emptied. Stop the reclaiming process, reduce its capacity, or increase the input tonnage.

Model parameters

Parameter	Val.	Unit	Limits	Description
Dimensions				
Stockpile type	Conical / Elongated			
Determination of volume capacity	Maximum radius – Angle of repose / Maximum height – Angle of repose / Volumetric capacity			Stockpile parameter known
Calculation method	Homogenizing / Buffering			Homogenization / Plug flow - For dynamic calculation only

Metso Outotec reserves the right to modify these specifications at any time without prior notice. Copyright © 2021, Metso Outotec Finland Oy

Metso:Outotec

HSC - Sim MinPro Unit Models
27/192
Antti Remes, Caroline Izart, et al.
May 27, 2021

Buffering effect	Low / Medium / High			Intensity of the buffering effect - For dynamic calculation only
Maximum known capacity	1000	m3	>0	Maximum stockpile volumetric capacity
Angle of repose	38	degrees	[0-55]	Material angle of repose
Radius	5	m	>0	Maximum stockpile radius
Height	8	m	>0	Maximum stockpile height
Length	20	m	>0	Length or arc length of the center section
Characteristics				
Void Fraction	0.2		[0-0.8]	Volume of voids / total volume
Live volume fraction	0.25		[0-1]	Volume of live stock / total volume
Reclaiming capacity	20	tph	>0	Maximum reclaiming capacity - For dynamic calculation only

Runtime values

Readable:

Parameter	Val.	Unit	Limits	Description
Total capacity		m3		Maximal capacity in cubic meters
Total capacity		t		Maximal capacity in metric tons
Actual volume		m3		In static calculation equals total capacity
Capacity percentage		%		Percentage of the total stockpile capacity filled - In static calculation equals 100%
Live volume		m3		Actual live volume
Residence Time		h		Based on live volume fraction
Time to empty		h		Estimated time after which the stockpile is completely emptied
Time to fill		h		Estimated time after which the stockpile reaches total capacity

Writable:

Parameter	Val.	Unit	Limits	Description
Reclaiming ON	TRUE /FALSE			Reclaiming is ongoing - For dynamic calculation only
Reclaiming capacity percentage	100	%	[0-100]	In percentage of the maximum reclaiming capacity - For dynamic calculation only

Metso Outotec reserves the right to modify these specifications at any time without prior notice. Copyright © 2021, Metso Outotec Finland Oy

Metso:Outotec

HSC - Sim MinPro Unit Models
28/192
Antti Remes, Caroline Izart, et al.
May 27, 2021

Model fitting and calibration **Limitations**

This model does not take into account the segregation of particles in the stockpile related to their density or size. The loading point and drawpoint are each limited to one occurrence.

References

1. Young CA (2019) SME Mineral Processing and Extractive Metallurgy Handbook

Metso:Outotec

HSC - Sim MinPro Unit Models
127/192
Antti Remes, Caroline Izart, et al.
May 27, 2021

46.3.27. Hydrocyclone : MU-240-10

Modeling scope:	DIMENSIONING	ADVANCED
Stream particle sizing:	SIZED	
Mode:	Static: <input checked="" type="checkbox"/> Dynamic: -	
Inputs:	Feed	
Outputs:	Overflow Underflow	

Description and equations

The hydrocyclone model is based on the physical dimension of a cyclone. Two calculation options are available, the Plitt and the Nageswararao. In the Plitt calculation, there are four constants that are used for model calibration. In the Nageswararao calculation, five variables are fitted to the process. This model can calculate the classification of each mineral separately as an option. In addition, the roping condition is estimated with selected methods and a warning message is given if it occurs.

The dimensions of the hydrocyclone used in the model are illustrated in **Fig. 25**.

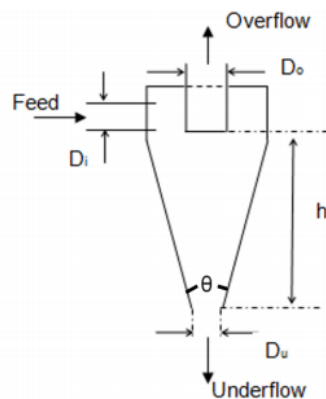


Fig. 25. Hydrocyclone dimensions required for the model.

Plitt model relationships:

The separation by size is calculated using the Plitt/Reid separation efficiency /1/:

$$E_o(d_i) = R_f + (1 - R_f) \left(1 - 0.5 \left(\frac{d_i}{d_{50c}} \right)^m \right)$$

The corrected cut size is obtained /1/:

Metso:Outotec

HSC - Sim MinPro Unit Models
128/192
Antti Remes, Caroline Izart, et al.
May 27, 2021

$$d_{50c} = F_1 \frac{39.7 D_c^{0.46} D_i^{0.6} D_o^{1.21} \eta^{0.5} \exp(0.063\phi)}{D_u^{0.71} h^{0.38} Q^{0.45} \left[\frac{(\rho_s - 1)}{1.6} \right]^k}$$

The separation of size by mineral can also be calculated (if selected) with the same equations as above, but the solids density ρ_s is then for the mineral concerned instead of the bulk average. A liberation size, above which the separation is made, can be set in the model parameters based on bulk solids properties.

Sharpness of the separation is described with efficiency exponent m /2/:

$$m = F_2 1.94 \exp\left(\frac{-1.58S}{1+S}\right) \left(\frac{D_c^2 h}{Q}\right)^{0.15}$$

Pressure drop over the cyclone is /1, 2/:

$$P = F_3 \frac{1.88 Q^{1.78} \exp(0.0055\phi)}{D_c^{0.37} D_i^{0.94} h^{0.28} (D_u^2 + D_o^2)^{0.87}}$$

Subsequently, the volumetric slurry split between underflow/overflow is calculated by /1, 2/:

$$S = F_4 \frac{18.62 \rho_p^{0.24} \left(\frac{D_u}{D_o}\right)^{3.31} h^{0.54} (D_u^2 + D_o^2)^{0.36} \exp(0.0054\phi)}{D_c^{1.11} P^{0.24}}$$

Finally, the water recovery to underflow is a function of volumetric solids split S (underflow/overflow) and solids mass recovery R_s (underflow/feed) with /2/:

$$R_f = \frac{\frac{S}{1+S} - \frac{R_s \phi}{100}}{1 - \frac{\phi}{100}}$$

Since the separation efficiency depends on the water recovery and solids split, and the water recovery is dependent on the solids split and solids recovery, the calculation procedure is iterative. The iteration is repeated until water recovery R_f is close to the value of the previous calculation round; usually 3 iterations is enough /1/. Here, for the first iteration, the water recovery is calculated, based on Brookes et al. and Rouse et al., using /3, p. 185/:

$$R_f = 7.62 \left[\frac{1}{1 + (D_o/D_u)} \right]^{3.59}$$

Nageswararao model relationships:

The following relationships were established by Nageswararao and are described in /4/.

First, the hindered settling factor, λ , is calculated based on the feed solid volumetric fraction ϕ .

Metso:Outotec

HSC - Sim MinPro Unit Models
129/192
Antti Remes, Caroline Izart, et al.
May 27, 2021

$$\lambda = \frac{10^{1.82\phi}}{8.05 (1 - \phi)^2}$$

The cyclone feed pressure can be computed based on the following throughput / pressure relation:

$$\frac{Q}{D_c \sqrt{P/\rho_p}} = K_{Q0} D_c^{-0.10} \left(\frac{D_o}{D_c}\right)^{0.68} \left(\frac{D_i}{D_c}\right)^{0.45} \left(\frac{L_c}{D_c}\right)^{0.20} \theta^{-0.10}$$

Once P has been calculated, d_{50c} can be estimated with the following d_{50c} / D_c relation:

$$\frac{d_{50c}}{D_c} = K_{D0} D_c^{-0.65} \left(\frac{D_o}{D_c}\right)^{0.52} \left(\frac{D_u}{D_c}\right)^{-0.50} \left(\frac{D_i}{D_c}\right)^{0.20} \left(\frac{L_c}{D_c}\right)^{0.20} \theta^{0.15} \left(\frac{P}{\rho_p g D_c}\right)^{-0.22} \lambda^{0.93}$$

d_{50c} can also be computed separately for each different mineral if the option is enabled:

$$d_{50c,min} = d_{50c} \frac{\rho_p - 1}{\rho_{min} - 1}$$

The water recovery to the underflow, R_f , is then calculated using the dimension ratio, pressure, hindered settling, and calibration constant K_{Wf} :

$$R_f = K_{Wf} \left(\frac{D_o}{D_c}\right)^{-1.19} \left(\frac{D_u}{D_c}\right)^{2.40} \left(\frac{D_i}{D_c}\right)^{0.50} \left(\frac{L_c}{D_c}\right)^{0.22} \theta^{-0.24} \left(\frac{P}{\rho_p g D_c}\right)^{-0.53} \lambda^{0.27}$$

Finally, the pulp volumetric recovery to the underflow, R_v , is calculated with the empirical relation:

$$R_v = K_{V1} \left(\frac{D_o}{D_c}\right)^{-0.94} \left(\frac{D_u}{D_c}\right)^{1.83} \left(\frac{D_i}{D_c}\right)^{0.25} \left(\frac{L_c}{D_c}\right)^{0.22} \theta^{-0.24} \left(\frac{P}{\rho_p g D_c}\right)^{-0.31}$$

The ratio of particles of mean size d going to the overflow is calculated as follows:

$$E_o(d/d_{50c}) = (1 - R_f) \frac{(1 + \beta \beta^* d/d_{50c})(e^\alpha - 1)}{(e^{\alpha d/d_{50c}} + e^\alpha - 2)}$$

The parameters α and β are constant for a given feed, where R_f and d_{50c} depend on the operating conditions (throughput, pulp SG, solid percentage etc.).

β^* is calculated iteratively, assuming that:

$$E_o(1) = \frac{(1 - R_f)}{2}$$

Roping criteria:

Metso:Outotec

HSC - Sim MinPro Unit Models
130/192
Antti Remes, Caroline Izart, et al.
May 27, 2021

If the capacity of the cyclone underflow apex is exceeded, the underflow discharge can turn gradually from a spray shape to a rope-like shape. Here the roping of a cyclone is estimated in the same way as in the Plitt model.

Roping occurs if the underflow volumetric solids fraction exceeds the value calculated by the criteria equation.

Plitt (1986, 1987) roping criteria /2/:

$$\phi_u > 62.3 \left[1 - \exp\left(\frac{-d_u}{60}\right) \right]$$

Roping criteria according to Laguitton (1985) /2/ (valid for feed densities less than 35 v/v % of solids):

$$\phi_u > 56 + 0.2(\phi - 20)$$

Power:

The work done in the cyclone is calculated based on the pressure drop and the volumetric flow rate. The calculated Power [kW] can be further used for estimation of the required pumping power.

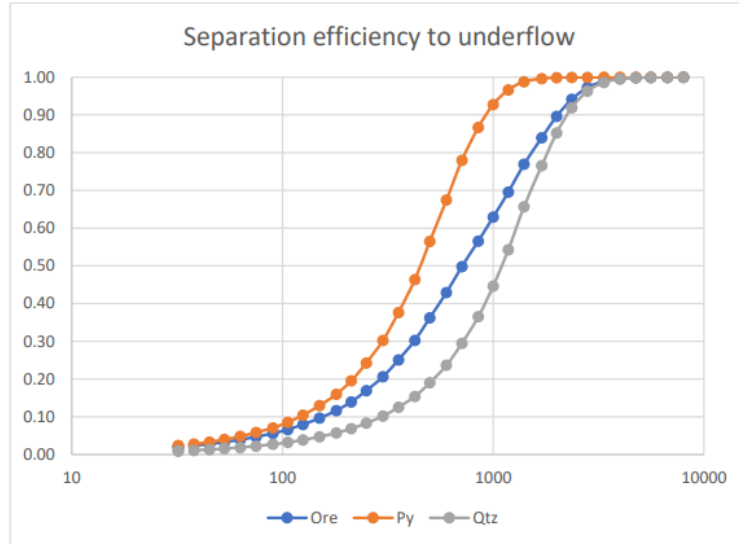
$$Power = \frac{P Q}{3600}$$

Partition and efficiency curves

The partition curve gives the actual repartition proportion to the underflow for each particle and each size class, considering the entrainment to be equal to $1-E_o$. The efficiency curve does not take entrainment into account.

Metso:Outotec

HSC - Sim MinPro Unit Models
131/192
Antti Remes, Caroline Izart, et al.
May 27, 2021



Separation parameters

The imperfection number I is a dimensionless parameter calculated as /6/:

$$I = \frac{d_{75} - d_{25}}{2 d_{50c}}$$

where d_{75} and d_{25} are the sizes for which 75% and 25% respectively of the particles of this size class are directed to the underflow. The imperfection number is calculated for each particle type when 'Separation by mineral' is selected.

Total and reduced separation efficiency

The total separation efficiency E_t is calculated as /7/:

$$E_t = \frac{G_u C_u}{G_e C_e}$$

where G_u and G_e are the mass flows of underflow and feed respectively and C_u and C_e are the solid weight concentrations of underflow and feed.

The reduced separation efficiency E_t' is calculated as:

$$E_t' = \frac{E_t - R_f}{1 - R_f}$$

where R_f is the flow ratio, i.e., the ratio of volume flow of underflow to that of the feed.

Notations:

Metso Outotec reserves the right to modify these specifications at any time without prior notice. Copyright © 2021, Metso Outotec Finland Oy

Metso:Outotec

HSC - Sim MinPro Unit Models
132/192
Antti Remes, Caroline Izart, et al.
May 27, 2021

▪ D_c	m	cyclone diameter
▪ D_i	m	inlet diameter
▪ D_o	m	overflow vortex finder diameter
▪ D_u	m	underflow apex diameter
▪ L_c	m	length of the cylindrical section
▪ $KV1$		Nageswararao calibration constant (UF pulp recovery)
▪ $KW1$		Nageswararao calibration constant (UF water recovery)
▪ $KQ0$		Nageswararao calibration constant (throughput/pressure relation)
▪ $KD0$		Nageswararao calibration constant (classification size)
▪ $F1$		Plitt calibration (d50c)
▪ $F2$		Plitt calibration (efficiency exponent)
▪ $F3$		Plitt calibration (pressure drop)
▪ $F4$		Plitt calibration (volumetric flow ratio)
▪ R_v		volumetric pulp recovery from feed to underflow
▪ R_f		water mass recovery from feed to underflow
▪ $E_0(d/d_{50c})$		ratio of particle of size d to overflow
▪ d_{50c}	µm	corrected cut size
▪ d	µm	size of given feed particle size class
▪ d_u	µm	mean size of the underflow stream
▪ ρ_p	t/m ³	density of the feed slurry (pulp)
▪ ρ_{min}	t/m ³	density of given mineral
▪ g	m/s ²	gravitational acceleration
▪ P	kPa	pressure drop of the cyclone
▪ $Power$	kW	power due to pressure drop
▪ Q	m ³ /h	volumetric slurry feed
▪ θ	degrees	full cone angle
▪ ϕ	%	solids fraction of the feed v/v %
▪ ϕ_u	%	underflow volumetric solids fraction
▪ α		Nageswararao - efficiency curve sharpness
▪ β		Nageswararao - efficiency curve hook parameter
▪ β^*		Nageswararao - calculated efficiency curve hook
parameter		

Messages from the model

Message	Reason / What to Do
Fish hook parameter could not be solved within tolerance of d50c	Iterative solution of β^* was not reached. Please increase the Max Iteration parameter or increase the Tolerance parameter (less accuracy).
Cyclone is roping according to SPOC criterion	Cyclone underflow might not be spray shaped and the cut size is no longer valid. Change the feed characteristics or modify the cyclone dimensions or increase the number of cyclones in the pattern.
Cyclone is roping according to Plitt criterion	Cyclone underflow might not be spray shaped and the cut size is no longer valid. Change the feed characteristics or modify the cyclone dimensions or increase the number of cyclones in the pattern.

Metso:Outotec

HSC - Sim MinPro Unit Models
133/192
Antti Remes, Caroline Izart, et al.
May 27, 2021

Model parameters

Parameter	Val.	Unit	Limits	Description
Settings				
Separation by Mineral	False			
Tolerance for fish-hook calculation	0.01			
Maximum iteration for fish-hook calculation	25			
Calculation option	-Nageswararao -Plitt			
Dimensions				
Dc	0.35	m	>0	Cyclone diameter
Di	0.11	m	>0	Inlet diameter
Dof	0.15	m	>0	Vortex finder (overflow) diameter
Duf	0.8	m	>0	Apex (underflow) diameter
Height	1.8	m	>0	Distance between apex and vortex finder
Θ (If Nageswararao option selected)	15	Degree	>0	Cone angle
Cyclones	1			Number of parallel cyclones
Calibration				
KD0 (If Nageswararao option selected)	0.0001			Calibration for cut size (d50c) (Typical: 1E-5 - 1E-3)
KQ0 (If Nageswararao option selected)	433			Calibration for pressure/flowrate relationship (Typical: 300 - 600)
KV1 (If Nageswararao option selected)	5.87			Calibration for pulp volume recovery in the UF
KW1 (If Nageswararao option selected)	7.74			Calibration for water recovery in the UF
α (If Nageswararao option selected)	1.15		>0	Sharpness of efficiency curve (Typical: 0.5 - 10)
β (If Nageswararao option selected)	0			Initial dip of efficiency curve (Typical: 0 - 0.5)

Metso Outotec reserves the right to modify these specifications at any time without prior notice. Copyright © 2021, Metso Outotec Finland Oy

Metso:Outotec

HSC - Sim MinPro Unit Models
134/192
Antti Remes, Caroline Izart, et al.
May 27, 2021

F1 (If Plitt option selected)	1			Calibration for cut size (d50c)
F2 (If Plitt option selected)	1			Calibration for efficiency exponent (m)
F3 (If Plitt option selected)	1			Calibration for pressure drop (P)
F4 (If Plitt option selected)	1			Calibration for uf/of flow ratio (S)
Physical parameters				
Calculate Water Viscosity	TRUE/FALSE			
k	0.5		>0	Hydrodynamic exponent
η	0.89	cP	>0	Liquid viscosity (if automatic calculation disabled)

Runtime values

Readable:

Parameter	Val.	Unit	Limits	Description
β^*				Corrected dip value
d50c		μm		Corrected 50% cut size
P		kPa		Pressure drop
Rf		%		Water recovery to underflow
Power		kW		Work done by the cyclone

Model fitting and calibration

The Nageswararao option of the model requires the physical dimensions of the hydrocyclone. The model can be calibrated to experimental data using the following K values:

- KD0, for calibrating the d_{50c} corrected cut size
- KQ0, for calibrating the P pressure drop / flowrate separation
- KW1, for calibrating the water underflow/overflow split
- α , for calibrating the PSD separation in the overflow/underflow
- β , for calibrating the fish hook effect of the separation

which depend on the feed characteristics. It must be noted that the K values vary over a substantial range, which limits the model applicability in process design.

The Plitt option of the model is parameterized with the physical dimensions of a hydrocyclone. The model calibration to experimental data is carried out using four factors:

Metso:Outotec

HSC - Sim MinPro Unit Models
135/192
Antti Remes, Caroline Izart, et al.
May 27, 2021

- F1, for calibrating the d_{50c} corrected cut size
- F2, for calibrating the m efficiency exponent
- F3, for calibrating the P pressure drop
- F4, for calibrating the S volumetric underflow/overflow split

The default values of all of them are one /1/, but they should be calibrated whenever operating data is available.

Limitations

- SPOC roping criterion is valid only for feed densities < 35 % vol./vol.

References

1. Flintoff, B.C., Plitt, L.R., and Turak, A.A. Cyclone modeling: a review of present technology. CIM Bulletin, 1987, Vol. 80, No 905, pp. 39-50.
2. Plitt, L.R. A mathematical model of the hydrocyclone classifier. CIM Bulletin, 1976, Vol. 69, pp. 114-123.
3. Heiskanen, K. Particle classification. 1st ed. London: Chapman & Hall, 1993. 321 p. ISBN 0 412 49300 4.
4. Nageswararao, K., Wiseman, D.M., and Napier-Munn, T.J. Two empirical hydrocyclone models revisited. Minerals Engineering, 2004, Vol. 17, pp. 671-687.
5. Vogel. H., Phys. Z., 1921, 22, p. 645.
6. Wills, B.A., and Napier-Munn, T., Mineral Processing Technology – An introduction to the practical aspects of ore treatment and mineral recovery, 7th ed., Elsevier Science & Technology Books, 2006, 444 p., ISBN: 0750644508,
7. Chu, L.Y., Yu, W., Wang, G.J., Zhou, X.T., Chen, W.M., Dai, G.Q., Enhancement of hydrocyclone separation performance by eliminating the air core, Chemical Engineering and Processing, 2004, 43-12.

6.3 Appendix 3: Murske size analysis and mineral reconstruction

Element / Sieve size (um)	20	32	45	63	75	90	125	250	500	1000	2000	3350	4000	10000
Fe	21.7	22.5	22.1	22.3	23.1	22.3	21.6	20.8	19.7	17.6	16.2	15.2	16.6	14.6
Ca	5.3	4.1	3.9	3.6	3.5	3.1	3.3	3.1	3.1	3.7	4.2	4.2	3.9	3.5
Cu	0.9	0.8	0.6	0.6	0.6	0.5	0.5	0.4	0.3	0.4	0.4	0.5	0.4	0.5
Ti	0.4	0.7	0.6	0.5	0.4	0.3	0.2	0.2	0.3	0.4	0.4	0.3	0.3	0.3
Zn	0.4	0.3	0.3	0.3	0.3	0.2	0.2	0.2	0.2	0.2	0.2	0.2	0.2	0.2
Ni	0.6	0.5	0.4	0.5	0.5	0.4	0.4	0.4	0.3	0.3	0.3	0.2	0.3	0.2
Co	0.3	0.3	0.2	0.2	0.2	0.2	0.2	0.2	0.2	0.2	0.1	0.1	0.1	0.1
Cr	0.1	0.1	0.1	0.1	0.1	0.1	0.1	0.1	0.1	0.1	0.1	0.1	0.1	0.1
Mn	0.1	0.1	0.1	0.0	0.1	0.0	0.0	0.0	0.0	0.0	0.0	0.0	0.0	0.0
Rest	70.4	70.8	71.7	71.9	71.4	72.9	73.5	74.6	75.8	77.2	78.1	79.2	78.0	80.6
Weight %	4.2	1.5	1.6	2.4	1.7	1.6	3.7	8.3	7.3	8.5	13.9	18.3	10.3	16.6
Min wt% per size fraction														
Chalcopyrite	0.3	0.3	0.2	0.2	0.2	0.2	0.2	0.1	0.1	0.1	0.1	0.2	0.1	0.2
Co-Pentlandite	0.1	0.1	0.1	0.1	0.1	0.1	0.1	0.1	0.1	0.1	0.1	0.0	0.1	0.0
Pyrite / Pyrrhotite	13.5	14.0	13.8	13.9	14.4	13.9	13.5	13.0	12.3	11.0	10.1	9.5	10.4	9.1
Sphalerite	0.2	0.2	0.2	0.2	0.2	0.1	0.1	0.1	0.1	0.1	0.1	0.1	0.1	0.1
NSG	85.9	85.4	85.8	85.7	85.2	85.8	86.2	86.7	87.4	88.8	89.6	90.2	89.3	90.6
Min proportion per size fraction														
Chalcopyrite	0.09	0.03	0.02	0.03	0.02	0.02	0.04	0.07	0.05	0.07	0.13	0.18	0.09	0.17
Co-Pentlandite	0.07	0.03	0.02	0.04	0.02	0.02	0.04	0.10	0.08	0.10	0.13	0.14	0.09	0.12
Pyrite / Pyrrhotite	0.05	0.02	0.02	0.03	0.02	0.02	0.05	0.10	0.08	0.09	0.13	0.16	0.10	0.14
Sphalerite	0.07	0.02	0.02	0.03	0.02	0.02	0.04	0.08	0.06	0.07	0.13	0.17	0.10	0.18
NSG	0.04	0.01	0.02	0.02	0.02	0.02	0.04	0.08	0.07	0.09	0.14	0.19	0.10	0.17
Min PSD														
Chalcopyrite Murske	8.6	11.1	13.3	16.6	18.7	20.4	24.2	31.3	36.6	43.6	56.1	74.3	83.5	100.0
Co-Pentlandite Murske	7.1	9.7	12.0	15.5	17.8	19.8	24.0	34.1	42.5	52.2	64.7	78.3	87.6	100.0
Pyrite / Pyrrhotite Murske	5.2	7.1	9.1	12.2	14.4	16.5	21.0	30.9	39.1	47.7	60.5	76.4	86.2	100.0
Sphalerite Murske	7.1	9.3	11.4	14.5	16.7	18.5	22.4	30.0	35.8	42.8	55.6	72.4	81.9	100.0
NSG Murske	4.1	5.5	7.1	9.4	11.0	12.6	16.2	24.3	31.5	40.0	54.0	72.7	83.0	100.0
Simplified min wt%														
Sulphides	14.1	14.6	14.2	14.3	14.8	14.3	13.8	13.3	12.6	11.2	10.4	9.8	10.7	9.4
NSG	85.9	85.4	85.8	85.7	85.2	85.7	86.2	86.7	87.4	88.8	89.6	90.2	89.3	90.6
Simplified min proportion														
Sulphides	0.05	0.02	0.02	0.03	0.02	0.02	0.05	0.10	0.08	0.09	0.13	0.16	0.10	0.14
NSG	0.04	0.01	0.02	0.02	0.02	0.02	0.04	0.08	0.07	0.09	0.14	0.19	0.10	0.17
Simplified min PSD														
Sulphides	5 %	7 %	9 %	12 %	15 %	17 %	21 %	31 %	39 %	48 %	60 %	76 %	86 %	100 %
NSG	4 %	6 %	7 %	9 %	11 %	13 %	16 %	24 %	31 %	40 %	54 %	73 %	83 %	100 %

6.4 Appendix 4: TMT size analysis and mineral reconstruction

Element / Sieve size (um)	20	32	45	63	75	90	125	250	500	1000
Fe	19.8	21.6	20.1	19.8	22.4	20.5	18.7	16.8	17.6	18.4
Ca	5.0	4.4	3.8	3.6	3.4	3.2	3.3	3.6	3.4	3.2
Cu	0.7	0.7	0.5	0.5	0.5	0.4	0.4	0.3	0.3	0.3
Ti	0.4	0.7	0.6	0.5	0.4	0.3	0.2	0.2	0.3	0.4
Zn	0.3	0.3	0.2	0.2	0.2	0.2	0.2	0.2	0.2	0.2
Ni	0.4	0.5	0.4	0.4	0.4	0.3	0.3	0.3	0.3	0.2
Co	0.2	0.2	0.2	0.2	0.2	0.2	0.2	0.1	0.2	0.2
Cr	0.1	0.1	0.1	0.1	0.1	0.1	0.1	0.1	0.1	0.1
Mn	0.1	0.1	0.1	0.0	0.1	0.0	0.0	0.0	0.0	0.0
Rest	72.9	71.7	74.0	74.8	72.3	74.7	76.6	78.4	77.7	77.0
Weight %	11.4	4.8	5.2	8.0	5.8	4.7	14.0	31.3	12.3	2.3
Min wt% per size fraction										
Chalcopyrite	0.3	0.2	0.2	0.2	0.2	0.1	0.1	0.1	0.1	0.1
Co-Pentlandite	0.1	0.1	0.1	0.1	0.1	0.1	0.1	0.1	0.1	0.1
Pyrite / Pyrrhotite	12.3	13.5	12.5	12.3	14.0	12.8	11.6	10.4	11.0	11.5
Sphalerite	0.2	0.2	0.1	0.1	0.1	0.1	0.1	0.1	0.1	0.1
NSG	87.2	86.1	87.1	87.3	85.6	86.9	88.1	89.3	88.8	88.3
Min proportion per size fraction										
Chalcopyrite	0.19	0.07	0.06	0.09	0.07	0.05	0.13	0.24	0.09	0.02
Co-Pentlandite	0.15	0.06	0.06	0.09	0.08	0.05	0.13	0.24	0.12	0.02
Pyrite / Pyrrhotite	0.12	0.06	0.06	0.09	0.07	0.05	0.14	0.28	0.12	0.02
Sphalerite	0.16	0.06	0.06	0.08	0.06	0.05	0.14	0.29	0.09	0.02
NSG	0.11	0.05	0.05	0.08	0.06	0.05	0.14	0.32	0.12	0.02
Min PSD										
Chalcopyrite TMT	19.1	26.5	32.8	41.6	48.5	53.0	65.7	89.5	98.3	100.0
Co-Pentlandite TMT	14.8	21.0	27.3	35.9	43.4	48.5	61.4	85.6	97.9	100.0
Pyrite / Pyrrhotite TMT	12.1	17.7	23.3	31.8	38.8	43.9	58.0	86.1	97.7	100.0
Sphalerite TMT	15.9	22.2	28.1	36.4	42.8	47.5	60.9	89.7	98.3	100.0
NSG TMT	11.3	16.0	21.2	29.1	34.8	39.4	53.5	85.3	97.7	100
Simplified min wt%										
Sulphides	12.8	13.9	12.9	12.7	14.4	13.1	11.9	10.7	11.2	11.8
NSG	87.2	86.1	87.1	87.3	85.6	86.9	88.1	89.3	88.8	88.2
Simplified min proportion										
Sulphides	0.12	0.06	0.06	0.09	0.07	0.05	0.14	0.28	0.12	0.02
NSG	0.11	0.05	0.05	0.08	0.06	0.05	0.14	0.32	0.12	0.02
Simplified min PSD										
Sulphides	12 %	18 %	23 %	32 %	39 %	44 %	58 %	86 %	98 %	100 %
NSG	11 %	16 %	21 %	29 %	35 %	39 %	53 %	85 %	98 %	100 %

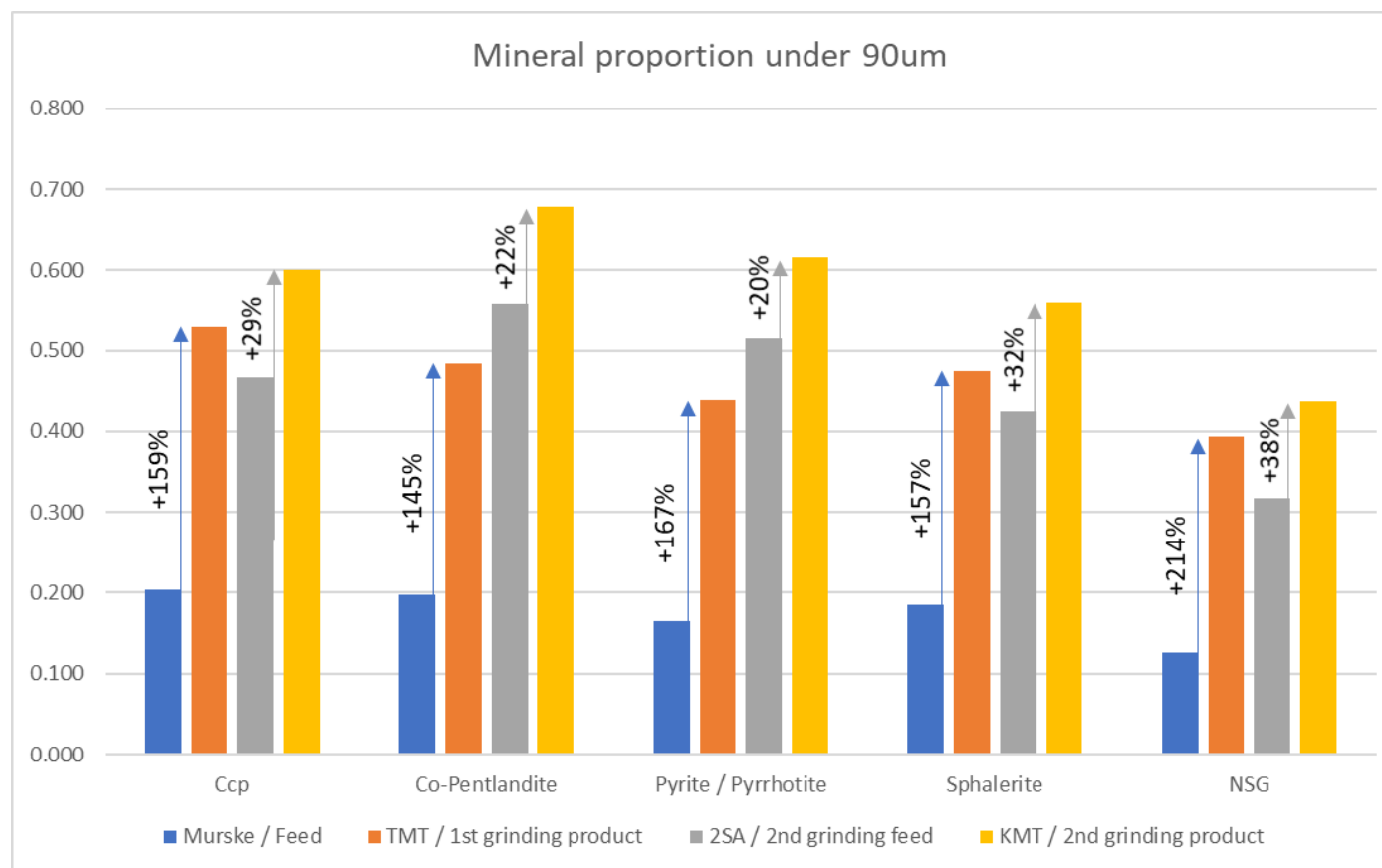
6.5 Appendix 5: 2SA size analysis and mineral reconstruction

Elements / Sieve size (um)	45	63	75	90	125	250	500
Fe	43.16	45.95	45.76	41.35	35.20	16.73	14.47
Ca	1.49	1.02	1.08	1.63	3.12	3.26	2.71
Cu	0.62	0.59	0.63	0.57	0.56	0.29	0.24
Ti	0.39	0.65	0.63	0.47	0.40	0.30	0.23
Zn	0.24	0.24	0.27	0.27	0.27	0.15	0.14
Ni	0.75	0.71	0.64	0.53	0.44	0.25	0.21
Co	0.44	0.43	0.37	0.33	0.25	0.13	0.09
Cr	0.12	0.07	0.08	0.08	0.09	0.11	0.09
Mn	0.09	0.06	0.05	0.04	0.05	0.04	0.04
Rest	52.70	50.27	50.50	54.73	59.60	78.74	81.78
Weight %	5.90	10.30	9.90	9.40	22.60	34.00	7.80
Min wt% per size fraction							
Chalcopyrite	0.21	0.21	0.22	0.2	0.19	0.1	0.08
Co-Pentlandite	0.17	0.16	0.14	0.12	0.1	0.05	0.03
Pyrite / Pyrrhotite	26.9	28.64	28.52	25.77	21.94	10.43	9.02
Sphalerite	0.14	0.14	0.16	0.16	0.16	0.09	0.08
NSG	72.58	70.85	70.97	73.75	77.61	89.33	90.78
Min proportion per size fraction							
Chalcopyrite	0.08	0.13	0.14	0.12	0.28	0.21	0.04
Co-Pentlandite	0.11	0.18	0.15	0.13	0.23	0.18	0.03
Pyrite / Pyrrhotite	0.08	0.16	0.15	0.13	0.26	0.19	0.04
Sphalerite	0.07	0.12	0.12	0.12	0.28	0.24	0.05
NSG	0.05	0.09	0.09	0.09	0.22	0.38	0.09
Min PSD							
Chalcopyrite 2SA	8.0	21.4	34.9	46.7	74.6	95.8	100.0
Co-Pentlandite 2SA	10.6	28.5	43.3	55.8	79.2	97.1	100.0
Pyrite / Pyrrhotite 2SA	8.4	23.9	38.8	51.5	77.6	96.3	100.0
Sphalerite 2SA	6.7	18.3	30.7	42.5	70.8	95.1	100.0
NSG 2SA	5.3	14.4	23.1	31.7	53.5	91.2	100.0
Simplified min wt%							
Sulphides	27.42	29.15	29.03	26.25	22.39	10.67	9.22
NSG	72.58	70.85	70.97	73.75	77.61	89.33	90.78
Simplified min proportion							
Sulphides	0.08	0.16	0.15	0.13	0.26	0.19	0.04
NSG	0.05	0.09	0.09	0.09	0.22	0.38	0.09
Simplified min PSD							
Sulphides	0.0835	24 %	39 %	51 %	78 %	96 %	100 %
NSG	0.0532	14 %	23 %	32 %	53 %	91 %	100 %

6.6 Appendix 6: KMT size analysis and mineral reconstruction

Element / Sieve size (um)	32	45	63	75	90	125	250	500
Fe	36.45	40.76	43.58	43.84	39.63	32.08	15.79	16.45
Ca	3.21	2.02	1.47	1.3	1.99	3.28	3.25	2.87
Cu	0.7	0.62	0.64	0.66	0.58	0.53	0.26	0.24
Ti	0.39	0.65	0.63	0.47	0.4	0.3	0.23	0.22
Zn	0.3	0.25	0.25	0.27	0.29	0.25	0.15	0.13
Ni	0.57	0.68	0.72	0.65	0.54	0.43	0.22	0.22
Co	0.32	0.4	0.42	0.38	0.3	0.22	0.1	0.12
Cr	0.12	0.07	0.08	0.08	0.09	0.11	0.09	0.08
Mn	0.09	0.06	0.05	0.04	0.05	0.04	0.04	0.04
Rest	57.86	54.49	52.16	52.32	56.12	62.76	79.87	79.63
Weight %	8.9	4.8	12.7	11.2	9.7	23.4	26.9	2.4
Min wt% per size fraction								
Chalcopyrite	0.24	0.21	0.22	0.23	0.2	0.18	0.09	0.08
Co-Pentlandite	0.12	0.15	0.16	0.14	0.11	0.08	0.04	0.04
Pyrite / Pyrrhotite	22.72	25.4	27.16	27.32	24.7	19.99	9.84	10.26
Sphalerite	0.17	0.15	0.15	0.16	0.17	0.15	0.09	0.07
NSG	76.75	74.08	72.31	72.15	74.81	79.59	89.94	89.54
Min proportion per size fraction								
Chalcopyrite	0.12	0.06	0.16	0.15	0.11	0.25	0.14	0.01
Co-Pentlandite	0.11	0.08	0.21	0.17	0.12	0.20	0.11	0.01
Pyrite / Pyrrhotite	0.10	0.06	0.18	0.16	0.12	0.24	0.13	0.01
Sphalerite	0.12	0.05	0.14	0.13	0.12	0.26	0.17	0.01
NSG	0.09	0.05	0.12	0.10	0.09	0.23	0.30	0.03
Min PSD								
Chalcopyrite KMT	12.4	18.2	34.3	48.9	60.1	84.7	98.8	100.0
Co-Pentlandite KMT	11.1	18.7	39.5	56.2	67.8	87.8	98.9	100.0
Pyrite / Pyrrhotite KMT	10.3	16.4	33.9	49.4	61.6	85.3	98.8	100.0
Sphalerite KMT	11.5	16.8	30.7	43.9	56.0	81.7	98.7	100.0
NSG KMT	8.6	13.0	24.5	34.6	43.7	67.0	97.3	100.0
Simplified min wt%								
Sulphides	23.3	25.9	27.7	27.9	25.2	20.4	10.1	10.5
NSG	76.7	74.1	72.3	72.1	74.8	79.6	89.9	89.5
Simplified min proportion								
Sulphides	0.10	0.06	0.18	0.16	0.12	0.24	0.13	0.01
NSG	0.09	0.05	0.12	0.10	0.09	0.23	0.30	0.03
Simplified min PSD								
Sulphides	10 %	16 %	34 %	49 %	62 %	85 %	99 %	100 %
NSG	9 %	13 %	25 %	35 %	44 %	67 %	97 %	100 %

6.7 Appendix 7: Mineral reconstruction in streams and enrichments

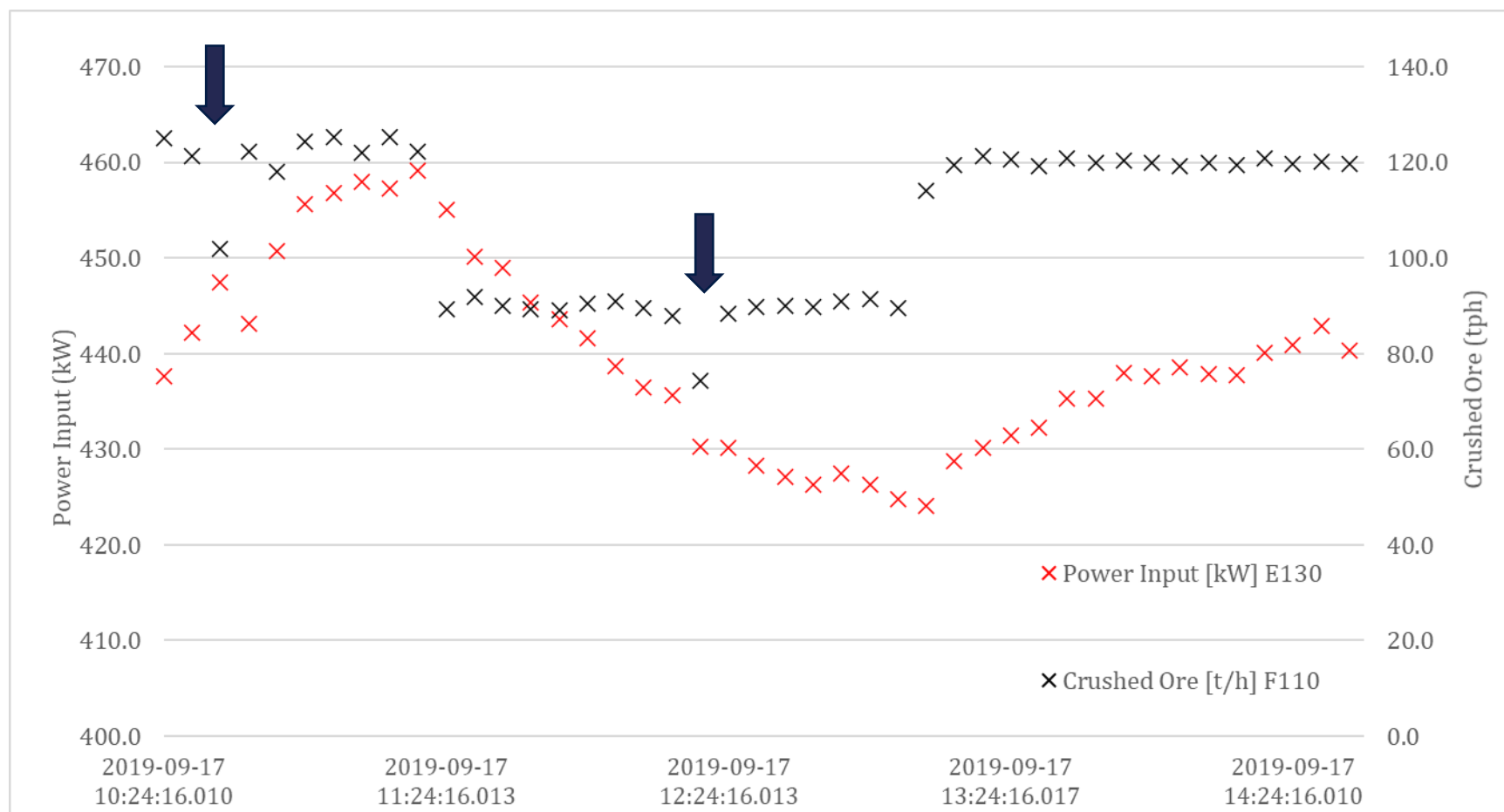


6.9 Appendix 9: Data table from Pyhäsalmi SAG automation process control during test

timestamp	Power Input [kW]	Lump Ore [t/h]	Crushed Ore [t/h]	Water [m ³ /h]	Power input Cone Crusher [kW]	Filling Factor [%]	Pulp Density [kg/dm ³]
	E130	F100	F110	F137	E080	MFILL2	D139
2019-09-17 14:36:16.007	440.3	19.2	119.7	41.3	39.3	36.4	2.5
2019-09-17 14:30:16.000	442.9	19.6	120.1	41.1	39.8	36.3	2.5
2019-09-17 14:24:16.010	440.9	19.2	119.9	41.2	39.9	36.4	2.5
2019-09-17 14:18:16.003	440.1	19.9	121.0	41.3	39.0	36.2	2.5
2019-09-17 14:12:16.027	437.8	19.1	119.4	41.3	39.0	36.0	2.5
2019-09-17 14:06:16.007	437.9	19.7	120.0	41.1	40.4	35.9	2.5
2019-09-17 14:00:16.013	438.6	19.5	119.2	41.4	39.5	36.1	2.5
2019-09-17 13:54:16.020	437.7	19.5	120.0	41.0	39.8	36.0	2.5
2019-09-17 13:48:16.000	438.1	19.8	120.4	41.3	39.8	35.9	2.5
2019-09-17 13:42:16.007	435.3	18.7	119.9	41.2	39.3	35.7	2.5
2019-09-17 13:36:16.023	435.3	19.5	120.8	41.2	39.5	35.7	2.5
2019-09-17 13:30:16.017	432.3	19.4	119.3	41.3	38.8	35.5	2.5
2019-09-17 13:24:16.017	431.4	19.5	120.7	41.3	39.0	35.4	2.5
2019-09-17 13:18:16.017	430.2	19.4	121.4	41.1	39.2	35.3	2.5
2019-09-17 13:12:16.000	428.7	19.7	119.6	41.4	39.0	35.2	2.5
2019-09-17 13:06:16.003	424.1	19.9	114.0	41.3	38.7	35.0	2.4
2019-09-17 13:00:16.027	424.7	19.8	89.7	41.1	38.4	35.0	2.3
2019-09-17 12:54:16.007	426.3	19.3	91.3	41.2	38.9	35.2	2.3
2019-09-17 12:48:16.010	427.5	20.4	90.9	41.1	39.2	35.2	2.3
2019-09-17 12:42:16.007	426.3	19.7	89.8	41.2	39.2	35.3	2.3
2019-09-17 12:36:16.017	427.1	19.1	90.1	41.1	38.9	35.4	2.3
2019-09-17 12:30:16.017	428.3	19.4	89.9	41.2	38.5	35.6	2.3

2019-09-17 12:24:16.013	430.2	19.1	88.5	41.2	39.0	35.6	2.3
2019-09-17 12:18:16.007	430.3	18.9	74.4	41.2	39.3	35.7	2.1
2019-09-17 12:12:16.007	435.7	19.4	88.0	40.9	39.7	35.8	2.3
2019-09-17 12:06:16.020	436.5	19.2	89.6	41.0	40.6	36.0	2.3
2019-09-17 12:00:16.023	438.7	19.6	91.0	41.0	40.8	36.2	2.3
2019-09-17 11:54:16.007	441.6	19.9	90.4	41.0	40.6	36.4	2.3
2019-09-17 11:48:15.007	443.6	19.9	89.2	41.1	40.6	36.5	2.3
2019-09-17 11:42:16.017	445.4	19.7	89.3	40.9	40.7	36.7	2.3
2019-09-17 11:36:16.017	449.0	20.0	90.0	41.0	40.8	36.9	2.3
2019-09-17 11:30:16.017	450.1	19.8	91.8	41.0	41.0	37.1	2.3
2019-09-17 11:24:16.013	455.0	21.0	89.4	40.9	40.8	37.5	2.3
2019-09-17 11:18:16.000	459.2	22.2	122.4	40.8	41.4	37.5	2.5
2019-09-17 11:12:16.010	457.3	22.3	125.3	40.9	41.8	37.5	2.5
2019-09-17 11:06:16.003	458.0	22.7	122.2	40.9	42.3	37.4	2.5
2019-09-17 11:00:16.023	456.8	22.8	125.4	40.8	41.9	37.5	2.6
2019-09-17 10:54:16.013	455.6	22.7	124.4	40.8	42.0	37.4	2.5
2019-09-17 10:48:16.007	450.8	22.2	118.2	40.9	41.6	37.2	2.5
2019-09-17 10:42:16.007	443.2	20.7	122.3	41.1	41.4	36.9	2.5
2019-09-17 10:36:16.013	447.5	21.2	102.0	40.9	40.5	37.0	2.3
2019-09-17 10:30:16.013	442.2	21.1	121.3	41.0	40.9	36.8	2.5
2019-09-17 10:24:16.010	437.7	19.5	125.0	41.2	41.0	36.6	2.5

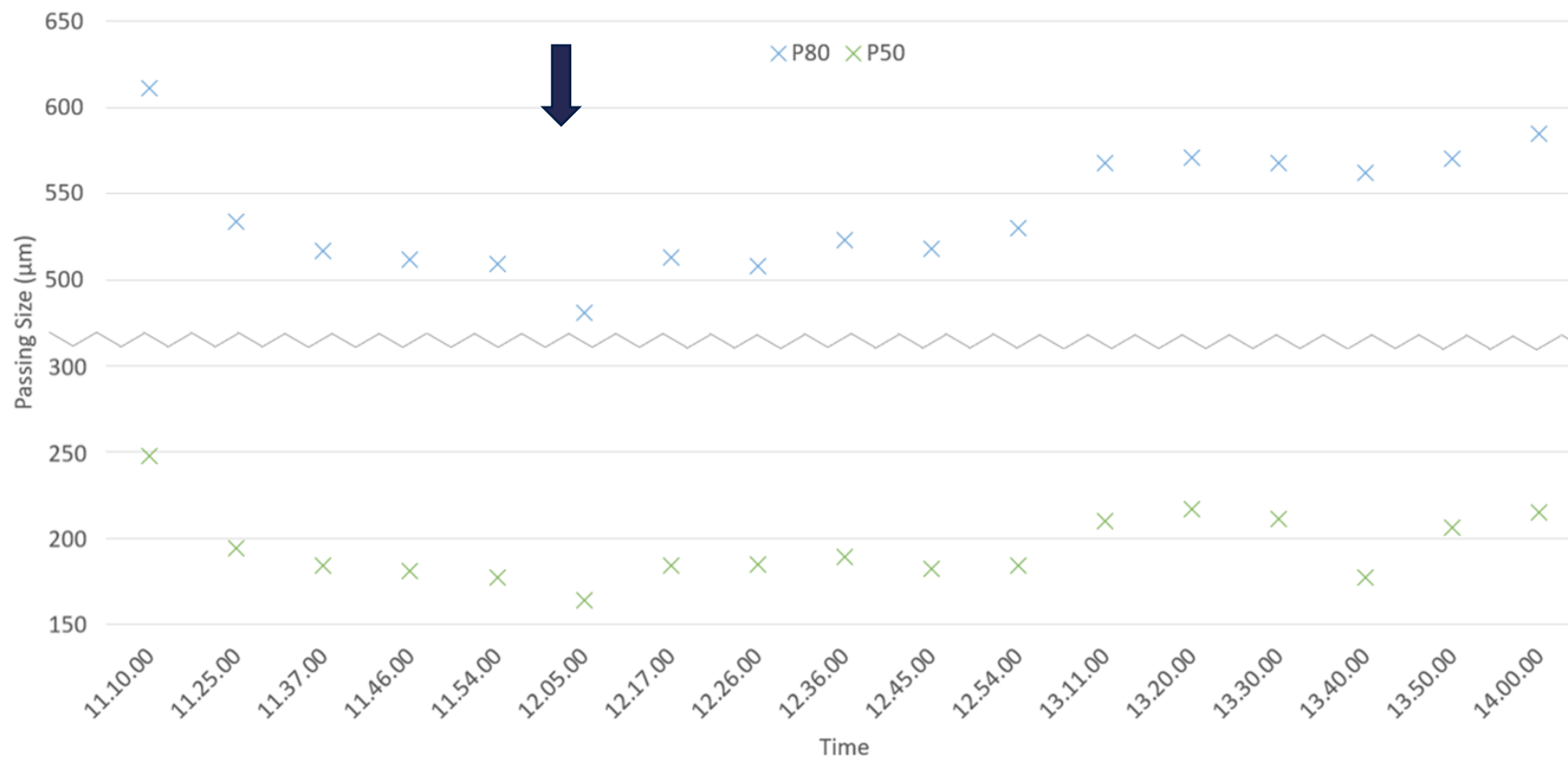
6.10 Appendix 10: LM2J power consumption (kW) and feed rate (tph) evolution graph. Blue arrows show when feed was momentarily interrupted



6.11 Appendix 11: Sample timing, D80, D50 and fine (-38µm) particles amount (%) table

		Percentage passing size (µm)										
		5000	3350	2360	1180	850	710	212	150	106	38	-38
Sample timing	11.10.00	100.0	99.7	99.2	98.7	95.5	90.8	86.5	46.0	36.9	29.3	13.8
	11.25.00	100.0	99.8	99.6	99.2	97.2	94.0	90.9	52.8	42.5	33.9	16.4
	11.37.00	100.0	99.9	99.7	99.3	97.5	94.7	91.7	54.4	44.2	35.9	17.5
	11.46.00	100.0	99.9	99.6	99.4	97.7	95.0	91.9	54.9	44.9	36.7	18.1
	11.54.00	100.0	99.9	99.6	99.4	97.8	95.1	92.1	55.2	45.6	37.3	17.6
	12.05.00	100.0	100.0	99.8	99.5	98.3	96.2	93.3	57.8	47.5	38.0	19.4
	12.17.00	100.0	99.5	99.1	98.9	97.9	95.1	92.1	54.6	44.1	35.8	17.9
	12.26.00	100.0	99.4	99.1	98.9	97.7	95.4	92.7	54.4	43.8	35.8	18.1
	12.36.00	100.0	99.6	99.4	99.0	97.3	94.6	91.6	53.5	43.3	34.9	18.8
	12.45.00	100.0	99.6	99.3	99.0	97.4	94.5	91.4	55.0	44.4	36.3	18.2
	12.54.00	100.0	98.7	98.2	97.8	96.3	93.4	90.4	54.5	44.0	35.6	17.6
	13.11.00	100.0	100.0	99.4	99.0	96.6	92.7	88.9	50.3	41.4	33.5	17.2
	13.20.00	100.0	100.0	99.4	99.0	96.6	92.8	88.9	49.5	39.7	32.8	16.4
	13.30.00	100.0	100.0	99.6	99.1	96.9	92.8	88.9	50.2	40.7	32.8	16.4
	13.40.00	100.0	100.0	99.7	99.2	96.2	91.7	87.3	55.7	45.2	36.7	18.5
	13.50.00	100.0	99.7	99.3	98.8	96.4	92.3	88.4	50.8	41.3	33.3	17.0
	14.00.00	100.0	98.9	98.3	97.8	95.5	91.4	87.6	49.7	40.4	32.8	16.3

6.12 Appendix 12: LM2J product size evolution graph. Blue arrow shows when feed was briefly interrupted



6.13 Appendix 13: Screenshot of the user interface of the economic calculator tool used in the VeX-Li training simulator

1	Parameters			
2				
3	Parameter	Value	Unit	Description
4	Calculation Configuration			
5	Enable Floor Losses calculation	<input checked="" type="checkbox"/>	*	
6	Number of valuable elements	1		
7				
8	Valuable Elements			
9	Element 1	Li2O	*	Valuable element (e.g. 'Cu')
12	Element 1 Price	8000	* \$/t	Price of the valuable element
15				
16	Reagent Consumption			
17	Number of conditioners where reagents are added	3	*	
18	Number of different reagents used	3	*	
19	Reagent 1 Price	0.0028	* \$/g	Price of reagent
20	Reagent 2 Price	0.0035	* \$/g	Price of reagent
21	Reagent 3 Price	0.0002	* \$/g	Price of reagent
22				

6.14 Appendix 14: Parameter simulation results from grinding / flotation circuits and expected results from plant survey. (Note: mass pulls and recoveries are not disclosed, and simulation results are given as a function of the expected results)

	Porphyry Simulation results HSC	Epithermal Simulation results HSC	Argillic Simulation results HSC	Expected Porphyry Results	Expected Epithermal Results	Expected Argillic Results
P80 to flotation (µm)	150.7	152.6	152	150.0	150.0	150.0
Grinding circuit specific energy (kwh/t)	16.8	17	10.8	16.9	17.2	10.4
FGO mass pull %	Expected x1.049	Expected x0.983	Expected x1.033	-	-	-
FGO Au rec%	Expected x1.020	Expected x1.010	Expected x0.969	-	-	-
FGO S rec%	Expected x0.994	Expected x0.976	Expected x1.020	-	-	-